Nonlinear Diffraction and Refraction of Regular and Random Waves

by

Meng-Yi Chen
M.S., Hydraulics and Ocean Engineering
National Cheng Kung University, 1998

Submitted to the Department of Civil and Environmental Engineering
in partial fulfillment of the requirements for the degree of

Doctor of Philosophy in the field of Coastal Engineering

at the

MASSACHUSETTS INSTITUTE OF TECHNOLOGY

February 2006

Author 11/17/2005
Department of Civil and Environmental Engineering
November 21, 2005

Certified by 11/17/2005
Chiang C. Mei
Ford Professor of Engineering
Thesis Supervisor

Accepted by .....
Andrew J. Whittle
Chairman, Departmental Committee on Graduate Students

Nonlinear Diffraction and Refraction of Regular and Random Waves

by

Meng-Yi Chen

M.S., Hydraulics and Ocean Engineering

National Cheng Kung University, 1998

Submitted to the Department of Civil and Environmental Engineering
on November 21, 2005, in partial fulfillment of the
requirements for the degree of
Doctor of Philosophy in the field of Coastal Engineering

Abstract

The mild-slope equation is an effective approximation for treating the combined effects of refraction and diffraction of infinitesimal water waves, for it reduces the spatial dimension of the linear boundary value problem from three to two. We extend this approximation to nonlinear waves up to the second order in wave steepness, in order to simplify the inherently three-dimensional task. Assuming that the geometrical complexity is restricted to a finite, though large, horizontal domain, the hybrid-element method designed earlier for linearized problems is modified for the two-dimensional elliptic boundary-value problems at the second order.

This thesis consists of two parts. In Part I, the incident waves are monochromatic. Application is first made to the special case of a a semi-circular peninsula (or a vertical cylinder on a cliff). Effects of the angle of incidence are examined for the free surface height along the cylinder. Numerical results for three examples involving radially varying depth are discussed. In Part II the second-order mild-slope approximation will be further extended for random waves with a broad frequency spectrum. A stochastic approach of Sclavounos is generalized for the prediction of spectral response in harbors. Focuss is on the low-frequency harbor resonance, so the third-order solution is unnecessary. Numerical examples are given for a simple square harbor of constant depth. Effects of harbor entrance are examined. Possible extensions and other applications are discussed.

Thesis Supervisor: Chiang C. Mei
Title: Ford Professor of Engineering

Acknowledgments

I would like to take this opportunity to express my gratitude and admiration to my advisor, Professor Chiang C. Mei for his support and guidance. His passion toward research has inspired me greatly. I also thank Professor Dick K. P. Yue, Professor Ole S. Madsen, Professor Triantaphyllos R. Akylas for their constructive suggestions. I am also indebted to Professor Paul D. Sclavounos whose guidance has contributed greatly to my thesis. I am especially grateful to Professor Dennis McLaughlin for letting me use itrda cluster. Thanks are also due to Mr. Chien-Kee Chang of the Institute of Harbor and Marine Technology in Taiwan who provided valuable field survey of Hualien harbor.

I am also grateful to all the people in my group and friends who have been there for me during my study. To Dr. Zhenhua Huang, Guangda Li, Blake Landry, Dr. Matthew Hancock, Aarow Chow, Brian White, Yo-Ming Hsieh, Yoshimitsu Tajima and Peter H. Israelsson, thanks for your support. I gratefully acknowledge the kindness of Yile Li for helping me on the computation and Matlab.

I appreciate the US Office of Naval Research (Grant N00014-04-1-0077) and US National Science Foundation (Grant CTS-0075713) for their financial support of this study.

Thanks to my parents for being wonderfully supportive. And finally, I thank my husband, Chih-Yuan Chuang for his endless love, patience and encouragement. Thank you.

Contents

1 Introduction **21**

1.1 Background and Motivation 21

1.2 Literature review 22

1.2.1 Nonlinear Diffraction 22

1.2.2 Mild-slope Equation 27

1.2.3 Harbor Oscillation 28

1.2.4 Random Waves 29

2 General Problem Formulation **31**

2.1 Mathematical Formulation of the Boundary Value Problem 31

2.2 Perturbation equations 33

2.2.1 First-order 34

2.2.2 Second-order 34

2.2.3 Third-order 35

I Monochromatic Incident Waves **37**

3 Mild-Slope Approximation **38**

3.1 First-order MSE 38

3.2 Second-order MSE 40

4 Solution Strategy: Hybrid-element Method **44**

4.1 First-order Far Field 46

4.2 Second-order Far Field 47
4.3 Forcing function F in the far-field Ω_F 49
4.3.1 Explicit expression for $\mathcal{P}$ in Ω_F 50
4.3.2 Fourier expansion for $\mathcal{Q}$ in Ω_F 51
4.4 ξ_ℓ^P and ξ_ℓ^Q in the far-field Ω_F 52
4.4.1 Response ξ_ℓ^P to Forcing $\mathcal{P}$ by progressive waves 52
4.4.2 Response ξ_ℓ^Q to forcing $\mathcal{Q}$ 54

5 Finite element analysis **63**
5.1 First-order problem 63
5.1.1 Weighted residual integral equation 64
5.1.2 Discretized by triangular elements 65
5.2 Second-order problem 73
5.2.1 Weighted residual integral equation 73
5.2.2 Discretized by triangular elements 75

6 Analytical Solution for a Semi-Circular Peninsula in Constant Depth **83**
6.1 First-order solution 83
6.2 Second-order solution 84
6.3 Numerical Validation 87
6.4 Effects of Incidence Angle and Cylinder Radius 91

7 Numerical Solution for problems involving a semi-circular shoal **98**
7.1 Example 1: A Semi-Circular Shoal near a Cliff 98
7.1.1 Computational Aspects and Validation 99
7.1.2 Results 100
7.2 Example 2: A Half Cylinder on top of a Semi-Circular Shoal 115
7.2.1 Compuational Aspects and Validation 115
7.2.2 Results 116
7.3 Example 3: A Square Harbor open to a Semi-Circular Shoal 125
7.3.1 Natural modes in a closed square basin with constant depth . 126

7.3.2 Numerical results 126

II Random Incident Waves **138**

8 Random Incident Sea **139**

8.1 Incident wave spectrum 139

8.2 TMA spectrum 141

8.3 First-order Diffraction 143

8.4 Second-order Diffraction 145

8.4.1 The potential 145

8.4.2 The free surface displacement 150

8.5 The Frequency Spectrum 151

8.5.1 Linear frequency spectrum S_2 154

8.5.2 Nonlinear Correction S_{22} 155

8.5.3 Nonlinear Corrections S_{13} and S_{31} 159

9 Calculations of nonlinear transfer functions and spectra **165**

9.1 Hybrid-element Method 165

9.2 Second-order analytic solution in the Far-field 166

9.3 Expression of $f(x, y, \omega_1, \omega_2)$ in the far-field Ω_F 168

9.3.1 Explicit Expression for $\mathcal{P}(\omega_1, \omega_2)$ in Ω_F 170

9.3.2 Fourier expression for $\mathcal{Q}(\omega_1, \omega_2)$ in Ω_F 171

9.4 $\xi_\ell^P(\omega_1, \omega_2)$ and $\xi_\ell^Q(\omega_1, \omega_2)$ in the far field Ω_F 172

9.4.1 Exact solution for $\xi_\ell^P(\omega_1, \omega_2)$ 173

9.4.2 Exact solution for $\xi_\ell^Q(\omega_1, \omega_2)$ by Green's theorem 173

9.5 Evaluation of spectrum S_{22} 177

10 Numerical Solution for a Square Harbor in constant depth **182**

10.1 Square Harbor in constant depth 182

10.2 Incident wave spectrum 184

10.3 Pairs of frequencies 185

10.4 Numerical result . . . 185

11 Conclusion **249**

A First-order MSE **253**

A.1 Derivation of the first-order MSE . . . 253

A.2 Derivation of $\frac{\partial k}{\partial h}$ . . . 257

A.3 Derivation of $\frac{\partial f}{\partial h}$ . . . 257

A.4 Derivation of U . . . 258

A.5 Derivation of V . . . 260

B Derivation of F **264**

B.1 Free surface boundary condition . . . 264

B.2 First term (Q_1) in Q . . . 265

B.3 Second term (Q_2) in Q . . . 266

B.4 Third Term (Q_3) in Q . . . 266

B.5 Fourth term (Q_4) in Q . . . 267

C Second-order MSE **268**

C.1 Derivation of the second-order MSE . . . 268

C.2 Derivation of $\frac{\partial \kappa_m}{\partial h}$ . . . 272

C.3 Derivation of $\frac{\partial f_m}{\partial h}$ . . . 272

C.4 Derivation of $U_{m,\ell}$ . . . 273

C.5 Derivation of $V_{m,\ell}$ . . . 276

D Fourier expression for $\mathcal{Q}$ **278**

E Equivalence to Stokes waves **280**

F Weak radiation condition for ξ_0^Q **282**

F.1 Asymptotic behavior of ξ_0^Q . . . 282

F.2 Weak radiation condition . . . 283

G Evaluation of Infinite Integrals **286**

H Jointly Gaussian distribution **290**

I Weak radiation condition for $\xi_0^Q(\omega_1, \omega_2)$ **293**

I.1 Asymptotic behavior of $\xi_0^Q(\omega_1, \omega_2)$ 293

I.2 Weak radiation condition 295

J Derivation of H_{31} **298**

List of Figures

1-1 Hualien Harbor, Taiwan, ROC. 23

1-2 Wave height v.s. wave period during Typhoon Tim at each station of Hualien Harbor 24

1-3 Surface elevation during Typhoon Tim at each station of Hualien Harbor 25

4-1 Near (Ω_A) and far (Ω_F) fields. Variable bathymetry and non-straight coastal boundaries in (Ω_A) behine the semi-circle $r = a$. (a): without a harbor (top) (b): with a harbor (bottom). 45

5-1 (a) Global and local nodes of finite elements . (b) Line elements on the semi-circular boundary ∂A 67

6-1 Method of image 84

6-2 Dimensionless amplitudes of the dimensionless second-order free-surface forcing terms, $\epsilon_m \mathcal{Q}_m/(2gk^2A^2/\omega)$ of the first three modes as a function of the dimensionless radial distance from the vertical cylinder, r/a 89

6-3 Comparison of our theory in the limit of $\theta_I = 0$ with Chau and Eatock Taylor(1992) and Kim and Yue (1989). 90

6-4 Dimensionless amplitudes of first-order $|\eta/A|$ along the semi-circular peninsula 93

6-5 Dimensionless amplitudes of second-order $\eta^{(1)}_{2,0}/(4kA^2)$ along the semi-circular peninsula 94

6-6 Dimensionless amplitudes of second-order $|\eta^{(1)}_{2,2}|/(2kA^2)$ along the semi-circular peninsula 95
6-7 Dimensionless amplitudes of second-order $|\eta^{(2)}_{2,2}|/(2kA^2)$ along the semi-circular peninsula 96
6-8 Dimensionless amplitudes of second-order $|\eta^{(2)}_{2,2} + \eta^{(1)}_{2,2}|/(2kA^2)$ along the semi-circular peninsula 97

7-1 Radial variation of depth profile of the circular shoal. 99
7-2 The first-order amplitude, $|\eta|/A$, over a circular shoal near a coast. Glancing incidence ($\theta_I = \pi$). 101
7-3 The first-order amplitude, $|\eta|/A$, over a semi-circular shoal near a coast. Normal incidence ($\theta_I = 3\pi/2$). 102
7-4 The first-order amplitude, $|\eta|/A$, over a semi-circular shoal near a coast. Oblique incidence ($\theta_I = 5\pi/4$). 102
7-5 Ray geometry for normal incidence 103
7-6 Variations of the first-order amplitude, $|\eta|/A$ along the centerline $x = 0\ m$. 104
7-7 The second-order setup/down, $\eta^{(1)}_{2,0}/4k_0A^2$, over a semi-circular shoal near a coast. Glancing incidence ($\theta_I = \pi$). 105
7-8 The second-order setup/down, $\eta^{(1)}_{2,0}/4k_0A^2$, over a semi-circular shoal near a coast. Normal incidence ($\theta_I = 3\pi/2$). 106
7-9 The second-order setup/down, $\eta^{(1)}_{2,0}/4k_0A^2$, over a semi-circular shoal near a coast. Oblique incidence ($\theta_I = 5\pi/4$). 107
7-10 Variations of the second-order setdown/up, $\eta^{(1)}_{2,0}/4k_0A^2$ along the centerline $x = 0\ m$. 107
7-11 The second-order amplitude, $|\eta^{(1)}_{2,2}|/2k_0A^2$, over a semi-circular shoal near a coast. Glancing incidence ($\theta_I = \pi$). 108
7-12 The second-order amplitude, $|\eta^{(1)}_{2,2}|/2k_0A^2$, over a semi-circular shoal near a coast. Normal incidence ($\theta_I = 3\pi/2$). 109

7-13 The second-order amplitude, $|\eta_{2,2}^{(1)}|/2k_0A^2$, over a semi-circular shoal near a coast. Oblique incidence ($\theta_I = 5\pi/4$). 109
7-14 The second-order amplitude, $|\eta_{2,2}^{(2)}|/2k_0A^2$, over a semi-circular shoal near a coast. Glancing incidence ($\theta_I = \pi$). 111
7-15 The second-order amplitude, $|\eta_{2,2}^{(2)}|/2k_0A^2$, over a semi-circular shoal near a coast. Normal incidence ($\theta_I = 3\pi/2$) 111
7-16 The second-order amplitude, $|\eta_{2,2}^{(2)}|/2k_0A^2$, over a semi-circular shoal near a coast. Oblique incidence ($\theta_I = 5\pi/4$) 112
7-17 The second-order amplitude, $|\eta_{2,2}^{(1)} + \eta_{2,2}^{(2)}|/2k_0A^2$, over a semi-circular shoal near a coast. Glancing incidence ($\theta_I = \pi$). 112
7-18 The second-order amplitude, $|\eta_{2,2}^{(1)} + \eta_{2,2}^{(2)}|/2k_0A^2$, over a semi-circular shoal near a coast. Normal incidence ($\theta_I = 3\pi/2$). 113
7-19 The second-order amplitude, $|\eta_{2,2}^{(1)} + \eta_{2,2}^{(2)}|/2k_0A^2$, over a semi-circular shoal near a coast. Oblique incidence ($\theta_I = 5\pi/4$). 113
7-20 Variations of the second-order amplitude $|\eta_{2,2}^{(1)}|/2k_0A^2$ along the centerline $x = 0\ m$. 114
7-21 Variations of the second-order $|\eta_{2,2}^{(2)}|/2k_0A^2$ along the centerline $x = 0\ m$. 114
7-22 Variations of the second-order $|\eta_{2,2}^{(1)} + \eta_{2,2}^{(2)}|/2k_0A^2$ along the centerline $x = 0\ m$. 114
7-23 The second-order amplitude $|\eta_{22}|/2k_0A^2$ along the semi-circular cylinder for example 2. $\circ$: $a = 310\ m$, $\times$: $a = 300\ m$. Left: glancing incidence. Right: normal incidence. 116
7-24 The first-order amplitude, $|\eta|/A$, over a semi-circular shoal around a cylinder. 118
7-25 The second-order setdown/setup, $\eta_{2,0}^{(1)}/4k_0A^2$, over a semi-circular shoal around a cylinder. 119
7-26 The second-harmonic amplitude computed from the first-harmonic, $|\eta_{2,2}^{(1)}|/2k_0A^2$, over a semi-circular shoal around a cylinder. 121

7-27 The second-order amplitude computed from the second-harmonic, $|\eta^{(2)}_{2,2}|/2k_0A^2$, over a semi-circular shoal around a cylinder. 122
7-28 The total second-order amplitude, $|\eta^{(1)}_{2,2} + \eta^{(2)}_{2,2}|/2k_0A^2$, over a semi-circular shoal around a cylinder. 123
7-29 Free-surface heights along the semi-circular cylinder of the same radius attacked by an incident wave of the same frequency. 124
7-30 Plane view of the square basin and locations of point A ($x = 150m,\ y = -305m$), B ($x = 0m,\ y = -305m$) and C ($x = 0m,\ y = -86m$) 125
7-31 The first-order response $|\eta/A|$ vs. frequency ω for normal incidence waves at three locations. Chain line : A(x=150 m, y=-305 m), Solid line: B(x=0 m, y=-305 m) and Dashed line: C(x=0 m, y=-86 m). 127
7-32 Contours of the free-surface amplitude of natural mode in a square basin for$(n, m) = (4, 4)$ 128
7-33 Contours of the first-order free-surface amplitude $|\eta/A|$ inside the square harbor with incident frequency $\omega = 0.7\ rad/s$ 128
7-34 The first-order amplitude, $|\eta|/A$, for a square harbor open to a semi-circular shoal near a coast. Incident wave frequency $\omega = 0.7$ rad/s. Normal incidence ($\theta_I = 3\pi/2$). 129
7-35 Variations of the first-order $|\eta|/A$ along the centerline $x = 0\ m$ for a square harbor open to a semi-circular shoal. Incident wave frequency $\omega = 0.7\ rad/s$. Normal incidence ($\theta_I = 3\pi/2$). 130
7-36 The second-order setup/down, $\eta^{(1)}_{2,0}/4k_0A^2$, for a square harbor with a semi-circular shoal near a coast. 132
7-37 Variations of the second-order setup/down $\eta^{(1)}_{2,0}/4k_0A^2$ along the centerline $x = 0\ m$. 132
7-38 Setup/setdown $\eta_{2,0}/k_0a_{n,m}$ of standing wave in a closed basin at mode $(n, m) = (4, 4)$ 133
7-39 The second-order amplitude, $|\eta^{(1)}_{2,2}|/2k_0A^2$, for a square harbor open to a semi-circular shoal near a coast. 133

7-40 Variations of the second-order amplitude $|\eta_{2,2}^{(1)}|/2k_0A^2$. along the centerline $x = 0\ m$. 134
7-41 The second-order amplitude, $|\eta_{2,2}^{(2)}|/2k_0A^2$, for a square harbor open to a semi-circular shoal near a coast. 134
7-42 Variations of the second-order amplitude $|\eta_{2,2}^{(2)}|/2k_0A^2$ along the centerline $x = 0\ m$. 135
7-43 Contours of the first-order free-surface amplitude of natural mode in a square basin for$(n, m) = (12, 15)$ 136
7-44 The dimensionless second-order amplitude, $|\eta_{2,2}^{(1)} + \eta_{2,2}^{(2)}|/2k_0A^2$,for a square harbor with a semi-circular shoal near a coast. 137
7-45 Variation of the second-order second-harmonic amplitude $|\eta_{2,2}^{(1)} + \eta_{2,2}^{(2)}|/2k_0A^2$ along the centerline $x = 0\ m$. 137

8-1 Transformation factor T as a function of dimensionless frequency $\omega(h/g)^{1/2}$. 141
8-2 Comparison between the TMA and the JONSWAP spectrum with $\gamma = 3.3$, $\bar{U} = 20\ m^2/sec$, $\bar{x} = 3000$. Solid line: S_{TMA} for $h = 20\ m$. Dashed line: S_{JON}. 143

9-1 Plane of (ω_1, ω_2). Γ_2 is computed for frequency pairs inside the shaded strips. Frequencies ω_a and ω_b are the truncated limits of the incident sea spectrum. 180

10-1 Plane view of the square basin and locations of St. $1 - 8$ 183
10-2 Comparison between TMA spectrum and our incident spectrum in frequency (a) ω (b) f space 184
10-3 Spatial-averaged response Γ_1 for (a): 60 m opening (Case 1) , (b): 30m opening without protection (Case 2) , (c): 30 m opening with protection (Case 3). 187
10-4 Free-surface contours of natural mode in a closed basin. 189
10-5 Free surface response Γ_1 at St. 1-4 for opening 60 m (Case 1) 194

10-6 Free surface response Γ_1 at St. 5-8 for opening 60 m (Case 1) 195
10-7 Free surface response Γ_1 at St. 1-4 for opening 30 m (Case 2) 196
10-8 Free surface response Γ_1 at St. 5-8 for opening 30 m (Case 2) 197
10-9 Free surface response Γ_1 at St. 1-4 for opening 30 m with breakwater (Case 3) 198
10-10 Free surface response Γ_1 at St. 5-8 for opening 30 m with breakwater (Case 3) 199
10-11Spatial-averaged spectrum $2\mathcal{S}_2(\omega)$. 200
10-12 Linear spectrum $2\mathcal{S}_2(\omega)$ at St. 1-4 for opening 60 m (Case 1) 201
10-13 Linear spectrum $2\mathcal{S}_2(\omega)$ at St. 5-8 for opening 60 m (Case 1) 202
10-14 Linear spectrum $2\mathcal{S}_2(\omega)$ at St. 1-4 for opening 30 m (Case 2) 203
10-15 Linear spectrum $2\mathcal{S}_2(\omega)$ at St. 5-8 for opening 30 m (Case 2) 204
10-16 Linear spectrum $2\mathcal{S}_2(\omega)$ at St. 1-4 for opening 30 m with breakwater(Case 3) 205
10-17 Linear spectrum $2\mathcal{S}_2(\omega)$ at St. 5-8 for opening 30 m with breakwater (Case 3) 206
10-18 The second-order setup/down for opening 60 m (Case 1). 207
10-19 The second-order setup/down for opening 30 m (Case 2). 207
10-20 The second-order setup/down for opening 30 m with breakwater (Case 3). 208
10-21 Setup/setdown $\eta_{20}/ka^2_{n,m}$ of standing wave in closed basin at mode (a) $(n,m) = (0,5)$ and (b) $(n,m) = (2,5)$ 209
10-22 Setup/setdown $\eta_{20}/ka^2_{n,m}$ of standing wave in closed basin at mode (a) $(n,m) = (4,4)$ and (b) $(n,m) = (0,6)$ 210
10-23 Setup/setdown $\eta_{20}/ka^2_{n,m}$ of standing wave in closed basin at mode (a) $(n,m) = (6,1)$ and (b) $(n,m) = (4,5)$ 211
10-24 Setup/setdown $\eta_{20}/ka^2_{n,m}$ of standing wave in closed basin at mode (a) $(n,m) = (6,3)$ and (b) $(n,m) = (0,7)$ 212
10-25 Spatial-averaged nonlinear correction $2\mathcal{S}_{22}(\omega)$. 213
10-26 Nonlinear correction $2\mathcal{S}_{22}(\omega)$ at St. 1-4 for $60\ m$ opening (Case 1). . . 214

10-27 Nonlinear correction $2\mathcal{S}_{22}(\omega)$ at St. 5-8 for 60 m opening (Case 1). . . 215
10-28 Nonlinear correction $2\mathcal{S}_{22}(\omega)$ at St. 1-4 for 30 m opening (Case 2). . . 216
10-29 Nonlinear correction $2\mathcal{S}_{22}(\omega)$ at St. 5-8 for 30 m opening (Case 2). . . 217
10-30 Nonlinear correction $2\mathcal{S}_{22}(\omega)$ at St. 1-4 for 30 m opening with breakwater (Case 3). 218
10-31 Nonlinear correction $2\mathcal{S}_{22}(\omega)$ at St. 5-8 for 30 m opening with breakwater (Case 3). 219
10-32 Layout of Hualien Harbor 220
10-33 Spectrum during Typhoon Tim of Hualien Harbor 221
10-34 Spatial-averaged spectrum $2\mathcal{S}(f)$ for 60 m opening (Case 1). 222
10-35 Spatial-averaged spectrum $2\mathcal{S}(f)$ for 30 m opening (Case 2). 223
10-36 Spatial-averaged spectrum $2\mathcal{S}(f)$ for 30 m opening with breakwater (Case 3). 224
10-37 $2\mathcal{S}(f)$ at St. 1 for 60 m opening (Case 1). 225
10-38 $2\mathcal{S}(f)$ at St. 1 for 30 m opening (Case 2). 226
10-39 $2\mathcal{S}(f)$ at St.1 for 30 m opening with breakwater (Case 3). 227
10-40 $2\mathcal{S}(f)$ at St.2 for 60 m opening (Case 1). 228
10-41 $2\mathcal{S}(f)$ at St. 2 for 30 m opening (Case 2). 229
10-42 $2\mathcal{S}(f)$ at St. 2 for 30 m opening with breakwater (Case 3). 230
10-43 $2\mathcal{S}(f)$ at St. 3 for 60 m opening (Case 1). 231
10-44 $2\mathcal{S}(f)$ at St. 3 for 30 m opening (Case 2). 232
10-45 $2\mathcal{S}(f)$ at St. 3 for 30 m opening with breakwater (Case 3). 233
10-46 $2\mathcal{S}(f)$ at St. 4 for 60 m opening (Case 1). 234
10-47 $2\mathcal{S}(f)$ at St. 4 for 30 m opening (Case 2). 235
10-48 $2\mathcal{S}(f)$ at St.4 for 30 m opening with breakwater (Case 3). 236
10-49 $2\mathcal{S}(f)$ at St.5 for 60 m opening (Case 1). 237
10-50 $2\mathcal{S}(f)$ at St.5 for 30 m opening (Case 2). 238
10-51 $2\mathcal{S}(f)$ at St.5 for 30 m opening with breakwater (Case 3). 239
10-52 $2\mathcal{S}(f)$ at St.6 for 60 m opening (Case 1). 240
10-53 $2\mathcal{S}(f)$ at St.6 for 30 m opening (Case 2). Region I: $2\mathcal{S}_2(f)$. 241

10-54 $2\mathcal{S}(f)$ at St.6 for $30\ m$ opening with breakwater (Case 3). 242
10-55 $2\mathcal{S}(f)$ at St.7 for $60\ m$ opening (Case 1). 243
10-56 $2\mathcal{S}(f)$ at St.7 for $30\ m$ opening with breakwater (Case 2). 244
10-57 $2\mathcal{S}(f)$ at St.7 for $30\ m$ opening with breakwater (Case 3). 245
10-58 $2\mathcal{S}(f)$ at St.8 for $60\ m$ opening (Case 1). 246
10-59 $2\mathcal{S}(f)$ at St.8 for $30\ m$ opening (Case2). 247
10-60 $2\mathcal{S}(f)$ at St.8 for $30\ m$ opening with breakwater(Case 3). 248

List of Tables

6.1 Number of terms (m, n) used in the double series for $\mathcal{Q}$. 92

9.1 Pairs of (ω_1, ω_2) for computing the first series of $\mathcal{I}(\omega)$ 181

9.2 Pairs of (ω_1, ω_2) for computing the second series of $\mathcal{I}(\omega)$ 181

10.1 Pairs of (ω_1, ω_2) for computing $S(\omega = 0.01)$ and $S(\omega = 0.02)$. 185

10.2 Pairs of (ω_1, ω_2) for computing $S(\omega = 0.59)$ and $S(\omega = 0.6)$. 186

10.3 The resonant frequencies for (1) closed basin (2) opening 60 m (Case 1) (3) 30 m opening without protection (Case 2) (4) 30 m opening with protection (Case 3). 188

Chapter 1

Introduction

1.1 Background and Motivation

In coastal dynamics there is a need for the prediction of the nonlinear diffraction and refraction of waves over varying bathymetry. Due to quadratic interactions of two first-order incident waves of nearly equal frequencies, second-order forcing at the difference frequency may induce significant slow oscillations inside a harbor. These long-period oscillations with periods of one to several minutes inside harbors often cause excessive sway of ships, resulting in damages of ship hulls, fenders, or mooring lines, or costly delay of loading and unloading operations. Oftentimes, when these long-period oscillations occur, ships are forced to leave a harbor and wait outside until the oscillations within subside. These damage and delay can cause a huge loss of money to a port authority.

Field reports [15] at Hualien Harbour, located in the center-eastern part of Taiwan facing to Pacific ocean, show that during typhoon seasons (1) many mooring lines were broken, (2) cargo operations were terminated, and (3) ships could not anchor at the harbor, all because of the long-period waves which cause large ship motions. Moreover, similar damages are common in other harbors in Japan, such as Tomakomai, Kashima, Norshiro, Shibushi, etc [32].

In many harbors, the natural modes have periods longer than one minute, and these modes can be excited by waves with a comparable long period. When these

modes are resonated, a small disturbance in water will induce large responses. This is called *harbor resonance*, which causes unpleasant long-period oscillations.

The long-period waves that create harbor resonances can be induced by transient winds. Although it is known that wind generated waves and swell usually have the periods less than 30 seconds, the long-period waves can be generated by the *nonlinear* interaction of the *short-period* wind waves. This is clearly seen in the wave records at many harbors.

Figure 1-2 and 1-3 are the field observations [15] at Hualien Harbour during Typhoon Tim, 1994 at several stations both inside and outside the harbor as indicated in Figure 1-1. Figure 1-2 represents the wave energy vs. a waves period. It shows that (1) outside the harbor the range of the wave periods is from 11 sec to 15 sec and no long-period waves exist, (2) near the entrance of the harbor the energy of short-period waves decreases slightly while the energy of long-period waves are significant, (3) inside the harbor the energy of long-period waves, around 160 sec, increases dramatically while short-period waves decrease significantly. It is also shown in Figure 1-3 that inside the harbor the water level oscillates with a period around 150 sec.

The study of the long-period waves induced by the *nonlinear* interaction of the short-period waves is of importance in the design of a harbor. Therefore, the objective of this thesis is to investigate the second-order nonlinear refraction and diffraction due to regular and random waves.

1.2 Literature review

1.2.1 Nonlinear Diffraction

The linearized diffraction problem for a vertical cylinder in a constant depth has been studied before. Because of its simplest geometry, the exact solution is well known and can be found in Mei [24].

The three-dimensional problem of nonlinear diffraction is difficult even for a

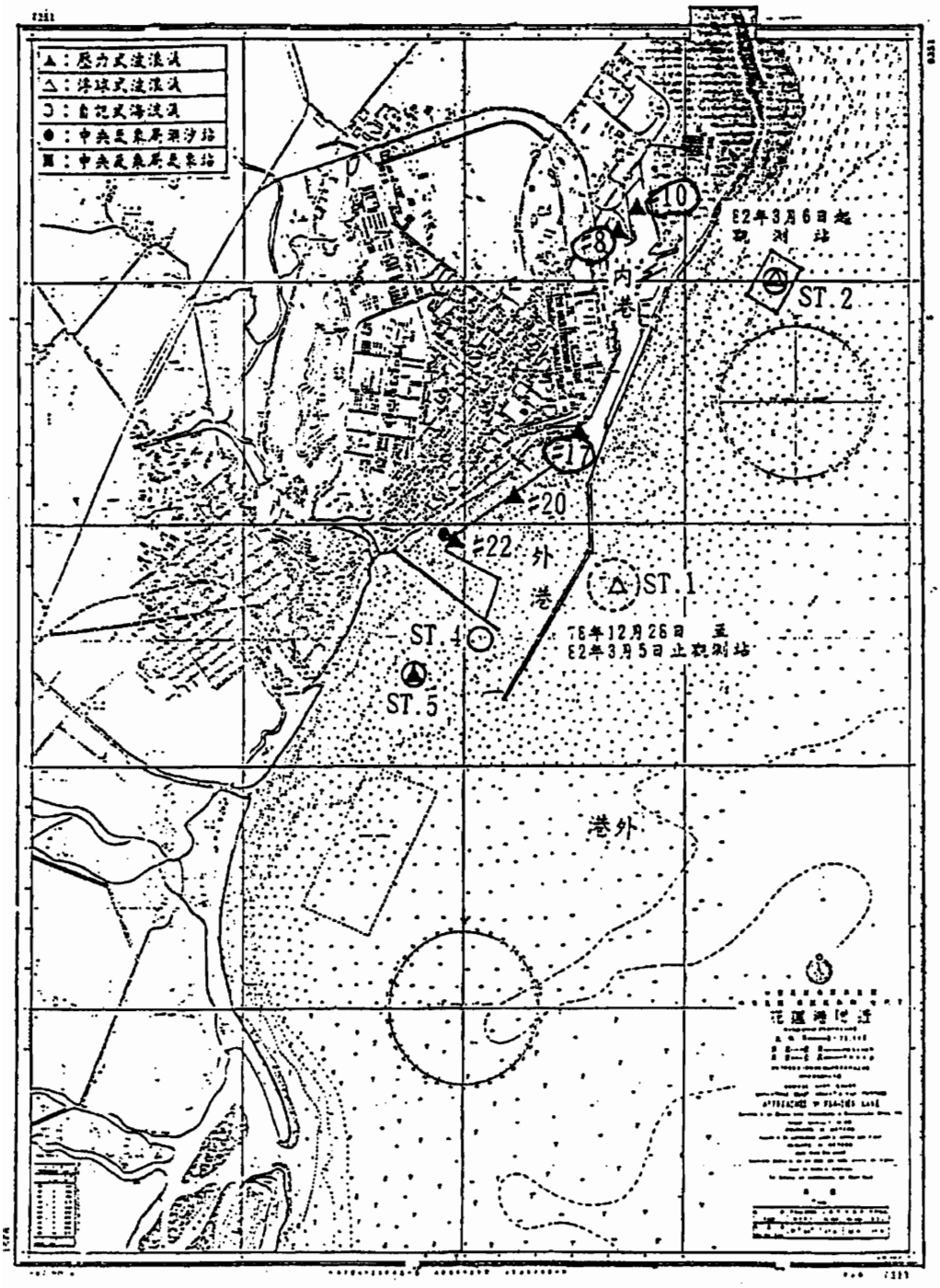

Figure 1-1: Hualien Harbor, Taiwan, ROC.

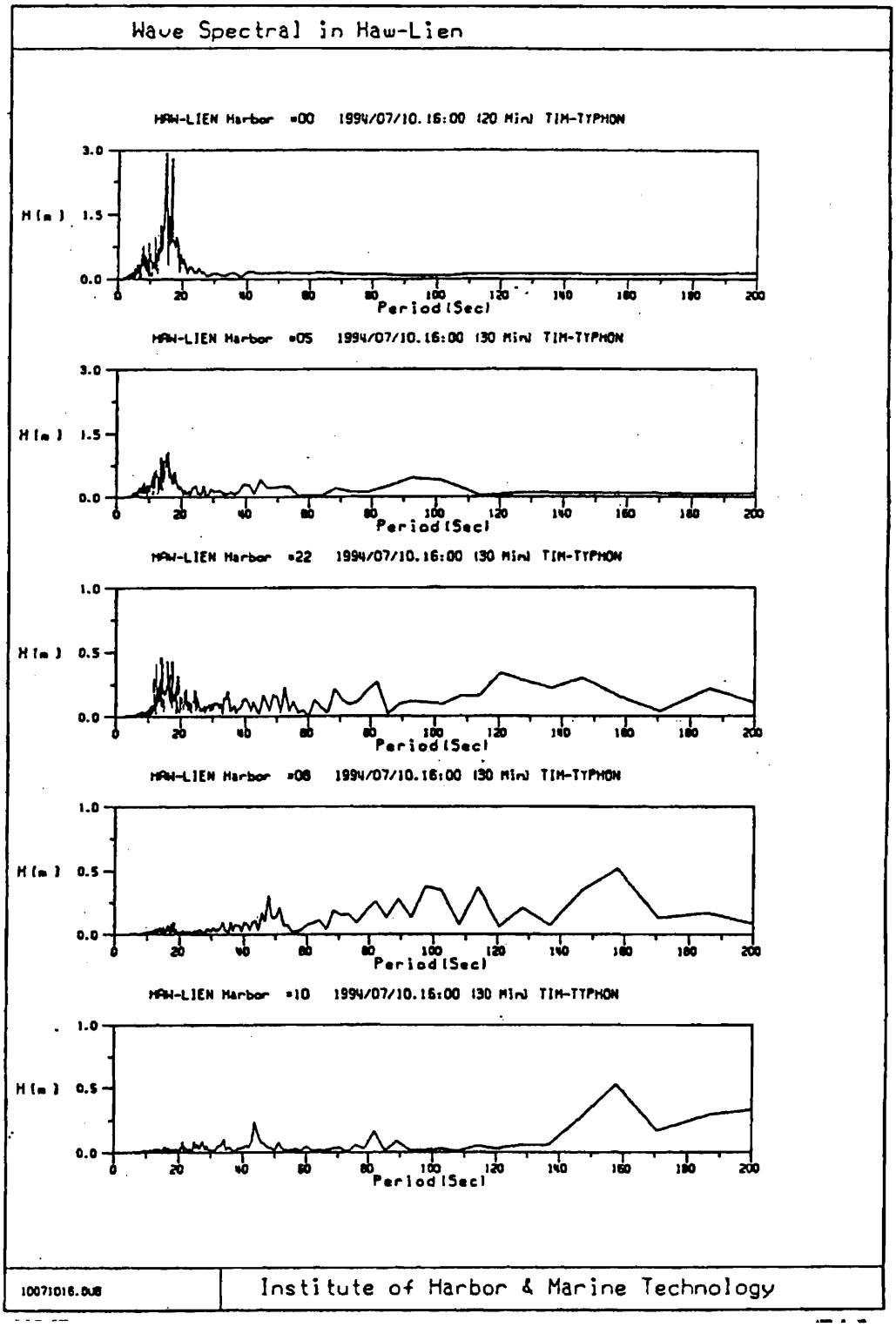

Figure 1-2: Wave height v.s. wave period during Typhoon Tim at each station of Hualien Harbor

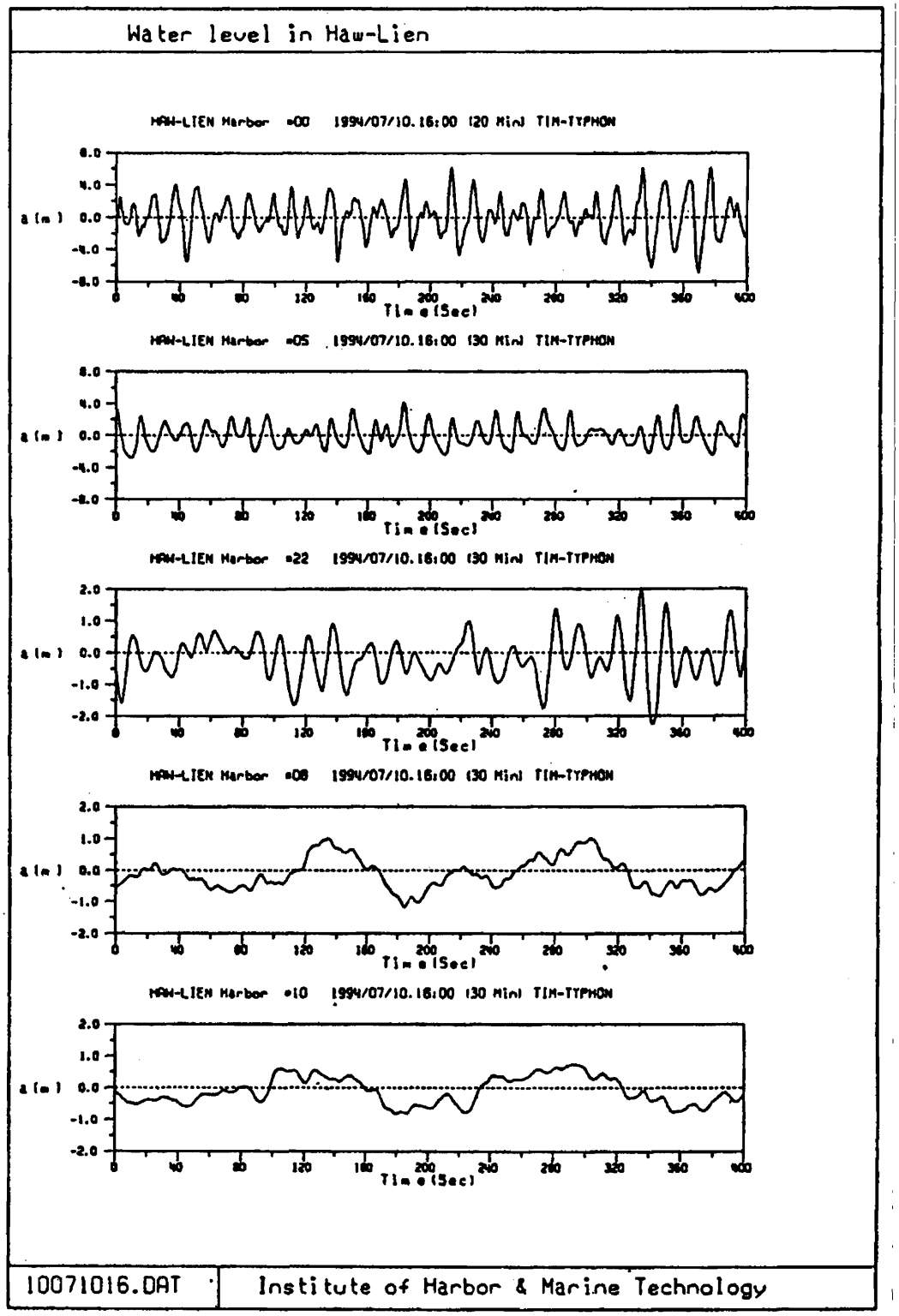

Figure 1-3: Surface elevation during Typhoon Tim at each station of Hualien Harbor

sea of constant depth bounded by vertical cliff-like coasts. Many researchers have studied the nonlinear diffraction by a vertical cylinder in constant depth. For constant depth and monochromatic incident waves, Molin [28] obtained an approximated second-order analytical solution for a large cylinder by decomposing the second-order potential into free and forced terms satisfying respectively homogeneous and inhomogeneous free-surface conditions. A weak radiation condition for the second-order diffracted waves is also obtained. In the study of a similar but large cylinder, Eatock Taylor and Hung [12] used an approximated first-order potentials for regular waves to obtain the second-order approximated solution for the second-order potential and forces. Zhou and Liu [44] used the multiple-scale perturbation method to investigate the diffraction of a nonlinear nearly periodic wavetrain by a vertical cylinder. Sclavounos [33] studied the second-order nonlinear radiation and diffraction by floating bodies of deep-water bichromatic and bidirectional surface waves and developed a theory for surface piercing bodies of arbitrary shape.

The second-order theory for an axially symmetric body was finally completed by Kim and Yue,[17] and [18]. In their theory, a ring-source integral equation is developed to treat the diffraction by an axisymmetric body for monochromatic incident waves [17] and also for bichromatic incident waves [18]. Besides, analytic free-surface integration over entire surface domain is also developed. Complete second-order forces, moments, surface pressures and run-up on the vertical cylinder as well as a truncated vertical cone are presented. They showed that the second-order potential cannot be neglected and its contribution can dominate the total load in many cases. In Chau and Eatock Taylor [10], a Green's function is employed to obtained an analytical solution which is in good agreement with Kim and Yue's numerical result [17].

However, for problems related to varying bathymetry and irregular boundaries, analytic solution is very difficult since the phenomenon combines refraction and diffraction.

1.2.2 Mild-slope Equation

The diffraction of infinitesimal waves by scatterers with vertical wall over a slowly varying bathymetry can be treated effectively by the mild-slope equation (MSE) originated by Berkhoff [6]. A special feature of MSE is that it combines the refraction and the diffraction effects and reduces the boundary value problem from three dimensions to two, hence, facilitates numerical computations. In the original derivation of Berkhoff (see also Smith and Sprinks [35] who derived MSE by weighted averaging via Green's formula.), terms proportional to the small ved slope ∇h were kept but those proportional to $(\nabla h)^2$, $\nabla^2 h$ were neglected. For applications to steeper bathymetries various modifications have been proposed(Massel [22]; Athanassoulis and Belibassakis [3]; Chamberlain and Porter [9]; Porter and Staziker [31].) In particular Chamberlain and Porter retain the second-order depth-gradient terms and show that the modified mild-slope equation has a better accuracy for scattering by corrugated sea bed of length scale comparable to the surface waves. Increased accuracy can be achieved for still steeper bed slopes by including all the evanescent modes, leading to an infinite set of two-dimensional modified mild-slope equations coupling all vertical modes(Massel [22] and Porter and Staziker [31].) Athanassoulis and Belibassakis [3] extend Massel's theory with one additional mode for the bottom slope in order to tackle a steeper bottom in which results of an one dimensional variable bottom with linear waves is demonstrated. Later a two dimensional problem for linear waves is shown in Belibassakis, Athanssoulis and Gerostathis [5]. Mei [25] use a multiple-scale perturbation method to obtain a MSE for the second-order long waves with including both slow scale and fast scale. In practice, it is difficult to separate the two scales when a numerical method is applied.

Extensions of the mild-slope approximation to nonlinear problems are so far limited to basic ideas but not yet fully implemented.

1.2.3 Harbor Oscillation

Monochromatic Incident Waves

Linearly excited oscillations by monochromatic incident long waves have been studied analytically for some simple geometries. Miles and Munk [27] gave a complete analysis for an open narrow bay. Ünlüata and Mei [38] studied the similar problem with a different approximation at the entrance. An analytic solution for a two coupled basins was also obtain by Ünlüata and Mei [39]. These linearized problem are reviewed by Mei [24] and by Mei and Liu [26].

Numerical methods are also developed for the linearized long waves. For harbors of constant depth but arbitrary plan form, numerical solutions have been obtained by Hwang and Tuck [16] and Lee [21] by method of integral equations. For varying depth integral equations is rather complicated and expensive (Lautenbacher [20]; Mattioli [23].) Chen and Mei [11] developed a hybrid finite element method for a incident long waves and the method is well suited for variable depth. The numerical scheme was applied on the incident short waves with a mild-slope equation by Houston [14]. Also the numerical scheme has been applied in many practical computation, e.g. for Long Beach harbor in U.S. [13] and Hualien harbor in Taiwan [15]. Some modifications are given by Tsay, Zhu and Liu [37] concerning dissipation at the boundary.

Narrow-banded Incident Waves Groups

Long-period harbor oscillations by groups of short-period wind waves with narrow band have been studied by several authors. Bowers [8] considered two narrow channels with the outer channel being wider. He found both locked long waves and free long waves theoretically and experimentally. Agnon and Mei [2] studied a rectangular harbor with a narrow entrance width that is much wider than the wavelength of the incident short waves but much smaller than the wavelength of the long waves. Besides, the harbor basin is exposed to the ocean without any protection and the depth is constant everywhere. Moreover, the straight coastline

intersects the longitudinal axis of the harbor. With these assumptions, they obtained an approximated analytical solution for the short waves. They showed that the free long wave can be resonated inside the harbor.

Wu and Liu [41] examined a similar problem concerning wave-group-induced harbor resonance. The two major features are (1) a protection of two breakwaters parallel to the coastline is imposed, and (2) the harbor mouth is wider than the wavelength of incident short waves but smaller than the wavelength of the wave envelope . In their study, oblique incident wave groups were considered. The first-order wave field is obtained exactly by an integral-equation method. Also analytical expressions for both locked and free long waves inside and outside the harbor were obtained. They demonstrated that only the free long waves are resonated at low frequencies and the locked long waves may be ignored for practical purposes. In the higher frequency range both locked and free long waves could be resonated.

All researches cited above considered narrow-banded incident waves. These theories are however inadequate for simulating waves in nature which are random and broad-banded.

1.2.4 Random Waves

Since waves are random in the real sea, a stochastic theory for nonlinear waves is of importance. At the first-order, the linear response spectrum is well known to be of Wiener-Khintchine form. For simple progressive or standing waves in deep water, Sclavounos [34] has advanced a systematic stochastic theory. By assuming the incident waves to be a stationary and Gaussian process, he showed that nonlinear correction to the frequency spectrum starts at the fourth order in wave steepness, and depends on the frequency responses at first, second and third orders. With emphasis on the nonlinear corrections for the entire frequency range, he presented numerical results for a simple nonlinear problem of random wave reflection from a long vertical cliff in a sea of constant depth.

In Part II of this thesis, his stochastic approach will be generalized for the prediction of spectral response in harbors.

Chapter 2

General Problem Formulation

In this chapter, a general boundary value problem for a varying bottom is formulated. Based on the assumption of small amplitude waves, $O(kA \ll 1)$, where kA is the wave slope, perturbation equations governing the potential function for each order are obtained.

2.1 Mathematical Formulation of the Boundary Value Problem

Let us assume that the fluid is incompressible, inviscid and in a conservative force field. The flow is initially irrotational, therefore remains irrotational. The velocity potential is defined as

$$\nabla_3 \Phi = \left(\frac{\partial \Phi}{\partial x}, \frac{\partial \Phi}{\partial y}, \frac{\partial \Phi}{\partial z} \right) = (u, v, w)\,, \tag{2.1.1}$$

where

$$\nabla_3 = \left(\frac{\partial}{\partial x}, \frac{\partial}{\partial y}, \frac{\partial}{\partial z} \right),$$

and u, v, w are the velocity in x, y, z direction, respectively.

For an irrotational flow, the velocity potential is governed by Laplace's equa-

tion

$$\nabla_3\Phi = \nabla^2\Phi + \frac{\partial^2\Phi}{\partial z^2} = 0, \quad -h(x,y) < z < \zeta(x,y,t), \tag{2.1.2}$$

where ∇ denotes the horizontal Laplacian

$$\nabla = \left(\frac{\partial}{\partial x}, \frac{\partial}{\partial y}\right),$$

and $\zeta(x,y,t)$ and $h(x,y)$ are the vertical displacement of the free surface and the water depth, respectively, measured from the still water free surface $z = 0$. On the fixed and impermeable seabed, $z = -h(x,y)$, the normal velocity must be zero

$$\frac{\partial\Phi}{\partial z} = -\nabla\Phi \cdot \nabla h, \quad z = -h(x,y). \tag{2.1.3}$$

All lateral boundaries, ∂B, including the coast are assumed to be vertical, so that

$$\frac{\partial\Phi}{\partial n} = \vec{n} \cdot \nabla_3\Phi = 0, \qquad (x,y) \in \partial B, \tag{2.1.4}$$

where $\vec{n}$ is the normal vector toward the rigid boundaries.

On the free surface, $z = \zeta(x,y,t)$, the kinematic and dynamics boundary conditions are

$$\frac{\partial\zeta}{\partial t} + \frac{\partial\Phi}{\partial x}\frac{\partial\zeta}{\partial x} + \frac{\partial\Phi}{\partial y}\frac{\partial\zeta}{\partial y} = \frac{\partial\Phi}{\partial z}, \quad z = \zeta(x,y,t), \tag{2.1.5}$$

and

$$g\zeta + \frac{\partial\Phi}{\partial t} + \frac{1}{2}\left(\nabla_3\Phi\right)^2 = 0, \quad z = \zeta(x,y,t), \tag{2.1.6}$$

where the zero pressure on the free surface is assumed. Eqns. (2.1.5) and (2.1.6) can be combined to give

$$\frac{\partial^2\Phi}{\partial t^2} + g\frac{\partial\Phi}{\partial z} + \frac{\partial}{\partial t}\left(\nabla_3\Phi\right)^2 + \frac{\nabla_3\Phi}{2} \cdot \nabla_3\left(\nabla_3\Phi\right)^2 = 0, \quad z = \zeta(x,y,t). \tag{2.1.7}$$

For small-amplitude waves, i.e., the wave steepness $\epsilon \equiv kA \ll 1$, where A is the amplitude of the incident waves, we expand Φ and its derivatives up to several

order in powers of ϵ by using the Taylor expansion about $z = 0$

$$f(x, y, \zeta, t) = f(x, y, 0, t) + \zeta \left(\frac{\partial f}{\partial z}\right)_{z=0} + \frac{\zeta^2}{2} \left(\frac{\partial^2 f}{\partial z^2}\right)_{z=0} + O\left(\zeta^3\right). \tag{2.1.8}$$

The free surface boundary conditions become

$$g\zeta + \frac{\partial \Phi}{\partial t} + \zeta \frac{\partial^2 \Phi}{\partial t \partial z} + \frac{\zeta^2}{2} \frac{\partial^3 \Phi}{\partial t \partial z^2} + \frac{1}{2} \left(\nabla_3 \Phi\right)^2 + \zeta \frac{\partial}{\partial z} \left[\frac{1}{2} \left(\nabla_3 \Phi\right)^2\right] = O(\epsilon^4), \quad z = 0, \tag{2.1.9}$$

and

$$\begin{aligned} \frac{\partial \Phi}{\partial z} + \frac{1}{g} \frac{\partial^2 \Phi}{\partial t^2} = & -\frac{\zeta}{g} \frac{\partial}{\partial z} \left(g \frac{\partial \Phi}{\partial z} + \frac{\partial^2 \Phi}{\partial t^2}\right) - \frac{1}{g} \frac{\partial}{\partial t} \left(\nabla_3 \Phi\right)^2 - \frac{\zeta^2}{2g} \frac{\partial^2}{\partial z^2} \left(g \frac{\partial \Phi}{\partial z} + \frac{\partial^2 \Phi}{\partial t^2}\right) \\ & - \zeta \frac{\partial}{\partial z} \left[\frac{1}{g} \frac{\partial}{\partial t} \left(\nabla_3 \Phi\right)^2\right] - \frac{\nabla_3 \Phi}{2g} \cdot \nabla_3 \left(\nabla_3 \Phi\right)^2 + O(\epsilon^4), \quad z = 0. \end{aligned} \tag{2.1.10}$$

In summary, Eqns. (2.1.2), (2.1.3), (2.1.4), (2.1.9) and (2.1.10) represent the generalized boundary value problem up to $O(\epsilon^3)$.

2.2 Perturbation equations

Because of the assumption of small wave steepness, $\epsilon \equiv kA \ll 1$, we introduce the perturbation expansions

$$\Phi = \epsilon \Phi_1 + \epsilon^2 \Phi_2 + \epsilon^3 \Phi_3 + \cdots = \sum_{n=1}^{\infty} \epsilon^n \Phi_n, \tag{2.2.1}$$

$$\zeta = \epsilon \zeta_1 + \epsilon^2 \zeta_2 + \epsilon^3 \zeta_3 + \cdots = \sum_{n=1}^{\infty} \epsilon^n \zeta_n, \tag{2.2.2}$$

into Eqns. (2.1.2), (2.1.3), (2.1.4), (2.1.9) and (2.1.10). By separating the orders, the first-order, second-order and third-order perturbation equations are presented below.

2.2.1 First-order

At the first order, $O(\epsilon)$, the velocity potential Φ_1 satisfies the governing equation

$$\frac{\partial^2 \Phi_1}{\partial x^2} + \frac{\partial^2 \Phi_1}{\partial y^2} + \frac{\partial^2 \Phi_1}{\partial z^2} = 0, \quad -h(x,y) < z < 0 \tag{2.2.3}$$

in water, the no-flux conditions

$$\frac{\partial \Phi_1}{\partial z} = -\nabla \Phi_1 \cdot \nabla h, \quad z = -h(x,y) \tag{2.2.4}$$

on the bottom and

$$\frac{\partial \Phi_1}{\partial n} = 0, \qquad (x,y) \in \partial B, \tag{2.2.5}$$

on all lateral boundaries, and the homogeneous free surface boundary condition

$$g\frac{\partial \Phi_1}{\partial z} + \frac{\partial^2 \Phi_1}{\partial t^2} = 0, \quad z = 0 \tag{2.2.6}$$

on the still water free surface.

The first-order free surface displacement, ζ_1, is related to Φ_1 by

$$\zeta_1 = -\frac{1}{g}\left[\frac{\partial \Phi_1}{\partial t}\right]_{z=0}. \tag{2.2.7}$$

2.2.2 Second-order

At the second order, $O(\epsilon^2)$, the velocity potential Φ_2 also satisfies Laplace's equation

$$\frac{\partial^2 \Phi_2}{\partial x^2} + \frac{\partial^2 \Phi_2}{\partial y^2} + \frac{\partial^2 \Phi_2}{\partial z^2} = 0 \quad -h(x,y) < z < 0, \tag{2.2.8}$$

in water, the no-flux conditions

$$\frac{\partial \Phi_2}{\partial z} = -\nabla \Phi_2 \cdot \nabla h, \quad z = -h(x,y) \tag{2.2.9}$$

on the bottom and

$$\frac{\partial \Phi_2}{\partial n} = 0, \qquad (x,y) \in \partial B, \tag{2.2.10}$$

on all lateral boundaries. On the still water free surface, $z = 0$, the boundary condition is now inhomogeneous

$$\frac{\partial \Phi_2}{\partial z} + \frac{1}{g}\frac{\partial^2 \Phi_2}{\partial t^2} = \frac{1}{g^2}\frac{\partial \Phi_1}{\partial t}\frac{\partial}{\partial z}\left[g\left(\frac{\partial \Phi_1}{\partial z}\right) + \frac{\partial^2 \Phi_1}{\partial t^2}\right] - \frac{1}{g}\frac{\partial}{\partial t}\left(\nabla_3 \Phi_1\right)^2, \quad z = 0. \tag{2.2.11}$$

The second-order free surface displacement, ζ_2, is given by

$$\zeta_2 = \left[-\frac{1}{g}\frac{\partial \Phi_2}{\partial t} + \frac{1}{g^2}\frac{\partial \Phi_1}{\partial t}\frac{\partial^2 \Phi_1}{\partial t \partial z} - \frac{1}{2g}\left(\nabla_3 \Phi_1\right)^2\right]_{z=0}. \tag{2.2.12}$$

It is convenient to decompose ζ_2 as follows,

$$\zeta_2 = \zeta_2^{(1)} + \zeta_2^{(2)} \tag{2.2.13}$$

where

$$\zeta_2^{(1)} = \left[\frac{1}{g^2}\frac{\partial \Phi_1}{\partial t}\frac{\partial^2 \Phi_1}{\partial t \partial z} - \frac{1}{2g}\left(\nabla_3 \Phi_1\right)^2\right]_{z=0}, \tag{2.2.14}$$

$$\zeta_2^{(2)} = \left[-\frac{1}{g}\frac{\partial \Phi_2}{\partial t}\right]_{z=0}. \tag{2.2.15}$$

The first part $\zeta_2^{(1)}$ can be calculated from the first-order potential Φ_1. The second part $\zeta_2^{(2)}$ is associated with the second-order potential Φ_2, which is the main objective of the mathematical task.

2.2.3 Third-order

At the third order, $O(\epsilon^3)$, the velocity potential Φ_3 satisfies the Laplace equation

$$\frac{\partial^2 \Phi_3}{\partial x^2} + \frac{\partial^2 \Phi_3}{\partial y^2} + \frac{\partial^2 \Phi_3}{\partial z^2} = 0, \quad -h(x,y) < z < 0 \tag{2.2.16}$$

in water, the no-flux conditions

$$\frac{\partial \Phi_3}{\partial z} = -\nabla \Phi_3 \cdot \nabla h, \quad z = -h(x,y) \tag{2.2.17}$$

on the bottom and

$$\frac{\partial \Phi_3}{\partial n} = 0, \qquad (x, y) \in \partial B \tag{2.2.18}$$

on all lateral boundaries, and the inhomogeneous boundary condition

$$\begin{aligned} \frac{\partial \Phi_3}{\partial z} + \frac{1}{g}\frac{\partial^2 \Phi_3}{\partial t^2} = & -\frac{\zeta_1}{g}\frac{\partial}{\partial z}\left(g\frac{\partial \Phi_2}{\partial z} + \frac{\partial^2 \Phi_2}{\partial t^2}\right) - \frac{\zeta_2}{g}\frac{\partial}{\partial z}\left(g\frac{\partial \Phi_1}{\partial z} + \frac{\partial^2 \Phi_1}{\partial t^2}\right) \\ & - \frac{2}{g}\frac{\partial}{\partial t}\left(\nabla_3 \Phi_1 \cdot \nabla_3 \Phi_2\right) - \frac{\zeta_1^2}{2g}\frac{\partial^2}{\partial z^2}\left(g\frac{\partial \Phi_1}{\partial z} + \frac{\partial^2 \Phi_1}{\partial t^2}\right) \\ & - \zeta_1 \frac{\partial}{\partial z}\left[\frac{1}{g}\frac{\partial}{\partial t}\left(\nabla_3 \Phi_1\right)^2\right] - \frac{\nabla_3 \Phi_1}{2g} \cdot \nabla_3 \left(\nabla_3 \Phi_1\right)^2, \quad z = 0 \end{aligned} \tag{2.2.19}$$

on the still water free surface.

The third-order free surface displacement, ζ_3, is related to the first-order, the second-order and the third-order potentials by

$$\zeta_3 = -\frac{1}{g}\frac{\partial \Phi_3}{\partial t} - \frac{\zeta_1}{g}\frac{\partial^2 \Phi_2}{\partial t \partial z} - \frac{\zeta_2}{g}\frac{\partial^2 \Phi_1}{\partial t \partial z} - \frac{\zeta_1^2}{2g}\frac{\partial^3 \Phi_1}{\partial t \partial z^2} - \frac{1}{g}\nabla_3 \Phi_1 \cdot \nabla_3 \Phi_2 - \frac{\zeta_1}{2g}\frac{\partial}{\partial z}\left(\nabla_3 \Phi_1\right)^2, \quad z = 0 \tag{2.2.20}$$

with ζ_1 given by Eq. (2.2.7) and ζ_2 given by Eq. (2.2.12).

In addition, radiation conditions at infinity for each order will be specified later. The study of combined nonlinear diffraction and refraction will be focussed on two types of incident waves, monochromatic and random. In Part I we consider monochromatic incident waves. After extending the mild-slope approximation. Applications are made to the geometries involving a mildly sloping seabed and a special case of a semi-circular cylinder on a cliff or an idealized peninsula, in a sea of constant depth. In Part II the second-order mild-slope approximation will be further extended for random waves with a broad frequency spectrum with applications to harbor oscillations due to short incident waves.

Part I

Monochromatic Incident Waves

Chapter 3

Mild-Slope Approximation

The mild-slope equation(MSE) is an effective approximation to combine refraction and diffraction and reduce the spatial dimension of the boundary value problem from three to two. In this chapter, we extend the mild-slope approximation to second-order in wave steepness. Attentions is limited to monochromatic incident waves through out Chapter 3 to 7.

3.1 First-order MSE

We assume the waves to be simple-harmonic in time at the first order with the velocity potential

$$\Phi_1 = \phi e^{-i\omega t} + *, \tag{3.1.1}$$

where $*$ denotes the complex conjugate of the preceding term, and ω the wave frequency.

Let all coastal boundaries be vertical. We take the first-order ϕ take to be

$$\phi = -\frac{ig\eta(x,y)}{\omega}\frac{\cosh k(z+h)}{\cosh kh}, \tag{3.1.2}$$

where $\eta(x,y)$ is the surface elevation for ω, and k is the wave number satisfying the dispersion relation

$$\omega^2 = gk\tanh kh. \tag{3.1.3}$$

By treating Laplace's equation as an ordinary differential equation in z and applying Green's formula (as in Sprinks and Smith [35]), we get the modified mild-slope equation for the first-order problem. The result by keeping all terms proportional to $\nabla h, \nabla^2 h$ and $(\nabla h)^2$ is the modified mild-slope equation by Chamberlain and Porter [9], (see Appendix A for details)

$$\nabla \cdot (CC_g \nabla \eta) + \left[k^2 CC_g + gU\nabla^2 h + gV\left(\nabla h\right)^2\right]\eta = 0, \tag{3.1.4}$$

where

$$U = \frac{\left(\sinh 2kh - 2kh\cosh 2kh\right)}{4\cosh^2\left(kh\right)\left(2kh + \sinh 2kh\right)}, \tag{3.1.5}$$

$$\begin{aligned} V = & \frac{k\left[\left(2kh\right)^4 + 4\left(2kh\right)^3 \sinh 2kh - 9\sinh 2kh \sinh 4kh\right]}{12\cosh^2\left(kh\right)\left(2kh + \sinh 2kh\right)^3} \\ & + \frac{k\left[kh\left(kh + \sinh 2kh\right)\left(\cosh^2 2kh - 2\cosh 2kh + 3\right)\right]}{\cosh^2\left(kh\right)\left(2kh + \sinh 2kh\right)^3}, \end{aligned} \tag{3.1.6}$$

C is the phase velocity,

$$C = \frac{\omega}{k}, \tag{3.1.7}$$

and C_g is the group velocity

$$C_g = \frac{C}{2}\left(1 + \frac{2kh}{\sinh 2kh}\right). \tag{3.1.8}$$

Note that while no terms related to the gradients of depth are omitted, the assumed potential Eq. (3.1.2) is not exact and does not satisfy the bottom condition strictly. The above approximation is therefore still restricted to mild slope. Over a constant depth, Eqn. (3.1.4) reduces to Helmholtz equation

$$\nabla^2 \eta + k^2 \eta = 0. \tag{3.1.9}$$

Eq. (3.1.4) with appropriate radiation condition can be solved numerically by hybrid element method of Chen & Mei [11] if the complex geometry is limited to a

finite near field. Afterwards by putting Eqs. (3.1.1) and (3.1.2) into Eqs. (2.2.7) and (2.2.12) , we obtain the first-order free surface displacement

$$\zeta_1 = \eta e^{-i\omega t} + *. \tag{3.1.10}$$

With these results the following part of the second-order free surface displacement can be computed immediately,

$$\zeta_2^{(1)} = \eta_{2,0}^{(1)} + \eta_{2,2}^{(1)} e^{-2i\omega t} + *. \tag{3.1.11}$$

In particular, the zeroth harmonic $\eta_{2,0}^{(1)}$ represents the mean-sea-level setup/setdown

$$\eta_{2,0}^{(1)} = \frac{\omega^2}{g}|\eta|^2 - \frac{g}{\omega^2}|\nabla\eta|^2, \tag{3.1.12}$$

and $\eta_{2,2}^{(1)}$ represents the second-harmonic amplitude due directly to quadratic interactions of the first-order motion

$$\eta_{2,2}^{(1)} = \frac{3\omega^2}{2g}\eta^2 + \frac{g}{2\omega^2}\left(\nabla\eta\right)^2. \tag{3.1.13}$$

Solution of the remaining second harmonic

$$\zeta_2^{(2)} = \eta_{2,2}^{(2)} e^{-2i\omega t} + * \tag{3.1.14}$$

must await the solution of Φ_2.

3.2 Second-order MSE

At the second order, the inhomogeneous free surface boundary condition, Eqn. (2.2.11), can be rewritten as follows

$$\frac{\partial\Phi_2}{\partial z} + \frac{1}{g}\frac{\partial^2\Phi_2}{\partial t^2} = Fe^{-2i\omega t} + *, \tag{3.2.1}$$

where the forcing function F is found to be

$$F = \widehat{\beta}\eta\eta + \bar{\beta}\nabla\eta \cdot \nabla\eta, \tag{3.2.2}$$

with

$$\widehat{\beta} = \frac{igk^2}{\omega} - \frac{3i\omega^3}{g}, \quad \bar{\beta} = -\frac{2ig}{\omega}. \tag{3.2.3}$$

Details are given in Appendix B. Note that the forcing term does not contain any zeroth harmonic in time.

Since the forcing term on the free surface contains the second time-harmonic, the second-order potential must be of the form

$$\Phi_2 = \psi e^{-2i\omega t} + *. \tag{3.2.4}$$

Putting Eqn. (3.2.4) into Eqns. (2.2.8), (2.2.9) and (3.2.1), we find that ψ satisfies the Laplace equation

$$\nabla^2\psi + \frac{\partial^2\psi}{\partial z^2} = 0, \quad -h(x,y) < z < 0, \tag{3.2.5}$$

in water,

$$\frac{\partial\psi}{\partial z} = -\nabla\psi \cdot \nabla h, \quad z = -h(x,y), \tag{3.2.6}$$

on the seabed,

$$\frac{\partial\psi}{\partial n} = 0, \qquad (x,y) \in \partial B \tag{3.2.7}$$

on the lateral boundaries,

$$\frac{\partial\psi}{\partial z} - \frac{4\omega^2}{g}\psi = F, \ z = 0 \tag{3.2.8}$$

on the still water free surface. Because the forcing term F involves quadratic interactions of first-order incident and scattered waves, the second-order problem is more complex vertically than the first order. Similar to the first-order mild-slope approximation of Porter and Staziker [31], we express the solution for ψ as the sum

of all vertical eigenmodes

$$\psi = -\frac{ig}{2\omega}\sum_{m=0}^{\infty}\xi_m\frac{\cos\kappa_m(z+h)}{\cos\kappa_m h}, \tag{3.2.9}$$

where κ_m, $m = 1, 2, \ldots$ are the real roots of the transcendental equation

$$-4\omega^2 = g\kappa_m \tan\kappa_m h, \quad (m-1/2)\,\pi \le \kappa_m h \le m\pi, \tag{3.2.10}$$

and κ_0 is pure imaginary $\kappa_0 = -i\widehat{\kappa}_0$, with $\widehat{\kappa}_0$ being the real root of the dispersion equation

$$4\omega^2 = g\widehat{\kappa}_0 \tanh\widehat{\kappa}_0 h. \tag{3.2.11}$$

Physically the subscript $m = 0$ corresponds to the propagating mode which propagates to infinity, while those with $m \ge 1$ to evanescent modes which represent local effects. Repeating the procedure of weighted vertical averaging via Green's formula, as in Appendix C, we obtain a matrix equation coupling all second-order modal amplitudes ξ_ℓ:

$$\sum_{\ell=0}^{\infty}\{\nabla\cdot(A_{m,\ell}\nabla\xi_\ell) + B_{m,\ell}\nabla h\cdot\nabla\xi_\ell + C_{m,\ell}\xi_\ell\} = -i2\omega F, \quad m = 0, 1, 2, 3, \cdots. \tag{3.2.12}$$

where

$$A_{m,\ell} = \begin{cases} \frac{gh}{2\cos^2\kappa_\ell h}\left(1 + \frac{\sin 2\kappa_\ell h}{2\kappa_\ell h}\right) & \text{for } m = \ell \\ 0 & \text{for } m \ne \ell \end{cases} \tag{3.2.13}$$

$$B_{m,\ell} = \begin{cases} 0 & \text{for } m = \ell \\ g\left(U_{m,\ell} - U_{\ell,m}\right), & \text{for } m \ne \ell \end{cases} \tag{3.2.14}$$

with

$$U_{m,\ell} = \begin{cases} \frac{\sin 2\kappa_m h - 2\kappa_m h\cos 2\kappa_m h}{4\cos^2(\kappa_m h)(2\kappa_m h + \sin 2\kappa_m h)} & \text{for, } m = \ell, \\ -\frac{\kappa_\ell^2}{\cos\kappa_m h\cos\kappa_\ell h\left(\kappa_\ell^2 - \kappa_m^2\right)}, & \text{for, } m \ne \ell, \end{cases} \tag{3.2.15}$$

and

$$C_{m,\ell} = -\kappa_m^2 A_{m,\ell} + gU_{m,\ell}\nabla^2 h + gV_{m,\ell}\left(\nabla h\right)^2 . \tag{3.2.16}$$

with $V_{m,\ell}$ being

$$\begin{aligned} V_{m,m} = & \frac{\kappa_m\left[-\left(2\kappa_m h\right)^4 - 4\left(2\kappa_m h\right)^3 \sin 2\kappa_m h - 9\sin\left(2\kappa_m h\right)\sin 4\kappa_m h\right]}{12\cos^2\left(\kappa_m h\right)\left(2\kappa_m h + \sin 2\kappa_m h\right)^3} \\ & + \frac{\kappa_m\left[\kappa_m h\left(\kappa_m h + \sin 2\kappa_m h\right)\left(\cos^2 2\kappa_m h - 2\cos 2\kappa_m h + 3\right)\right]}{\cos^2\left(\kappa_m h\right)\left(2\kappa_m h + \sin 2\kappa_m h\right)^3} \end{aligned} \tag{3.2.17}$$

for $m = \ell$, and

$$V_{m,\ell} = \frac{-2\kappa_\ell \sec\kappa_m h \sec\kappa_\ell h}{\left(2\kappa_\ell h + \sin 2\kappa_\ell h\right)} \frac{\left[4\kappa_\ell^2\kappa_m^2 + \left(\kappa_\ell^4 - \kappa_m^4\right)\sin^2\kappa_\ell h\right]}{\left(\kappa_\ell^2 - \kappa_m^2\right)^2} \tag{3.2.18}$$

for $m \neq \ell$. These Coefficients $A_{m,\ell}$, $B_{m,\ell}$,and $C_{m,\ell}$ are equivalent to those in the modified system of mild-slope equations of Porter and Staziker [31] for linearized waves and $F = 0$, after changing 2ω to ω. We have now reduced the second-order task to the solution of coupled two-dimensional elliptic problems, subject to certain boundary conditions.

In the region of constant depth, terms multiplied by $B_{m,\ell}$ vanish, while $A_{m,\ell}$ and $C_{m,l}$ are diagonal matrices. Eqns. (3.2.12) are no longer coupled and reduced to

$$\nabla^2\xi_\ell - \kappa_\ell^2\xi_\ell = -i\frac{2\omega}{A_{\ell,\ell}}F, \quad \ell = 0, 1, 2, 3, \cdots . \tag{3.2.19}$$

In the simple case where h is constant everywhere and the coastline is simple, Eqn. (3.2.19) can be solved analytically as will be described in Chapter 6.

Chapter 4

Solution Strategy: Hybrid-element Method

For coastal waters where only the complexities of local topography and coastline is of major concern, we can simplify the geometry in areas far from the local region. With reference to Figure 4-1, let us divide the horizontal fluid domain into two regions : the near field Ω_A in which the bathymetry and coastal boundary are complex, and the far field Ω_F where the depth is constant and the coastline straight. The two fields are separated by a semi-circular cylindrical surface ∂A of radius $r = a$.

For the first-order problem, the far-field solution in Ω_F can be represented analytically as an eigenfunction expansion. In the near field Ω_A, discrete solutions will be sought via finite elements. The unknown nodal coefficients in Ω_A and the expansion coefficients in Ω_F will be found together by Galerkin's method, subject to the continuity of η and $\partial\eta/\partial r$ at $r = a$

$$(\eta)_{\Omega_A} = (\eta)_{\Omega_F}, \qquad r = a, \tag{4.0.1}$$

$$\left(\frac{\partial \eta}{\partial r}\right)_{\Omega_A} = \left(\frac{\partial \eta}{\partial r}\right)_{\Omega_F}, \qquad r = a. \tag{4.0.2}$$

where $()_{\Omega_A}$ denotes the solution in Ω_A, $()_{\Omega_F}$ denotes the solution in Ω_F. This is the hybrid-element method developed for linearized wave problems by Chen & Mei

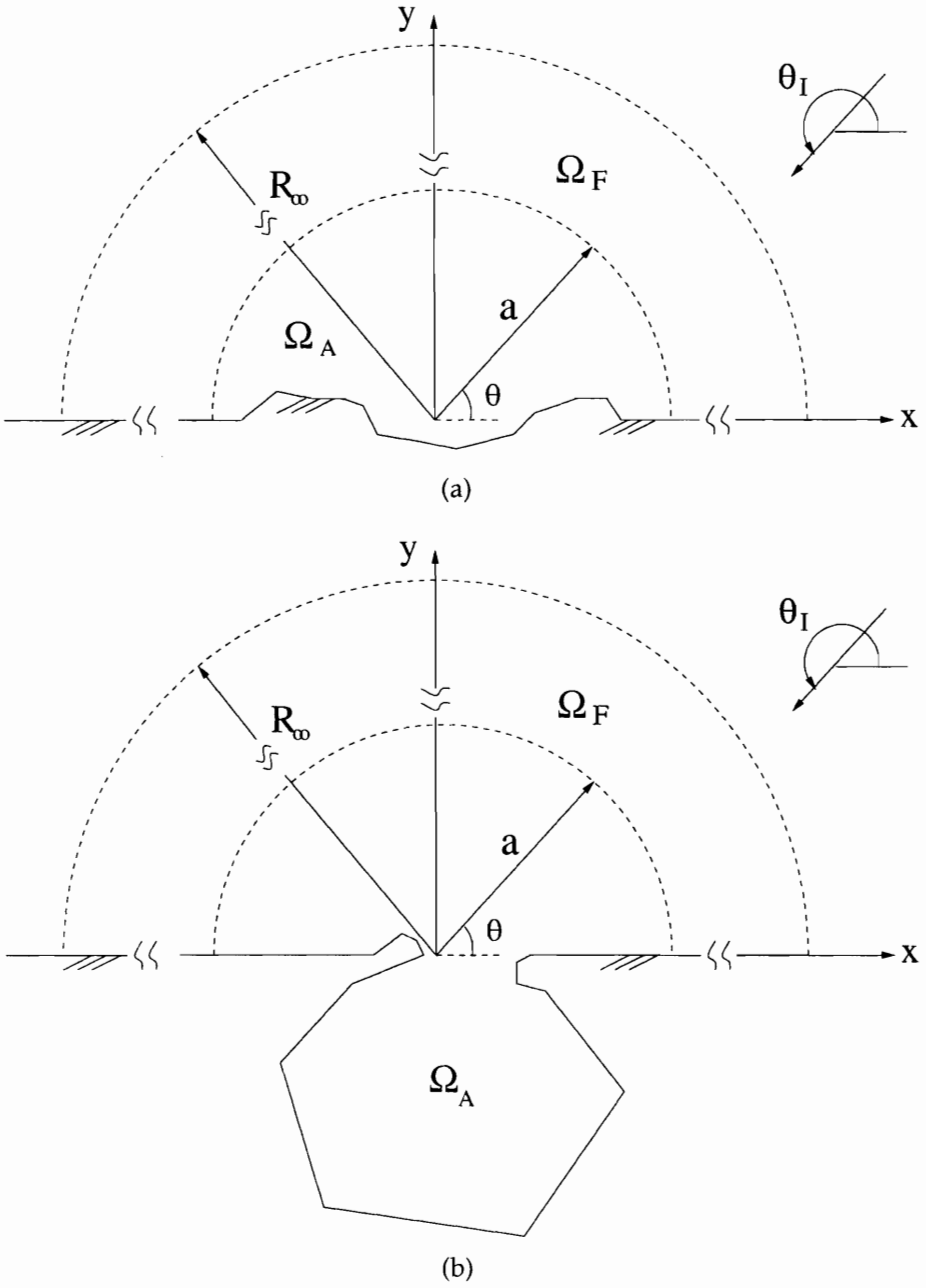

Figure 4-1: Near (Ω_A) and far (Ω_F) fields. Variable bathymetry and non-straight coastal boundaries in (Ω_A) behine the semi-circle $r = a$. (a): without a harbor (top) (b): with a harbor (bottom).

(1974) and Bai & Yeung (1974) [4] for two dimensions and Yue, Chen & Mei (1976, 1978) [42] [43] for three dimensions. The method is extended to the second-order problem here with the requirement of continuity of ξ_ℓ and $\partial\xi_\ell/\partial r$ at $r = a$

$$(\xi_\ell)_{\Omega_A} = (\xi_\ell)_{\Omega_F}, \qquad r = a, \quad \ell = 0, 1, 2, 3, \cdots, \tag{4.0.3}$$

$$\left(\frac{\partial \xi_\ell}{\partial r}\right)_{\Omega_A} = \left(\frac{\partial \xi_\ell}{\partial r}\right)_{\Omega_F}, \qquad r = a, \quad \ell = 0, 1, 2, 3, \cdots. \tag{4.0.4}$$

As a part of the hybrid-element analysis, let us first present the analytical solutions in the far field Ω_F where the depth is constant and the coastline is along the x axis.

4.1 First-order Far Field

In the far field, the first-order waves consists of the incident, reflected and scattered (diffracted) waves given together by

$$(\eta)_{\Omega_F} = \eta^{(T)} + \eta^{(S)}, \tag{4.1.1}$$

where

$$\eta^{(T)} = \eta^{(I)} + \eta^{(R)}, \tag{4.1.2}$$

The part $\eta^{(I)}$is the first-order incident wave

$$\eta^{(I)} = \frac{A}{2} e^{ikr\cos(\theta-\theta_I)}, \tag{4.1.3}$$

with θ_I being the incident angle and A the amplitude. The part $\eta^{(R)}$ is the first-order reflected wave

$$\eta^{(R)} = \frac{A}{2} e^{ikr\cos(\theta+\theta_I)}, \tag{4.1.4}$$

while $\eta^{(S)}$ is the first-order scattered wave which can be represented by

$$\eta^{(S)} = \sum_{m=0}^{\infty} \epsilon_m i^m \alpha_m H_m(kr) \cos m\theta, \tag{4.1.5}$$

where ϵ_m is the Jacobi symbol, being 1 for $m = 0$ and 2 for $m \leq 1$, $H_m(kr) \equiv H_m^{(1)}(kr)$ is the Hankel function of the first kind, and the coefficients α_m, $m = 0, 1, 2, \cdots$ are yet unknown.

In the near field of complex bathymetry and coastline, discrete finite elements are used. The first-order two-dimensional finite element analysis is shown in section 5.1, and the coupled problem of near and far fields are then solved numerically as in Chen & Mei [11]. After which the nodal values of η in the near field and the coefficients α_m of the far field are found.

4.2 Second-order Far Field

The analytic solutions in Ω_F are sought as follows. As will be shown in the next-section, F can be split into two parts

$$F = \mathcal{P} + \mathcal{Q}, \tag{4.2.6}$$

representing respectively self interaction of progressive waves, and quadratic interactions involving scattered waves (progressive-scattered and scattered-scattered). In accordance with the form of the forcing term, the second-order response $(\xi_\ell)_{\Omega_F}$ defined by Eqn. (3.2.9) can be separated into three parts

$$(\xi_\ell)_{\Omega_F} = \xi_\ell^P + \xi_\ell^Q + \xi_\ell^H, \qquad \ell = 0, 1, 2, 3, \cdots. \tag{4.2.7}$$

The first part ξ_ℓ^P is the response to forcing $\mathcal{P}$ as if the complex geometry in the near field does not exist. Thus it satisfies the following inhomogeneous equation

$$\left(\nabla^2 - \kappa_\ell^2\right) \xi_\ell^P = -i\frac{2\omega\mathcal{P}}{A_{\ell,\ell}}, \qquad \ell = 0, 1, 2, 3, \cdots, \tag{4.2.8}$$

and

$$\frac{\partial \xi_\ell^P}{\partial \theta} = 0, \quad r > a; \quad \theta = 0 \text{ and } \theta = \pi, \qquad \ell = 0, 1, 2, 3, \cdots \tag{4.2.9}$$

along the coast. No conditions are imposed elsewhere. It will be solved in section 4.4.1.

The second part ξ_ℓ^Q is the response to forcing $\mathcal{Q}$ and is required to satisfy the inhomogeneous equation

$$\left(\nabla^2 - \kappa_\ell^2\right) \xi_\ell^Q = -i\frac{2\omega \mathcal{Q}}{A_{\ell,\ell}}, \qquad \ell = 0, 1, 2, 3, \cdots, \tag{4.2.10}$$

the no-flux condition along the straight coast

$$\frac{\partial \xi_\ell^Q}{\partial \theta} = 0, \quad r > a; \quad \theta = 0, \ \theta = \pi, \qquad \ell = 0, 1, 2, 3, \cdots. \tag{4.2.11}$$

and along the semi-circle $r = a$

$$\frac{\partial \xi_\ell^Q}{\partial r} = 0, \quad r = a, \ 0 \le \theta \le \pi, \qquad \ell = 0, 1, 2, 3, \cdots. \tag{4.2.12}$$

For the evanescent modes, $\ell = 1, 2, 3, \cdots$, ξ_ℓ^Q diminishes to zero at large enough r. For the propagating mode, $\ell = 0$, ξ_ℓ^Q must satisfy the weak (integral) radiation condition at infinity due to the slow attenuation of $\mathcal{Q}$. We shall call both ξ_ℓ^P and ξ_ℓ^Q the *forced waves*.

Finally, the *free wave* ξ_ℓ^H is defined to satisfy the homogeneous Helmholtz equation

$$\left(\nabla^2 - \kappa_\ell^2\right) \xi_\ell^H = 0, \qquad \ell = 0, 1, 2, 3, \cdots, \tag{4.2.13}$$

and the no-flux condition along the straight coast,

$$\frac{\partial \xi_\ell^H}{\partial \theta} = 0, \ r = a; \ \theta = 0, \ \pi, \qquad \ell = 0, 1, 2, 3, \cdots \tag{4.2.14}$$

In addition, ξ_ℓ^H must satisfy the usual (strong) radiation condition at infinity. The

formal solution to the free wave ξ_ℓ^H is immediate

$$\xi_\ell^H = \sum_{m=0}^{\infty} \epsilon_m \widehat{\alpha}_{\ell,m} K_m(\kappa_\ell r) \cos m\theta, \qquad \ell = 0, 1, 2, 3, \cdots \tag{4.2.15}$$

where K_m is the modified Bessel function of the second kind of order m. For $\ell = 0$, $\kappa_0 = -i\widehat{\kappa}_0$ is pure imaginary and $K_m(\kappa_0 r)$ is proportional to $H_m^{(1)}(\widehat{\kappa}_0 r)$. The unknown coefficients $\widehat{\alpha}_{\ell,m}$ will be found jointly with the discrete solution in the near field by the hybrid-element analysis(in section 5.2), which requires the continuity of the near and far fields and their radial derivatives along $r = a$

$$\xi_\ell^H = (\xi_\ell)_{\Omega_A} - \xi_\ell^Q - \xi_\ell^P, \quad r = a, \quad 0 \le \theta \le \pi, \qquad \ell = 0, 1, 2, 3, \cdots, \tag{4.2.16}$$

$$\frac{\partial \xi_\ell{}^H}{\partial r} = \left(\frac{\partial \xi_\ell}{\partial r}\right)_{\Omega_A} - \frac{\partial \xi_\ell{}^P}{\partial r}, \quad r = a, \quad 0 \le \theta \le \pi \qquad \ell = 0, 1, 2, 3, \cdots. \tag{4.2.17}$$

The solutions for ξ_ℓ^P and ξ_ℓ^Q can be obtained explicitly, as shown in section 4.4.

4.3 Forcing function F in the far-field Ω_F

Referring to Eqn. (3.2.2), F contains quadratic products of the first-order waves and can be decomposed as

$$F = \mathcal{P} + \mathcal{Q} \tag{4.3.1}$$

where $\mathcal{P}$ denotes the part associated with the self- and cross-interactions of progressive waves(incident and reflected waves),

$$\mathcal{P}(r, \theta) = \widehat{\beta} \eta^{(T)} \eta^{(T)} + \bar{\beta} \nabla \eta^{(T)} \cdot \nabla \eta^{(T)}, \tag{4.3.2}$$

with $\widehat{\beta}$ and $\bar{\beta}$ are given by Eq. (3.2.3), and

$$\mathcal{Q}(r, \theta) = \widehat{\beta} \left[2\eta^{(T)} + \eta^{(S)}\right] \eta^{(S)} + \bar{\beta} \left[2\nabla \eta^{(T)} + \nabla \eta^{(S)}\right] \cdot \nabla \eta^{(S)}, \tag{4.3.3}$$

is the part due to mutual interactions between the plane progressive waves and the scattered waves, and the self-interaction of the scattered waves.

4.3.1 Explicit expression for $\mathcal{P}$ in Ω_F

By definition, $\mathcal{P}$ is

$$\mathcal{P}(r,\theta) = \widehat{\beta}\eta^{(T)}\eta^{(T)} + \bar{\beta}\nabla\eta^{(T)} \cdot \nabla\eta^{(T)} \tag{4.3.4}$$

with

$$\eta^{(T)} = \frac{A}{2}e^{ikr\cos(\theta-\theta_I)} + \frac{A}{2}e^{ikr\cos(\theta+\theta_I)}. \tag{4.3.5}$$

To get $\mathcal{P}$, we must obtain $\eta^{(T)}\eta^{(T)}$ and $\nabla\eta^{(T)} \cdot \nabla\eta^{(T)}$

$$\eta^{(T)}\eta^{(T)} = \frac{A}{4}e^{i2kr\cos(\theta-\theta_I)} + \frac{A}{4}e^{i2kr\cos(\theta+\theta_I)} + \frac{A}{2}e^{i2kr\cos\theta_I\cos\theta}, \tag{4.3.6}$$

and

$$\nabla\eta^{(T)} \cdot \nabla\eta^{(T)} = -\frac{A^2}{4}k^2\left[e^{i2kr\cos(\theta-\theta_I)} + e^{i2kr\cos(\theta+\theta_I)} + 2\cos(2\theta_I)\,e^{i2kr\cos\theta_I\cos\theta}\right] \tag{4.3.7}$$

Therefore, putting Eqns. (4.3.6) and (4.3.7) into Eqn. (4.3.4), we obtain

$$\begin{aligned}\mathcal{P}(r,\theta) = \mathcal{M}(r,\theta) + \mathcal{N}(r,\theta) =& \frac{A^2}{4}\left(\widehat{\beta} - \bar{\beta}k^2\right)\left[e^{i2kr\cos(\theta-\theta_I)} + e^{i2kr\cos(\theta+\theta_I)}\right] \\ &+ \frac{A^2}{2}\left[\widehat{\beta} - \bar{\beta}k^2\cos(2\theta_I)\right]e^{i2kr\cos\theta_I\cos\theta}.\end{aligned} \tag{4.3.8}$$

Clearly the first line

$$\mathcal{M}(r,\theta) = \frac{A^2}{4}\left(\widehat{\beta} - \bar{\beta}k^2\right)\left[e^{i2kr\cos(\theta-\theta_I)} + e^{i2kr\cos(\theta+\theta_I)}\right] \tag{4.3.9}$$

represents a pair of obliquely incident and reflected plane waves of wavenumber $2k$, and the second line

$$\mathcal{N}(r,\theta) = \frac{A^2}{2}\left[\widehat{\beta} - \bar{\beta}k^2\cos(2\theta_I)\right]e^{i2kr\cos\theta_I\cos\theta} \tag{4.3.10}$$

is a plane incident waves of wavenumber $2k\cos\theta_I$ propagating along the coastline.

4.3.2 Fourier expansion for $\mathcal{Q}$ in Ω_F

To calculate the forcing function $\mathcal{Q}$, we shall first abbreviate the first-order progressive waves as

$$\eta^{(T)} = \sum_{m=-\infty}^{\infty} T_m(r)e^{im\theta} \tag{4.3.11}$$

with

$$T_m(r) = Ai^m J_m(kr)\cos m\theta_I, \tag{4.3.12}$$

and the first-order scattered waves as

$$\eta^{(S)} = \sum_{m=-\infty}^{\infty} S_m(r)e^{im\theta} \tag{4.3.13}$$

where

$$S_m(r) = i^m \alpha_m H_m(kr) \tag{4.3.14}$$

with the coefficients α_m are solved by the hybrid-element method. Because of the no flux condition on the straight coast,

$$\frac{\left(\partial\eta^{(T)}, \eta^{(S)}\right)}{\partial\theta} = 0, \quad r > a; \quad \theta = 0, \text{ and } \pi, \tag{4.3.15}$$

and the properties of Bessel functions

$$J_{-m}(x) = (-1)^m J_m(x), \quad H_{-m}(x) = (-1)^m H_m(x), \tag{4.3.16}$$

it is evident that

$$T_{-m}(r) = Ai^{-m}J_{-m}(kr)\cos(-m\theta_I) = Ai^m J_m(kr)\cos m\theta_I = T_m(r),$$

$$S_{-m}(r) = \frac{A}{2}i^{-m}\alpha_{-m}H_{-m}(kr) = \frac{A}{2}i^m\alpha_m H_m(kr) = S_m(r)$$

$$\alpha_m = \alpha_{-m}.$$

i.e., T_m, S_m, α_m are even in m.

We now calculate $\mathcal{Q}$ according to Eq. (4.3.3). A typical quadratic product in Eq. (4.3.3) is of the form

$$\begin{aligned}\eta^{(T)}\eta^{(S)} &= \sum_{m=-\infty}^{\infty} T_m e^{im\theta} \sum_{n=-\infty}^{\infty} S_n e^{in\theta} \\ &= \sum_{m=-\infty}^{\infty} \left[\sum_{n=-\infty}^{\infty} T_{m-n} S_n\right] e^{im\theta}\end{aligned} \tag{4.3.17}$$

It follows that $\mathcal{Q}$ can be expressed as a Fourier series shown in Appendix D

$$\mathcal{Q}(r,\theta) = \sum_{m=-\infty}^{\infty} \mathcal{Q}_m(r) e^{im\theta}, \tag{4.3.18}$$

or equivalently

$$\mathcal{Q}(r,\theta) = \sum_{m=0}^{\infty} \epsilon_m \mathcal{Q}_m(r) \cos m\theta, \tag{4.3.19}$$

with

$$\begin{aligned}\mathcal{Q}_m(r) = \sum_{n=-\infty}^{\infty} \Bigg\{ &\left[\widehat{\beta} - \frac{n(m-n)}{r^2}\bar{\beta}\right] S_n \left(2T_{m-n} + S_{m-n}\right) \\ &+ \bar{\beta}\frac{\partial S_n}{\partial r}\left(2\frac{\partial T_{m-n}}{\partial r} + \frac{\partial S_{m-n}}{\partial r}\right)\Bigg\}.\end{aligned} \tag{4.3.20}$$

4.4 ξ_ℓ^P and ξ_ℓ^Q in the far-field Ω_F

The analytical solutions for ξ_ℓ^P and ξ_ℓ^Q are obtained in the following sections.

4.4.1 Response ξ_ℓ^P to Forcing $\mathcal{P}$ by progressive waves

Let us recall that ξ_ℓ^P satisfies Eqn. (4.2.8)

$$\left(\nabla^2 - \kappa_\ell^2\right)\xi_\ell^P = -i\frac{2\omega\mathcal{P}}{A_{\ell,\ell}}, \qquad \ell = 0, 1, 2, 3\cdots \tag{4.4.1}$$

with $\mathcal{P}$ being Eqn. (4.3.8)

After inspecting the form of $\mathcal{P}$ we expect ξ_ℓ^P also has the same form,

$$\xi_\ell^P = \xi_\ell^I + \xi_\ell^R + \xi_\ell^{IR}, \quad \ell = 0, 1, 2, 3 \cdots \tag{4.4.2}$$

where

$$\xi_\ell^I = L_\ell^M e^{i2kr\cos(\theta-\theta_I)}, \ \xi_\ell^R = L_\ell^M e^{i2kr\cos(\theta+\theta_I)}, \ \xi_\ell^{IR} = L_\ell^N e^{i2kr\cos\theta_I\cos\theta}. \tag{4.4.3}$$

In the preceding equation, ξ_ℓ^I and ξ_ℓ^R represent the second-order oblique incident waves and reflected waves, respectively, and ξ_ℓ^{IR} is radiated plane wave induced by the interaction between the first-order incident and reflected waves. Substituting the above equations into Eqn. (4.4.1), we obtain

$$L_\ell^M = \frac{2i\omega}{A_{\ell,\ell}}\frac{A^2}{4}\frac{\left(\widehat{\beta}-\bar{\beta}k^2\right)}{4k^2+\kappa_\ell^2}, \tag{4.4.4}$$

and

$$L_\ell^N = \frac{2i\omega}{A_{\ell,\ell}}\frac{A^2}{2}\frac{\left[\widehat{\beta}-\bar{\beta}k^2\cos\left(2\theta_I\right)\right]}{\left(2k\cos\theta_I\right)^2+\kappa_\ell^2}. \tag{4.4.5}$$

In summary, we obtain

$$\begin{aligned}\xi_\ell^P =& \frac{2i\omega}{A_{\ell,\ell}}\frac{A^2}{4}\frac{\left(\widehat{\beta}-\bar{\beta}k^2\right)}{4k^2+\kappa_\ell^2}\left[e^{i2kr\cos(\theta-\theta_I)}+e^{i2kr\cos(\theta+\theta_I)}\right] \\ &+\frac{2i\omega}{A_{\ell,\ell}}\frac{A^2}{2}\frac{\left[\widehat{\beta}-\bar{\beta}k^2\cos\left(2\theta_I\right)\right]}{\left(2k\cos\theta_I\right)^2+\kappa_\ell^2}e^{i2kr\cos\theta_I\cos\theta}, \quad \ell = 0, 1, 2, 3\cdots.\end{aligned} \tag{4.4.6}$$

Substituting Eqn. (4.4.3) into (3.2.4) and (3.2.9), we obtain the corresponding second-order potentials Φ_2^I, Φ_2^R and Φ_2^{IR},

$$\begin{pmatrix}\Phi_2^I \\ \Phi_2^R\end{pmatrix} = \sum_{\ell=0}^{\infty}\frac{g\left(\widehat{\beta}-\bar{\beta}k^2\right)}{A_{\ell,\ell}\left(4k^2+\kappa_\ell^2\right)}\frac{A^2}{4}\frac{\cos\kappa_\ell\left(z+h\right)}{\cos\kappa_\ell h}e^{i2krcos(\theta\mp\theta_I)-i2\omega t}+*, \tag{4.4.7}$$

and

$$\Phi_2^{IR} = \sum_{\ell=0}^{\infty} \frac{g\left(\widehat{\beta} - \bar{\beta}k^2\cos 2\theta_I\right)}{A_{\ell,\ell}\left[(2k\cos\theta)^2 + \kappa_\ell^2\right]} \frac{A^2}{2} \frac{\cos\kappa_\ell(z+h)}{\cos\kappa_\ell h} e^{i2kr\cos\theta_I\cos\theta - i2\omega t} + *, \tag{4.4.8}$$

For normal incidence $\theta_I = 3\pi/2$, the second-harmonic potential Φ_2^{IR} becomes independent of (x, y, z) (or r, θ, z); the associated second harmonic pressure persists for all depth down to the seabed and can induce microseisms, as shown first by Longuet-Higgins (1950) for a pure standing wave in deep water on a straight coast.

We remark that each potential above is just the series expansion of the second-order part of the classical Stokes wave (see Appendix E for details). While the Stokes form is more compact, the series form here is more convenient for later computations.

4.4.2 Response ξ_ℓ^Q to forcing $\mathcal{Q}$

To solve the inhomogeneous equations, we shall employ the method of Green's function, $G_\ell(r, \theta; r_0, \theta_0)$, defined here by the following equations

$$\nabla^2 G_\ell(r,\theta;r_0,\theta_0) - \kappa_\ell^2 G_\ell(r,\theta;r_0,\theta_0) = \frac{1}{r}\delta(r-r_0)\left[\delta(\theta-\theta_0) + \delta(\theta+\theta_0)\right] \quad \text{in } \Omega_F, \tag{4.4.9}$$

$$\frac{\partial G_\ell}{\partial\theta} = 0, \quad \theta = 0,\ \pi, \tag{4.4.10}$$

$$\frac{\partial G_\ell}{\partial r} = 0, \quad r = a. \tag{4.4.11}$$

with $\ell = 0, 1, 2, 3\cdots$.

For $\ell = 0$, the usual(strong) radiation condition is required, i.e., at infinity, G_0 behaves as an outgoing waves,

$$\sqrt{r}\left(\frac{\partial G_0}{\partial r} - i\widehat{\kappa_0}G_0\right) \to 0, \quad r \to \infty, \tag{4.4.12}$$

For $\ell = 1, 2, 3, \cdots$, we require that the evanescent modes die out at infinity

$$G_\ell \to 0, \quad r \to \infty, \quad \ell = 1, 2, 3 \cdots . \tag{4.4.13}$$

The Green's function $G_\ell(r, \theta; r_0, \theta_0)$ is then obtained as follows. Let us expand the Dirac delta function for θ into complete orthogonal sets of eigenfunctions

$$\delta(\theta - \theta_0) = \frac{1}{2\pi} \sum_{m=0}^{\infty} \epsilon_m \cos m(\theta - \theta_0), \tag{4.4.14}$$

$$\delta(\theta + \theta_0) = \frac{1}{2\pi} \sum_{m=0}^{\infty} \epsilon_m \cos m(\theta + \theta_0). \tag{4.4.15}$$

Substituting the above expression into Eqn. (4.4.9), yields

$$\nabla^2 G_\ell(r, \theta; r_0, \theta_0) - \kappa_\ell^2 G_\ell(r, \theta; r_0, \theta_0) = \frac{\delta(r - r_0)}{2\pi r} \sum_{m=0}^{\infty} \epsilon_m \left[\cos m(\theta - \theta_0) + \cos m(\theta + \theta_0)\right]. \tag{4.4.16}$$

Let us assume $G_\ell(r, \theta; r_0, \theta_0)$ to take the form

$$\begin{aligned} G_\ell(r, \theta; r_0, \theta_0) &= \frac{1}{2\pi} \sum_{m=0}^{\infty} \epsilon_m g_{\ell,m}(r; r_0) \left[\cos m(\theta - \theta_0) + \cos m(\theta + \theta_0)\right] \\ &= \frac{1}{\pi} \sum_{m=0}^{\infty} \epsilon_m g_{\ell,m}(r; r_0) \cos m\theta \cos m\theta_0 \end{aligned} \tag{4.4.17}$$

where $g_{\ell,m}(r; r_0)$ is yet to be determined. Putting $G_\ell(r, \theta; r_0, \theta_0)$ into equation (4.4.16), we obtain

$$\frac{d^2 g_{\ell,m}}{dr^2} + \frac{1}{r}\frac{d}{dr} g_{\ell,m} - \frac{1}{r^2}\left[\kappa_\ell^2 r^2 + m^2\right] g_{\ell,m} = \frac{\delta(r - r_0)}{r}. \tag{4.4.18}$$

Defining $g_{\ell,m} = g^-_{\ell,m}$ for $r < r_0$ and $g_{\ell,m} = g^+_{\ell,m}$ for $r > r_0$, we get

$$\frac{d^2 g^\pm_{\ell,m}}{dr^2} + \frac{1}{r}\frac{d}{dr} g^\pm_{\ell,m} - \frac{1}{r^2}\left[\kappa_\ell^2 r^2 + m^2\right] g^\pm_{\ell,m} = 0. \tag{4.4.19}$$

The above equation is the Modified Bessel equation with integer order m, with the solution

$$g^+_{\ell,m}(r, r_0) = pK_m(\kappa_\ell r) + qI_m(\kappa_\ell r), \tag{4.4.20}$$

$$g^{-}_{\ell,m}(r,r_0) = cK_m(\kappa_\ell r) + dI_m(\kappa_\ell r), \tag{4.4.21}$$

where I_m is the modified Bessel function of the first kind of order m, and K_m is the modified Bessel function of the second kind of order m. The following boundary conditions must be required

$$g^{+}_{\ell,m}(r;r_0) = g^{-}_{\ell,m}(r;r_0), \quad r = r_0, \tag{4.4.22}$$

$$\frac{d}{dr}g^{-}_{\ell,m}(r;r_0) = 0, \quad r = a. \tag{4.4.23}$$

In addition, we integrate equation (4.4.18) with respect to r from r_0^- to r_0^+ to obtain another matching condition at $r = r_0$

$$\frac{d}{dr}g^{+}_{\ell,m}(r;r_0) - \frac{d}{dr}g^{-}_{\ell,m}(r;r_0) = \frac{1}{r_0}, \quad r = r_0. \tag{4.4.24}$$

Since for large r, $g^{+}_{\ell,m}(r;r_0)$ should satisfy Eqns. (4.4.12) and (4.4.13), the solution can only consist of Modified Bessel functions of the second kind,

$$g^{+}_{\ell,m}(r;r_0) = pK_m(\kappa_\ell r). \tag{4.4.25}$$

For $g^{-}_{\ell,m}(r;r_0)$ to satisfy the boundary condition at $r = a$, we require

$$\left(\frac{dg^{-}_{\ell,m}}{dr}\right)_{r=a} = \kappa_\ell\left[cK'_m(\kappa_\ell a) + dI'_m(\kappa_\ell a)\right] = 0, \tag{4.4.26}$$

so that

$$d = -\frac{K'_m(\kappa_\ell a)}{I'_m(\kappa_\ell a)}c, \tag{4.4.27}$$

$$g^{-}_{\ell,m}(r;r_0) = cK_m(\kappa_\ell r) - c\frac{K'_m(\kappa_\ell a)}{I'_m(\kappa_\ell a)}I_m(\kappa_\ell r). \tag{4.4.28}$$

To satisfy the matching conditions at $r = r_0$, we need

$$pK_m(\kappa_\ell r_0) = cK_m(\kappa_\ell r_0) - c\frac{K'_m(\kappa_\ell a)}{I'_m(\kappa_\ell a)}I_m(\kappa_\ell r_0), \tag{4.4.29}$$

and

$$pK'_m(\kappa_\ell r_0) - cK'_m(\kappa_\ell r_0) + c\frac{K'_m(\kappa_\ell a)}{I'_m(\kappa_\ell a)} I'_m(\kappa_\ell r_0) = \frac{1}{\kappa_\ell r_0}. \tag{4.4.30}$$

We shall make use of the Wronskian relation for modified Bessel functions

$$K_{v+1}(z) I_v(z) + K_v(z) I_{v+1}(z) = \frac{1}{z}, \tag{4.4.31}$$

and the recurrence relations for $K_{v+1}(z)$ and for $I_{v+1}(z)$

$$K_{v+1}(z) = -K'_v(z) + \frac{v}{z} K_v(z), \tag{4.4.32}$$

and

$$I_{v+1}(z) = I'_v(z) - \frac{v}{z} I_v(z). \tag{4.4.33}$$

Putting the recurrence relations, Eqns. (4.4.32) and (4.4.33), into Eqn. (4.4.31), we get another expression for the Wronskian relation

$$-K'_v(z) I_v(z) + K_v(z) I'_v(z) = \frac{1}{z}. \tag{4.4.34}$$

Let us rewrite Eqn. (4.4.30) as

$$(p-c) K'_m(\kappa_\ell r_0) + c\frac{K'_m(\kappa_\ell a)}{I'_m(\kappa_\ell a)} I'_m(\kappa_\ell r_0) = \frac{1}{\kappa_\ell r_0}. \tag{4.4.35}$$

and compare the above equation with the Wronskian relation, Eq. (4.4.34), we get

$$c = \frac{I'_m(\kappa_\ell a)}{K'_m(\kappa_\ell a)} K_m(\kappa_\ell r_0), \tag{4.4.36}$$

$$p = \left[\frac{I'_m(\kappa_\ell a)}{K'_m(\kappa_\ell a)} K_m(\kappa_\ell r_0) - I_m(\kappa_\ell r_0)\right], \tag{4.4.37}$$

$$d = -c\frac{K'_m(\kappa_\ell a)}{I'_m(\kappa_\ell a)} = -K_m(\kappa_\ell r_0). \tag{4.4.38}$$

We finally obtain

$$g_{\ell,m}^{+}\left(r;r_0\right)=\left[\frac{I_m'\left(\kappa_\ell a\right)}{K_m'\left(\kappa_\ell a\right)}K_m\left(\kappa_\ell r_0\right)-I_m\left(\kappa_\ell r_0\right)\right]K_m\left(\kappa_\ell r\right), \tag{4.4.39}$$

and

$$g_{\ell,m}^{-}\left(r;r_0\right)=\left[\frac{I_m'\left(\kappa_\ell a\right)}{K_m'\left(\kappa_\ell a\right)}K_m\left(\kappa_\ell r_0\right)K_m\left(\kappa_\ell r\right)-K_m\left(\kappa_\ell r_0\right)I_m\left(\kappa_\ell r\right)\right]. \tag{4.4.40}$$

Green function can thus be written as

$$\begin{aligned}G_\ell\left(r,\theta;r_0,\theta_0\right)=&\sum_{m=0}^{\infty}\frac{\epsilon_m}{\pi}\left[\frac{I_m'\left(\kappa_\ell a\right)}{K_m'\left(\kappa_\ell a\right)}K_m\left(\kappa_\ell r_>\right)K_m\left(\kappa_\ell r_<\right)\right]\cos m\theta\cos m\theta_0\\&-\sum_{m=0}^{\infty}\frac{\epsilon_m}{\pi}\left[K_m\left(\kappa_\ell r_>\right)I_m\left(\kappa_\ell r_<\right)\right]\cos m\theta\cos m\theta_0\end{aligned} \tag{4.4.41}$$

with

$$r_>=Max\left\{r,r_0\right\},\quad r_<=Min\left\{r,r_0\right\}. \tag{4.4.42}$$

This is the two-dimensional counterpart of the three-dimensional Green's function by Chau and Eatock Taylor(1992) [10]. Also, it is clear that the arguments in G_ℓ are interchangeable, i.e.

$$G_\ell\left(r,\theta;r_0,\theta_0\right)=G_\ell\left(r_0,\theta_0;r,\theta\right). \tag{4.4.43}$$

After obtaining Green's function, we can solve $\xi_\ell^Q(r,\theta)$ by making use of Green's theorem

$$\begin{aligned}&\int_0^\pi\int_a^\infty\left[\xi_\ell^Q(r,\theta)\nabla^2G_\ell\left(r,\theta;r_0,\theta_0\right)-G_\ell\left(r,\theta;r_0,\theta_0\right)\nabla^2\xi_\ell^Q(r,\theta)\right]rd\theta dr\\&=\oint_{\partial\Omega_F}\left[\xi_\ell^Q(r,\theta)\frac{\partial G_\ell\left(r,\theta;r_0,\theta_0\right)}{\partial n}-G_\ell\left(r,\theta;r_0,\theta_0\right)\frac{\partial\xi_\ell^Q(r,\theta)}{\partial n}\right]dS\end{aligned} \tag{4.4.44}$$

where $\partial\Omega_F$ is the boundary of Ω_F,

$$\partial\Omega_F=\partial A+\partial B+\partial F, \tag{4.4.45}$$

with ∂A being the semi-circular cylindrical boundary between Ω_A and Ω_F, ∂B the coastline and ∂F the semi-circular cylindrical boundary at infinity $r = R_\infty \to \infty$.

Putting the boundary conditions Eqns. (4.2.12), (4.2.11), (4.4.10) and (4.4.11) into Eqn. (4.4.44), we get

$$\begin{aligned}\int_0^\pi\int_a^\infty \left[\xi_\ell^Q(r,\theta)\nabla^2 G_\ell\left(r,\theta;r_0,\theta_0\right) - G_\ell\left(r,\theta;r_0,\theta_0\right)\nabla^2\xi_\ell^Q(r,\theta)\right] r d\theta dr \\ = \int_{\partial F}\left[\xi_\ell^Q(r,\theta)\frac{\partial G_\ell\left(r,\theta;r_0,\theta_0\right)}{\partial n} - G_\ell\left(r,\theta;r_0,\theta_0\right)\frac{\partial \xi_\ell^Q(r,\theta)}{\partial n}\right] dS.\end{aligned} \tag{4.4.46}$$

Making use of the facts that (i) for $\ell = 1, 2, 3, \cdots$, the evanescent modes die out exponentially at infinity, and (ii) for $\ell = 0$, the propagating mode satisfies the weak radiation condition, i.e. the line integral along the boundary at infinity ∂F below vanishes in the limit of large r

$$\begin{aligned}I_{\partial F} &= \int_0^\pi\left[\xi_\ell^Q(R_\infty,\theta)\frac{\partial G_\ell(R_\infty,\theta;r_0,\theta_0)}{\partial n} - G_\ell(R_\infty,\theta;r_0,\theta_0)\frac{\partial\xi_\ell^Q(R_\infty,\theta)}{\partial n}\right] R_\infty d\theta \\ &\approx O\left(\frac{1}{\sqrt{R_\infty}}\right)\to 0, \qquad R_\infty\to\infty\end{aligned} \tag{4.4.47}$$

The details are shown in Appendix F.2. Therefore, Eqn. (4.4.46) becomes

$$\int_0^\pi\int_a^\infty \left[\xi_\ell^Q(r,\theta)\nabla^2 G_\ell\left(r,\theta;r_0,\theta_0\right) - G_\ell\left(r,\theta;r_0,\theta_0\right)\nabla^2\xi_\ell^Q(r,\theta)\right] r d\theta dr = 0. \tag{4.4.48}$$

Putting Eqn. (4.2.10) and (4.4.9) into Eqn. (4.4.48), we get

$$\xi_\ell^Q\left(r_0,\theta_0\right) = \int_0^\pi\int_a^\infty -i\frac{2\omega\mathcal{Q}(r,\theta)}{A_{\ell,\ell}}G_\ell(r,\theta;r_0,\theta_0) r d\theta dr. \tag{4.4.49}$$

Due to the symmetry of the obtained Green's function, Eq. (4.4.43), the preceding equation can be further rewritten as

$$\xi_\ell^Q\left(r,\theta\right) = \int_0^\pi\int_a^\infty -i\frac{2\omega\mathcal{Q}(r_0,\theta_0)}{A_{\ell,\ell}}G_\ell(r_0,\theta_0;r,\theta) r_0 d\theta_0 dr_0, \qquad \ell = 0, 1, 2, 3\cdots. \tag{4.4.50}$$

By making use of Green function Eqn. (4.4.41) into Eqn. (4.4.50), $\xi_\ell^Q(r,\theta)$ is finally obtained

$$\xi_\ell^Q(r,\theta) = \int_a^\infty r_0 dr_0 \int_0^\pi d\theta_0 \left[-i\frac{2\omega\mathcal{Q}(r_0,\theta_0)}{A_{\ell,\ell}}\right] \sum_{m=0}^\infty \frac{\epsilon_m}{\pi} \cos m\theta \cos m\theta_0 K_m(\kappa_\ell r_>) \times \left[\frac{I_m'(\kappa_\ell a)}{K_m'(\kappa_\ell a)} K_m(\kappa_\ell r_<) - I_m(\kappa_\ell r_<)\right], \quad \ell = 0,1,2,3\cdots. \tag{4.4.51}$$

From Eqn. (4.3.19), $\mathcal{Q}(r_0,\theta_0)$ is written in terms of a Fourier series

$$\mathcal{Q}(r_0,\theta_0) = \sum_{p=0}^\infty \epsilon_p \mathcal{Q}_p(r_0)\cos p\theta_0, \tag{4.4.52}$$

where $\mathcal{Q}_p(r_0,\theta_0)$ is

$$\mathcal{Q}_p(r_0) = \sum_{q=-\infty}^\infty \left\{\left[\widehat{\beta} - \frac{q(p-q)}{r_0^2}\bar{\beta}\right] S_q(2T_{p-q} + S_{p-q}) + \bar{\beta}\frac{\partial S_q}{\partial r_0}\left(2\frac{\partial T_{p-q}}{\partial r_0} + \frac{\partial S_{p-q}}{\partial r_0}\right)\right\} \tag{4.4.53}$$

with

$$T_{p-q}(r_0) = \frac{A}{2} i^n \left[H_{p-q}^{(1)}(kr_0) + H_{p-q}^{(2)}(kr_0)\right]\cos(p-q)\theta_I, \tag{4.4.54}$$

$$S_q(r_0) = i^q \alpha_q H_q(kr_0). \tag{4.4.55}$$

Putting the identities of the eigenfunction of θ_0

$$\int_0^\pi \cos m\theta_0 \cos p\theta_0 d\theta_0 = \begin{cases} 0 & m \neq p \\ \pi/2 & m = p \neq 0 \\ \pi & m = p = 0 \end{cases}, \tag{4.4.56}$$

into Eqn. (4.4.51), we obtain

$$\xi_\ell^Q(r,\theta) = \sum_{m=0}^{\infty} \epsilon_m \cos(m\theta) \int_a^\infty r_0 dr_0 \left[-i\frac{2\omega \mathcal{Q}_m(r_0)}{A_{\ell,\ell}}\right] K_m(\kappa_\ell r_>) \times \left[\frac{I_m'(\kappa_\ell a)}{K_m'(\kappa_\ell a)} K_m(\kappa_\ell r_<) - I_m(\kappa_\ell r_<)\right], \quad \ell = 0,1,2,3\cdots. \tag{4.4.57}$$

In particular, for $r = a$ (i.e. on the boundary between Ω_A and Ω_F):

$$\xi_\ell^Q(a,\theta) = \sum_{m=0}^{\infty} \epsilon_m \cos(m\theta) \int_a^\infty r_0 dr_0 \left[-i\frac{2\omega \mathcal{Q}_m(r_0)}{A_{\ell,\ell}}\right] K_m(\kappa_\ell r_0) \times \left[\frac{I_m'(\kappa_\ell a)}{K_m'(\kappa_\ell a)} K_m(\kappa_\ell a) - I_m(\kappa_\ell a)\right], \quad \ell = 0,1,2,3\cdots. \tag{4.4.58}$$

Making use of Eqn. (4.4.34), the previous equation can be reduced as

$$\xi_\ell^Q(a,\theta) = \sum_{m=0}^{\infty} \frac{\epsilon_m}{\kappa_\ell a} \cos(m\theta) \int_a^\infty r_0 dr_0 \left[-i\frac{2\omega \mathcal{Q}_m(r_0)}{A_{\ell,\ell}}\right] \frac{K_m(\kappa_\ell r_0)}{K_m'(\kappa_\ell a)}, \quad \ell = 0,1,2,3\cdots. \tag{4.4.59}$$

For all $\ell > 0$, $K_m(\kappa_\ell r_0)$ decays exponentially for large r_0, so the integral above converges rapidly. For $\ell = 0$, $\kappa_0 = -i\widehat{\kappa}_0$ is pure imaginary

$$I_m(\kappa_0 r_0) = I_m(-i\widehat{\kappa}_0 r_0) = e^{\frac{3}{2}im\pi} J_m(\widehat{\kappa}_0 r_0), \tag{4.4.60}$$

$$K_m(\kappa_0 r_0) = K_m(-i\widehat{\kappa}_0 r_0) = \frac{\pi}{2} i e^{\frac{1}{2}im\pi} H_m^{(1)}(\widehat{\kappa}_0 r_0), \tag{4.4.61}$$

and

$$K_m'(\kappa_0 r_0) = K_m'(-i\widehat{\kappa}_0 r_0) = -\frac{\pi}{2} e^{\frac{1}{2}im\pi} H_m^{(1)'}(\widehat{\kappa}_0 r_0). \tag{4.4.62}$$

Thus the infinite integral Eq. (4.4.59) can be computed by first rewriting

$$\xi_0^Q(a,\theta) = \sum_{m=0}^{\infty} \frac{\epsilon_m}{\widehat{\kappa}_0 a} \cos(m\theta) \frac{1}{H_m^{(1)'}(\widehat{\kappa}_0 a)} (I_{F_1} + I_{F_\infty}) \tag{4.4.63}$$

where

$$I_{F_1} = \int_a^{r_s} r_0 dr_0 \left[-i \frac{2\omega \mathcal{Q}_m(r_0)}{A_{0,0}} \right] H_m^{(1)}(\widehat{\kappa}_0 r_0), \tag{4.4.64}$$

and

$$I_{F_\infty} = \int_{r_s}^{\infty} r_0 dr_0 \left[-i \frac{2\omega \mathcal{Q}_m(r_0)}{A_{0,0}} \right] H_m^{(1)}(\widehat{\kappa}_0 r_0). \tag{4.4.65}$$

The integral I_{F_1} is evaluated by the Guassian quadrature integral method. Evaluation of the integral I_{F_∞} can be expedited by the scheme of Chau and Eatock Taylor(1992) [10] and the details are given in Appendix G.

In summary, the second-order solution in the far-field is known analytically except for the unknown coefficients $\widehat{\alpha}_{\ell,m}$ of the second-order free wave.

Chapter 5

Finite element analysis

The detailed finite element analysis for solving the first-order and the second-order mild-slope equation will be described in this chapter.

5.1 First-order problem

In this section, the finite element equations using Galerkin's approximation are formulated for the first-order mild-slope equation

$$\nabla \cdot (CC_g \nabla \eta) + \left[k^2 CC_g + gU\nabla^2 h + gV\left(\nabla h\right)^2\right]\eta = 0, \tag{5.1.1}$$

the no-flux condition on the solid boundaries ∂B which is the union of the complex coastline (peninsula, harbor, breakwaters,etc.),

$$\left(\frac{\partial \eta}{\partial n}\right)_{\Omega_A} = 0, \quad (x, y) \in \partial B, \tag{5.1.2}$$

and the continuities of pressure along and flux across the semi-circle ∂A : $(r = a, 0 \leq \theta \leq \pi)$

$$\left(\frac{\partial \eta}{\partial r}\right)_{\Omega_A} = \frac{\partial \eta^{(T)}}{\partial r} + \frac{\partial \eta^{(S)}}{\partial r}, \quad r = a, \tag{5.1.3}$$

$$(\eta)_{\Omega_A} = \eta^{(T)} + \eta^{(S)}, \quad r = a, \tag{5.1.4}$$

These conditions are imposed on the nodal points along the semi-circle. Recall that the far field solutions $\eta^{(T)}$ and $\eta^{(S)}$ are given by Eq. (4.1.2) and Eq. (4.1.5), the last of which still contains the unknown coefficients α_m.

5.1.1 Weighted residual integral equation

Instead of solving Eq. (5.1.1) directly, we use the weighted residual integral equation as follows.

$$\iint_{\Omega_A} \left\{\nabla \cdot (CC_g \nabla\eta) + \left[k^2 CC_g + gU\nabla^2 h + gV\left(\nabla h\right)^2\right]\eta\right\} W d\Omega_A = 0 \tag{5.1.5}$$

where W is a weighting function to be chosen below. Instead of getting the exact solution, we try to get an approximate numerical solution in which the residual or error is forced to be zero in a spatially averaged sense. The first term of the integrand on the left hand side of Eq. (5.1.5) can be written as

$$\left[\nabla \cdot (CC_g \nabla\eta)\right] W = \nabla \cdot (WCC_g \nabla\eta) - CC_g \nabla\eta \cdot \nabla W. \tag{5.1.6}$$

Then, by Green's theorem, the following surface integral is transformed into a closed line integral along boundary Γ of the domain Ω_A

$$\iint_{\Omega_A} \nabla \cdot (WCC_g \nabla\eta)\, d\Omega = \oint_{\Gamma} WCC_g \frac{\partial\eta}{\partial n} d\Gamma, \tag{5.1.7}$$

Therefore, Eq. (5.1.5) becomes

$$\iint_{\Omega_A} \left\{CC_g \nabla\eta \cdot \nabla W - \left[k^2 CC_g + gU\nabla^2 h + gV\left(\nabla h\right)^2\right]\eta W\right\} d\Omega = \oint_{\Gamma} WCC_g \frac{\partial\eta}{\partial n} d\Gamma. \tag{5.1.8}$$

By employing the boundary condition, Eqns. (5.1.2)-(5.1.3), the preceding equation becomes

$$\begin{aligned}&\iint_{\Omega}\left\{CC_g\nabla\eta\cdot\nabla W-\left[k^2CC_g+gU\nabla^2h+gV\left(\nabla h\right)^2\right]\eta W\right\}d\Omega\\&=\int_0^{\pi}WCC_g\frac{\partial\eta^{(T)}}{\partial r}ad\theta+\int_0^{\pi}WCC_g\frac{\partial\eta^{(S)}}{\partial r}ad\theta.\end{aligned}\tag{5.1.9}$$

5.1.2 Discretized by triangular elements

We shall employ three-node triangular elements. Within each triangle η^e is approximated by a linear interpolation function

$$\eta^e(x,y)=\sum_{i=1}^{3}w_i^e\eta_i^e=\begin{bmatrix}w_1^e & w_2^e & w_3^e\end{bmatrix}\begin{bmatrix}\eta_1^e\\ \eta_2^e\\ \eta_3^e\end{bmatrix}\tag{5.1.10}$$

where superscripts e represent quantities associated with an element, η_i^e is the local i-th nodal coefficient of η. The local weighting function w_i^e for nodal point is defined as

$$w_i^e=\frac{1}{2\Delta^e}\left(a_i+b_ix+c_iy\right),\quad i=1,2,3\tag{5.1.11}$$

with

$$a_1=x_2^ey_3^e-x_3^ey_2^e,\quad b_1=y_2^e-y_3^e,\quad c_1=x_3^e-x_2^e,\tag{5.1.12}$$

and Δ^e being the area of element e

$$\Delta^e=\frac{1}{2}\begin{vmatrix}1 & x_1^e & y_1^e\\ 1 & x_2^e & y_2^e\\ 1 & x_3^e & y_3^e\end{vmatrix}=\frac{1}{2}\left(b_1*c_2-b_2*c_1\right),\tag{5.1.13}$$

where (x_i^e,y_i^e) denote the x, y coordinates at node i. The other coefficients a_2, a_3, b_2, b_3, c_2, c_3 can be obtained by permutation $1\rightarrow2\rightarrow3\rightarrow1$. Note that at local node i,

w_i is unity, while outside the immediately adjacent elements $w_i = 0$; i.e.,

$$w_1^e = \begin{cases} 1, & \text{at } (x_1, y_1) \\ 0, & \text{at } (x_2, y_2), (x_3, y_3) \end{cases}, \quad w_2^e = \begin{cases} 1, & \text{at } (x_2, y_2) \\ 0, & \text{at } (x_1, y_1), (x_3, y_3) \end{cases}, \tag{5.1.14}$$

$$w_3^e = \begin{cases} 1, & \text{at } (x_3, y_3) \\ 0, & \text{at } (x_1, y_1), (x_2, y_2) \end{cases}. \tag{5.1.15}$$

In the finite element analysis, domain Ω_A is approximated as an assemblage of N_E discrete triangular elements with N_P nodes in which N_B boundary nodes are placed from node $N_P - N_B + 1$ to node N_B. Therefore, there are $N_P - N_B$ interior nodes. In addition, the continuous field η is replaced by

$$\eta = \sum_{n=1}^{N_P} \mathcal{W}_n \eta_n, \tag{5.1.16}$$

where η_n is the n-th global nodal coefficient of η, and $\mathcal{W}_n$, with $n = 1, 2 \cdots N_P$, is the global weighting function. η_n and $\mathcal{W}_n^e$ are assembled by the local nodal parameter η_i^e and the local weighted function w_i^e respectively (Figure 5-1a). Therefore, at global node n, $\mathcal{W}_n = 1$, while outside the immediately adjacent elements $\mathcal{W}_n = 0$.

Based on the Galerkin assumption, W in the weighted integral equation is chosen to be the global weighting function $\mathcal{W}_n$. Therefore, with Eq. (5.1.16) and Galerkin assumption, Eq. (5.1.9) is approximated as

$$\sum_{n=1}^{N_P} \eta_n \left\{ \sum_{\Omega_e=1}^{N_E} \iint_{\Omega_e} \left\{ CC_g \nabla \mathcal{W}_n \cdot \nabla \mathcal{W}_m - \left[k^2 CC_g + gU\nabla^2 h + gV\left(\nabla h\right)^2 \right] \mathcal{W}_n \mathcal{W}_m \right\} d\Omega \right\}$$
$$- \int_0^\pi \mathcal{W}_m CC_g \frac{\partial \eta^{(S)}}{\partial r} a d\theta = \int_0^\pi \mathcal{W}_m CC_g \frac{\partial \eta^{(T)}}{\partial r} a d\theta, \qquad m = 1, 2, 3, \cdots, N_P. \tag{5.1.17}$$

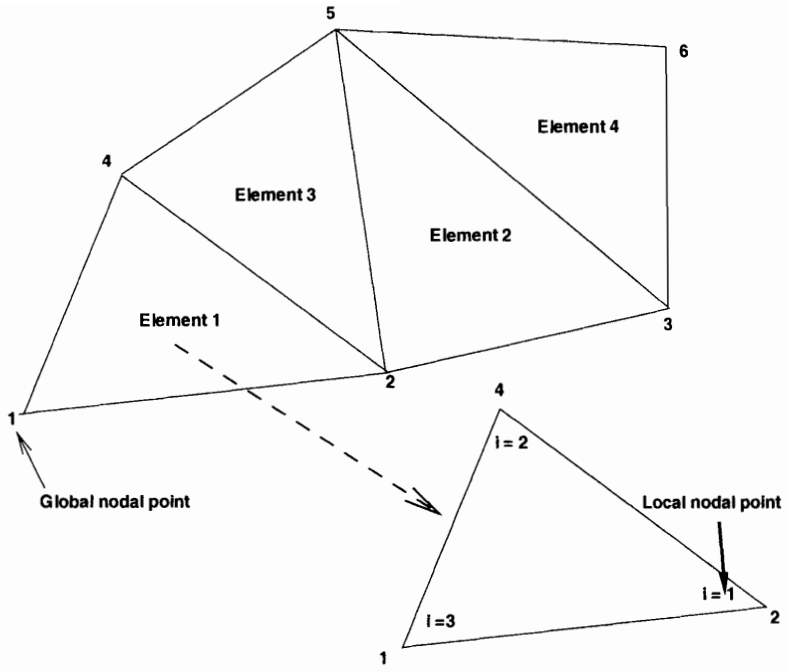

(a)

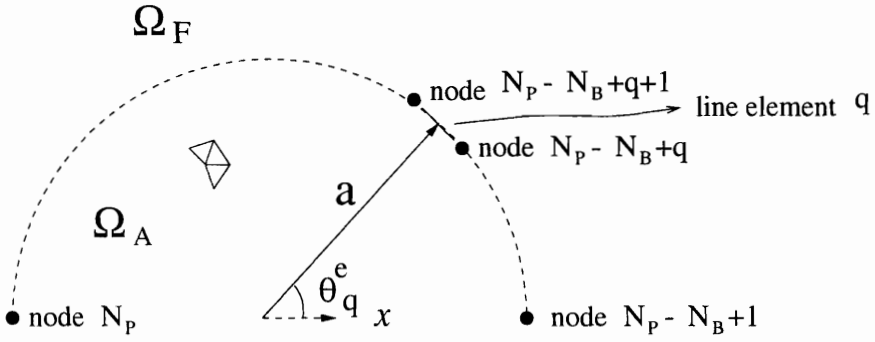

(b)

Figure 5-1: (a) Global and local nodes of finite elements . (b) Line elements on the semi-circular boundary ∂A

Recalling that

$$\eta^{(T)} = \frac{A}{2} e^{ikr\cos(\theta-\theta_I)} + \frac{A}{2} e^{ikr\cos(\theta+\theta_I)} = \sum_{n=0}^{\infty} A\epsilon_n i^n \cos n\theta_I J_n(kr)\cos n\theta, \tag{5.1.18}$$

and the scattered waves with $N_\alpha + 1$ unknown coefficients α_p after truncation is

$$\eta^{(S)} = \sum_{p=0}^{N_\alpha} \epsilon_p i^p \alpha_p H_p\left(kr\right)\cos p\theta, \tag{5.1.19}$$

we can write Eq. (5.1.17) as

$$\begin{aligned}
&\sum_{n=1}^{N_P} \eta_n \left\{ \sum_{\Omega_e=1}^{N_E} \iint_{\Omega_e} \left\{ CC_g \nabla \mathcal{W}_n \cdot \nabla \mathcal{W}_m - \left[k^2 CC_g + gU\nabla^2 h + gV\left(\nabla h\right)^2 \right] \mathcal{W}_n \mathcal{W}_m \right\} d\Omega_e \right\} \\
&- \sum_{p=0}^{N_\alpha} \alpha_p \left\{ \epsilon_p i^p kaCC_g H_p'\left(ka\right) \int_0^\pi \mathcal{W}_m \cos p\theta d\theta \right\} \\
&= ikaCC_g \frac{A}{2} \int_0^\pi \mathcal{W}_m \left[\cos\left(\theta - \theta_I\right) e^{ika\cos(\theta-\theta_I)} + \cos\left(\theta + \theta_I\right) e^{ika\cos(\theta+\theta_I)} \right] d\theta, \\
&\qquad\qquad m = 1, 2, 3, \cdots, N_p.
\end{aligned} \tag{5.1.20}$$

Now let us define two column vectors $\mathcal{X}^{(1)}$ and $\mathcal{X}^{(2)}$ by the unknown η_n and α_p

$$\mathcal{X}^{(1)} = \begin{bmatrix} \eta_1 \\ \eta_2 \\ \vdots \\ \eta_{N_P} \end{bmatrix}, \quad \mathcal{X}^{(2)} = \begin{bmatrix} \alpha_0 \\ \alpha_1 \\ \vdots \\ \alpha_{N_\alpha} \end{bmatrix}. \tag{5.1.21}$$

Eq. (5.1.20) can be written in matrix form

$$\begin{bmatrix} \mathbb{K}^{(1)} & \mathbb{K}^{(2)} \end{bmatrix} \begin{bmatrix} \mathcal{X}^{(1)} \\ \mathcal{X}^{(2)} \end{bmatrix} = \mathcal{Y}^{(1)} \tag{5.1.22}$$

or equivalently

$$\sum_{n=1}^{N_P} \mathcal{K}^{(1)}_{m,n}\eta_n + \sum_{p=0}^{N_\alpha} \mathcal{K}^{(2)}_{m,p}\alpha_p = \mathcal{Y}^{(1)}_m, \qquad m = 1, 2, 3, \cdots, N_p, \tag{5.1.23}$$

where the entries for $\mathbb{K}^{(1)}$, $\mathbb{K}^{(2)}$, and $\mathcal{Y}^{(1)}$ are $\mathcal{K}^{(1)}_{m,n}$, $\mathcal{K}^{(2)}_{m,p}$ and $\mathcal{Y}^{(1)}_m$ respectively ; they are defined as

$$\mathcal{K}^{(1)}_{m,n} = \sum_{\Omega_e=1}^{N_e} \iint_{\Omega_e} \left\{ CC_g \nabla \mathcal{W}_n \cdot \nabla \mathcal{W}_m - \left[k^2 CC_g + gU\nabla^2 h + gV\left(\nabla h\right)^2 \right] \mathcal{W}_n \mathcal{W}_m \right\} d\Omega,$$

$$\mathcal{K}^{(2)}_{m,p} = -\epsilon_p i^p kaCC_g H'_p\left(ka\right) \int_0^\pi \mathcal{W}_m \cos p\theta d\theta$$

and

$$\mathcal{Y}^{(1)}_m = ikaCC_g \frac{A}{2} \int_0^\pi \mathcal{W}_m \left[\cos\left(\theta - \theta_I\right) e^{ika\cos(\theta - \theta_I)} + \cos\left(\theta + \theta_I\right) e^{ika\cos(\theta + \theta_I)} \right] d\theta.$$

The above integrals $\mathcal{K}^{(1)}_{m,n}$, $\mathcal{K}^{(2)}_{m,p}$ and $\mathcal{Y}^{(1)}_m$ are obtained as follows.

$\mathcal{K}^{(1)}_{m,n}$ is an assemblage of local element stiffness matrices $E_{i,j}$,

$$\mathcal{K}^{(1)}_{m,n} = \sum_{\Omega_e=1}^{N_E} E_{i,j}, \quad \text{with} \begin{cases} i, j & \Rightarrow \text{local node}, \\ m, n & \Rightarrow \text{corresponding global node}, \end{cases} \tag{5.1.24}$$

with

$$E_{i,j} = \int_{\triangle_e} \left\{ CC_g \nabla w^e_i \cdot \nabla w^e_j - \left[k^2 CC_g + gU\nabla^2 h + gV\left(\nabla h\right)^2 \right] w^e_i w^e_j \right\} d\Omega \tag{5.1.25}$$

obtained as

$$E_{i,j} = \frac{\overline{CC_g}}{4\Delta^e}\left(b_i^2 + c_i^2\right) - \frac{\Delta^e}{6}\left[\overline{k^2 CC_g + gU\nabla^2 h + gV\left(\nabla h\right)^2}\right], \quad i = j, \tag{5.1.26}$$

$$E_{i,j} = \frac{\overline{CC_g}}{4\Delta^e}\left(b_i b_j + c_i c_j\right) - \frac{\Delta^e}{12}\left[\overline{k^2 CC_g + gU\nabla^2 h + gV\left(\nabla h\right)^2}\right], \quad i \neq j. \tag{5.1.27}$$

where $\overline{()}$ is the averaged value within each element.

For a semi-circular boundary, ∂A, $N_B - 1$ boundary line elements are formed by two of the adjacent boundary nodal points (Figure 5-1b). For example, $\eta_{N_P-N_B+1}$ and $\eta_{N_P-N_B+2}$ form line element 1. Also, the weighting function $\mathcal{W}_n$ is unity at the global node n and is zero outside the adjacent nodes. The boundary integral can be represented by the sum of the integral over each line element. Let the length l^e of the element be very small and equal for each element. Let θ_q^e be the angle at the mid-point of the line element q. The weighting function $W_{N_P-N_B+q}$ is nonzero only within the line element q and $q+1$. $W_{N_P-N_B+q} = 1/2$ at the mid-point of the line element q and $q+1$. We take the mid-point value to represent the average value of the integrand. Therefore,

$$\mathcal{Y}_m^{(1)} = \begin{cases} 0, & m < N_P - N_B + 1, \\ iCC_g \frac{A}{2} \frac{kl^e}{2} Y_q, & m = N_P - N_B + 1, \\ iCC_g \frac{A}{2} \frac{kl^e}{2} \left(Y_{q-1} + Y_q\right), & N_P - N_B + 1 < m < N_P, \\ iCC_g \frac{A}{2} \frac{kl^e}{2} Y_{q-1}, & m = N_P, \end{cases} \tag{5.1.28}$$

with

$$Y_q = \cos\left(\theta_q^e - \theta_I\right) e^{ika\cos\left(\theta_q^e - \theta_I\right)} + \cos\left(\theta_q^e + \theta_I\right) e^{ika\cos\left(\theta_q^e + \theta_I\right)}, \qquad q = m - N_P + N_B, \tag{5.1.29}$$

and

$$\mathcal{K}_{m,p}^{(2)} = \begin{cases} 0, & m < N_P - N_B + 1, \\ -\epsilon_p i^p CC_g \frac{A}{2} \frac{kl^e}{2} H_p'(ka)\, \Theta_q, & m = N_P - N_B + 1, \\ -\epsilon_p i^p CC_g \frac{A}{2} \frac{kl^e}{2} H_p'(ka) \left(\Theta_{q-1} + \Theta_q\right), & N_P - N_B + 1 < m < N_P, \\ -\epsilon_p i^p CC_g \frac{A}{2} \frac{kl^e}{2} H_p'(ka)\, \Theta_{q-1}, & m = N_P, \end{cases} \tag{5.1.30}$$

with

$$\Theta_q = \cos p\theta_q^e. \tag{5.1.31}$$

Since $m = 1, \cdots N_P$, we have N_P equations. There are however the same num-

ber of unknown nodal coefficients plus $N_\alpha + 1$ unknown coefficients α_p. The remaining equations are found from the boundary condition, Eq. (5.1.4) as follows. Let us rewrite Eq. (5.1.4) as

$$-\sum_{n=1}^{N_P} \eta_n \mathcal{W}_n + \sum_{p=0}^{N_\alpha} \epsilon_p i^p \alpha_p \cos p\theta H_p(ka) = -\sum_{m=0}^{\infty} \epsilon_p i^p A \cos m\theta_I J_p(ka) \cos m\theta \quad (5.1.32)$$

where Eqs. (5.1.16), (5.1.18) and (5.1.19) are applied. Let us multiply Eq. (5.1.32) by a factor of $\left[\epsilon_p i^p CC_g k H_p'(ka) \cos p\theta\right]$, integrate along the semi-circle at $r = a$ and use the identity

$$\int_0^\pi \cos m\theta \cos p\theta d\theta = \begin{cases} 0, & n \neq p \\ \pi/2, & n = p \neq 0 \\ \pi, & n = p = 0 \end{cases} . \quad (5.1.33)$$

We get $N_\alpha + 1$ additional equations

$$\left[\sum_{n=1}^{N_P} \mathcal{K}_{p,n}^{(3)} \eta_n\right] + \mathcal{K}_{p,p}^{(4)} \alpha_p = \mathcal{Y}_p^{(2)}, \quad \text{with } p = 0, 1, 2, \cdots, N_\alpha \quad (5.1.34)$$

where

$$\mathcal{K}_{p,n}^{(3)} = -\epsilon_p i^p CC_g k H_p'(ka) \int_0^\pi \mathcal{W}_n a \cos p\theta d\theta,$$

$$\mathcal{K}_{p,p}^{(4)} = \epsilon_p^2 i^{2p} CC_g ka H_p(ka) H_p'(ka) \int_0^\pi \cos^2 p\theta d\theta,$$

and

$$\mathcal{Y}_p^{(2)} = -\epsilon_p^2 i^{2p} CC_g Aka \cos p\theta_I J_p(ka) H_p'(ka) \int_0^\pi \cos^2 p\theta d\theta,$$

or equivalently in matrix form

$$\begin{bmatrix} \mathbb{K}^{(3)} & \mathbb{K}^{(4)} \end{bmatrix} \begin{bmatrix} \mathcal{X}^{(1)} \\ \mathcal{X}^{(2)} \end{bmatrix} = \mathcal{Y}^{(2)} \quad (5.1.35)$$

where the entries for $\mathbb{K}^{(3)}$ and $\mathcal{Y}^{(2)}$ are $\mathcal{K}_{p,n}^{(3)}$and $\mathcal{Y}_p^{(2)}$ respectively, and $\mathbb{K}^{(4)}$, is a diagonal matrix with entries $\mathcal{K}_{p,p}^{(4)}$ The above integrals $\mathcal{K}_{p,p}^{(4)}$, $\mathcal{K}_{p,n}^{(3)}$, and $\mathcal{Y}_p^{(2)}$ are obtained

as follows.

$$\mathcal{K}^{(4)}_{p,p} = \epsilon_n i^{2p} \pi C C_g k a H_p\left(ka\right) H'_p\left(ka\right), \tag{5.1.36}$$

$$\mathcal{Y}^{(2)}_{p} = -A\epsilon_n i^{2p} C C_g k a \pi \cos n\theta_I J_p(ka) H'_p\left(ka\right), \tag{5.1.37}$$

and

$$\mathcal{K}^{(3)}_{p,n} = \begin{cases} 0, & n < N_P - N_B + 1, \\ -\epsilon_p i^p C C_g \frac{A}{2} \frac{kl^e}{2} H'_p\left(ka\right) \Theta_q, & n = N_P - N_B + 1, \\ -\epsilon_p i^p C C_g \frac{A}{2} \frac{kl^e}{2} H'_p\left(ka\right) \left(\Theta_{q-1} + \Theta_q\right), & N_P - N_B + 1 < n < N_P, \\ -\epsilon_p i^p C C_g \frac{A}{2} \frac{kl^e}{2} H'_p\left(ka\right) \Theta_{q-1}, & n = N_P, \end{cases} \tag{5.1.38}$$

with

$$\Theta_q = \cos p\theta^e_q. \tag{5.1.39}$$

In summary, by combining Eqns. (5.1.22) and (5.1.35), we can write a matrix equation with the $N_P + N_\alpha + 1$ unknown variables

$$\begin{bmatrix} \mathbb{K}^{(1)} & \mathbb{K}^{(2)} \\ \mathbb{K}^{(3)} & \mathbb{K}^{(4)} \end{bmatrix} \begin{bmatrix} \mathcal{X}^{(1)} \\ \mathcal{X}^{(2)} \end{bmatrix} = \begin{bmatrix} \mathcal{Y}^{(1)} \\ \mathcal{Y}^{(2)} \end{bmatrix} \tag{5.1.40}$$

where the entries for $\mathbb{K}^{(1)}$, $\mathbb{K}^{(2)}$, and $\mathbb{K}^{(3)}$ are $\mathcal{K}^{(1)}_{m,n}$, $\mathcal{K}^{(2)}_{m,p}$ and $\mathcal{K}^{(3)}_{p,n}$ respectively , $\mathbb{K}^{(4)}$ is diagonal matrix with entries being $\mathcal{K}^{(4)}_{p,p}$,

$$\mathcal{X}^{(1)} = \begin{bmatrix} \eta_1 \\ \vdots \\ \eta_{N_P} \end{bmatrix}, \quad \mathcal{X}^{(2)} = \begin{bmatrix} \alpha_0 \\ \vdots \\ \alpha_{N_\alpha} \end{bmatrix}, \quad \mathcal{Y}^{(1)} = \begin{bmatrix} 0 \\ \vdots \\ 0 \\ \mathcal{Y}^{(1)}_{N_P - N_B + 1} \\ \vdots \\ \mathcal{Y}^{(1)}_{N_P} \end{bmatrix}, \quad \mathcal{Y}^{(2)} = \begin{bmatrix} \mathcal{Y}^{(2)}_0 \\ \vdots \\ \mathcal{Y}^{(2)}_{N_\alpha} \end{bmatrix}.$$

The matrix equation, (5.1.40), can be solved numerically by using the UC Berkeley programme *Distributed SupterLU* which is designed for distributed memory paral-

lel processors, using MPI for interprocess communications.

5.2 Second-order problem

In this section, we repeat the finite element analysis for the second-order system of mild-slope equations

$$\sum_{\ell=0}^{\infty}\{\nabla\cdot(A_{m,\ell}\nabla\xi_\ell)+B_{m,\ell}\nabla h\cdot\nabla\xi_\ell+C_{m,\ell}\xi_\ell\}=-i2\omega F,\qquad m=0,1,2,3,\cdots \text{ in } \Omega_A \tag{5.2.1}$$

with the no-flux condition on the solid boundary ∂B which is the union of the complex coastline(peninsula, harbor, breakwater, etc.)

$$\left(\frac{\partial\xi_\ell}{\partial n}\right)_{\Omega_A}=0,\qquad \ell=0,1,2,3,\cdots,\qquad (x,y)\in\partial B, \tag{5.2.2}$$

and the continuities of pressure along and flux across the semi-circle ∂A : $(r=a, 0\le\theta\le\pi)$

$$(\xi_\ell)_{\Omega_A}=\xi_\ell^P+\xi_\ell^Q+\xi_\ell^H,\qquad \ell=0,1,2,3,\cdots,r=a, \tag{5.2.3}$$

$$\left(\frac{\partial\xi_\ell}{\partial r}\right)_{\Omega_A}=\frac{\partial\xi_\ell^P}{\partial r}+\frac{\partial\xi_\ell^H}{\partial r},\qquad \ell=0,1,2,3,\cdots,\quad r=a. \tag{5.2.4}$$

These conditions are imposed on the nodal points along the semi-circle. Recall that the far field solutions ξ_ℓ^P, ξ_ℓ^Q and ξ_ℓ^H are given by Eqs. (4.4.6), (4.4.58) and (4.2.15), the last of which still contains the unknown coefficients $\widehat{\alpha}_{\ell,m}$.

5.2.1 Weighted residual integral equation

To obtain finite element matrices, Eq. (5.2.1) is truncated to a finite number of $N_\xi+1$ modes; that is, $\ell=0,1...,N_\xi$ and $m=0,1...,N_\xi$. Afterwards we applied the method

of weighted residuals and form the integrals for the truncated equation

$$\iint_{\Omega_A} \left\{ -\sum_{\ell=0}^{N_\xi} [\nabla \cdot (A_{m,\ell} \nabla \xi_\ell) + B_{m,\ell} \nabla h \cdot \nabla \xi_\ell + C_{m,\ell} \xi_\ell] = i2\omega F \right\} W d\Omega, \tag{5.2.5}$$

where the W is a weighting function to be chosen below.

The first term of the integrand on the left hand side of Eq. (5.2.5) can be written as

$$-[\nabla \cdot (A_{m,\ell} \nabla \xi_\ell)] W = -\nabla \cdot (W A_{m,\ell} \nabla \xi_\ell) + A_{m,\ell} \nabla \xi_\ell \cdot \nabla W. \tag{5.2.6}$$

With the Green's theorem, the following surface integral is transformed into a closed line integral along boundary Γ of the domain Ω_A

$$\iint_{\Omega_A} \nabla \cdot (W A_{m,\ell} \nabla \xi_\ell)\, d\Omega = \oint_\Gamma W A_{m,\ell} \frac{\partial \xi_\ell}{\partial n} d\Gamma. \tag{5.2.7}$$

Therefore, Eq. (5.2.5) becomes

$$\begin{aligned} &\iint_{\Omega_A} \left[\sum_{\ell=0}^{N_\xi} (A_{m,\ell} \nabla \xi_\ell \cdot \nabla W - B_{m,\ell} W \nabla h \cdot \nabla \xi_\ell - C_{m,\ell} \xi_\ell W) \right] d\Omega \\ &= \oint_\Gamma \left[\sum_{\ell=0}^{N_\xi} W A_{m,\ell} \frac{\partial \xi_\ell}{\partial n} \right] d\Gamma + \iint_{\Omega_A} i2\omega F W d\Omega, \\ &\qquad m = 0, 1, 2, 3, \cdots, N_\xi. \end{aligned} \tag{5.2.8}$$

Recall that $A_{m,\ell}$ is diagonal; therefore, the previous equation becomes

$$\begin{aligned} &\iint_{\Omega_A} \left[\sum_{\ell=0}^{N_\xi} (A_{m,\ell} \nabla \xi_\ell \cdot \nabla W - B_{m,\ell} W \nabla h \cdot \nabla \xi_\ell - C_{m,\ell} \xi_\ell W) \right] d\Omega \\ &= \oint_\Gamma \left[A_{m,m} \frac{\partial \xi_m}{\partial n} \right] d\Gamma + \iint_{\Omega_A} i2\omega F W d\Omega, \\ &\qquad m = 0, 1, 2, 3, \cdots, N_\xi. \end{aligned} \tag{5.2.9}$$

By employing the boundary conditions, Eqs. (5.2.2) and (5.2.4), the preceding equa-

tion becomes

$$\iint_{\Omega_A} \left[\sum_{\ell=0}^{N_\xi} (A_{m,\ell} \nabla \xi_\ell \cdot \nabla W - B_{m,\ell} W \nabla h \cdot \nabla \xi_\ell - C_{m,\ell} \xi_\ell W) \right] d\Omega$$
$$= \int_0^\pi \left[W A_{m,m} \left(\frac{\partial \xi_m^P}{\partial r} + \frac{\partial \xi_m^H}{\partial r} \right) \right] a d\theta + \iint_{\Omega_A} i2\omega F W d\Omega, \tag{5.2.10}$$
$$m = 0, 1, 2, 3, \cdots, N_\xi.$$

5.2.2 Discretized by triangular elements

Similar to Section 5.1.2, domain Ω_A is approximated as an assemblage of N_E discrete triangular elements with N_P nodes in which N_B boundary nodes are from node $N_P - N_B + 1$ to node N_P. Therefore, there are t $N_P - N_B$ interior nodal points. In addition, the continuous field variable ξ_ℓ is replaced by

$$\xi_\ell = \sum_{n=1}^{N_P} \xi_{\ell,n} \mathcal{W}_n \tag{5.2.11}$$

where $\mathcal{W}_n$ is the global weighting function (same as the ones in Section 5.1.2), and $\xi_{\ell,n}$ denotes the n-th unknown nodal coefficient of ξ_ℓ, which is assembled by the local nodal parameter $\xi^e_{\ell,i}$, $i = 1, 2, 3$.

W in the weighted integral equation is chosen to be the global weighting function $\mathcal{W}_\tau$. Therefore, with Eq. (5.2.11) and the Galerkin assumption, Eq. (5.2.10) is approximated as

$$\sum_{\ell=0}^{N_\xi} \sum_{n=1}^{N_P} \xi_{\ell,n} \left\{ \sum_{\Omega_e=1}^{N_E} \iint_{\Omega_e} \left[(A_{m,\ell} \nabla \mathcal{W}_n \cdot \nabla \mathcal{W}_\tau - B_{m,\ell} \mathcal{W}_\tau \nabla h \cdot \nabla \mathcal{W}_n - C_{m,\ell} \mathcal{W}_n \mathcal{W}_\tau) \right] d\Omega \right\}$$
$$- \int_0^\pi \mathcal{W}_\tau A_{m,m} \frac{\partial \xi_m^H}{\partial r} a d\theta = \int_0^\pi \mathcal{W}_\tau A_{m,m} \frac{\partial \xi_m^P}{\partial r} a d\theta + \sum_{\Omega_e=1}^{N_E} \iint_{\Omega_e} i2\omega F \mathcal{W}_\tau d\Omega,$$
$$m = 0, 1, 2, 3, \cdots, N_\xi, \qquad \tau = 0, 1, 2, 3, \cdots, N_\xi, \tag{5.2.12}$$

Recalling that

$$\xi_\ell^P = L_\ell^M \left[e^{i2kr\cos(\theta-\theta_I)} + e^{i2kr\cos(\theta+\theta_I)}\right] + L_\ell^N e^{i2kr\cos\theta_I\cos\theta}$$

with L_ℓ^M and L_ℓ^N being Eqns. (4.4.4) and (4.4.5) respectively, and the free waves ξ_ℓ^H with $N_{\widehat{\alpha}}+1$ unknown coefficients $\widehat{\alpha}_{\ell,p}$,

$$\xi_\ell^H = \sum_{p=0}^{N_{\widehat{\alpha}}} \epsilon_p \widehat{\alpha}_{\ell,p} K_p\left(\kappa_\ell r\right)\cos p\theta, \tag{5.2.13}$$

we can write Eq. (5.2.12) as

$$\begin{aligned}
&\sum_{\ell=0}^{N_\xi}\sum_{n=1}^{N_P}\xi_{\ell,n}\left\{\sum_{\Omega_e=1}^{N_E}\iint_{\Omega_e}\left(A_{m,\ell}\nabla\mathcal{W}_n\cdot\nabla\mathcal{W}_\tau - B_{m,\ell}\mathcal{W}_\tau\nabla h\cdot\nabla\mathcal{W}_n - C_{m,\ell}\mathcal{W}_n\mathcal{W}_\tau\right)d\Omega\right\}\\
&\quad - \sum_{p=0}^{N_\alpha}\widehat{\alpha}_{m,p}\left\{\left[\epsilon_p a\kappa_m A_{m,m}K_p'\left(\kappa_m a\right)\right]\int_0^\pi \mathcal{W}_\tau\cos p\theta d\theta\right\}\\
&= i2kaA_{m,m}L_m^M\int_o^\pi \mathcal{W}_\tau\left[\cos\left(\theta-\theta_I\right)e^{i2ka\cos(\theta-\theta_I)} + \cos\left(\theta+\theta_I\right)e^{i2ka\cos(\theta+\theta_I)}\right]d\theta\\
&\quad + i2kaA_{m,m}\cos\theta_I L_m^N\int_0^\pi \mathcal{W}_\tau e^{i2ka\cos\theta_I\cos\theta}\cos\theta d\theta + \sum_{\Omega_e=1}^{N_E} i2\omega\iint_{\Omega_e} F\mathcal{W}_\tau d\Omega,\\
&\qquad\qquad m=0,1,2,3,\cdots,N_\xi, \qquad \tau=0,1,2,3,\cdots,N_\xi.
\end{aligned} \tag{5.2.14}$$

Let us introduce the following abbreviation

$$\mathcal{K}_{\tau,n}^{(m,\ell)} = \sum_{\Omega_e=1}^{N_E}\iint_{\Omega_e}\left(A_{m,\ell}\nabla\mathcal{W}_n\cdot\nabla\mathcal{W}_\tau - B_{m,\ell}\mathcal{W}_\tau\nabla h\cdot\nabla\mathcal{W}_n - C_{m,\ell}\mathcal{W}_n\mathcal{W}_\tau\right)d\Omega, \tag{5.2.15}$$

$$\widehat{\mathcal{K}}_{\tau,p}^{(m,m)} = -\epsilon_p a\kappa_m A_{m,m}K_p'\left(\kappa_m a\right)\int_0^\pi \mathcal{W}_\tau\cos p\theta d\theta, \tag{5.2.16}$$

$$\mathcal{Y}_\tau^{(m)} = i2kaA_{m,m}L_m^M \int_0^\pi \mathcal{W}_\tau \left[\cos(\theta-\theta_I)\, e^{i2ka\cos(\theta-\theta_I)} + \cos(\theta+\theta_I)\, e^{i2ka\cos(\theta+\theta_I)}\right] d\theta + i2kaA_{m,m}\cos\theta_I L_m^N \int_0^\pi \mathcal{W}_\tau e^{i2ka\cos\theta_I\cos\theta}\cos\theta d\theta, \tag{5.2.17}$$

$$\widehat{\mathcal{Y}}_\tau^{(m)} = \sum_{\triangle_e=1}^{N_E} i2\omega \iint_{\triangle_e} F\mathcal{W}_\tau d\Omega, \tag{5.2.18}$$

Eq. (5.2.14) can then be expressed more compactly as

$$\sum_{\ell=0}^{N_\xi}\sum_{n=1}^{N_P} \xi_{\ell,n}\mathcal{K}_{\tau,n}^{(m,\ell)} + \sum_{p=0}^{N_\alpha-1} \alpha_{m,p}\widehat{\mathcal{K}}_{\tau,p}^{(m,m)} = \mathcal{Y}_\tau^{(m)} + \widehat{\mathcal{Y}}_\tau^{(m)}, \qquad m = 0,1,2,3,\cdots,N_\xi, \quad \tau = 0,1,2,3,\cdots,N_\xi. \tag{5.2.19}$$

The above integrals, $K_{\tau,n}^{(m,\ell)}$, $\widehat{K}_{\tau,p}^{(m,m)}$, $\mathcal{Y}_\tau^{(m)}$, $\widehat{\mathcal{Y}}_\tau^{(m)}$ are obtained as follows.

$\mathcal{K}_{\tau,n}^{(m,\ell)}$ is an assemblage of element stiffness matrices $E_{i,j}^{(m,\ell)}$,

$$\mathcal{K}_{\tau,n}^{(m,\ell)} = \sum_{\Omega_e=1}^{N_E} E_{i,j}^{(m,\ell)}, \quad \text{with} \begin{cases} i,j & \Rightarrow \text{local node,} \\ \tau,n & \Rightarrow \text{corresponding global node.} \end{cases} \tag{5.2.20}$$

The element stiffness matrices are obtained as follows. For a triangular element (see Section 5.1.2), we denote the centroid coordinates of a triangular element is

$$(\overline{x},\overline{y}) = \left(\frac{x_1+x_2+x_3}{3}, \frac{y_1+y_2+y_3}{3}\right) \tag{5.2.21}$$

Therefore, the element stiffness

$$E_{i,j}^{(m,\ell)} = \int_{\Omega_e} \left(A_{m,\ell}\nabla w_i^e \nabla w_j^e - B_{m,\ell} w_i^e \nabla h\cdot\nabla w_j^e - C_{m,\ell} w_i^e w_j^e\right) d\Omega \tag{5.2.22}$$

is obtained as

$$E_{i,j}^{(m,\ell)} = \frac{1}{4\Delta^e}\left[\overline{A_{m,\ell}}\left(b_i^2+c_i^2\right) - \overline{B_{m,\ell}}\left(\overline{\frac{\partial h}{\partial x}}b_i + \overline{\frac{\partial h}{\partial y}}c_i\right)\left(a_i+b_i\overline{x}+c_i\overline{y}\right) - \frac{2\Delta^2}{3}\overline{C_{m,\ell}}\right], \quad i=j, \tag{5.2.23}$$

$$E_{i,j}^{(m,\ell)} = \frac{1}{4\Delta^e}\left[\overline{A_{m,\ell}}\left(b_ib_j+c_ic_j\right) - \overline{B_{m,\ell}}\left(\overline{\frac{\partial h}{\partial x}}b_j + \overline{\frac{\partial h}{\partial y}}c_j\right)\left(a_i+b_i\overline{x}+c_i\overline{y}\right) - \frac{\Delta^2}{3}\overline{C_{m,\ell}}\right], \quad i\neq j, \tag{5.2.24}$$

where $\overline{()}$ is the averaged value within each element, and $\triangle^e$, w_i, a_i, b_i and c_i are defined in Section 5.1.2.

Using the facts that

$$A_{m,\ell}=0,\ m\neq\ell, \qquad B_{m,\ell}=0,\ m=\ell.$$

we obtain, when $m=\ell$

$$E_{i,j}^{(m,m)} = \frac{1}{4\Delta^e}\left[\overline{A_{m,m}}\left(b_i^2+c_i^2\right) - \frac{2\Delta^2}{3}\overline{C_{m,m}}\right], \quad i=j, \tag{5.2.25}$$

$$E_{i,j}^{(m,m)} = \frac{1}{4\Delta^e}\left[\overline{A_{m,m}}\left(b_ib_j+c_ic_j\right) - \frac{\Delta^2}{3}\overline{C_{m,m}}\right], \quad i\neq j, \tag{5.2.26}$$

and when $m\neq\ell$

$$E_{i,j}^{(m,\ell)} = \frac{1}{4\Delta^e}\left[-\overline{B_{m,\ell}}\left(\overline{\frac{\partial h}{\partial x}}b_i + \overline{\frac{\partial h}{\partial y}}c_i\right)\left(a_i+b_i\overline{x}+c_i\overline{y}\right) - \frac{2\Delta^2}{3}\overline{C_{m,\ell}}\right], \quad i=j, \tag{5.2.27}$$

$$E_{i,j}^{(m,\ell)} = \frac{1}{4\Delta^e}\left[-\overline{B_{m,\ell}}\left(\overline{\frac{\partial h}{\partial x}}b_j + \overline{\frac{\partial h}{\partial y}}c_j\right)\left(a_i+b_i\overline{x}+c_i\overline{y}\right) - \frac{\Delta^2}{3}\overline{C_{m,\ell}}\right], \quad i\neq j. \tag{5.2.28}$$

Therefore,

$$\mathcal{Y}_{\tau}^{(1)}=\begin{cases}0, & \tau<N_P-N_B+1,\\ iA_{m,m}kl^eY_q^{(m)}, & \tau=N_P-N_B+1,\\ iA_{m,m}kl^e\left(Y_{q-1}^{(m)}+Y_q^{(m)}\right), & N_P-N_B+1<\tau<N_P,\\ iA_{m,m}kl^eY_{q-1}^{(m)}, & \tau=N_P,\end{cases} \tag{5.2.29}$$

with

$$\begin{aligned}Y_q^{(m)}=&L_m^M\left[\cos\left(\theta_q^e-\theta_I\right)e^{ika\cos\left(\theta_q^e-\theta_I\right)}+\cos\left(\theta_q^e+\theta_I\right)e^{ika\cos\left(\theta_q^e+\theta_I\right)}\right]\\ &+L_m^N\cos\theta_I\cos\theta_q^e e^{i2ka\cos\theta_I\cos\theta_q^e},\qquad q=\tau-N_P+N_B,\end{aligned} \tag{5.2.30}$$

and

$$\mathcal{K}_{\tau,p}^{(m,m)}=\begin{cases}0, & \tau<N_P-N_B+1,\\ -\epsilon_pA_{m,m}\kappa_m\frac{l^e}{2}K_p'\left(\kappa_ma\right)\Theta_q, & \tau=N_P-N_B+1,\\ -\epsilon_pA_{m,m}\kappa_m\frac{l^e}{2}K_p'\left(\kappa_ma\right)\left(\Theta_{q-1}+\Theta_q\right), & N_P-N_B+1<\tau<N_P,\\ -\epsilon_pA_{m,m}\kappa_m\frac{l^e}{2}K_p'\left(\kappa_ma\right)\Theta_{q-1}, & \tau=N_P,\end{cases} \tag{5.2.31}$$

with

$$\Theta_q=\cos p\theta_q^e. \tag{5.2.32}$$

$\widehat{\mathcal{Y}}_{\tau}^{(m)}$ is an assemblage of the element integral $\widehat{\mathcal{Y}}_i^{(m^e)}$

$$\widehat{\mathcal{Y}}_{\tau}^{(m)}=\sum_{\Omega_e=1}^{N_E}\widehat{\mathcal{Y}}_i^{(m^e)} \tag{5.2.33}$$

with

$$\widehat{\mathcal{Y}}_i^{(m^e)}=i2\omega\iint_{\Omega_e}Fw_id\Omega=i2\omega\overline{F}\left(a_i+b_i\overline{x}+c_i\overline{y}\right) \tag{5.2.34}$$

where $\overline{F}$ is the averaged F over element e, and $i=1,2,3$.

Since $m=0,1,\cdots,N_\xi$, and $\tau=1,2,\cdots,N_P$, these constitute $(N_\xi+1)\times N_P$

equations. There are however, the same number of unknown nodal coefficients plus $(N_\xi + 1) \times (N_\alpha + 1)$ free-wave coefficients $\widehat{\alpha}_{m,p}$. The remaining equations are found from the matching condition Eq. (5.2.3), and let us rewrite it as

$$-\sum_{n=1}^{N_P} \xi_{\ell,n} \mathcal{W}_n + \sum_{p=0}^{N_{\widehat{\alpha}}} \epsilon_p \widehat{\alpha}_{\ell,p} K_p(\kappa_\ell a) \cos p\theta = -\xi_\ell^P - \xi_\ell^Q. \tag{5.2.35}$$

where Eqs. (5.2.11) and (5.2.13) are applied. Let us multiply Eq. (5.2.35) by a factor of $\left[\epsilon_p A_{\ell,\ell} \kappa_\ell K_p'(\kappa_\ell a) \cos p\theta\right]$, with $\ell = 0, 1, 2, \cdots, N_\xi$ and $p = 0, 1, 2, 3, \cdots, N_{\widehat{\alpha}}$ integrate along the semi-circle at $r = a$ and use of the identity of Eq. (5.1.33) We get

$$\left[\sum_{n=1}^{N_P} \widetilde{\mathcal{K}}_{p,n}^{(\ell,\ell)} \xi_{\ell,n}\right] + \check{\mathcal{K}}_{p,p}^{(\ell,\ell)} \widehat{\alpha}_{\ell,p} = \widetilde{\mathcal{Y}}_p^{(\ell)}, \qquad p = 0, 2, \cdots, N_\alpha, \tag{5.2.36}$$

where

$$\check{\mathcal{K}}_{p,p}^{(\ell,\ell)} = \epsilon_p^2 a A_{\ell,\ell} \kappa_\ell K_p'(\kappa_\ell a) K_p(\kappa_\ell a) \int_0^\pi \cos^2 \tau\theta d\theta = \epsilon_p \pi a A_{\ell,\ell} \kappa_\ell K_p'(\kappa_\ell a) K_p(\kappa_\ell a) \tag{5.2.37}$$

$$\widetilde{\mathcal{K}}_{p,n}^{(\ell,\ell)} = -\epsilon_p A_{\ell,\ell} \kappa_\ell K_p'(\kappa_\ell a) \int_0^\pi \mathcal{W}_n a \cos p\theta d\theta, \tag{5.2.38}$$

and

$$\widetilde{\mathcal{Y}}_p^{(\ell)} = -A_{\ell,\ell} \kappa_\ell a K_p'(\kappa_\ell a) \int_0^\pi \left(\xi_\ell^P + \xi_\ell^Q\right) \cos p\theta d\theta.$$

$\widetilde{\mathcal{Y}}_p^{(\ell)}$ is evaluated numerically, and $\widetilde{\mathcal{K}}_{p,n}^{(\ell,\ell)}$, is as follows.

$$\widetilde{\mathcal{K}}_{p,n}^{(\ell,\ell)} = \begin{cases} 0, & \tau < N_P - N_B + 1, \\ -\epsilon_p A_{\ell,\ell} \kappa_\ell \frac{l^e}{2} K_p'(\kappa_\ell a) \Theta_q, & n = N_P - N_B + 1, \\ -\epsilon_p A_{\ell,\ell} \kappa_\ell \frac{l^e}{2} K_p'(\kappa_\ell a) (\Theta_{q-1} + \Theta_q), & N_P - N_B + 1 < n < N_P, \\ -\epsilon_p A_{\ell,\ell} \kappa_\ell \frac{l^e}{2} K_p'(\kappa_\ell a) \Theta_{q-1}, & n = N_P, \end{cases} \tag{5.2.39}$$

with

$$\Theta_q = \cos p\theta_q^e. \tag{5.2.40}$$

Combining Eqs. (5.2.19) and (5.2.36), we can get a matrix equation as follows.

$$\begin{bmatrix} \mathbb{K}^{(0,0)} & \widehat{\mathbb{K}}^{(0,0)} & \cdots & \mathbb{K}^{(0,\ell)} & [0] & \cdots & \mathbb{K}^{(0,N_\xi)} & [0] \\ \check{\mathbb{K}}^{(0,0)} & \widetilde{\mathbb{K}}^{(0,0)} & \cdots & [0] & [0] & \cdots & [0] & [0] \\ \vdots & \vdots & \cdots & \vdots & \vdots & \cdots & \vdots & \vdots \\ \mathbb{K}^{(\ell,0)} & [0] & \cdots & \mathbb{K}^{(\ell,\ell)} & \widehat{\mathbb{K}}^{(\ell,\ell)} & \cdots & \mathbb{K}^{(\ell,N_\xi)} & [0] \\ [0] & [0] & \cdots & \check{\mathbb{K}}^{(\ell,\ell)} & \widetilde{\mathbb{K}}^{(\ell,\ell)} & \cdots & [0] & [0] \\ \vdots & \vdots & \cdots & \vdots & \vdots & \cdots & \vdots & \vdots \\ \mathbb{K}^{(N_\xi,0)} & [0] & \cdots & \mathbb{K}^{(N_\xi,\ell)} & [0] & \cdots & \mathbb{K}^{(N_\xi,N_\xi)} & \widehat{\mathbb{K}}^{(N_\xi,N_\xi)} \\ [0] & [0] & \cdots & [0] & [0] & \cdots & \check{\mathbb{K}}^{(N_\xi,N_\xi)} & \widetilde{\mathbb{K}}^{(N_\xi,N_\xi)} \end{bmatrix} \begin{bmatrix} \mathcal{X}^{(0)} \\ \widehat{\mathcal{X}}^{(0)} \\ \vdots \\ \mathcal{X}^{(\ell)} \\ \widehat{\mathcal{X}}^{(\ell)} \\ \vdots \\ \mathcal{X}^{(N_\xi)} \\ \widehat{\mathcal{X}}^{(N_\xi)} \end{bmatrix} = \begin{bmatrix} \mathcal{Y}^{(0)} \\ \widehat{\mathcal{Y}}^{(0)} \\ \vdots \\ \mathcal{Y}^{(m)} \\ \widehat{\mathcal{Y}}^{(m)} \\ \vdots \\ \mathcal{Y}^{(N_\xi)} \\ \widehat{\mathcal{Y}}^{(N_\xi)} \end{bmatrix} \tag{5.2.41}$$

with

$$\mathcal{X}^{(\ell)} = \begin{bmatrix} \xi_{\ell,1} \\ \vdots \\ \xi_{\ell,n} \\ \vdots \\ \xi_{\ell,N_\xi} \end{bmatrix}, \quad \widehat{\mathcal{X}}^{(\ell)} = \begin{bmatrix} \widehat{\alpha}_{\ell,0} \\ \vdots \\ \widehat{\alpha}_{\ell,p} \\ \vdots \\ \widehat{\alpha}_{\ell,N_\alpha} \end{bmatrix},$$

$$\mathcal{Y}^{(m)} = \begin{bmatrix} \mathcal{Y}_1^{(m)} \\ \vdots \\ \mathcal{Y}_{N_P-N_B}^{(m)} \\ \mathcal{Y}_{N_P-N_B+1}^{(m)} + \widehat{\mathcal{Y}}_{N_P-N_B+1}^{(m)} \\ \vdots \\ \mathcal{Y}_{N_P}^{(m)} + \widehat{\mathcal{Y}}_{N_P}^{(m)} \end{bmatrix}, \quad \widetilde{\mathcal{Y}}^{(m)} = \begin{bmatrix} \widetilde{\mathcal{Y}}_0^{(m)} \\ \vdots \\ \widetilde{\mathcal{Y}}_p^{(m)} \\ \vdots \\ \widetilde{\mathcal{Y}}_{N_\alpha}^{(m)} \end{bmatrix}.$$

The entries for $\mathbb{K}^{(m,\ell)}$, $\widehat{\mathbb{K}}^{(m,\ell)}$ and $\check{\mathbb{K}}^{(\ell,\ell)}$ are $\mathcal{K}_{\tau,n}^{(m,\ell)}$, $\widehat{\mathcal{K}}_{\tau,n}^{(m,\ell)}$, $\check{\mathcal{K}}_{\tau,n}^{(\ell,\ell)}$ respectively , $\widetilde{\mathbb{K}}^{(\ell,\ell)}$ is diagnal matrix with entries being $\widetilde{\mathcal{K}}_{\tau,\tau}^{(\ell,\ell)}$. These matrix equations can be solved numerically again by using the UC Berkeley programme *Distributed SuperLU*.

In the limit of constant depth everywhere, the above matrix equation can be

separated in to $N_\xi + 1$ uncoupled matrix equations as follows,

$$\begin{bmatrix} \mathbb{K}^{(m,m)} & \widehat{\mathbb{K}}^{(m,m)} \\ \check{\mathbb{K}}^{(m,m)} & \widetilde{\mathbb{K}}^{(m,m)} \end{bmatrix} \begin{bmatrix} \mathcal{X}^{(m)} \\ \widehat{\mathcal{X}}^{(m)} \end{bmatrix} = \begin{bmatrix} \mathcal{Y}^{(m)} \\ \widehat{\mathcal{Y}}^{(m)} \end{bmatrix}, \qquad m = 0, 1, 2, 3, \cdots, N_\xi. \tag{5.2.42}$$

Before discussing numerical example, let us examine a special case of constant depth in the next chapter.

Chapter 6

Analytical Solution for a Semi-Circular Peninsula in Constant Depth

For a semi-circular peninsula (or a vertical cylinder on a cliff) along a straight coast and in constant depth, no finite elements are needed. The region Ω_A is not needed and the radius of the semi-circular cylinder R_a is equal to radius a of the semi circle ∂A. Hence, an exact analytical solution can be found. Effects of the angle of incidence are examined for the free surface height along the cylinder.

6.1 First-order solution

We recall the familiar first-order result of diffraction by a vertical cylinder in an open sea without a coast

$$\eta_{cylinder} = \frac{A}{2}\left[e^{ikr\cos(\theta-\theta_I)} - \sum_{m=0}^{\infty}\epsilon_m i^m \frac{J'_m(ka)}{H'_m(ka)} H_m(kr)\cos m(\theta-\theta_I)\right]. \qquad (6.1.1)$$

The first-order result for a semi-circular peninsula can be obtained easily by using the method of images and summing up the two first-order results for a vertical cylinder with opposite incident angles(see Figure 6-1). Hence, with the effect of a

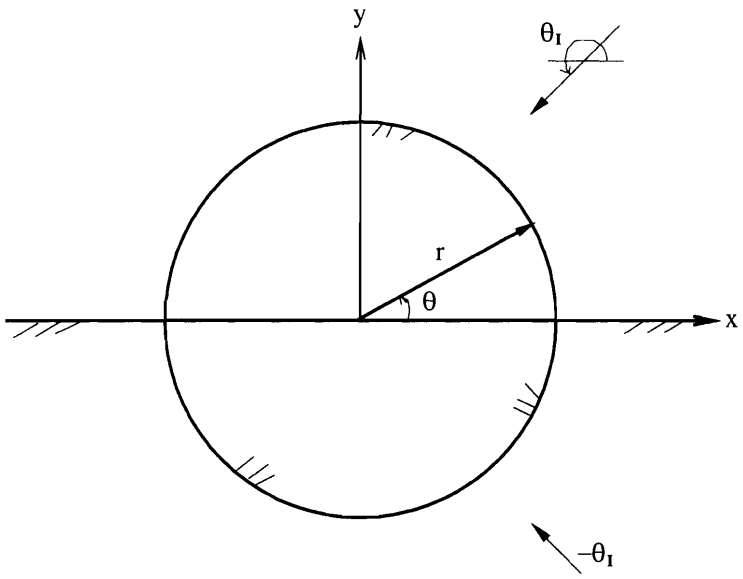

Figure 6-1: Method of image

coastline, the first-order result becomes

$$\eta = \eta^{(T)} + \eta^{(S)} \tag{6.1.2}$$

where $\eta^{(T)}$ being Eq. (4.1.2) and the scattered wave $\eta^{(S)}$ being Eq. (4.1.5) with coefficients

$$\alpha_m = 2\frac{J'_m(ka)}{H'_m(ka)}\cos m\theta_I, \quad m = 0, 1, 2, 3, \cdots .$$

6.2 Second-order solution

At the second-order, the free wave satisfies the boundary conditions along the coast

$$\frac{\partial \xi_\ell^H}{\partial \theta} = 0, \quad \theta = 0,\ \pi, \quad \ell = 0, 1, 2, 3, \cdots , \tag{6.2.3}$$

and on the peninsula

$$\frac{\partial \xi_\ell^H}{\partial r} = -\frac{\partial \xi_\ell^P}{\partial r}, \quad r = a,\ 0 \le \theta \le \pi, \quad \ell = 0, 1, 2, 3, \cdots . \tag{6.2.4}$$

Using the partial wave expansions for the plane waves

$$e^{i2kr\cos(\theta\mp\theta_I)} = \sum_{m=0}^{\infty} \epsilon_m i^m J_m(2kr)\cos m(\theta \mp \theta_I), \tag{6.2.5}$$

$$e^{i2kr\cos\theta_I\cos\theta} = \sum_{m=0}^{\infty} \epsilon_n i^m J_m(2kr\cos\theta_I)\cos m\theta, \tag{6.2.6}$$

and

$$e^{i2kr\cos(\theta-\theta_I)} + e^{i2kr\cos(\theta+\theta_I)} = \sum_{m=0}^{\infty} \epsilon_m i^m J_m(2kr) 2\cos m\theta_I \cos m\theta, \tag{6.2.7}$$

we rewrite ξ_ℓ^P as

$$\xi_\ell^P = L_\ell^M \sum_{m=0}^{\infty} \epsilon_m i^m J_m(2kr) 2\cos m\theta_I \cos m\theta + L_\ell^N \sum_{m=0}^{\infty} \epsilon_m i^m J_m(2kr\cos\theta_I)\cos m\theta \tag{6.2.8}$$

Using Eq. (4.1.5) for ξ_ℓ^H and applying Equation (6.2.4), we obtain

$$\begin{aligned} -\frac{\partial \xi_\ell^P}{\partial r} =& - L_\ell^M \sum_{m=0}^{\infty} \epsilon_m i^m J'_m(2ka) 2k 2\cos m\theta_I \cos n\theta \\ & - L_\ell^N \sum_{m=0}^{\infty} \epsilon_m i^m J'_m(2ka\cos\theta_I) 2k\cos\theta_I \cos m\theta, \quad r = a,\ 0 \le \theta \le \pi, \end{aligned} \tag{6.2.9}$$

and

$$\frac{\partial \xi_\ell^H}{\partial r} = \sum_{m=0}^{\infty} \epsilon_m \alpha_{\ell,m} K'_m(\kappa_\ell a)\kappa_\ell \cos m\theta. \qquad r = a,\ \ 0 \le \theta \le \pi, \tag{6.2.10}$$

Therefore,

$$\alpha_{\ell,m} = -i^m L_\ell^M \frac{J'_m(2ka)}{K'_m(\kappa_\ell a)\kappa_\ell} 4k\cos m\theta_I - i^m L_\ell^N \frac{J'_m(2ka\cos\theta_I)}{K'_m(\kappa_\ell a)\kappa_\ell} 2k\cos\theta_I. \tag{6.2.11}$$

In summary

$$\xi_\ell^H = \sum_{m=0}^{\infty} \epsilon_m i^m K_m(\kappa_\ell r)\cos m\theta \left[-L_\ell^M \frac{J'_m(2ka)}{K'_m(\kappa_\ell a)\kappa_\ell} 4k\cos m\theta_I \right. \\ \left. -L_\ell^N \frac{J'_m(2ka\cos\theta_I)}{K'_m(\kappa_\ell a)\kappa_\ell} 2k\cos\theta_I \right]. \tag{6.2.12}$$

The corresponding potential Φ_2^H is

$$\Phi_2^H = \sum_{\ell=0}^{\infty} \xi_\ell^H f_\ell = \sum_{\ell=0}^{\infty} \frac{\cos(\kappa_\ell(z+h))}{\cos\kappa_\ell h} \sum_{m=0}^{\infty} \epsilon_m i^m K_m(\kappa_\ell r)\cos m\theta \times \\ \left[-L_\ell^M \frac{J'_m(2ka)}{K'_m(\kappa_\ell a)\kappa_\ell} 4k\cos m\theta_I - L_\ell^N \frac{J'_m(2ka\cos\theta_I)}{K'_m(\kappa_\ell a)\kappa_\ell} 2k\cos\theta_I \right] \tag{6.2.13}$$

In summary, the amplitude of the second-order displacement $\eta_{2,2}^{(2)}$ is obtained as the sum of Eqs. (4.4.6), (4.4.57) and (6.2.12),

$$\eta_{2,2}^{(2)}(r,\theta) = \sum_{\ell=0}^{\infty}\sum_{m=0}^{\infty} \epsilon_m \cos m\theta \left\{ i^m L_\ell^M 2\cos m\theta_I \left[J_m(2kr) - \frac{2k}{\kappa_\ell} \frac{J'_m(2ka)}{K'_m(\kappa_\ell a)} K_m(\kappa_\ell r) \right] \right. \\ + i^m L_\ell^N \left[J_m(2kr\cos\theta_I) - \frac{2k\cos\theta_I}{\widehat{\kappa_\ell}} \frac{J'_m(2ka\cos\theta_I)}{K'_m(\kappa_\ell a)} K_m(\kappa_\ell r) \right] \\ \left. + \int_a^{\infty} r_0 dr_0 \left[-i\frac{2\omega \mathcal{Q}_m(r_0)}{A_{\ell,\ell}} \right] K_m(\kappa_\ell r_>) \left[\frac{I'_m(\kappa_\ell a)}{K'_m(\kappa_\ell a)} K_m(\kappa_\ell r_<) - I_m(\kappa_\ell r_<) \right] \right\}. \tag{6.2.14}$$

In particular, the value on the peninsula is

$$\eta_{2,2}^{(2)}(a,\theta) = \sum_{\ell=0}^{\infty}\sum_{m=0}^{\infty} \epsilon_m \cos m\theta \left\{ i^m L_\ell^M 2\cos m\theta_I \left[J_m(2ka) - \frac{2k}{\kappa_\ell} \frac{J'_m(2ka)}{K'_m(\kappa_\ell a)} K_m(\kappa_\ell a) \right] \right. \\ + i^m L_\ell^N \left[J_m(2ka\cos\theta_I) - \frac{2k\cos\theta_I}{\widehat{\kappa_\ell}} \frac{J'_m(2ka\cos\theta_I)}{K'_m(\kappa_\ell a)} K_m(\kappa_\ell a) \right] \\ \left. + \frac{1}{\kappa_l a} \int_a^{\infty} r_0 dr_0 \left[-i\frac{2\omega \mathcal{Q}_m(r_0)}{A_{\ell,\ell}} \right] \frac{K_m(\kappa_\ell r_0)}{K'_m(\kappa_\ell a)} \right\}. \tag{6.2.15}$$

Combined with (3.1.11), the second-order free surface displacement for semi-

circular peninsula is completely determined.

6.3 Numerical Validation

When the incident wave is parallel to the coastline either from the left ($\theta_I = 0$), the first-order incident and reflected waves are in the same direction

$$\eta^{(I)} = \eta^{(R)} = \frac{A}{2} e^{\pm ikr\cos\theta},\ \eta^{(T)} = 2\eta^{(I)} = Ae^{\pm ikr\cos\theta} \tag{6.3.16}$$

so that their total amplitude is $2A$ which can be treated as the full cylinder attacked by one incident waves. The second-order progressive waves ξ^I and ξ^{IR} now have the same direction with amplitude

$$L_\ell^N = \frac{2i\omega}{A_{\ell,\ell}} \frac{A^2}{2} \frac{\left(\widehat{\beta} - \bar{\beta}k^2\right)}{4k^2 + \kappa_\ell^2} = 2L_\ell^M. \tag{6.3.17}$$

The total second-order progressive waves is four times of that of the Stokes waves

$$\varphi_2^P = \sum_{\ell=0}^{\infty} \xi_\ell^P \frac{\cos\kappa_\ell(h+z)}{\cos\kappa_\ell h} = \frac{3A^2\omega^2}{2g} \frac{\cosh 2kh}{\sinh^4 kh} e^{\pm i2kr\cos\theta}. \tag{6.3.18}$$

The complete solution $\eta_{2,2}^{(2)}$ of a vertical cylinder is

$$\begin{aligned}\eta_{2,2}^{(2)}(r,\theta) = \sum_{\ell=0}^{\infty}\sum_{m=0}^{\infty} \epsilon_m \cos m\theta \Bigg\{ & i^m 4L_\ell^M 2 \left[J_m(2kr) - \frac{2k}{\kappa_\ell} \frac{J_m'(2ka)}{K_m'(\kappa_\ell a)} K_m(\kappa_\ell r) \right] \\ & + \int_a^\infty r_0 dr_0 \left[-i\frac{2\omega \mathcal{Q}_m(r_0)}{A_{l,l}} \right] K_m(\kappa_l r_>) \left[\frac{I_m'(\kappa_l a)}{K_m'(\kappa_l a)} K_m(\kappa_l r_<) - I_m(\kappa_l r_<) \right] \Bigg\}.\end{aligned} \tag{6.3.19}$$

In particular, the run up on the cylinder is

$$\begin{aligned}\eta_{2,2}^{(2)}(a,\theta) = \sum_{\ell=0}^{\infty}\sum_{m=0}^{\infty} \epsilon_m \cos m\theta \Bigg\{ & i^m 4L_\ell^M 2 \left[J_m(2ka) - \frac{2k}{\kappa_\ell} \frac{J_m'(2ka)}{K_m'(\kappa_\ell a)} K_m(\kappa_\ell a) \right] \\ & + \frac{1}{\kappa_l a} \cos m\theta \int_a^\infty r_0 dr_0 \left[-i\frac{2\omega \mathcal{Q}_m(r_0)}{A_{l,l}} \right] \frac{K_m(\kappa_l r_0)}{K_m'(\kappa_l a)} \Bigg\}.\end{aligned} \tag{6.3.20}$$

This closed-form solution is equivalent to the result of Chau & Eatock Taylor (1992) who started with a three-dimensional Green's function involving the eigenfunctions in z.

As a check for the correctness and accuracy, we have carried out computations for the earlier works (Kim & Yue ,1989) for the case of $\theta_I = 0$ with $r/a = 1, h/a = 1$, $\omega^2 a/g = 2$. Fig. 6-2 shows the agreement of the radial variation of the amplitudes of the second-order free-surface forcing terms, $\epsilon_m \mathcal{Q}_m/(2gk^2A^2/\omega)$ away from the vertical cylinder, r/a with the numerical results of Kim and Yue(1989). The first-order solution is trivial. Therefore, only the second-order amplitudes, $\eta^{(1)}_{2,0}$, $\eta^{(1)}_{2,2}$, $\eta^{(2)}_{2,2}$ are shown in Fig. 6-3. As seen in Figure 6-2- 6-3, our solution agrees well with numerical solution of Kim and Yue (1989) and Chau and Eatock Taylor(1992). Note that our $2A$ is their amplitude of the incident wave.

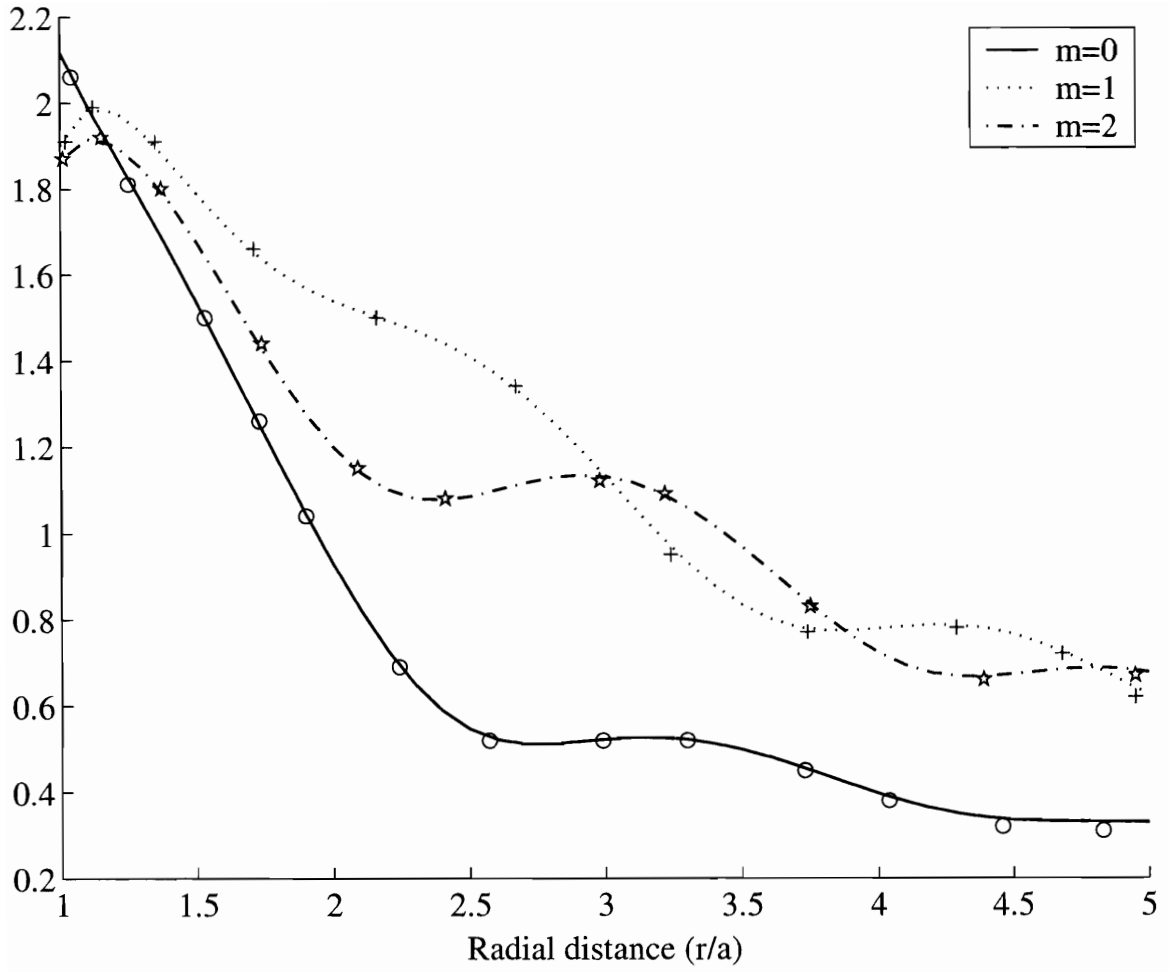

Figure 6-2: Dimensionless amplitudes of the dimensionless second-order free-surface forcing terms, $\epsilon_m \mathcal{Q}_m/(2gk^2A^2/\omega)$ of the first three modes as a function of the dimensionless radial distance from the vertical cylinder, r/a . Input: $h/a = 1$, $\omega^2 a/g = 2$. $+$, $\star$ and $\circ$ are the data from Kim and Yue(1989). Solid, dot, and dash-dot lines are our numerical result.

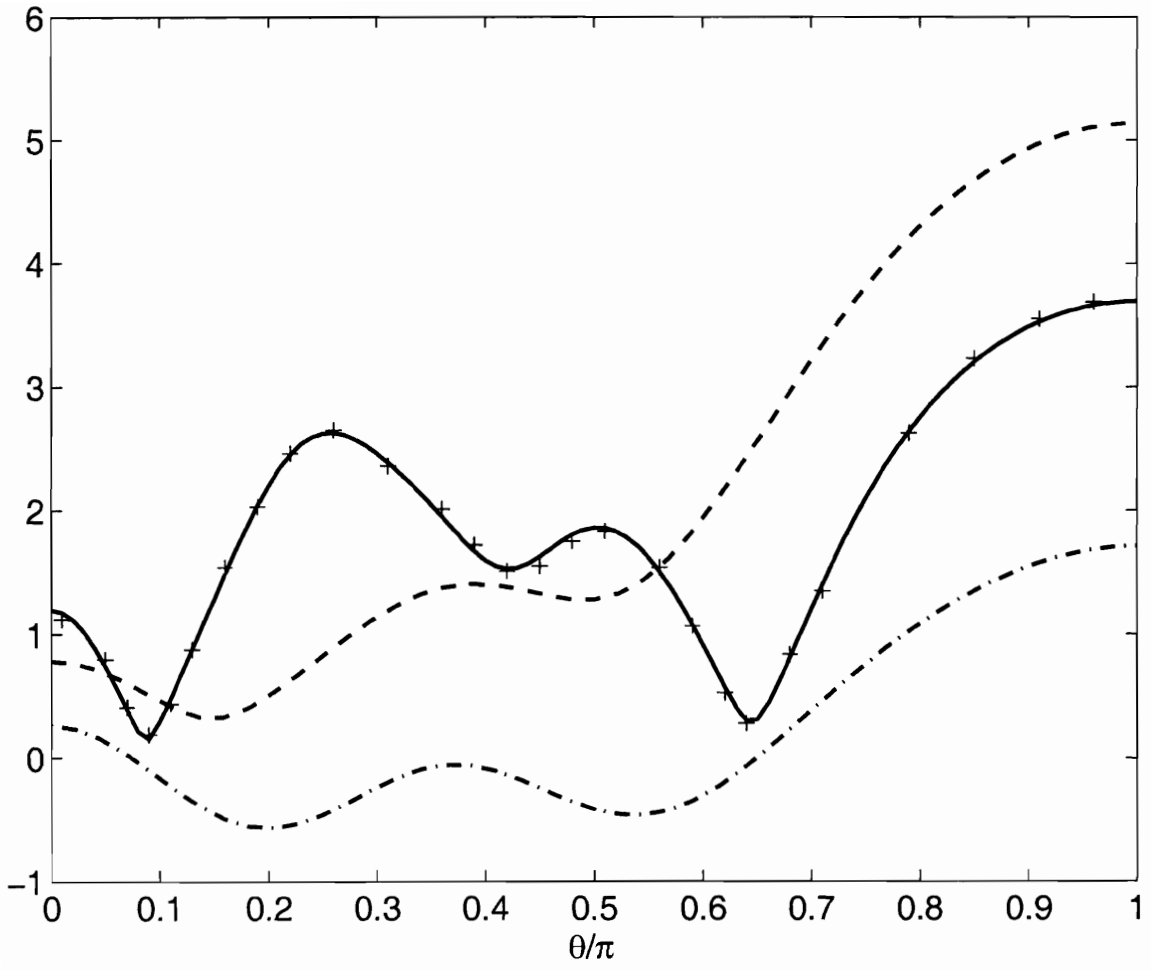

Figure 6-3: Comparison of our theory in the limit of $\theta_I = 0$ with Chau and Eatock Taylor(1992) and Kim and Yue (1989)(+++). Dimensionless amplitudes of $\eta^{(1)}_{2,0}/(4A^2/a)$ $(\cdot - \cdot -)$, $|2\eta^{(1)}_{2,2}|/(4A^2/a)$ $(- -)$ and $|2\eta^{(2)}_{2,2}|/(4A^2/a)$ (—) are evaluated along the semicircle $r = a$. Input data are : $h/a = 1, \omega^2 a/g = 2$.

6.4 Effects of Incidence Angle and Cylinder Radius

We have carried out a number of computations to study the effects of incidence angle and the cylinder radius. The free-surface displacements (runup) along the circumference of the cylinder are shown for a fixed depth-to-wavelength ratio $kh = 1$. Three angle of incidences : $\theta_I = \pi$ (glancing), $5\pi/4$ (oblique) and $3\pi/2$ (normal) and four radius-to-wavelength ratios are considered.

In computing the double series of $\mathcal{Q}$ defined in (4.3.19) and (D.1.12), both m and n must be truncated after a finite number of terms. These numbers are found by numerical experiments for a fixed error allowance, chosen to be 10^{-5}. As shown in Table 6.1 the numbers increase for larger ka. In addition, the integral for the propagating mode $\ell = 0$ in (6.3.20) is evaluated by sectioning the integration path. Over one section from a to a finite but large R numerical integration is performed by the Gaussian 3-points adaptive method. In the remaining section from R to ∞, asymptotic approximatons are used as in Chau & Eatock Taylor (1992). To limit the number of evanescent modes in the ℓ series converges, we use Domb-Sykes extrapolation scheme. By defining the truncated sum as

$$y_m^{(l)} = \sum_{\ell=0}^{l} \kappa_l a \int_a^\infty r_0 dr_0 \left[-i \frac{2\omega \mathcal{Q}_m(r_0)}{A_{\ell,\ell}} \right] \frac{K_m(\kappa_l r_0)}{K'_m(\kappa_\ell a)}. \tag{6.4.21}$$

The final result is obtained from the limit of $1/l = 0$. Choosing just two values l and $l+1$, the limit by linear extrapolation gives

$$y_m^{(\infty)} = y_m^{(l+1)} - \ell \left[y_m^{(l)} - y_m^{(l+1)} \right], \tag{6.4.22}$$

In all the computations, the number of the evanescent modes is chosen to be MAX $l = 10$; the relative error of $y_m^{(\infty)}$ is less than 10^{-3}.

To help understand the second-order results we first display in Figure 6-4 the first-order runup along the cylinder. As is well known, for the smallest cylinder $ka = 0.1$, the runup is quite uniform in all directions, and the effect of incidence angle is small. As the cylinder radius increases relative to the wavelength, the

m, n	$ka = 0.1$	$ka = 1$	$ka = 0.5$	$ka = 10$
$\theta_I = \pi$	6,7	10,11	23,19	34,26
$\theta_I = 5\pi/4$	6,7	10,11	22,19	34,27
$\theta_I = 3\pi/2$	5,6	10,10	21,18	35,27

Table 6.1: Number of terms (m, n) used in the double series for Q.

effect of incidence angle becomes more pronounced. For glancing incidence, the runup is the greatest on the incidence side (small θ), and the smallest in the shadow ($\theta \approx \pi$). For normal incidence the runup varies strongly in different directions with the greatest run-up at the corners($\theta = 0, \pi$). The directional variation is oscillatory and symmetrical about the shore-normal axis. With increasing ka, oscillations become more prominant.

The second-order setup and setdown along the semi-circle is shown in Figure 6-5. This quantity is the time-averaged part of the Bernoulli effect on the free surface (cf. Eq. (2.2.12)). For the smallest cylinder, the maximum setdown occurs in the direction $\theta = \pi/2$, being the largest for glancing incidence and smallest for normal incidence. With increasing ka the setup and setdown vary with direction in ways similar to the first-order, first-harmonic runup. The largest mean setup occurs near $\theta = 0$.

The second-harmonic runup contains two parts. The part due to the first-order interations (cf. Eq. (2.2.12)) is shown in Figure 6-6. For glancing incidence, the greatest runup is at $\theta = \pi/2$ for the smallest cylinder but near the corner facing the incoming wave for the largest cylinder. For normal incidence, the runup is oscillatory in θ and symmetrical with respect to the axis $\theta = \pi/2$, similar to the first-order, first-harmonic runup. The part due to second-order potential is shown in Figure 6-7. For glancing incidence, the greatest response appears at $\theta = 0$ for the smallest cylinder, but near $\theta = \pi/2$ for the larger cylinders. The total second-harmonic runup is also shown in Figure 6-8. The relative magnitudes and phases between $\eta_{2,2}^{(1)}$ and $\eta_{2,2}^{(2)}$ depend on θ. The magnitudes of two parts in the total second-harmonic runup are comparable.

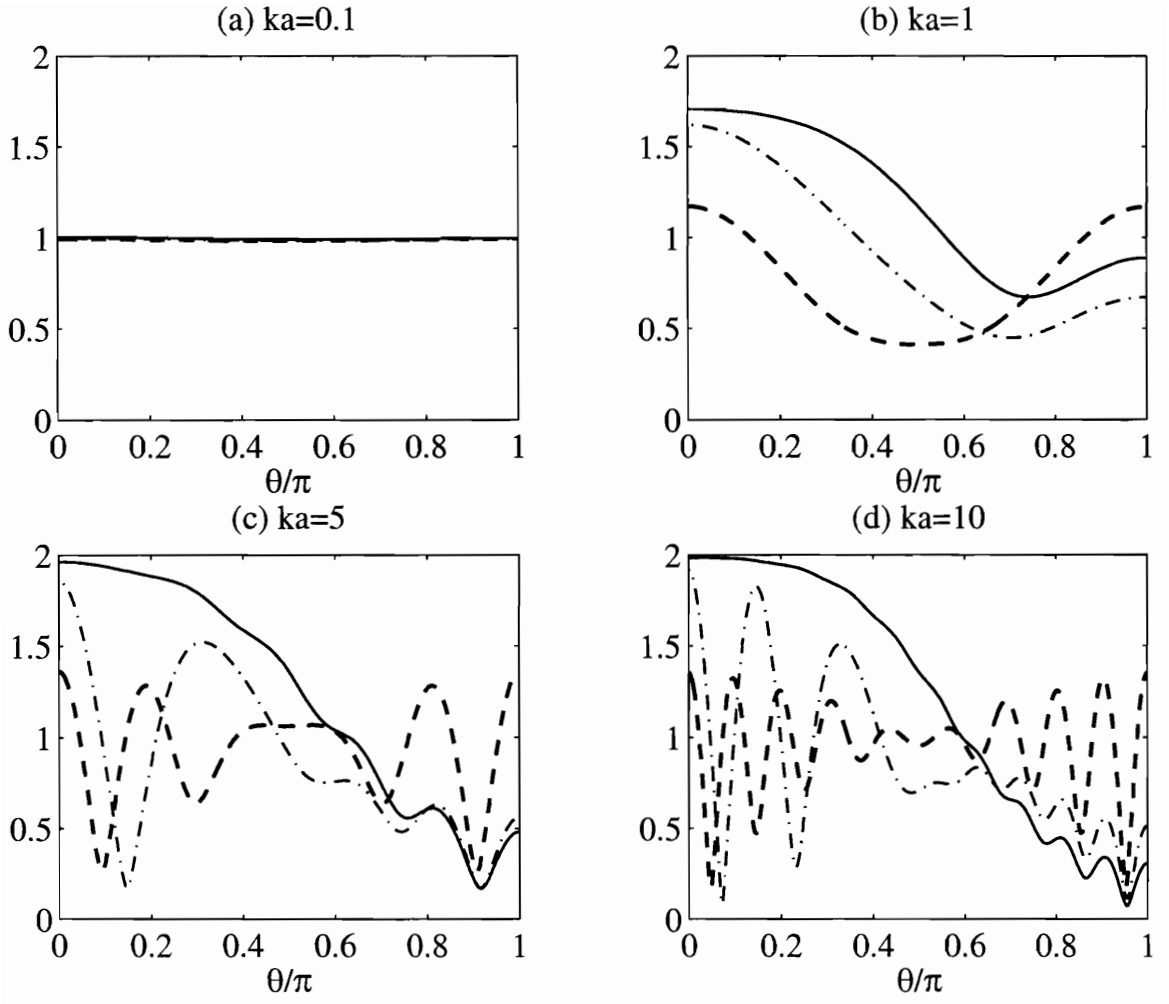

Figure 6-4: Dimensionless amplitudes of first-order $|\eta/A|$ along the semi-circular peninsula, for different angle of incidence $\theta_I = \pi$(—), $5\pi/4$(– · –), $3\pi/2$(– –). Input data are $kh = 1$, (a) $ka = 0.1$ (b) $ka = 1$(c) $ka = 5$ (d) $ka = 10$.

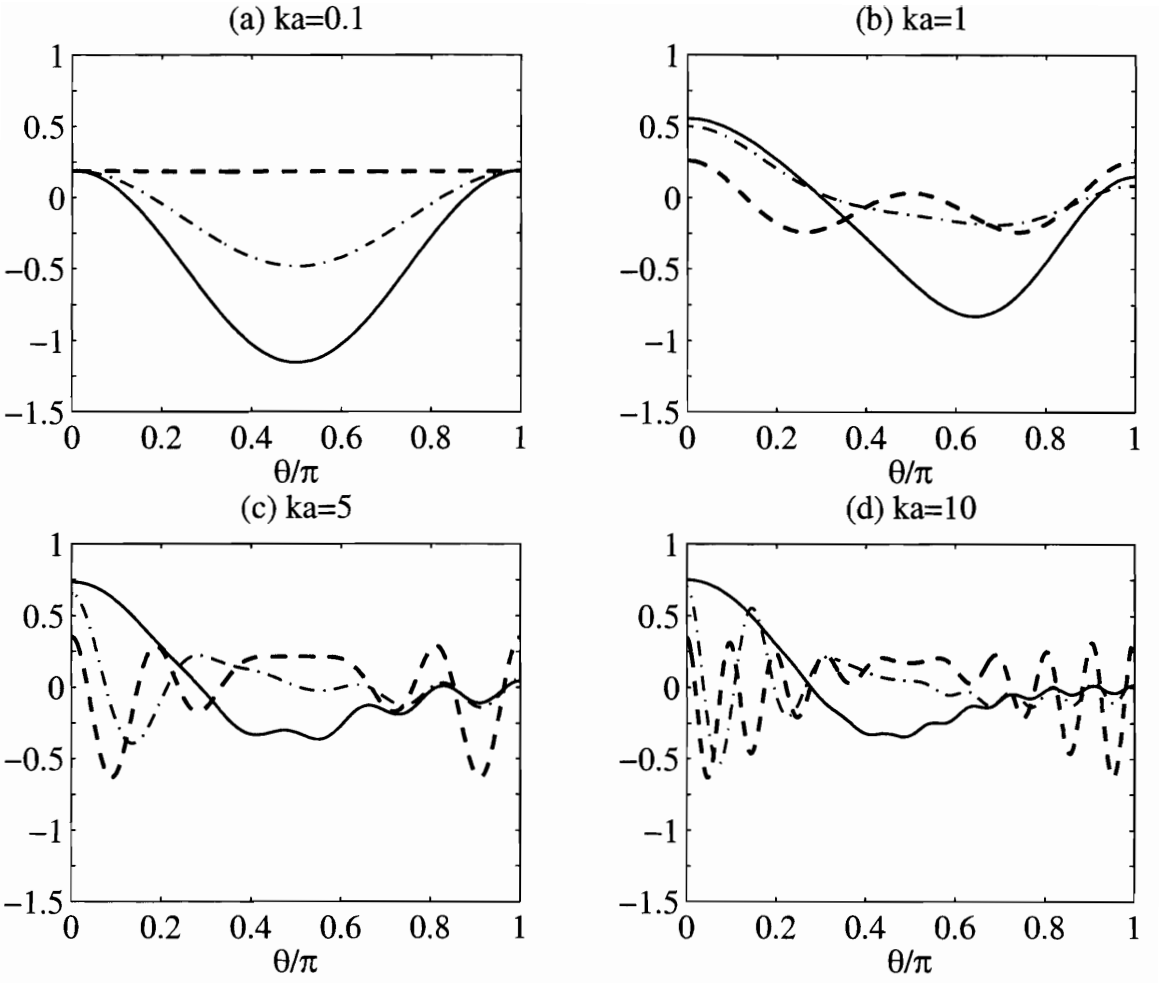

Figure 6-5: Dimensionless amplitudes of second-order $\eta^{(1)}_{2,0}/(4kA^2)$ along the semi-circular peninsula, for different angle of incidence $\theta_I = \pi$(—), $5\pi/4$(– · –), $3\pi/2$(– –). Input data are $kh = 1$, (a) $ka = 0.1$ (b) $ka = 1$(c) $ka = 5$ (d) $ka = 10$.

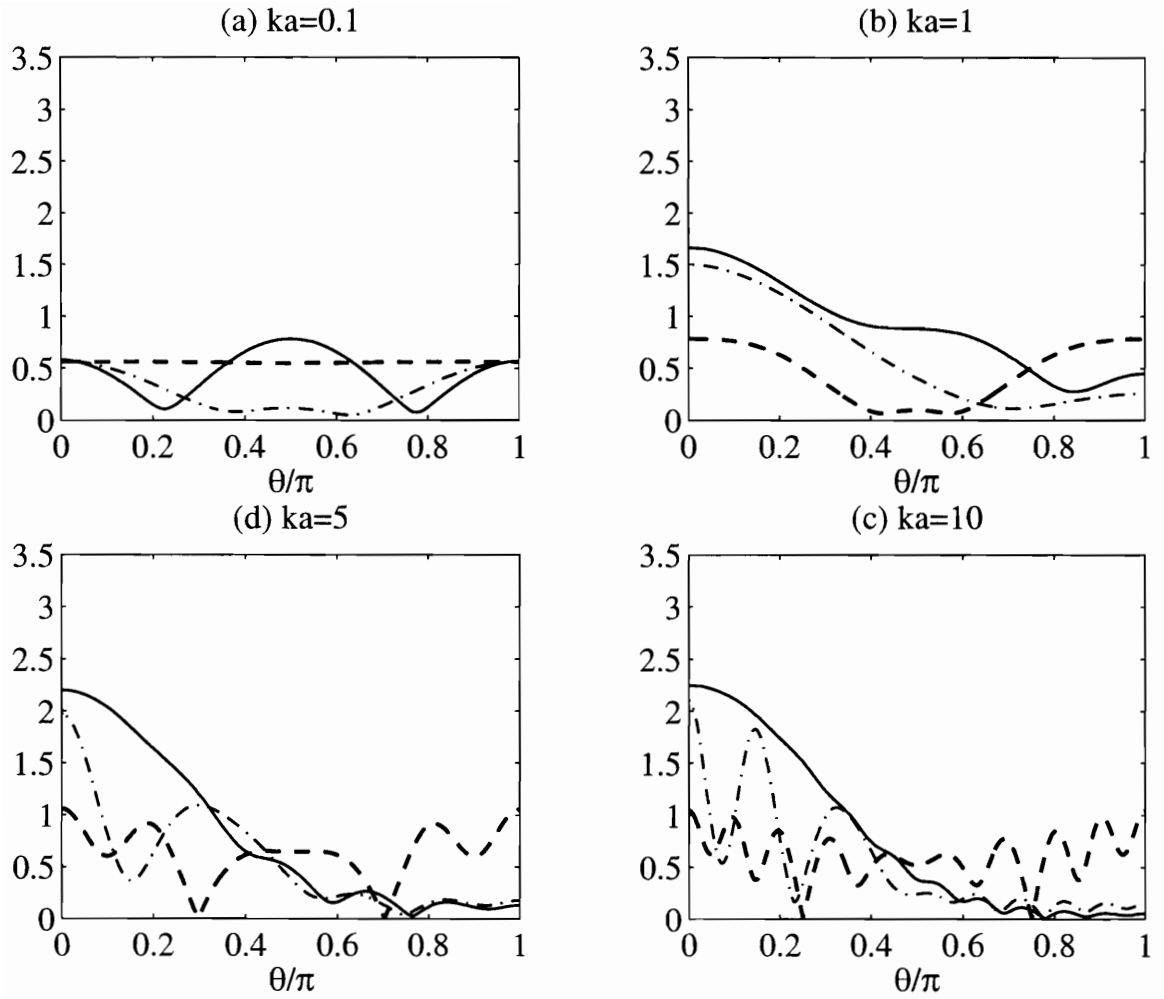

Figure 6-6: Dimensionless amplitudes of second-order $|\eta^{(1)}_{2,2}|/(2kA^2)$ along the semi-circular peninsula, for different angle of incidence $\theta_I = \pi$(—), $5\pi/4$(– · –), $3\pi/2$(– –). Input data are $kh = 1$, (a) $ka = 0.1$ (b) $ka = 1$(c) $ka = 5$ (d) $ka = 10$.

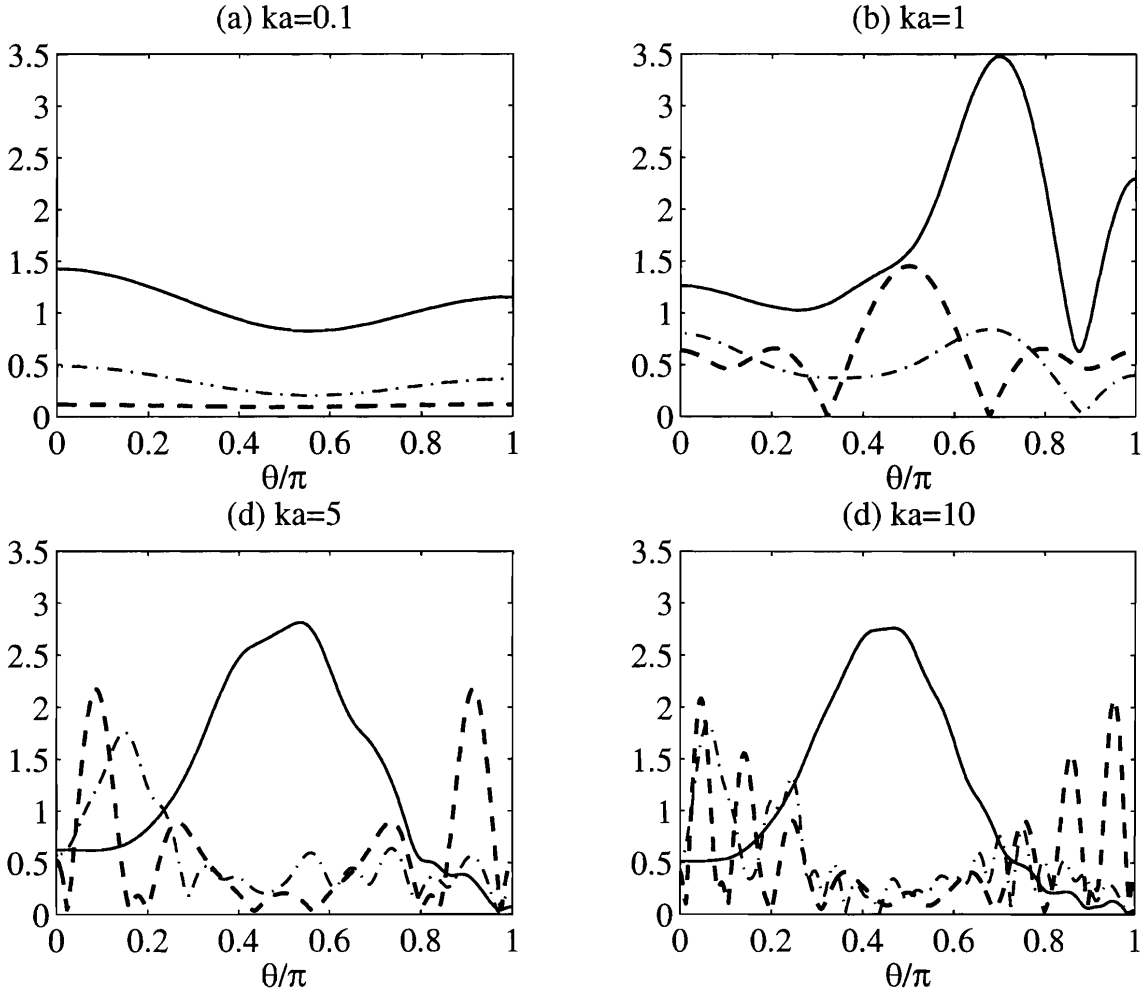

Figure 6-7: Dimensionless amplitudes of second-order $|\eta_{2,2}^{(2)}|/(2kA^2)$ along the semi-circular peninsula, for different angle of incidence $\theta_I = \pi$(—), $5\pi/4$(– · –), $3\pi/2$(– –). Input data are $kh = 1$, (a) $ka = 0.1$ (b) $ka = 1$(c) $ka = 5$ (d) $ka = 10$.

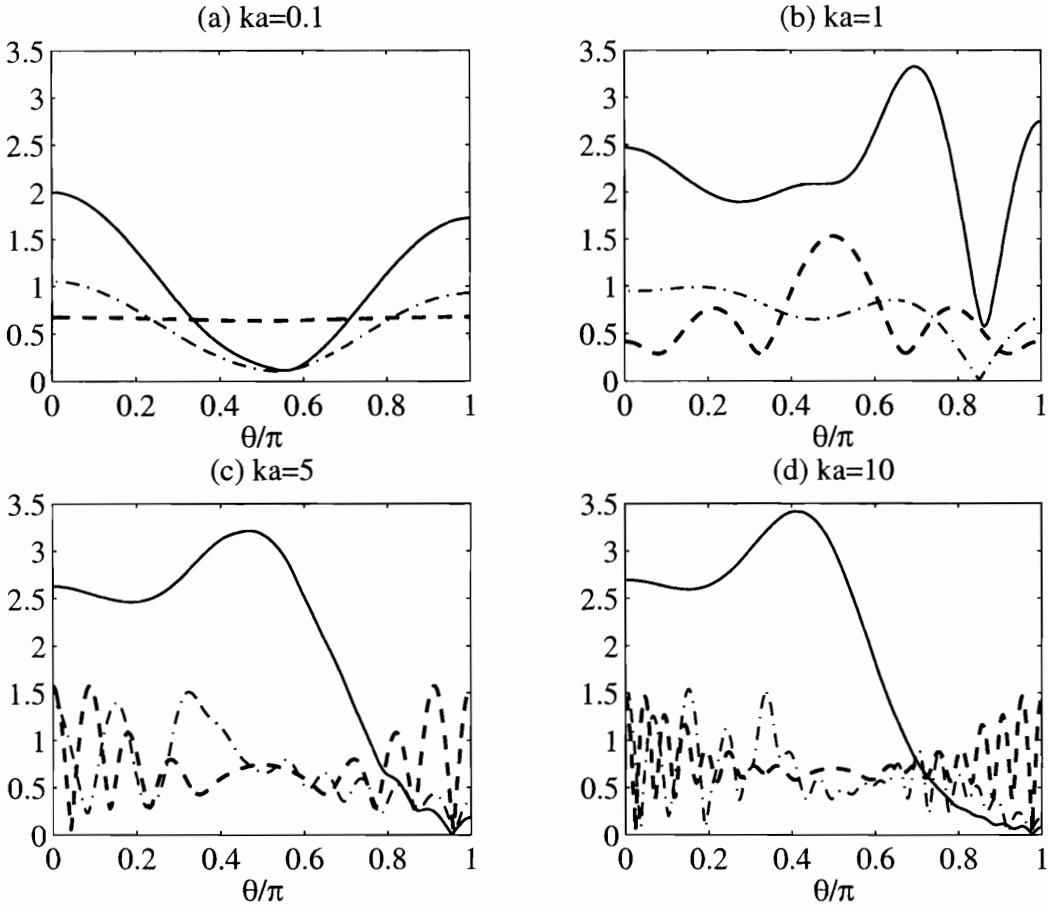

Figure 6-8: Dimensionless amplitudes of second-order $|\eta_{2,2}^{(2)} + \eta_{2,2}^{(1)}|/(2kA^2)$ along the semi-circular peninsula, for different angle of incidence $\theta_I = \pi$(—), $5\pi/4$(– · –), $3\pi/2$(– –).Input data are $kh = 1$, (a) $ka = 0.1$ (b) $ka = 1$(c) $ka = 5$ (d) $ka = 10$.

Chapter 7

Numerical Solution for problems involving a semi-circular shoal

Three examples involving radially varying depth are discussed in this chapter. First is a semi-circular shoal near a vertical cliff, followed by a semi-circular cylinder on top of a semi-circular shoal, and the last example is a square harbor open to a semi-circular shoal.

7.1 Example 1: A Semi-Circular Shoal near a Cliff

We consider a circular shoal next to a straight and cliff-like coast. The top of the shoal is a flat semicircle of radius 30 m at depth 20 m. The sea depth increases monotonically with r until $r = 300$ m, outside of which the surrounding sea has the greater constant depth of 40 m. The radial variation of the sea depth is given by

$$h = \begin{cases} 20m, & r \leq 30m \\ 30 - 10\cos\left[\frac{\pi}{270}(r-30)\right] m, & 30m \leq r \leq 300m, \end{cases} \tag{7.1.1}$$

as shown in Fig. 7-1.

Three incidence angles ($\theta_I = \pi$ (glancing), $5\pi/4$ (oblique) and $3\pi/2$ (normal)) are considered. The frequency is chosen to be $\omega = 0.7$ rad/s for all cases; the

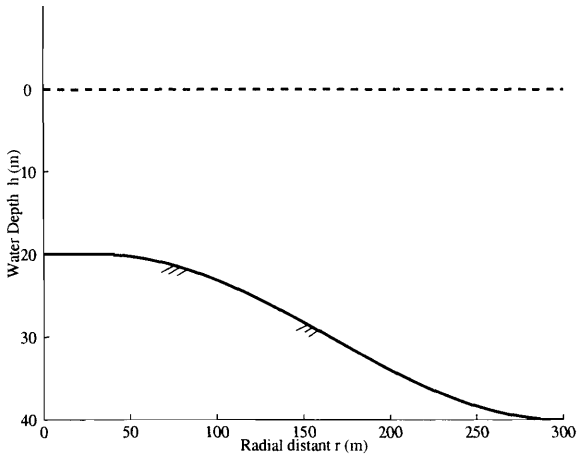

Figure 7-1: Radial variation of depth profile of the circular shoal.

corresponding kh varies from 2.06 at $h = 40m$ to 1.2 at $h = 20m$.

It is known for this type of bathymetry, that caustics may appear in the lee of the shoal so that the linearized ray approximation may fail (Stoker, 1957 pp. 136-137) [36]. Remedy by accounting for diffraction is needed and can be performed for simple caustics by asymptotic methods (see e.g., Mei, 1989). More conveniently, the linearized MSE makes it possible to account for refraction and diffraction in one unified approximation without having to locate the caustics first and to refine the calculation.

7.1.1 Computational Aspects and Validation

In the hybrid-element scheme, the analytical region (far-field Ω_F) is the region outside the shoal $r > a, 0 < \theta < \pi$. Finite elements are used to discretize the shoal.

Numerical accuracy of the first-order computations depends on the number of finite element nodes N_P (or the grid size), and the number of angular modes N_α included in the scattered waves. Two finite element grids: coarse grid with $N_P = 45451$ and fine grid with $N_P = 80601$ are tested. Let $k_0 = 0.0515\ m^{-1}$ denote the incident wavenumber at $h = 40m$. The maximum element size L_e is such that $k_0 L_e = 0.1$ for the coarse grid, and 0.075 for the fine grid. The corresponding ratios of L_e to wavelength are quite small: 0.016 and 0.012 respectively. For either grid,

the solution converges to six decimal places if the number of angular modes is $N_\alpha = 21$ or more. Using 201 angular modes in the outer region, the amplitude at one sample point $2\eta(x = 0m, y = 30m)/A$ is 0.47036911 (coarse) and 0.4710272 (fine); the relative error is approximately 10^{-3}. Our first-order results are obtained with the coarse grid and $N_\alpha = 201$.

For the second-order problems, we tested the number N_ξ of evanescent modes needed. With the coarse grid and 51 angular modes, the $2\eta^{(2)}_{2,2}(0m, 30m)/kA^2$ is 3.64316 for $N_\xi = 3$ and 3.6798 for $N_\xi = 4$. Based on these tests, the following choices are made in all our second-order computations: $N_P = 45451$ (coarse grid) and $N_{\widehat{\alpha}} = 51$. To limit the number of evanescent modes in the l series, we use the following Domb-Sykes extrapolation scheme. By defining the truncated sum as

$$y^{(l)} = \sum_{\ell=0}^{l} \xi_\ell, \tag{7.1.2}$$

By plotting $y^{(l)}$ vs. $1/l$, the final result is obtained from the limit of $1/l = 0$. Choosing just two values l and $l + 1$, the limit by linear extrapolation gives

$$y^{(\infty)} = y^{(l+1)} - l\left[y^{(l)} - y^{(l+1)}\right]. \tag{7.1.3}$$

We test the number N_ξ of evanescent modes needed, based on the numerical results with $l = N_\xi - 1$ and $l + 1 = N_\xi$ in Domb-Sykes method to extrapolate $y^{(\infty)}$. At the sample point (x=20 m, y=0 m) the numerical results for $\eta^{(2)}_{2,2}/2k_0A^2$ are found to be 1.82158 for $N_\xi = 3$ and 1.8399 for $N_\xi = 4$.

7.1.2 Results

We now discuss the numerical results displayed below only for the shoaling region: $r \leq a = 300\ m,\ 0 < \theta < \pi$.

The first-order free-surface amplitude η/A for three incidence angles shown in Figure 7-2 , 7-3 and 7-4. The mathematical problem for glancing incidence is equivalent to a full circular shoal in the open sea with an incident wave of amplitude $2A$.

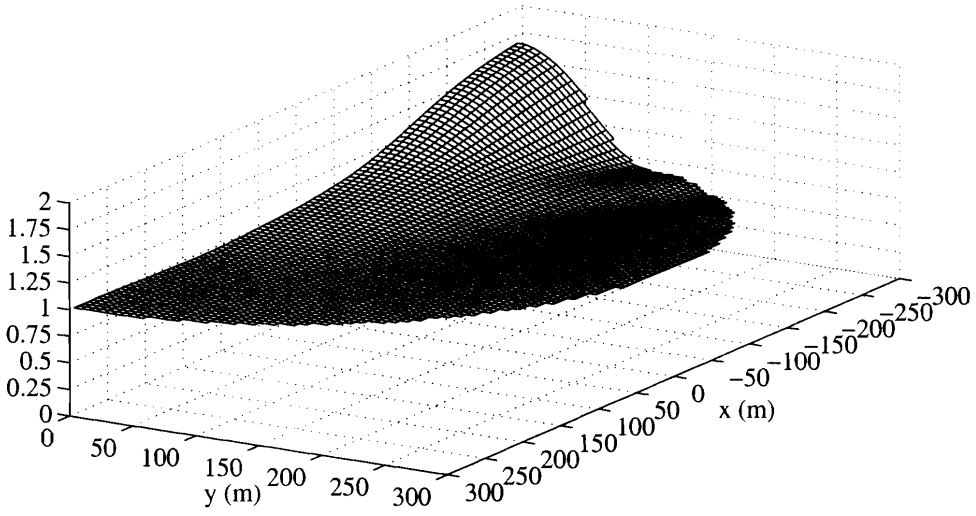

Figure 7-2: The first-order amplitude, $|\eta|/A$, over a circular shoal near a coast. Glancing incidence ($\theta_I = \pi$). At glancing incidence, waves are from left to right. The coast coincides with the plane $y = 0\ m$.

The incident rays are originally parallel to the x axis. The rays entering the shoal first bend toward then away from the center of the shoal. On the incidence side of the shoal the amplitude grows slightly towards the orgin. On the lee side, rays reflect from the coast and intersect with those farther away from the coast, resulting in constructive interference and the greater amplitude. The greatest amplification is around 1.75 near the exit at $x = -300\ m, y = 0\ m$. For normal incidences, Figure 7-5, the incident rays first bend towards the y axis by refraction, are then reflected specularly from the coast, and finally bend away from the y axis. Interference between the incident and reflected rays results in strong spatial variations in the direction normal to the shore (Figure 7-3). For oblique incidence, Figure 7-4, the amplitude variations are of course not symmetrical with respect to $\theta = \pi/2$, unlike the case of normal incidence. The greater amplification of the waves for oblique incidence is along the line around $\theta = 3\pi/4$ with a peaks near the edge of the shoal. Figure 7-6 gives a clearer comparison of the profiles of first-oder amplitudes along

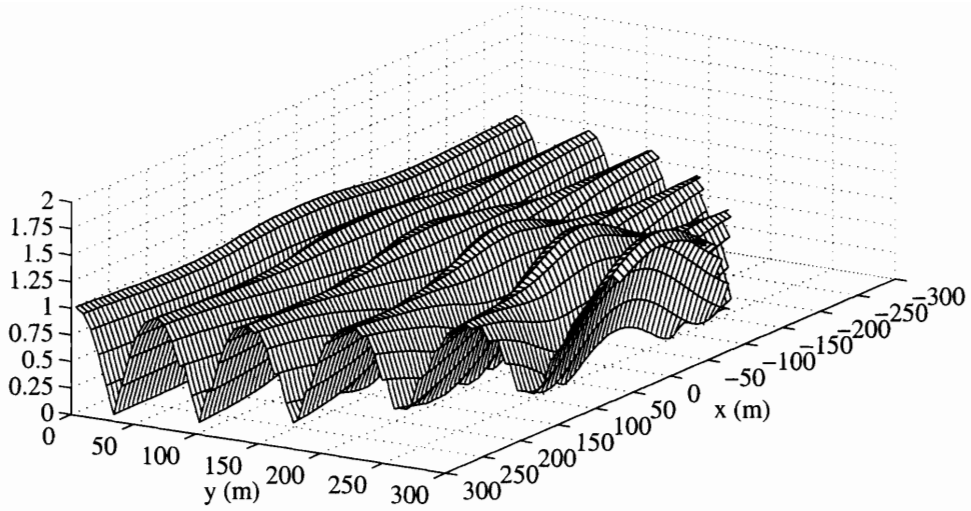

Figure 7-3: The first-order amplitude, $|\eta|/A$, over a semi-circular shoal near a coast. Normal incidence ($\theta_I = 3\pi/2$). The coast coincides with the plane $y = 0$ m.

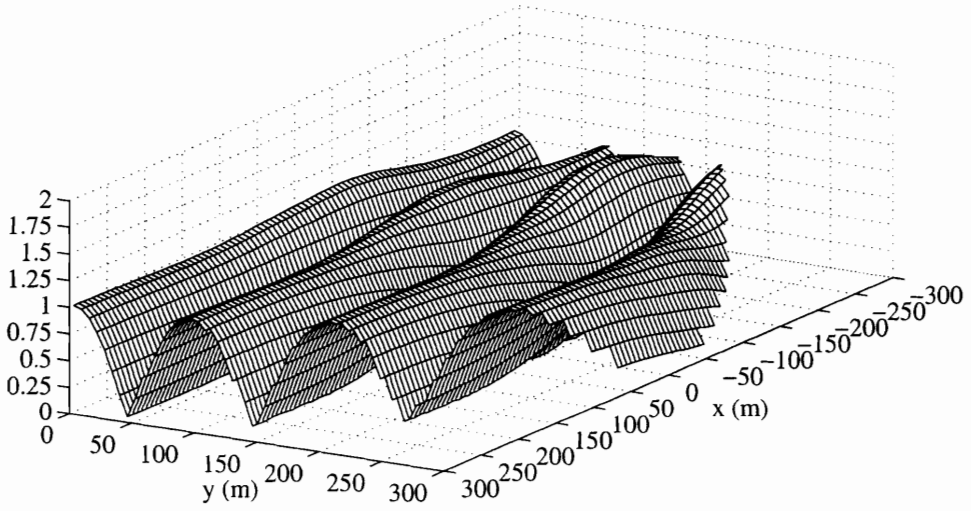

Figure 7-4: The first-order amplitude, $|\eta|/A$, over a semi-circular shoal near a coast. Oblique incidence ($\theta_I = 5\pi/4$). The coast coincides with the plane $y = 0$ m.

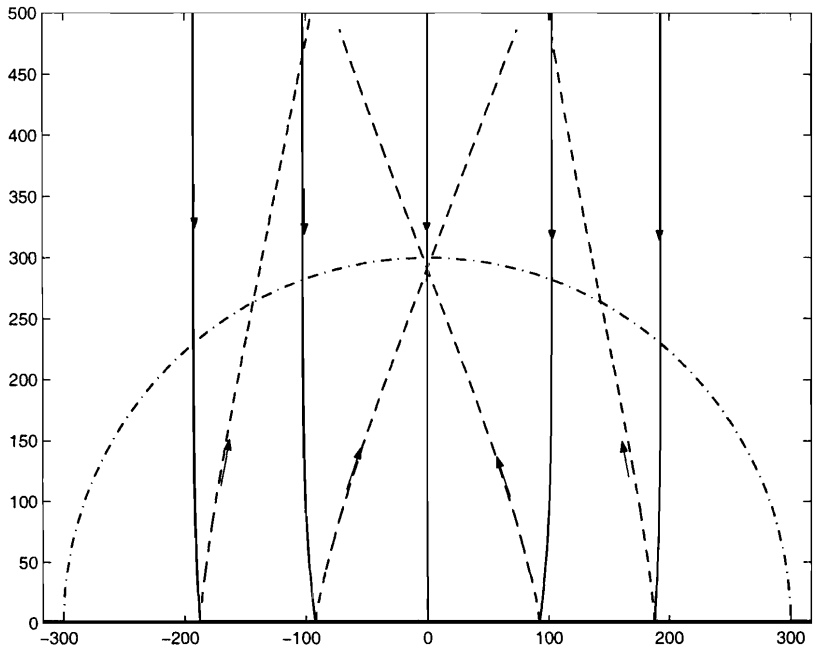

Figure 7-5: Ray geometry for normal incidence

the y axis for glancing, oblique ($\theta_I = 5\pi/4$) and normal incidences. Along this centerline, both incident and reflected waves are affected by refraction, strong interference is again evident except for glancing incidence. For normal incidence, the greatest amplitude of $\eta/A = 1.3$ occurs near the outer edge of the shoal. The location of this peak depends of course on the incident wave frequency. Since longer waves (of lower-frequency) are more influenced by refraction, the peak amplification should occur closer to the flat top. For glancing incidence the variation along the y axis is imperceptible in Figure 7-6; the numerical values are $\eta/A = 1.032$ at $x = 0$ m, and 0.9946 at $x = 300$ m.

The mean-sea-level setup/setdown is shown in Figure 7-7 , 7-8 and 7-9 for three incidence angles. Figure 7-10 compares their variations along the y axis. For normalization the amplitude ($2A$) and steepness ($2k_0A$) of the incident wave are used as references. As can be seen in Figure 7-7, at glancing incidence the mean-sea level is negative over most of the shoal except near the coast on the lee side where the first-order wave experiences inteference due to reflection and refraction. It is well known that the setdown of a progressive wave of amplitude $2A$ on a sea of

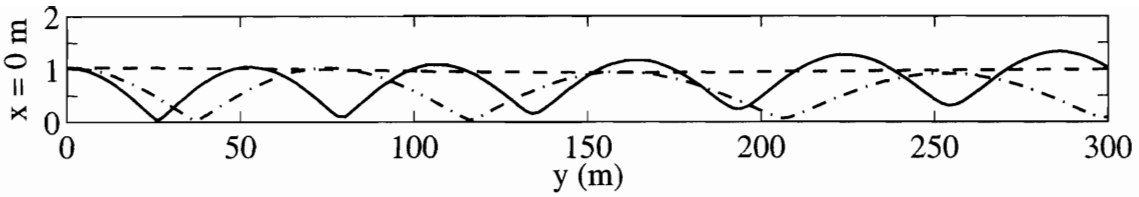

Figure 7-6: Variations of the first-order amplitude, $|\eta|/A$ along the centerline $x = 0\ m$. Glancing incidence ($\theta_I = \pi$): (– –). Oblique incidence ($\theta_I = 5\pi/4$) : (– · –). Normal incidence ($\theta_I = 3\pi/2$) : (——).

constant depth is

$$\eta_{20}^{(1)} = -\frac{4kA^2}{2\sinh 2kh} \tag{7.1.4}$$

At the entry point $x = 300\ m, y = 0\ m$, where $k_0 h = 2.06$, this formula gives $\eta_{20}^{(1)}/4k_0A^2 = -0.0162$ which provides a check of the numerical result $\eta_{20}^{(1)}/4k_0A^2 = -0.016$. The numerical results at the center top $x = y = 0$ m, $\eta_{20}^{(1)}/4k_0A^2 = -0.113406$ is twice the estimate result, which shows the effect of the shoal.

To better understand the computed mean sea-level at normal incidence shown in Figure 7-8, it is helpful to examine the limiting result under a simple standing wave over a horizontal seabed,

$$\begin{aligned} \eta_{20} &= kA^2\left[\frac{\omega^2}{gk}\cos^2 ky - \frac{gk}{\omega^2}\sin^2 ky\right] \\ &= \frac{kA^2}{2}\frac{1}{\tanh kh}\left[-(1-\tanh^2 kh) + \cos 2ky(1+\tanh^2 kh)\right] \end{aligned} \tag{7.1.5}$$

which follows from (3.1.12) by taking $\eta = A\cos ky$. The maximum setup occurs along the lines $2ky = 0, 2\pi, 4\pi, ...$ where $|\eta| = A|\cos ky| = A$ is also the greatest. The maximum setdown occurs at $2ky = \pi, 3\pi, 5\pi, ...$, where $|\eta| = A|\cos ky| = 0$ is the smallest. These features are qualitatively preserved in the numerical results, as can be more clearly seen from Figures 7-6 and 7-10. For oblique incidence, these features are also preserved as can be seen in Figures 7-4 and 7-9. The maximum setup and setdown of the normal incidence is the greatest among three incidence angles.

The second-order second-harmonic amplitudes has two parts. In Figures 7-11,

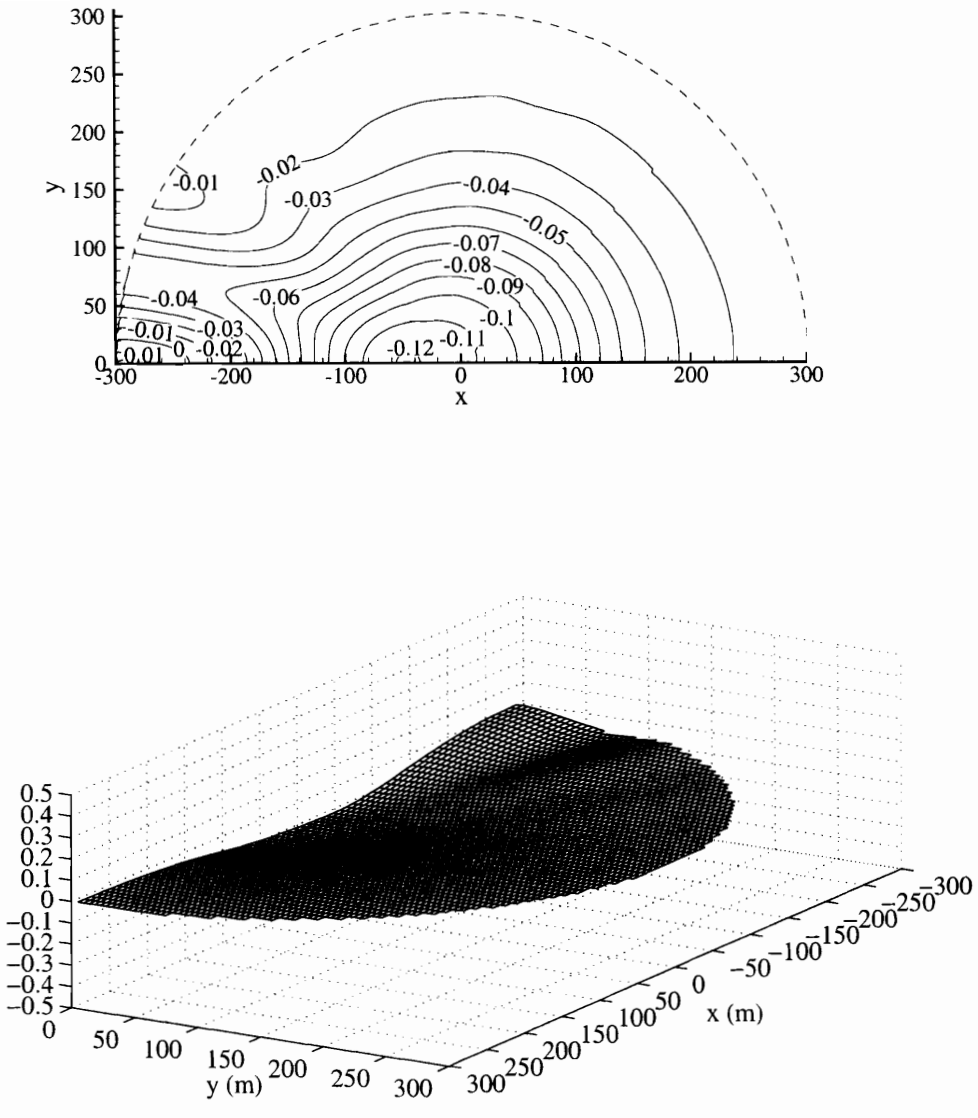

Figure 7-7: The second-order setup/down, $|\eta^{(1)}_{2,0}|/4k_0A^2$, over a semi-circular shoal near a coast. Glancing incidence ($\theta_I = \pi$). TOP: Contours. BOTTOM: 3-D view.

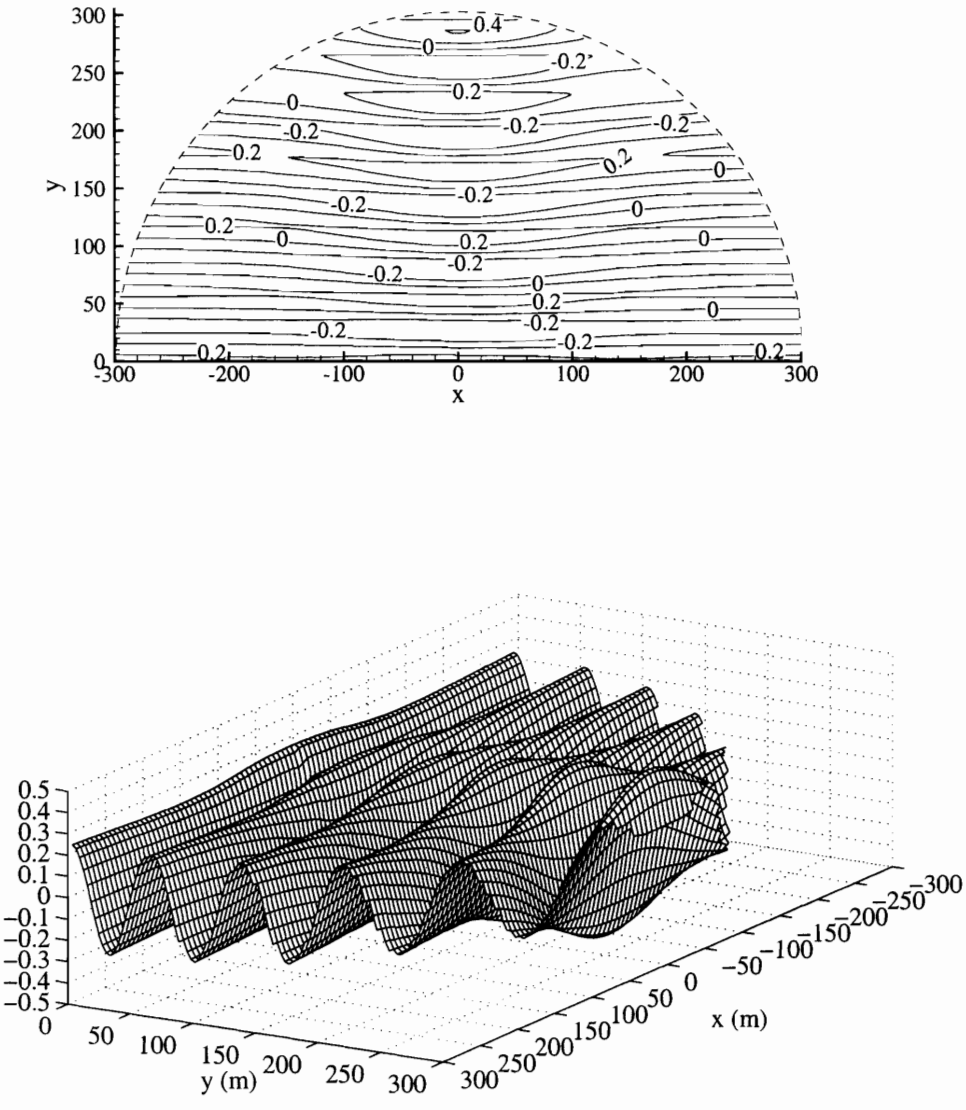

Figure 7-8: The second-order setup/down, $\eta^{(1)}_{2,0}/4k_0A^2$, over a semi-circular shoal near a coast. Normal incidence ($\theta_I = 3\pi/2$). TOP: Contours. BOTTOM: 3-D view.

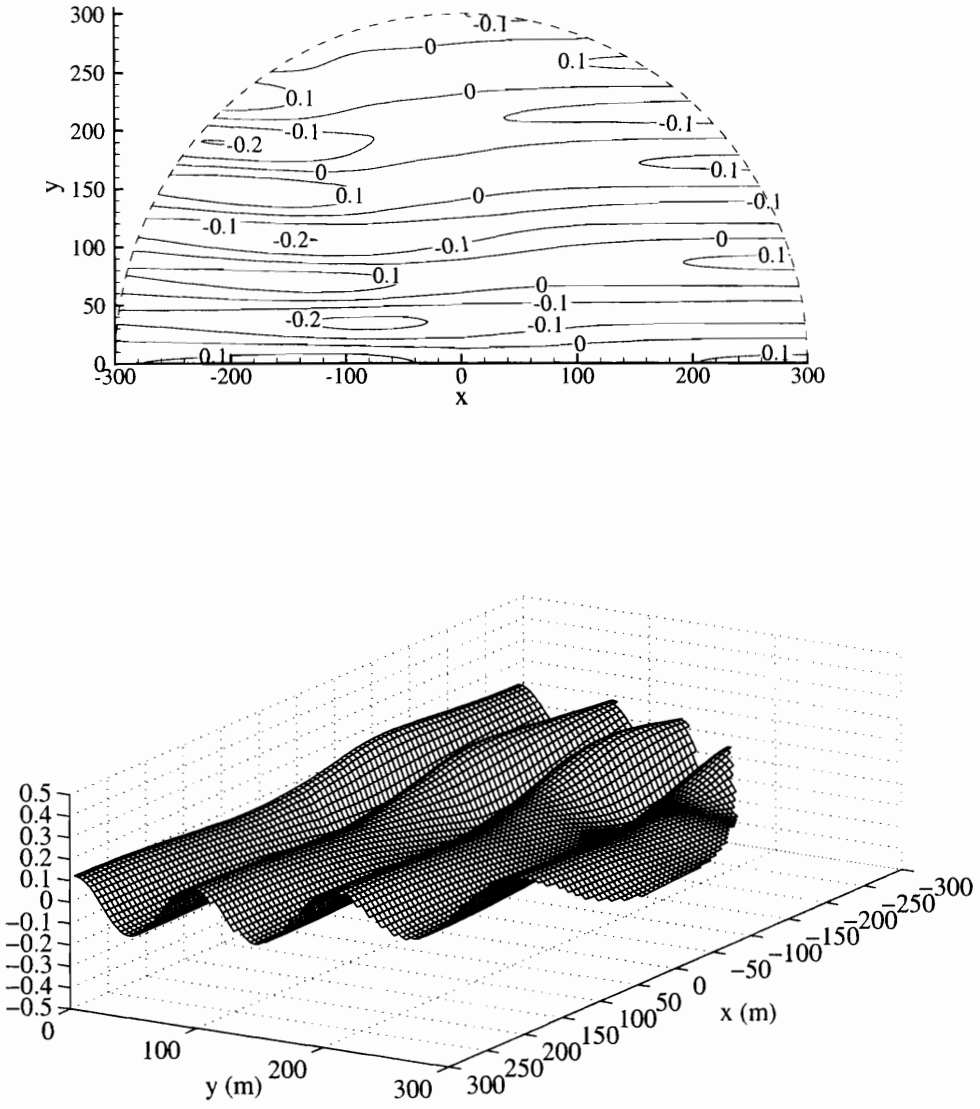

Figure 7-9: The second-order setup/down, $\eta^{(1)}_{2,0}/4k_0A^2$, over a semi-circular shoal near a coast. Oblique incidence ($\theta_I = 5\pi/4$). TOP: Contours. BOTTOM: 3-D view.

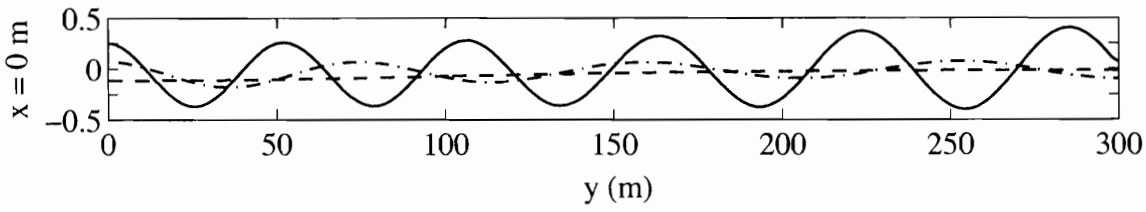

Figure 7-10: Variations of the second-order setdown/up, $\eta^{(1)}_{2,0}/4k_0A^2$ along the centerline $x = 0\ m$. Glancing incidence ($\theta_I = \pi$): (– –). Oblique incidence ($\theta_I = 5\pi/4$) : (– · –). Normal incidence ($\theta_I = 3\pi/2$) : (——).

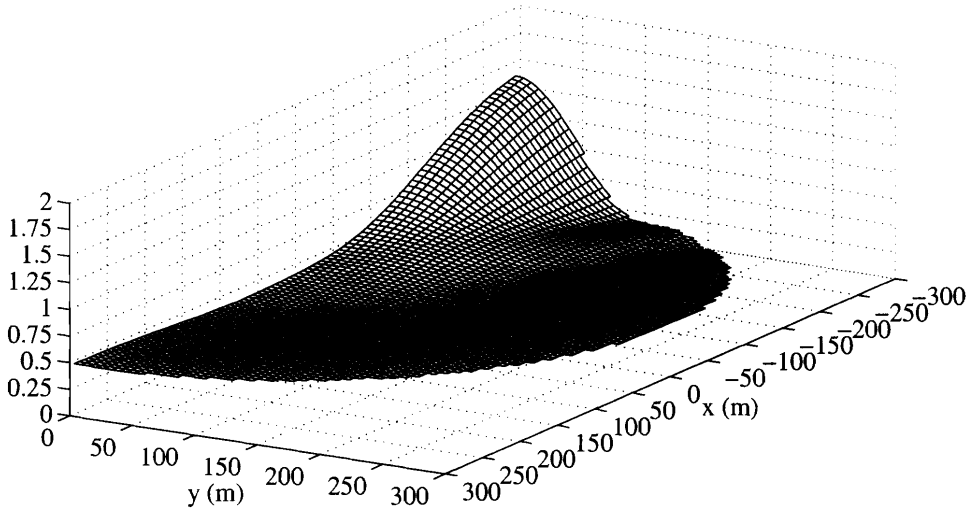

Figure 7-11: The second-order amplitude, $|\eta^{(1)}_{2,2}|/2k_0A^2$, over a semi-circular shoal near a coast. Glancing incidence ($\theta_I = \pi$).

7-12 and 7-13, we show $|\eta^{(1)}_{2,2}|/2k_0A^2$ for three incidence angles which is computed from the first-order potential Φ_1. The corresponding maximum amplitude of $\zeta^{(1)}_2$ is $2|\eta^{(1)}_{2,2}|$, hence $2k_0A^2$ is used as the normalizing scale. The variations resemble those of the first-order amplitude. Figure 7-20 shows the variations along the y axis. For glancing incidence seen in Figures 7-11, $|\eta^{(1)}_{2,2}|$ is amplified with a peak on the lee side of the coast near the edge of the shoal. For normal incidence seen in Figures 7-12, $|\eta^{(1)}_{2,2}|$ is amplified at the centerline due to refraction and reflection, with a peak near the foot of the shoal. The part $\eta^{(2)}_{2,2}$ associated with Φ_2 is shown in Figures 7-14, 7-15 and 7-16. Figure 7-21 compares their variations along the y axis . For glancing incidence, $\eta^{(2)}_{2,2}$ is again nearly flat and larger for smaller radii and near the coast. For oblique and normal incidences, the response is relatively large along the coast and become smaller near the outer edge $r = 300$ m. The magnitude of the sum of the two complex amplitudes $|\eta^{(1)}_{2,2} + \eta^{(2)}_{2,2}|$ is shown in Figures 7-17, 7-18 and 7-19 after accounting for their phases, and is also shown in Figure 7-22 for the variations along the y axis. For glancing incidence, the total second-harmonic is

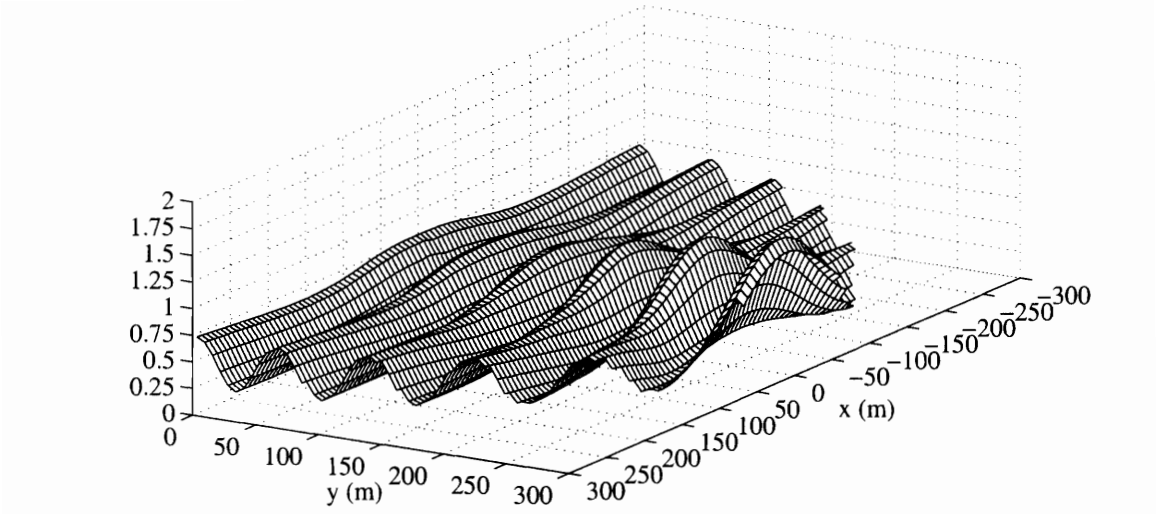

Figure 7-12: The second-order amplitude, $|\eta_{2,2}^{(1)}|/2k_0A^2$, over a semi-circular shoal near a coast. Normal incidence ($\theta_I = 3\pi/2$).

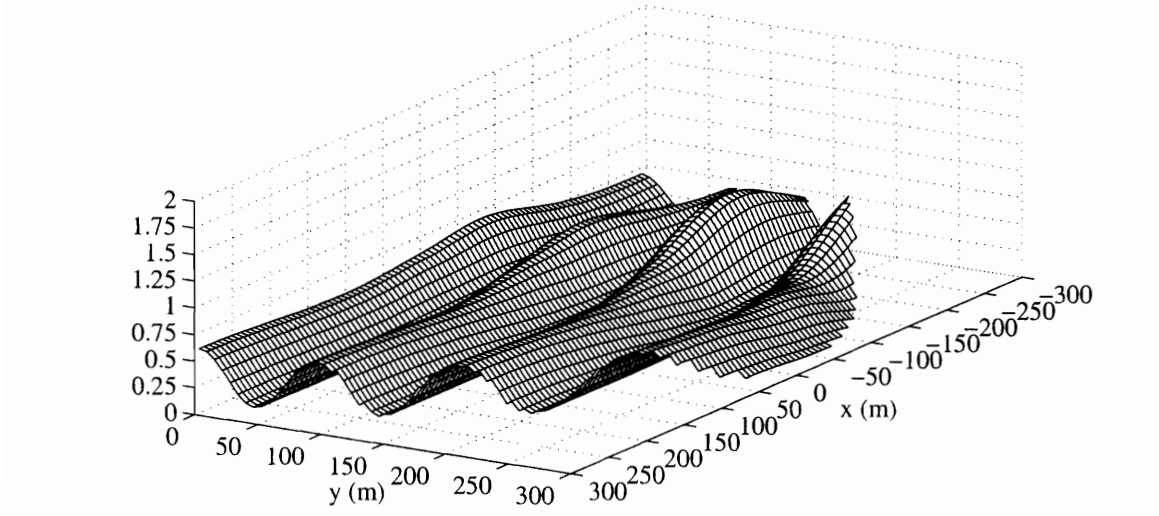

Figure 7-13: The second-order amplitude, $|\eta_{2,2}^{(1)}|/2k_0A^2$, over a semi-circular shoal near a coast. Oblique incidence ($\theta_I = 5\pi/4$).

dominated by $\eta_{2,2}^{(2)}$ and remains the greatest along the coast. Due to the staggering of the lines of maxima and minima, as can be seen by comparing Figures 7-20 with 7-21, the resulting sum is doubly as complex as each individual components.

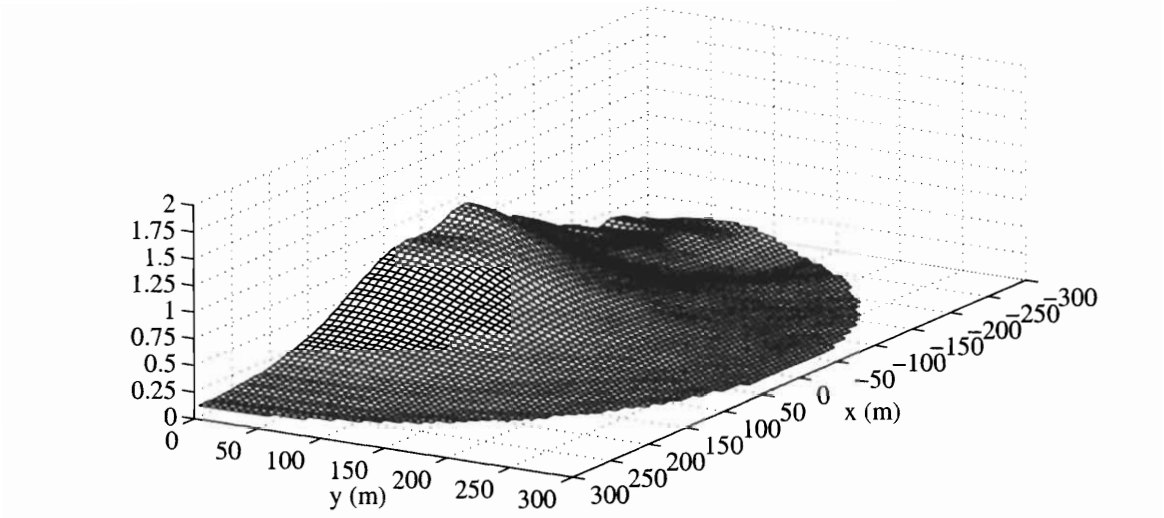

Figure 7-14: The second-order amplitude, $|\eta^{(2)}_{2,2}|/2k_0A^2$, over a semi-circular shoal near a coast. Glancing incidence ($\theta_I = \pi$).

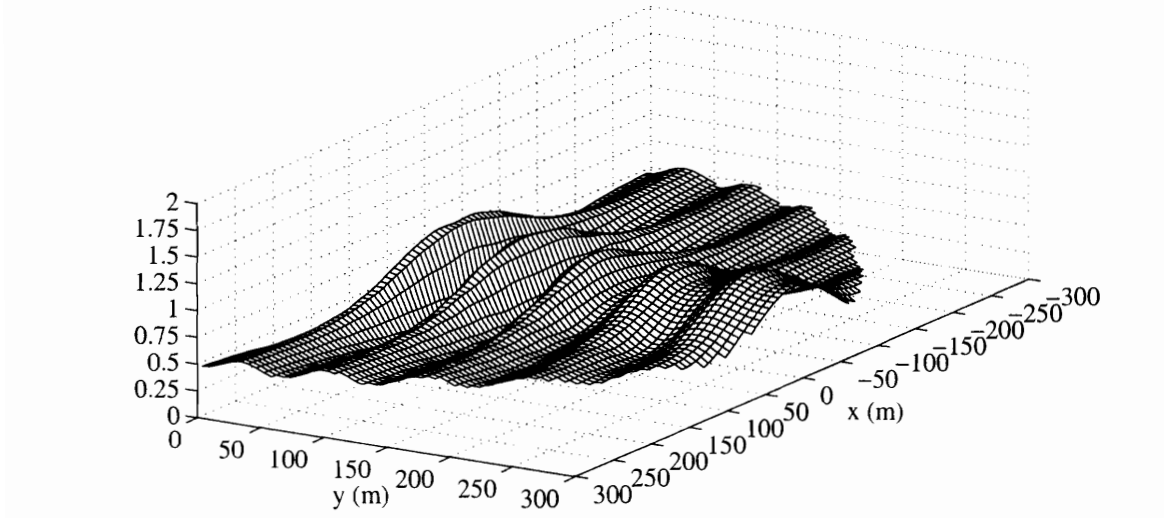

Figure 7-15: The second-order amplitude, $|\eta^{(2)}_{2,2}|/2k_0A^2$, over a semi-circular shoal near a coast. Normal incidence ($\theta_I = 3\pi/2$) .

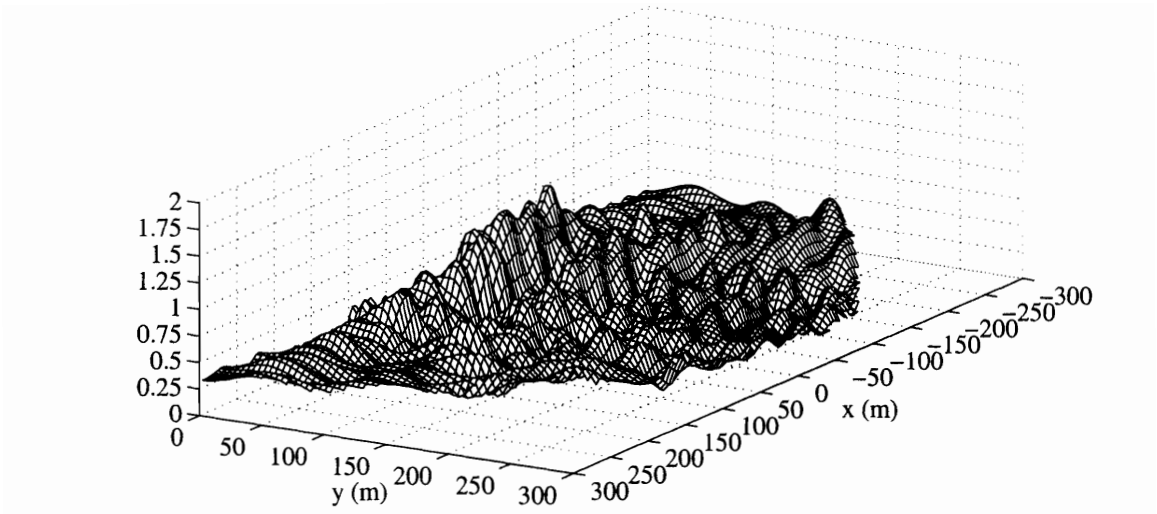

Figure 7-16: The second-order amplitude, $|\eta^{(2)}_{2,2}|/2k_0A^2$, over a semi-circular shoal near a coast. Oblique incidence ($\theta_I = 5\pi/4$) .

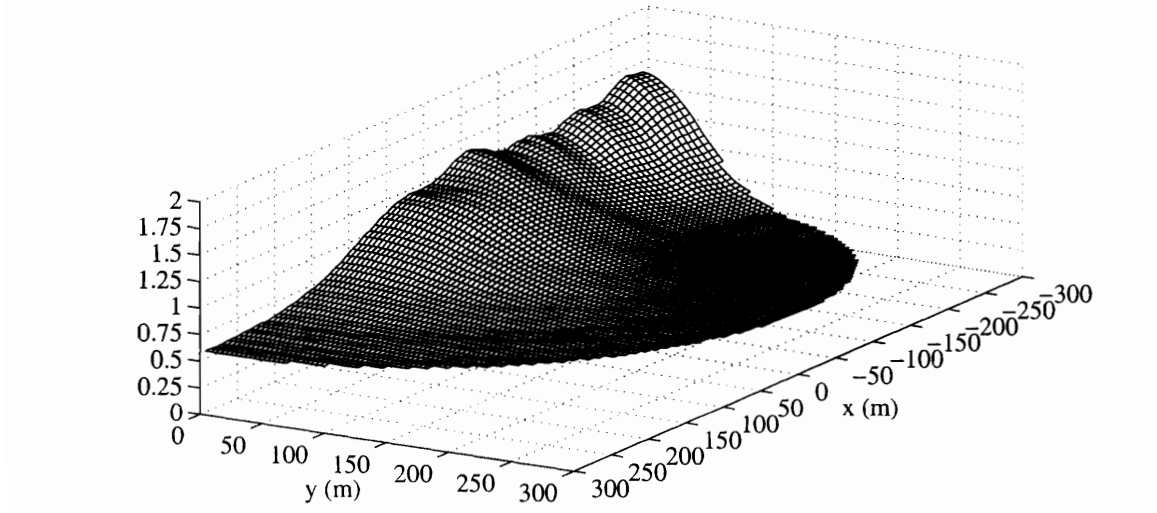

Figure 7-17: The second-order amplitude, $|\eta^{(1)}_{2,2} + \eta^{(2)}_{2,2}|/2k_0A^2$, over a semi-circular shoal near a coast. Glancing incidence ($\theta_I = \pi$).

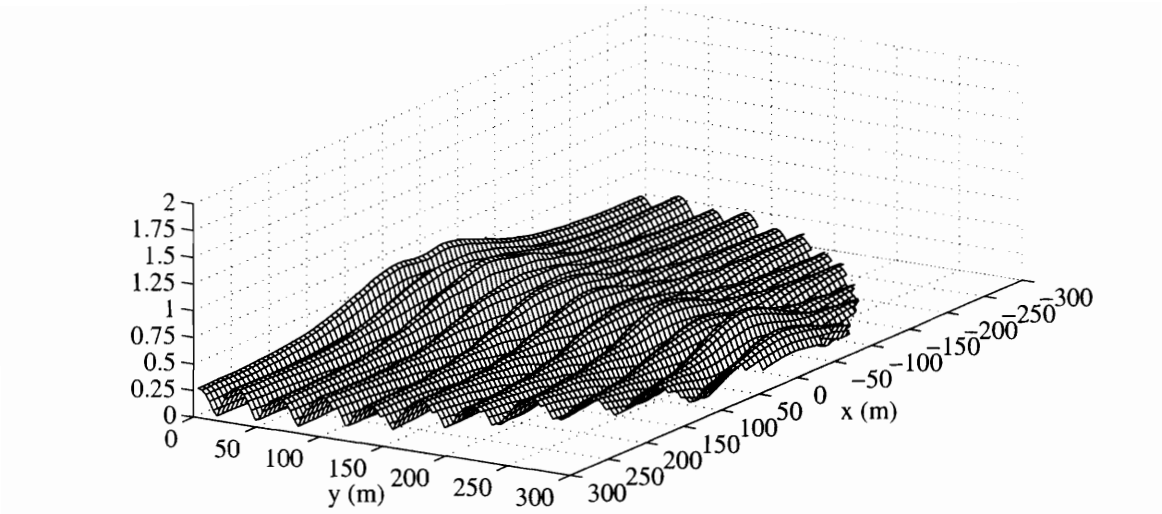

Figure 7-18: The second-order amplitude, $|\eta_{2,2}^{(1)} + \eta_{2,2}^{(2)}|/2k_0A^2$, over a semi-circular shoal near a coast. Normal incidence ($\theta_I = 3\pi/2$).

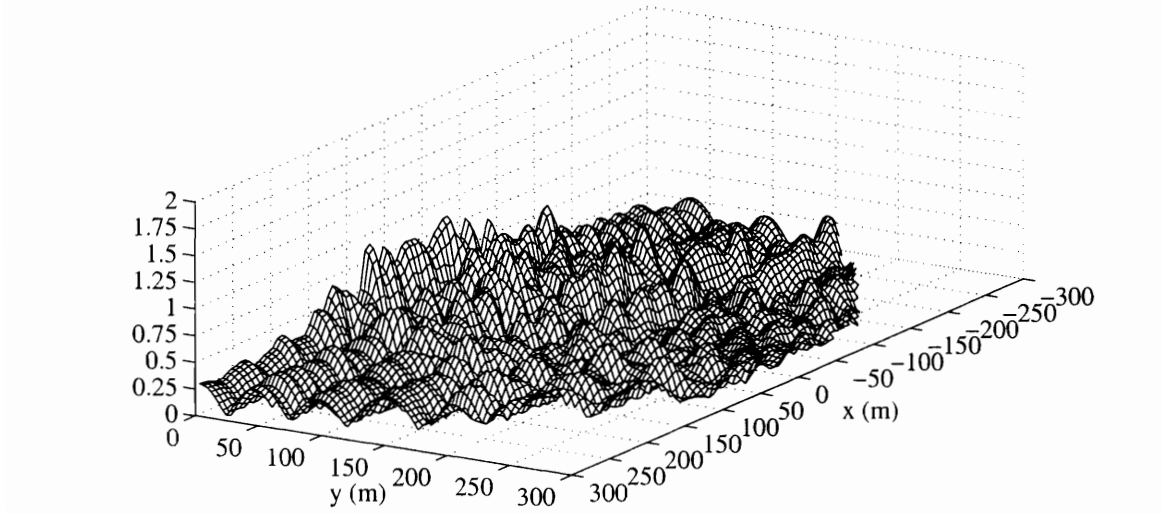

Figure 7-19: The second-order amplitude, $|\eta_{2,2}^{(1)} + \eta_{2,2}^{(2)}|/2k_0A^2$, over a semi-circular shoal near a coast. Oblique incidence ($\theta_I = 5\pi/4$).

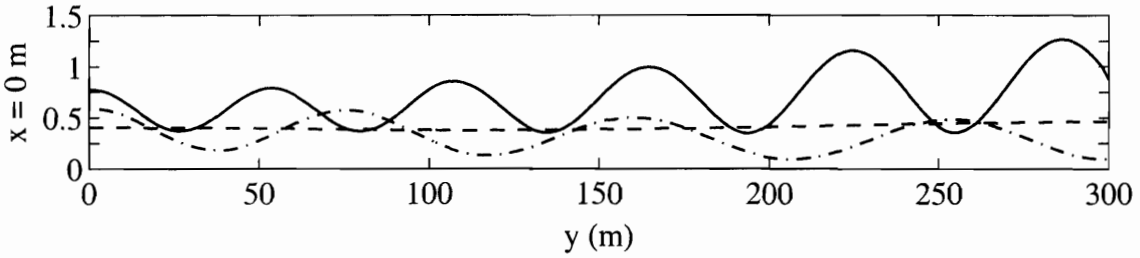

Figure 7-20: Variations of the second-order amplitude $|\eta_{2,2}^{(1)}|/2k_0A^2$ along the centerline $x = 0\ m$. Glancing incidence ($\theta_I = \pi$): (– –). Oblique incidence ($\theta_I = 5\pi/4$) : (– · –). Normal incidence ($\theta_I = 3\pi/2$) : (——).

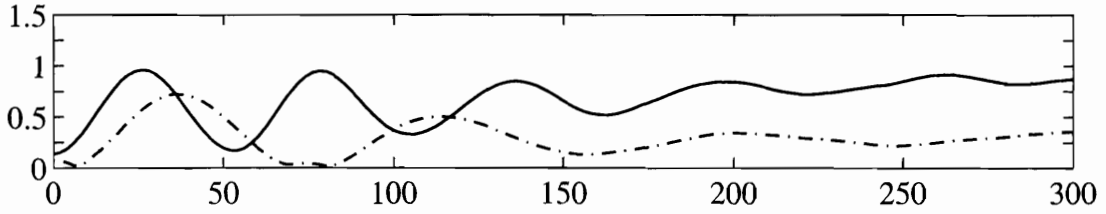

Figure 7-21: Variations of the second-order $|\eta_{2,2}^{(2)}|/2k_0A^2$ along the centerline $x = 0\ m$. Glancing incidence ($\theta_I = \pi$): (– –). Oblique incidence ($\theta_I = 5\pi/4$) : (– · –). Normal incidence ($\theta_I = 3\pi/2$) : (——).

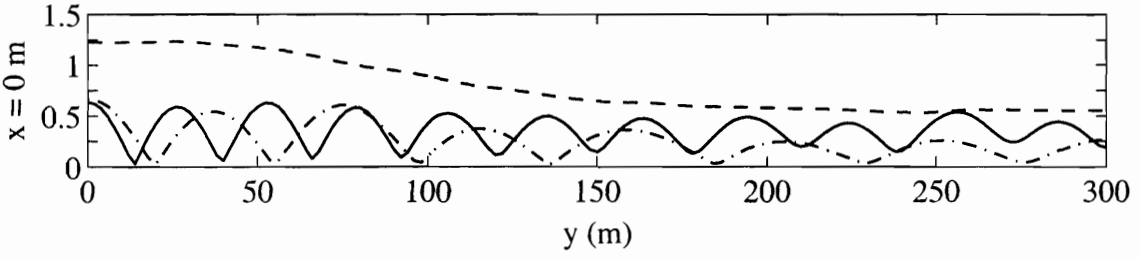

Figure 7-22: Variations of the second-order $|\eta_{2,2}^{(1)} + \eta_{2,2}^{(2)}|/2k_0A^2$ along the centerline $x = 0\ m$. Glancing incidence ($\theta_I = \pi$): (– –). Oblique incidence ($\theta_I = 5\pi/4$) : (– · –). Normal incidence ($\theta_I = 3\pi/2$) : (——).

7.2 Example 2: A Half Cylinder on top of a Semi-Circular Shoal

We now apply the theory for an example combining diffraction and refraction. Consider a semi-circular cylinder with radius $R_a = 20$ m standing at the center of a semi-circular shoal next to a straight and cliff-like coast. The top of the shoal is a flat semicircle of radius 20 m at depth 20 m. The sea depth increases monotonically with r until $r = 300$ m, outside of which the surrounding sea has the greater constant depth of 40 m. The radial variation of the sea depth is given by

$$h = \begin{cases} 20m, & r \leq 20m \\ 30 - 10\cos\left[\frac{\pi}{280}(r-20)\right] m, & 20m \leq r \leq 300m. \end{cases} \tag{7.2.1}$$

The frequency is chosen to be $\omega = 0.6873$ rad/s such that $kh = k_0 h = 2$ in the open sea where $h = 40m$. At depth $h = 20m$ the local wavenumber is increased so that $kh = 1.1697$. Two incidence angles ($\theta_I = \pi$ (glancing) and $3\pi/2$ (normal)) are considered.

7.2.1 Compuational Aspects and Validation

In the hybrid-element scheme, finite elements are used to discretize the shoal, $r < a = 300\ m,\ 0 < \theta < \pi$, outside which ($\Omega_F : r > 300\,m,\ 0 < \theta < \pi$) the solution is analytical.

We have tested two finite elements grids : coarse grid with $N_P = 73040$ and fine grid with $N_P = 175625$. Let $k_0 = 0.05\ m^{-1}$ denote the incident wavenumber at $h = 40\,m$. The maximum element size L_e is such that $k_0 L_e = 0.08$ for the coarse grid, and 0.05 for the fine grid. The corresponding ratios of L_e to wavelength are quite small: 0.012 and 0.008 respectively. For either grid, the solution converges to six decimal places if the number of angular modes is $N_\alpha = 21$ or more. Using 201 angular modes in the outer region, the amplitude for normal incidence at one sample point $\eta(x = 0\,m, y = 20\,m)/A$ is 0.49802(coarse) and 0.49824 (fine); the

relative error is approximately 4×10^{-4}. Our first-order results are obtained with the fine grid and $N_\alpha = 201$.

For the second-order problems, we use $N_P = 175625$ (fine grid) and $N_{\widehat{\alpha}} = 91$ (number of angular modes) based on several tests. Again, Domb-Sykes extrapolation scheme is used to limit the number of the evancensent modes. At the sample point (x=20 m, y=0 m) the numerical results for $\eta^{(2)}_{2,2}/2k_0A^2$ are found to be 1.9060 for $N_\xi = 3$ and 1.9117 for $N_\xi = 4$. We now discuss the numerical results displayed below only for the shoaling region: $r \leq a = 300\ m,\ 0 < \theta < \pi$. We have tested different radius a of the semi-circle boundary ∂A which separates the far field(analytic solution) and near field(discrete solution). The convergence tests of radius a of the second-order amplitude η_{22} along the semi-circular cylinder are plotted in Figure 7-23. The agreement between $a = 300\ m$ and $a = 310\ m$ are excellent.

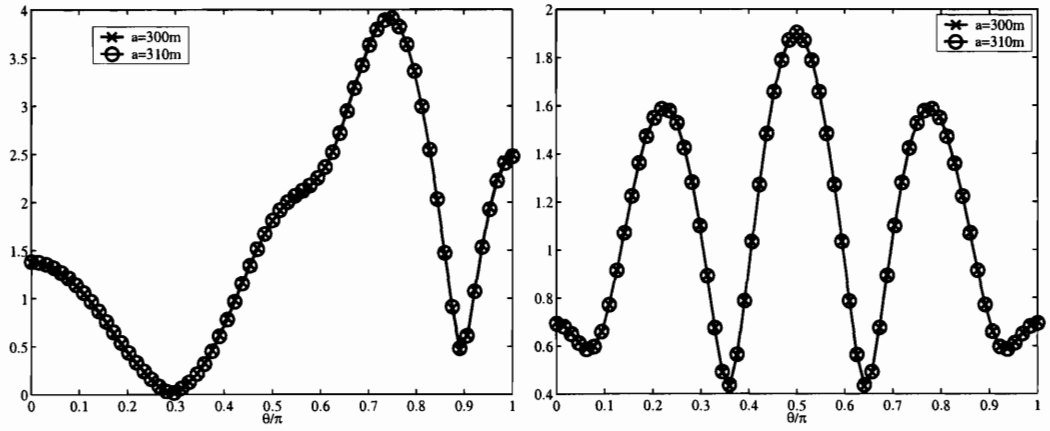

Figure 7-23: The second-order amplitude $|\eta_{22}|/2k_0A^2$ along the semi-circular cylinder for example 2. $\circ$: $a = 310\ m$, $\times$: $a = 300\ m$. Left: glancing incidence. Right: normal incidence.

7.2.2 Results

The first-order free-surface amplitudes $|\eta|/A$ for glancing and normal incidences are shown in Figure 7-24 (a) and (b). For glancing incidence, the problem is equivalent to a full cylinder on a circular shoal in the open sea, attacked by an incident wave of amplitude $2A$ propagating from left to right. If the cylinder were absent(

cf. section 7.1), the incident rays would enter the shoal first bend toward the center of the shoal; the amplitude grows slowly towards the orgin. On the lee side, rays would be reflected from the coast and intersect with those farther away from the coast, resulting in constructive interference and the greater amplitude. With a cylinder of fairly large radius $k_0 R_a = 1$, strong back-scattering results as indicated by the wavy envelope in Figure 7-24 (a). On the shadow side, only a mild increase with r is seen due to the constructive inteference between incident and reflected rays which are not interupted by the cylinder. All variations gradually diminish far outside the shoal not shown here. For normal incidence without the cylinder, the plot of $|\eta/A|$ would resemble that of a simple standing wave with crests and troughs parallel to the x axis. Now scattering from the cylinder adds modulations in all directions as is evident in Figure 7-24 (b).

The second-order setup/setdown of the mean sea level is shown in Figure 7-25 (a) and (b) for two incidence angles. Depending solely on the first-order result, the qualitative features resemble those of Figure 7-24 (a) and (b). For reference we recall that the mean-sea-level of a progressive wave of amplitude $2A$ on a sea of constant depth is negative and hence a pure set-down is Eq. (7.1.4). On the other hand the mean sea-level under a simple standing wave over a horizontal seabed is Eq. (7.1.5). Unlike the simple progressive wave the maximum setup occurs along the lines $2ky = 0, 2\pi, 4\pi, ...$ where $|\eta| = A|\cos ky| = A$ is also the greatest. The maximum setdown occurs at $2ky = \pi, 3\pi, 5\pi, ...$, where $|\eta| = A|\cos ky| = 0$ is the smallest. These features are qualitatively preserved in the numerical results, as can be seen from Figure 7-25 (b). In particular the mean-sea-level along the coast is positive everywhere.

The second-order second-harmonic amplitudes has two parts. In Figure 7-26 (a) and (b), we show for two incidence angles $|\eta^{(1)}_{2,2}|/2k_0A^2$ which is computed from the first-order potential Φ_1. The corresponding maximum amplitude of $\zeta^{(1)}_2$ is $2|\eta^{(1)}_{2,2}|$, hence $2k_0A^2$ is used as the normalizing scale. The variations again resemble those of the first-order amplitude.

Completing the second-order solution is the part $\eta^{(2)}_{2,2}$ associated with Φ_2, shown

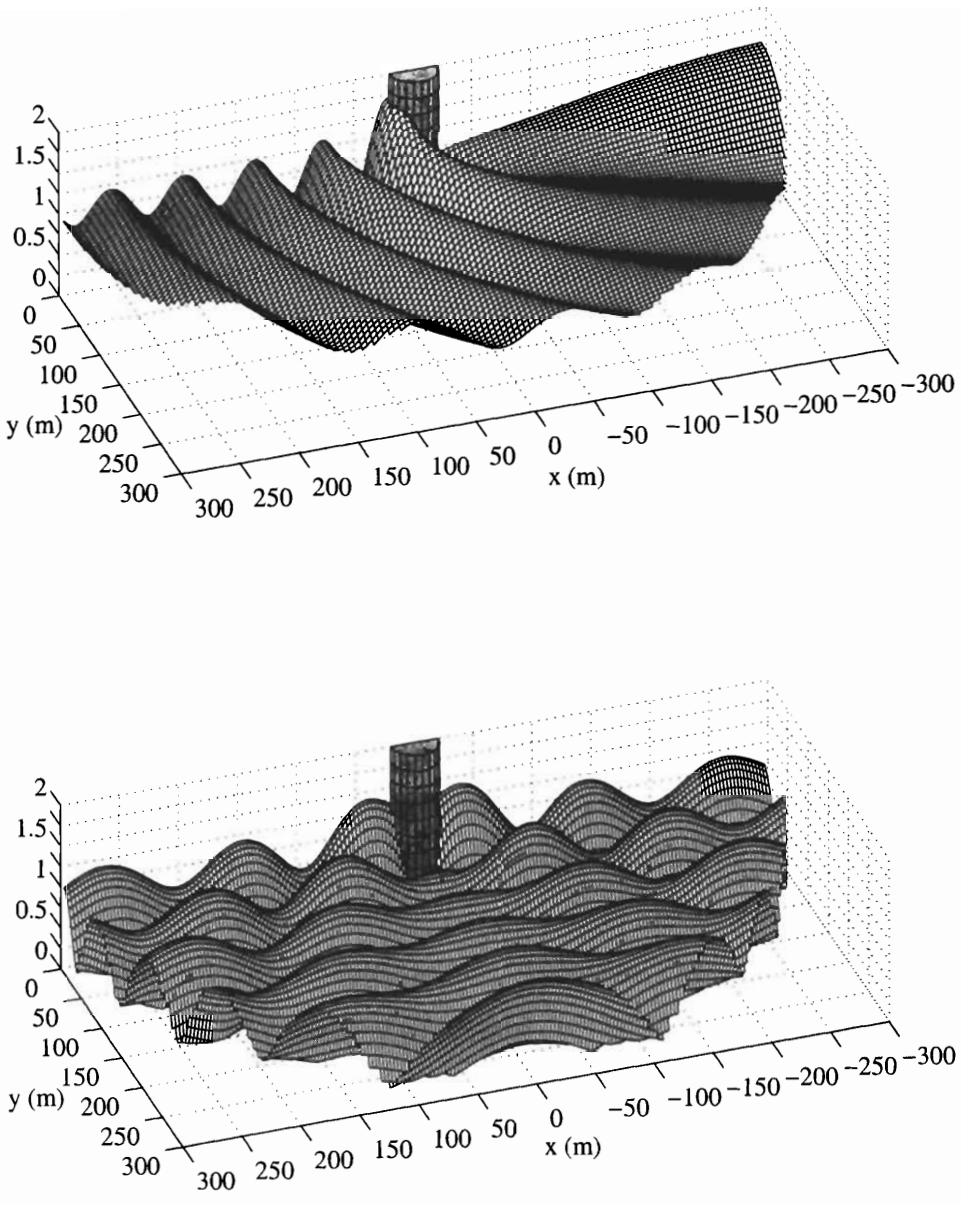

Figure 7-24: The first-order amplitude, $|\eta|/A$, over a semi-circular shoal around a cylinder. (a) : Glancing incidence (top). (b) : Normal incidence (bottom).

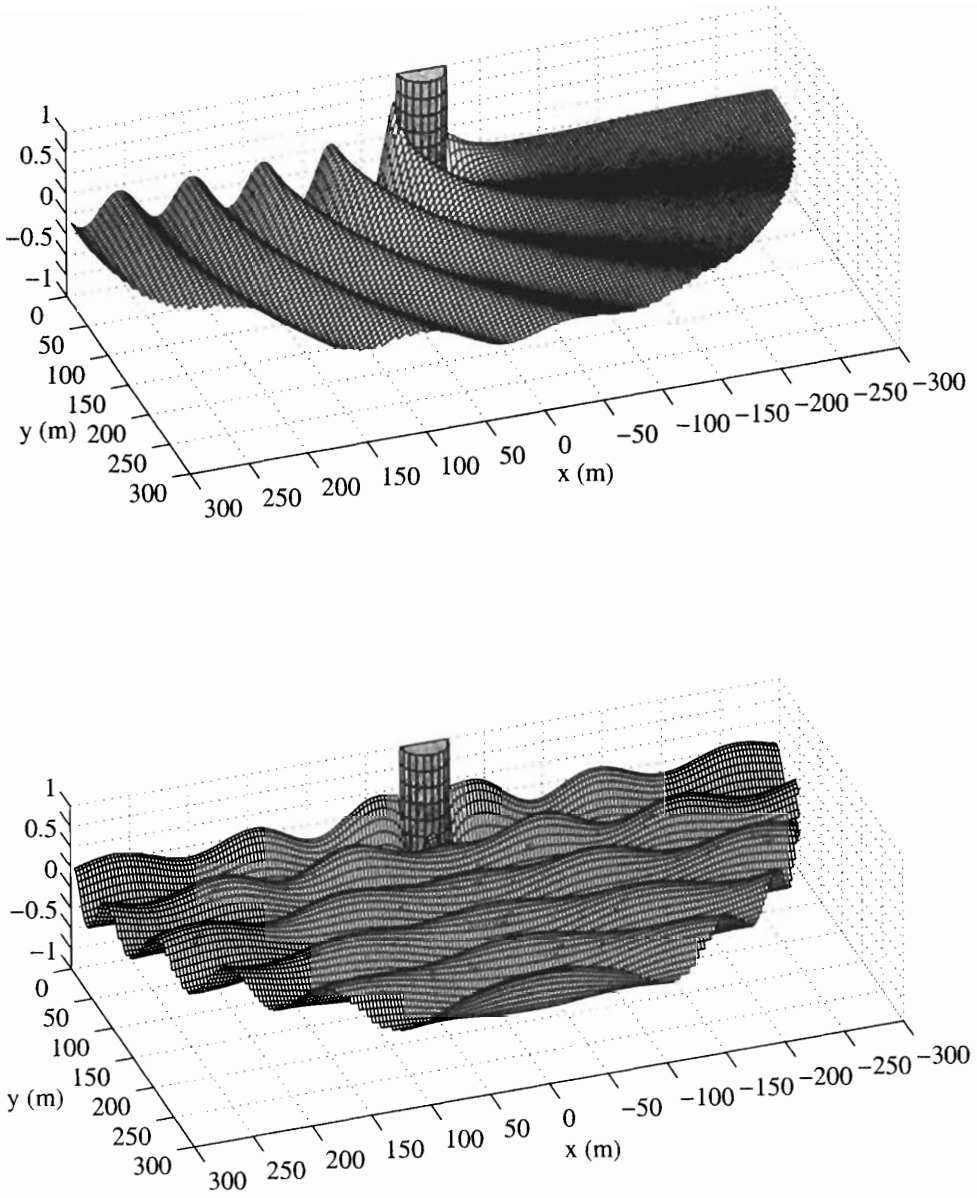

Figure 7-25: The second-order setdown/setup, $|\eta^{(1)}_{2,0}|/4k_0A^2$, over a semi-circular shoal around a cylinder. (a): Glancing incidence (top). (b) : Normal incidence (bottom).

in Figures 7-27 (a) and (b). Note that for both incidence angles the spatial undulations are much more rapid, due to the fact the characteristic wavenumber is now $\widehat{\kappa}_0$ which is nearly four times the magnitude of k (see (3.2.11)). As a consequence the magnitude of the sum of the two complex amplitudes $|\eta_{2,2}^{(1)} + \eta_{2,2}^{(2)}|$ oscillates nearly twice as fast in space, as is shown in Figures 7-28 (a) and (b) after accounting for the phases of the two components.

Finally, we compare the free-surface heights along the circumference of two cylinders of the same radius, $r = R_a = 20\,m$: one on a sea of constant depth ($40\,m$) and the other on top of a shoal just discussed. The incident wave has the same frequency $\omega = 0.6873$ rad/s so that $k_0 h_0 = 2$ in the sea. Note first by comparing Figure 7-29 (a)-(d) with Figures 6-4-6-8 that all results here for constant depth ($k_0 h = 2$) are very similar to those for a smaller depth ($kh = 1$); this is likely because the cylinder radius is the same ($kR_a = 1$). Secondly for both incidence angles, shoaling tends to increase mildly the first-order amplitude $|\eta|$ as well as $|\eta_{2,2}^{(1)}|$, but to decrease the mean-sea-level $|\eta_{2,0}^{(1)}|$, all of which depend solely on the first order. However the part $|\eta_{2,2}^{(2)}|$ is considerably more enhanced by shoaling.

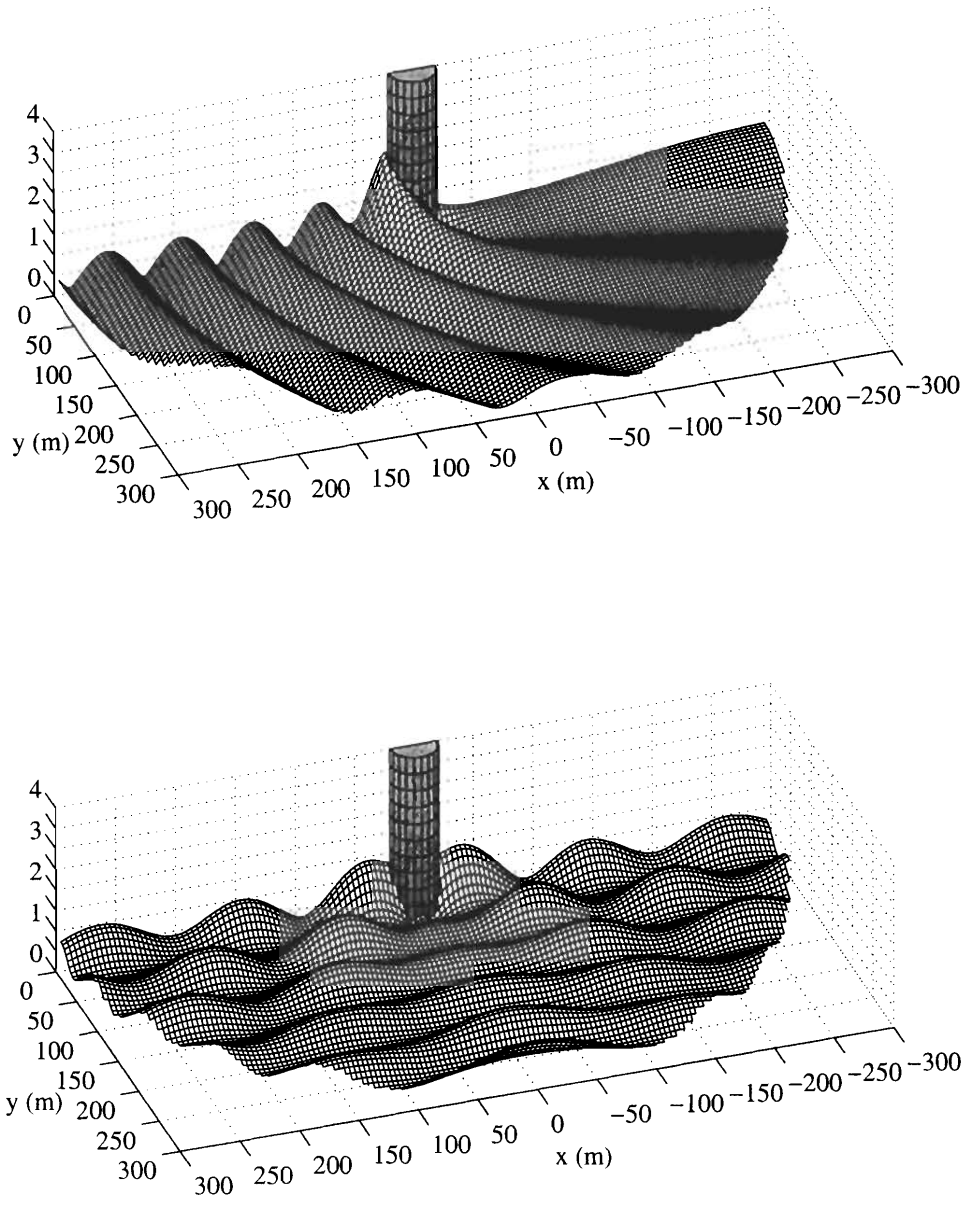

Figure 7-26: The second-harmonic amplitude computed from the first-harmonic, $|\eta^{(1)}_{2,2}|/2k_0A^2$, over a semi-circular shoal around a cylinder. (a) : Glancing incidence (top). (b) : Normal incidence (bottom).

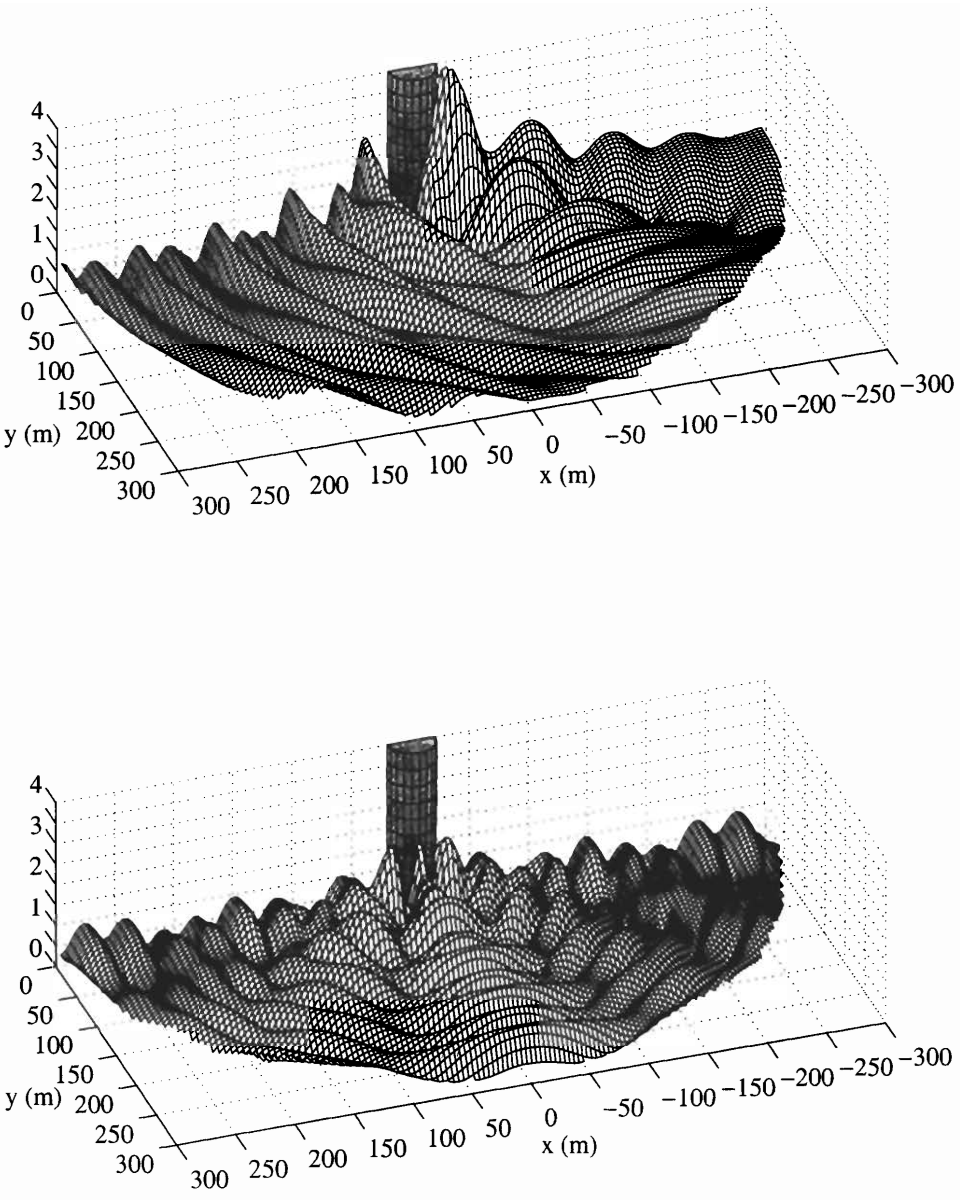

Figure 7-27: The second-order amplitude computed from the second-harmonic, $|\eta^{(2)}_{2,2}|/2k_0A^2$, over a semi-circular shoal around a cylinder. (a) : Glancing incidence (top). (b): Normal incidence (bottom).

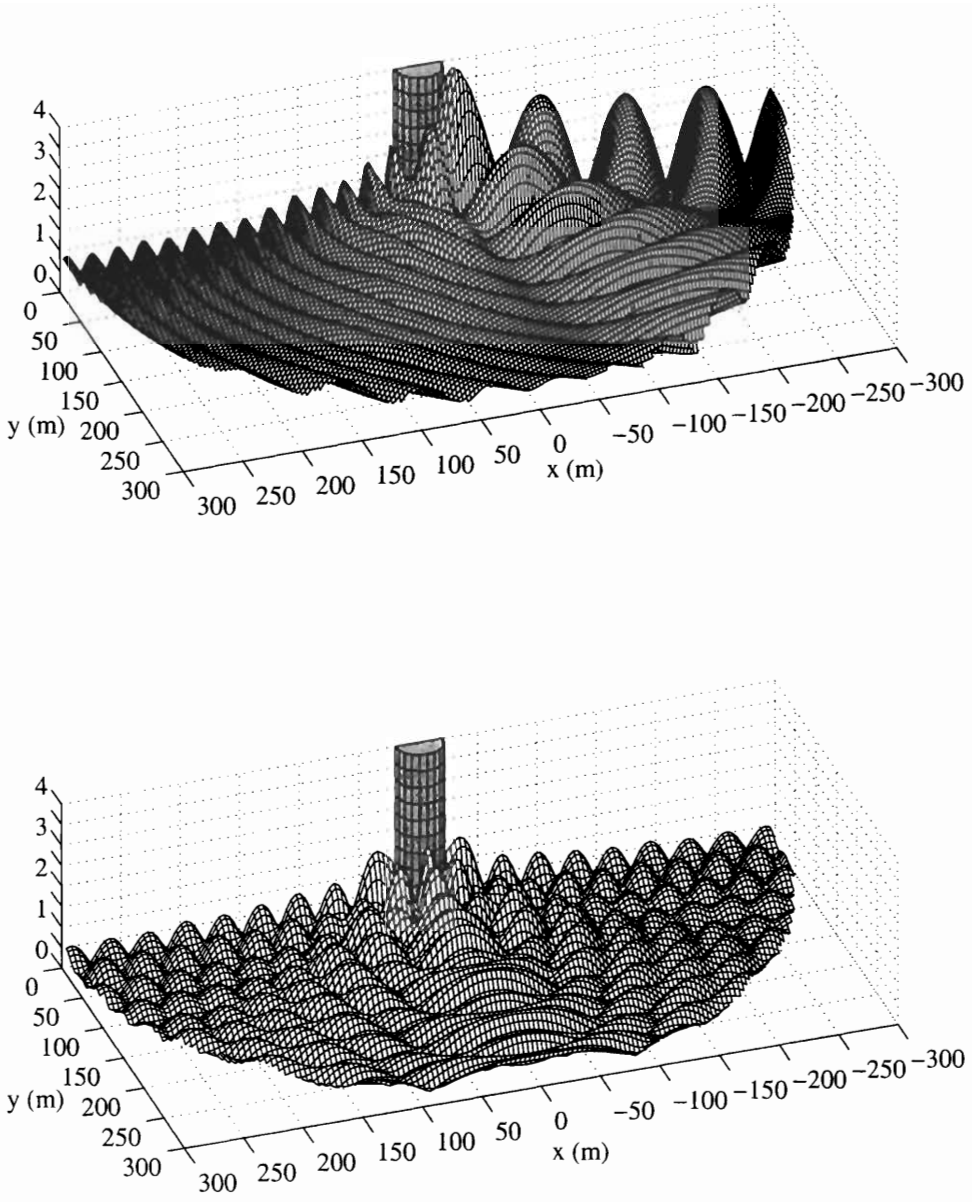

Figure 7-28: The total second-order amplitude, $|\eta_{2,2}^{(1)} + \eta_{2,2}^{(2)}|/2k_0A^2$, over a semi-circular shoal around a cylinder. (a) : Glancing incidence (top). (b) : Normal incidence (bottom).

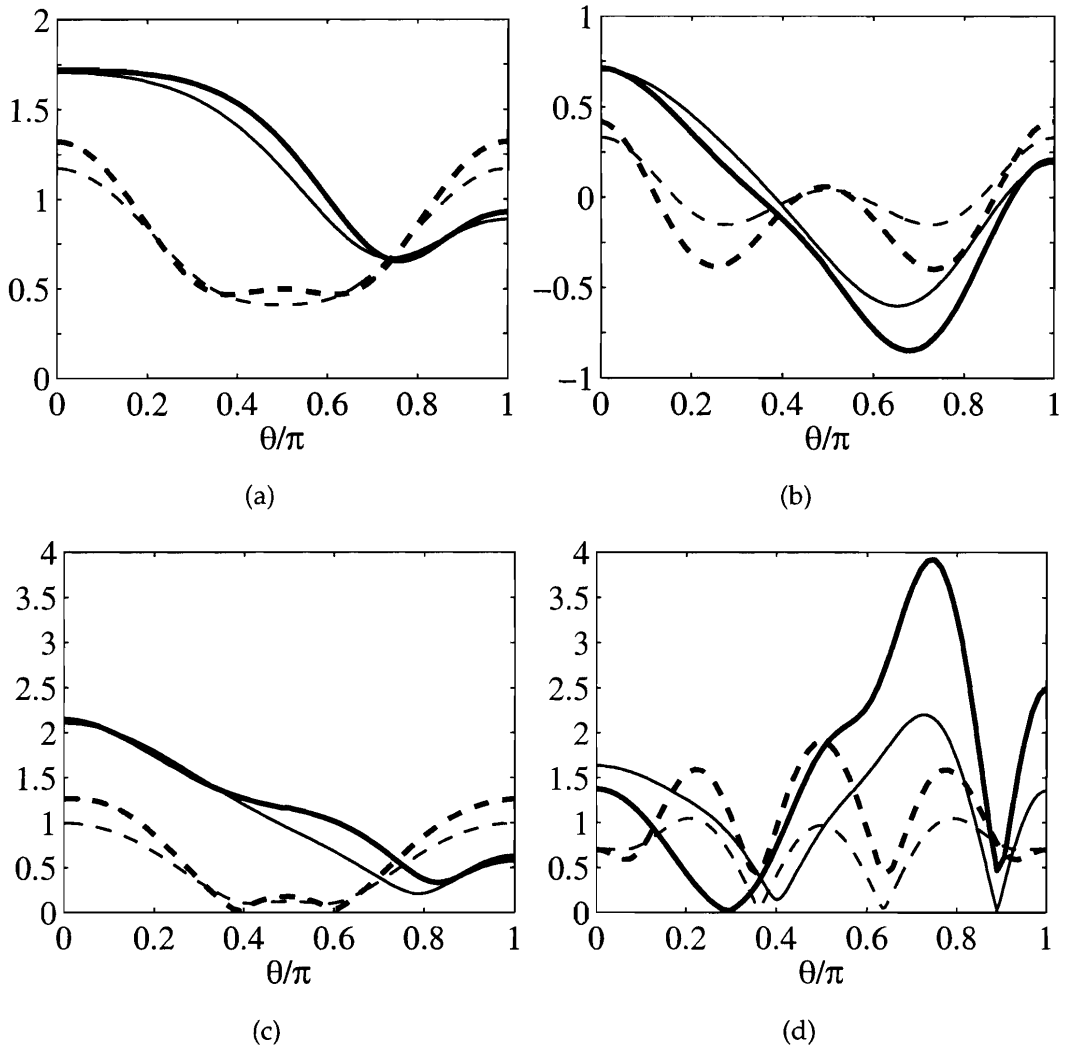

Figure 7-29: Free-surface heights along the semi-circular cylinder of the same radius attacked by an incident wave of the same frequency. For incident wave in deeper water : $k_0 h_0 = 2$. Thick lines are for variable depth, $h = h(r)$ varying from $40\,m$ to $20\,m$. Thin lines are for constant depth $h = h_0 = 40\,m$. Solid lines(—): Glancing incidence ($\theta_I = \pi$). Dashed lines (– –): Normal incidence ($\theta_I = 3\pi/2$). (a) $|\eta|/A$, (b) $|\eta^{(1)}_{2,0}|/(4k_0A^2)$, (c)$|\eta^{(1)}_{2,2}|/(2k_0A^2)$, (d) $|\eta^{(2)}_{2,2}|/(2k_0A^2)$.

7.3 Example 3: A Square Harbor open to a Semi-Circular Shoal

We consider a square harbor of constant depth behind the straight coast and open to the same semi-circular shoal studied in Section 7.1 . The width and length of the basin is 300 m while the depth is $h = 20$ m. The centered harbor entrance is 60 m wide and is formed by a pair of breakwaters of 5 m thickness, as sketched in Fig. 7-30. Outside the harbor the depth profile of the circular shoal has been defined in Eq. (7.1.1). Only normal incidence angle ($\theta_I = 3\pi/2$) is considered and the incident

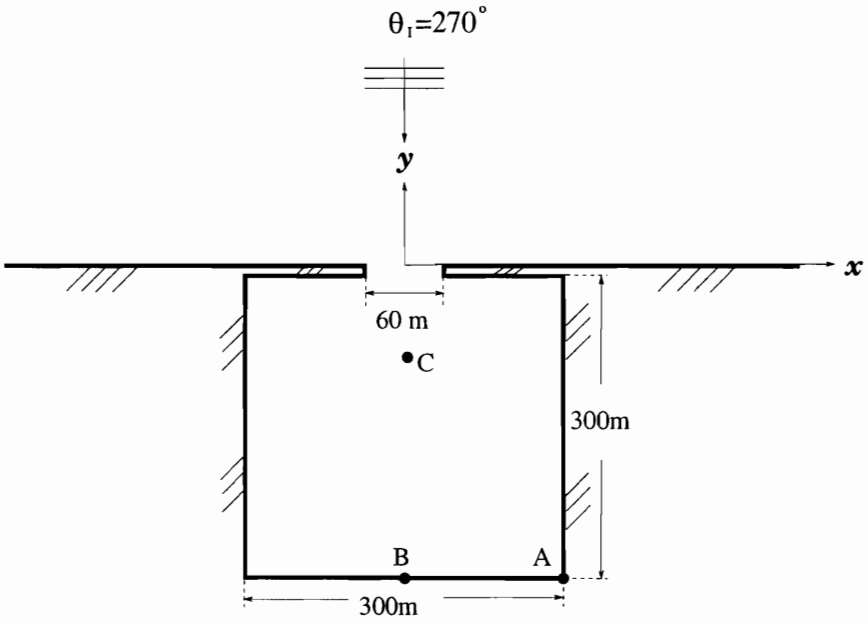

Figure 7-30: Plane view of the square basin and locations of point A ($x = 150m,\ y = -305m$), B ($x = 0m,\ y = -305m$) and C ($x = 0m,\ y = -86m$)

frequency is chosen to be $\omega = 0.7$ rad/s ; the corresponding kh varies from 2.06 at $h = 40\ m$ to 1.2 at $h = 20m$.

In the hybrid-element scheme, finite elements are used to discretize the square basin as well as the shoal, $r < a = 300\ m$, $0 < \theta < \pi$, Outside which ($\Omega_F : r > 300\ m,\ 0 < \theta < \pi$) the solution is analytical. Number of the elements used is $N_P = 145791$. The number of angular modes used in $N_\alpha = 201$ for the first-order problem and $N_{\widehat{\alpha}} = 91$ for the second-order problem. Domb-Sykes extrapolation is

used with three evanescent modes.

7.3.1 Natural modes in a closed square basin with constant depth

In order to understand the features of the computed result, it is useful to know the natural modes in a closed square basin with 300 m length with constant depth. Let the lateral boundaries of the square basin be $x = -150,\ 150$ m and $y = -305,\ -5$ m. For later reference, the eigensolutions for a closed square basin can be found by separation of variables

$$\eta = a_{n,m} \cos\left[\frac{n\pi}{300}(x + 150)\right] \cos\left[\frac{m\pi}{300}(y + 305)\right] \tag{7.3.1}$$

with $n, m = 0, 1, 2, 3, \cdots$. The corresponding eigenvalues are

$$k_{n,m} = \left[\left(\frac{n\pi}{300}\right)^2 + \left(\frac{m\pi}{300}\right)^2\right]^{1/2}. \tag{7.3.2}$$

The natural frequencies are

$$w_{n,m} = \left[g k_{n,m} \tanh\left(k_{n,m} h\right)\right]^{1/2}. \tag{7.3.3}$$

7.3.2 Numerical results

Figure 7-31 shows the first-order response curve $|\eta/A|$ with respect to the incident frequency ω at three locations : A ($x = 150m,\ y = -305m$), B ($x = 0m,\ y = -305m$) and near the opening C ($x = 0m,\ y = -86m$) (see Figure 7-30). It is shown that the chosen incident frequency ($\omega = 0.7$ rad/s) is close to the resonant peak $\omega_{re} = 0.696\ rad/s$ and the second-order double frequency ($2\omega = 1.4$ rad/s) is also close to another resonant peak.

The resonant frequency $\omega_{re} = 0.696\ rad/s$ observed from Fig. 7-31 corresponds to the mode $(n, m) = (4, 4)$ of the closed square basin which the natural frequency $\omega_{4,4} = 0.6937\ rad/s$, the corresponding wavenumber $k_{4,4} = 0.0592\ m^{-1}$ and wavelength $L_{4,4} = 106.067\ m$. According to Eq. (7.3.1), the absolute value of the corre-

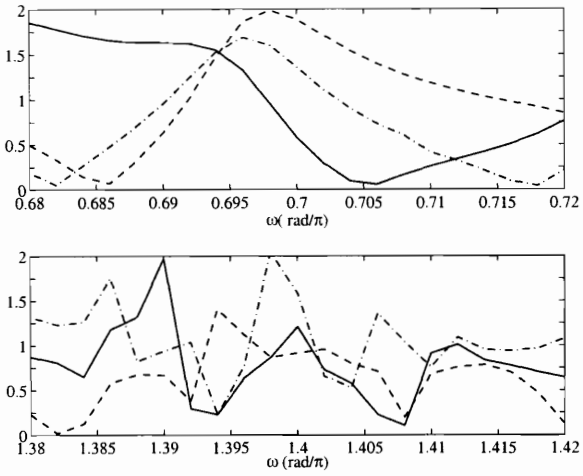

Figure 7-31: The first-order response $|\eta/A|$ vs. frequency ω for normal incidence waves at three locations. Chain line : A(x=150 m, y=-305 m), Solid line: B(x=0 m, y=-305 m) and Dashed line: C(x=0 m, y=-86 m).

sponding eigensolutions or natural mode $(4, 4)$ of the closed basin is

$$\left|\frac{\eta_{4,4}}{a_{4,4}}\right| = \left|\cos\left[\frac{4\pi}{300}(x+150)\right]\cos\left[\frac{\pi}{300}(y+305)\right]\right| \tag{7.3.4}$$

whose spatial structure is illustrated in Figure 7-32. It can be seen from Figure 7-32, at the four corners and the center of the circles, the amplitude is the greatest. On the other hand, the amplitude is zero along the eight nodal lines $x = \pm 37.5,\ \pm 112.5$ m and $y = -42.5,\ -117.5,\ -192.5,\ 267.5$ m. Because the chosen incident wave frequency, $\omega = 0.7\ rad/s$ is close to the resonant frequency $\omega = 0.696\ rad/s$, the contours of the first-order free surface amplitude inside the square basin, Figure 7-33, are similar to Figure 7-32. Inside the harbor, the standing waves with roughly $60\ m$ wavelength can be seen. Eight nodal lines are observed as well. Figure 7-34 is the 3D view of the first-order free surface amplitude η/A. By comparing the amplitude of the first-order runup within the shoal with example 1, diffraction due to the breakwater and the harbor entrance can be seen especially in front of the entrance. In particular, the first-order runup of example 3 is more oscillatory near the harbor entrance than that of example 1 (section 7.1). The five nodal points along the centerline in example 3 are closer to $y = 0\ m$ than in example 1, Fig-

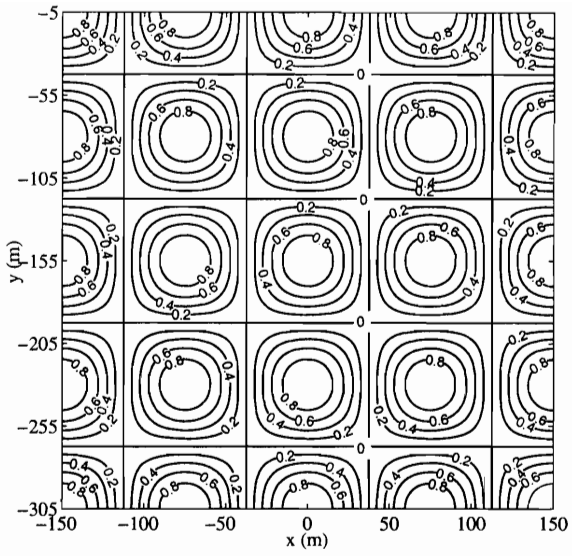

Figure 7-32: Contours of the free-surface amplitude of natural mode in a square basin for$(n, m) = (4, 4)$

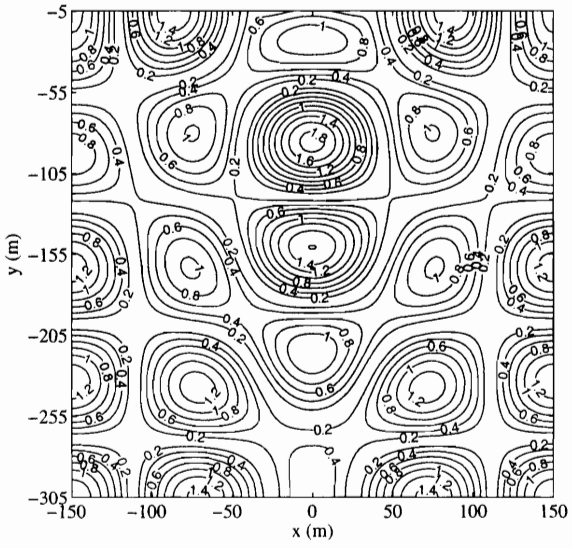

Figure 7-33: Contours of the first-order free-surface amplitude $|\eta/A|$ inside the square harbor with incident frequency $\omega = 0.7\ rad/s$

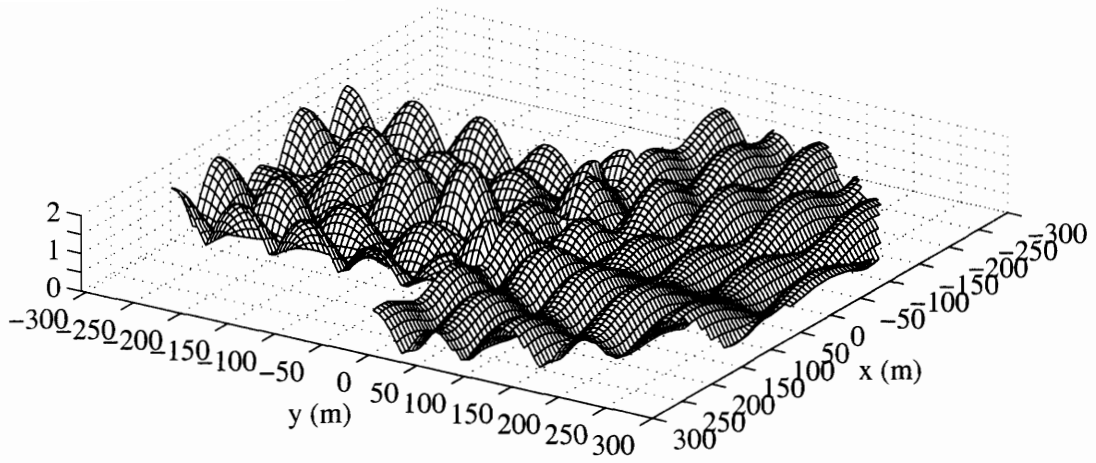

Figure 7-34: The first-order amplitude, $|\eta|/A$, for a square harbor open to a semi-circular shoal near a coast. Incident wave frequency $\omega = 0.7$ rad/s. Normal incidence ($\theta_I = 3\pi/2$).

ure 7-35. Also the magnitude of the peak ampification at the $y = \ 300\ m$ on the centerline($x = 0m$) is reduced from $1.25A$ (example 1) to around $1A$. The amplitude at $y = 0\ m$ on the centerline is also reduced from $1A$ (example 1) to $0.25A$. These can be understood because part of the wave energy is diffracted through the entrance into the harbor and reflected by the interior boundaries. Among the reflected waves, some escape the harbor and interfere with the diffracted wave by breakwater and the incident wave. In particular, for normal incidence, the greatest around $2A$ is on the centerline near the entrance due to the converging effect of the shoal and the diffraction from the breakwater.

The mean-sea-level setdown/setup is shown in Figure 7-36. Variations along the y axis is shown in Figure 7-37. As can be seen in Figure 7-36, the maximum setdown occurs along lines $x = \pm 37.5, \ \pm 112.5$ m and $y = -42.5, \ -117.5, \ -192.5, \ 267.5$ m where $|\eta| = 0$ is the smallest. The maximum setup occurs when $|\eta|$ is the greatest. The greatest setup and setdown are inside the harobr at $y =$

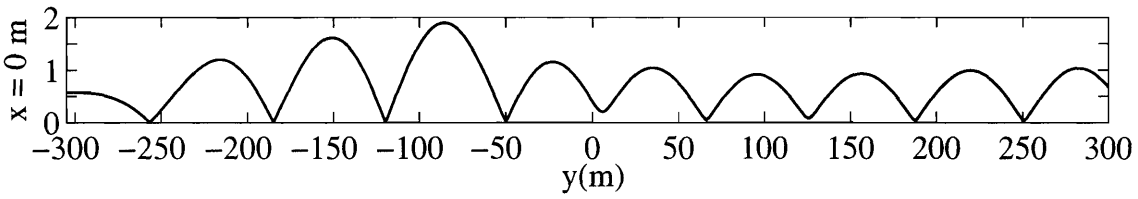

Figure 7-35: Variations of the first-order $|\eta|/A$ along the centerline $x = 0\ m$ for a square harbor open to a semi-circular shoal. Incident wave frequency $\omega = 0.7\ rad/s$. Normal incidence ($\theta_I = 3\pi/2$).

$-86\ m$ and $y = -120\ m$, respectively. By comparing the setdown/setup within the shoal with example 1, example 3 is more oscillatory than example 1. At $x = 0\ m$ on the centerline the mean-sea-level is negative(setdown) in example 3 while postive(setup) in example 1. Inside the harbor, its setup/setdown can be compared to the analytical formula for a standing wave mode (n, m) in a closed harbor

$$\begin{aligned}\frac{\eta_{20}}{a_{n,m}^2} =& \frac{\omega_{n,m}^2}{g}\left|\cos\left[\frac{n\pi}{300}(x+150)\right]\cos\left[\frac{m\pi}{300}(y+305)\right]\right|^2 \\ &- \frac{g}{\omega_{n,m}^2}\frac{n\pi}{300}\left\{\sin\left[\frac{n\pi}{300}(x+150)\right]\cos\left[\frac{m\pi}{300}(y+305)\right]\right\}^2 \\ &- \frac{g}{\omega_{n,m}^2}\frac{m\pi}{300}\left\{\cos\left[\frac{n\pi}{300}(x+150)\right]\sin\left[\frac{m\pi}{300}(y+305)\right]\right\}^2,\end{aligned} \tag{7.3.5}$$

Fig. (7-38) shows $\eta_{2,0}$ for $n = 4$, $m = 4$ which is close to that shown in Fig. 7-36.

The two parts of the second harmonic response at the second order are shown in figure 7-39 and 7-41. Again, similar to the first-order runup, eight nodal lines for $\eta_{2,2}^{(1)}$ are observed inside the harbor and has a peak at point $C(x = 0\ m, y = -86\ m)$ near the harbor entrance on the centerline($x = 0$)(Figure 7-40). The magnitude of the peak ampification at point C is around 3 times larger than the peaks on the shoal. By comparing $\eta_{2,2}^{(1)}$ within the shoal with example 1, the magnitude of the peak ampification near the $y = 300\ m$ on the centerline($x = 0m$) is reduced from $1.25A$(example 1) to around $0.75A$. The part $\eta_{2,2}^{(2)}$ associated with Φ_2 is shown in Figure 7-41 and Figure 7-42. For $\eta_{2,2}^{(2)}$, the value inside the harbor is much bigger than the value outside the harbor because the standing wave is excited by the

second-order double frequency. Inside the harbor there are roughly, 12 peaks along the boundary of the harbor ($y = -305\ m$,) the wavelenth of the standing wave is around 25m. It is useful to compare with Figure 7-43 for the spatial structure of the nature mode $(n, m) = (12, 15)$ of the closed square basin whose natural frequency is $\omega_{12,15} = 1.4036\ rad/s$, wavenumber $k_{12,15} = 0.2012\ m^{-1}$ and wavelength $L_{12,15} = 31.2348\ m$. According to Eq. (7.3.1), the absolute value of the corresponding eigensolutions or natural mode $(12, 15)$ of the closed basin is

$$\left|\frac{\eta_{12,15}}{a_{12,15}}\right| = \left|\cos\left(\frac{12\pi}{2} + \frac{15\pi x}{300}\right)\cos\left[12\pi\left(1 + \frac{5}{300}\right) + \frac{15\pi y}{300}\right]\right|. \tag{7.3.6}$$

By comparing $\eta_{2,2}^{(2)}$ within the shoal with example 1, unlike η,$\eta_{2,0,}^{(1)}$ and $\eta_{2,2}^{(1)}$, the response in example 3 is in general larger than example 1, especially near the entrance of the harbor. Due to the effect of diffraction, the spatial undulations for example 3 are much more rapid than example 1. The amplitude of the sum of the two complex amplitudes $\eta_{2,2}^{(1)} + \eta_{2,2}^{(2)}$ is shown in Figure 7-44, after accounting for their phases. It can be seen that $\eta_{2,2}^{(1)} + \eta_{2,2}^{(2)}$ oscillates nearly three times as fast as $\eta_{2,2}^{(1)}$ and 1.5 times as fast as $\eta_{2,2}^{(2)}$ in space. In general, $\eta_{2,2}^{(1)} + \eta_{2,2}^{(2)}$ inside the harbor is greater than the response within the shoal. The greatest $\eta_{2,2}^{(1)} + \eta_{2,2}^{(2)}$ is now at point $B(x = 0\ m, y = -305\ m)$. Within the shoal, near the entrance of the harbor the total response is much larger than near the edge of the shoal. Since within the shoal the magnitudes of $\eta_{2,2}^{(2)}$ is in general greater than $\eta_{2,2,}^{(1)}$, the features of the spatial variations of $\eta_{2,2}^{(2)}$ are preserved in $\eta_{2,2}^{(1)} + \eta_{2,2}^{(2)}$ (Figure 7-45).

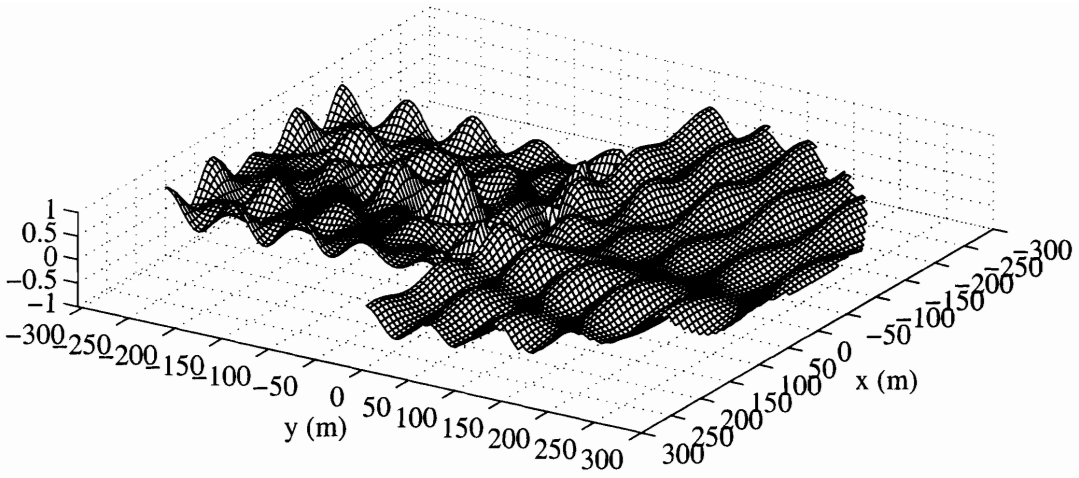

Figure 7-36: The second-order setup/down, $\eta^{(1)}_{2,0}/4k_0A^2$, for a square harbor with a semi-circular shoal near a coast. Incident wave frequency $\omega = 0.7$ rad/s. Normal incidence ($\theta_I = 3\pi/2$).

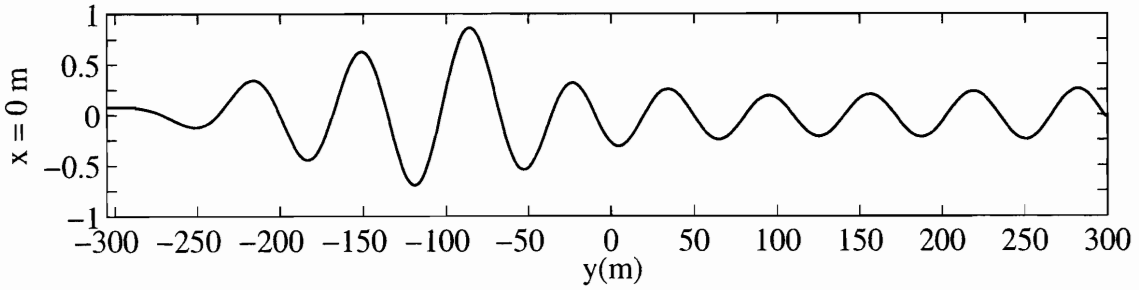

Figure 7-37: Variations of the second-order setup/down $\eta^{(1)}_{2,0}/4k_0A^2$ along the centerline $x = 0\ m$. Incident wave frequency $\omega = 0.7$ rad/s. Normal incidence ($\theta_I = 3\pi/2$).

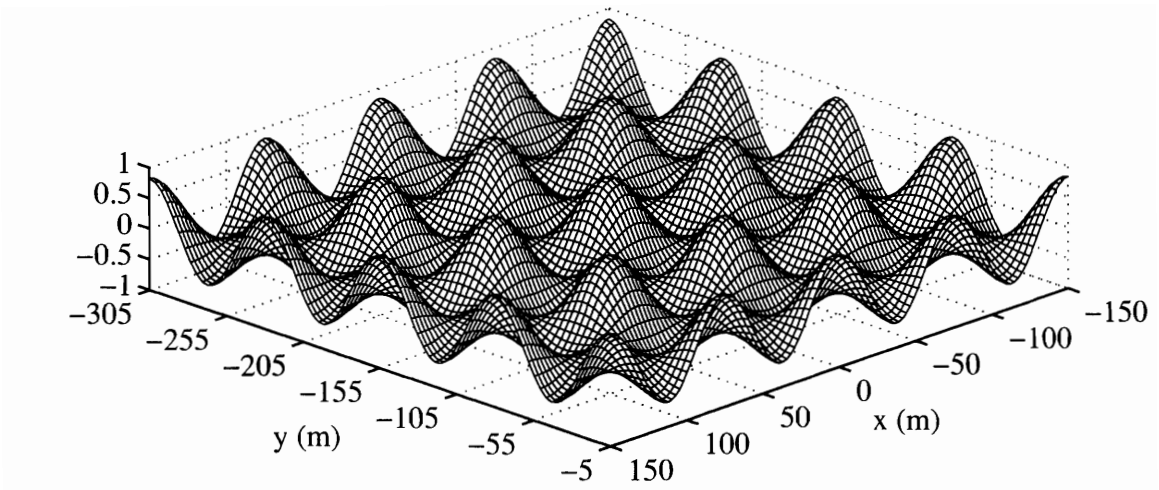

Figure 7-38: Setup/setdown $\eta_{2,0}/k_0 a_{n,m}$ of standing wave in a closed basin at mode $(n, m) = (4, 4)$

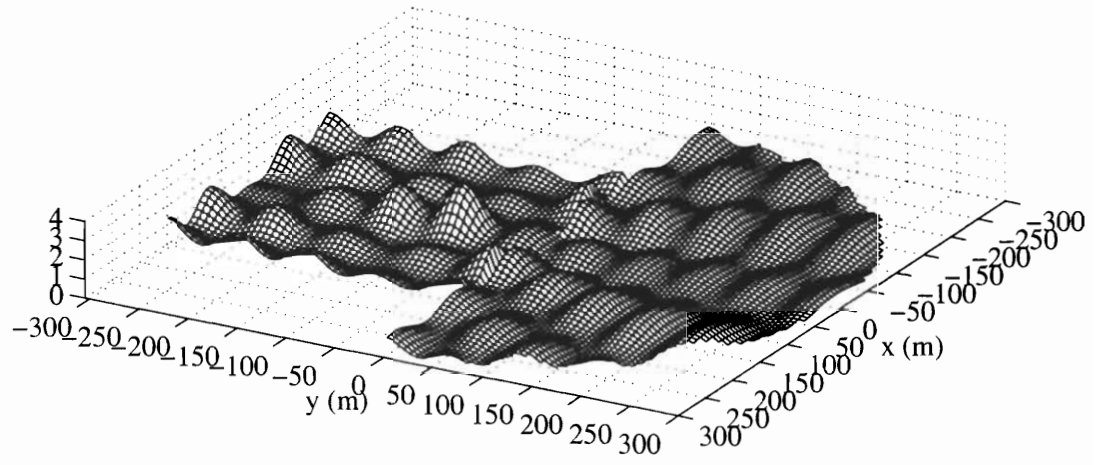

Figure 7-39: The second-order amplitude, $|\eta_{2,2}^{(1)}|/2k_0A^2$, for a square harbor open to a semi-circular shoal near a coast. Incident wave frequency $\omega = 0.7$ rad/s. Normal incidence ($\theta_I = 3\pi/2$).

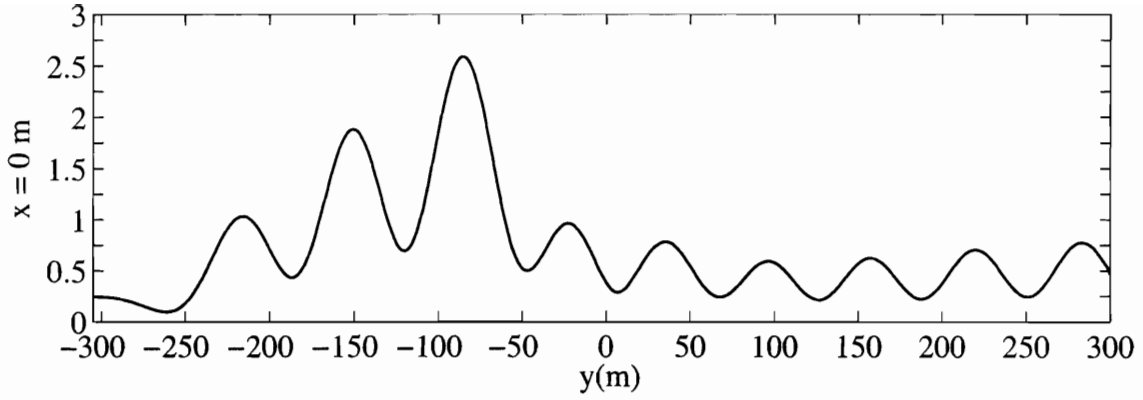

Figure 7-40: Variations of the second-order amplitude $|\eta_{2,2}^{(1)}|/2k_0A^2$. along the centerline $x = 0\ m$. Incident wave frequency $\omega = 0.7$ rad/s. Normal incidence ($\theta_I = 3\pi/2$).

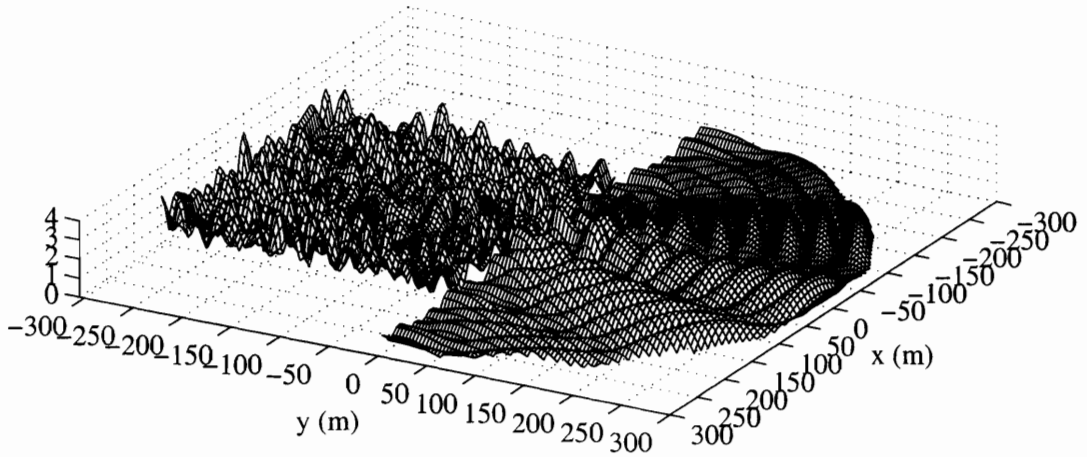

Figure 7-41: The second-order amplitude, $|\eta_{2,2}^{(2)}|/2k_0A^2$, for a square harbor open to a semi-circular shoal near a coast. Incident wave frequency $\omega = 0.7$ rad/s. Normal incidence ($\theta_I = 3\pi/2$).

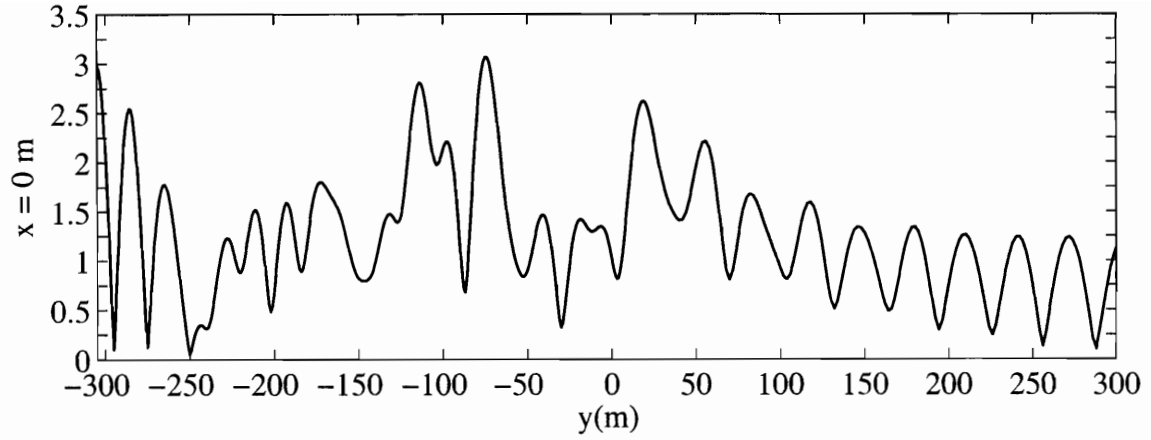

Figure 7-42: Variations of the second-order amplitude $|\eta^{(2)}_{2,2}|/2k_0A^2$ along the centerline $x = 0\ m$. Incident wave frequency $\omega = 0.7$ rad/s. Normal incidence ($\theta_I = 3\pi/2$).

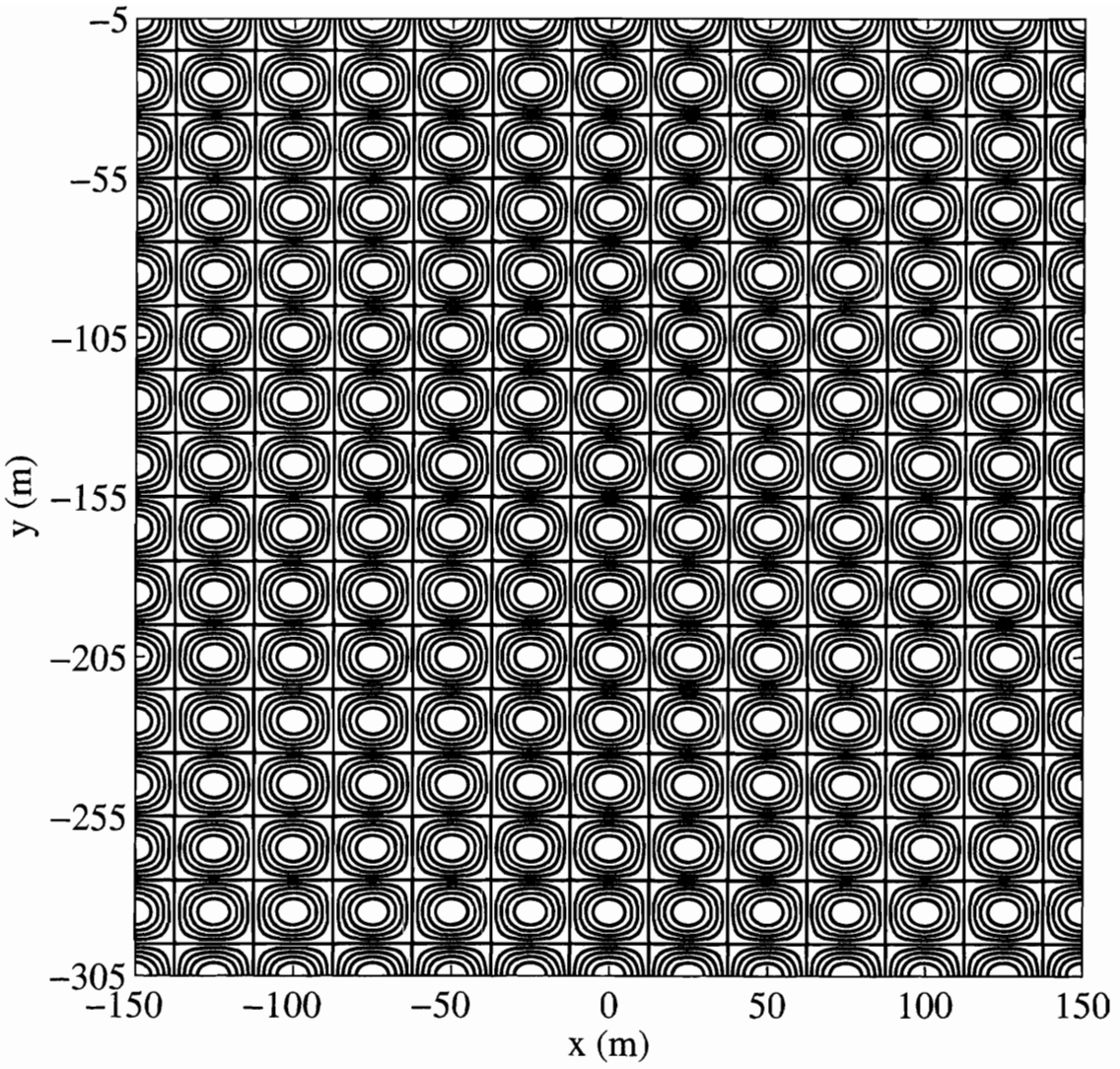

Figure 7-43: Contours of the first-order free-surface amplitude of natural mode in a square basin for$(n, m) = (12, 15)$

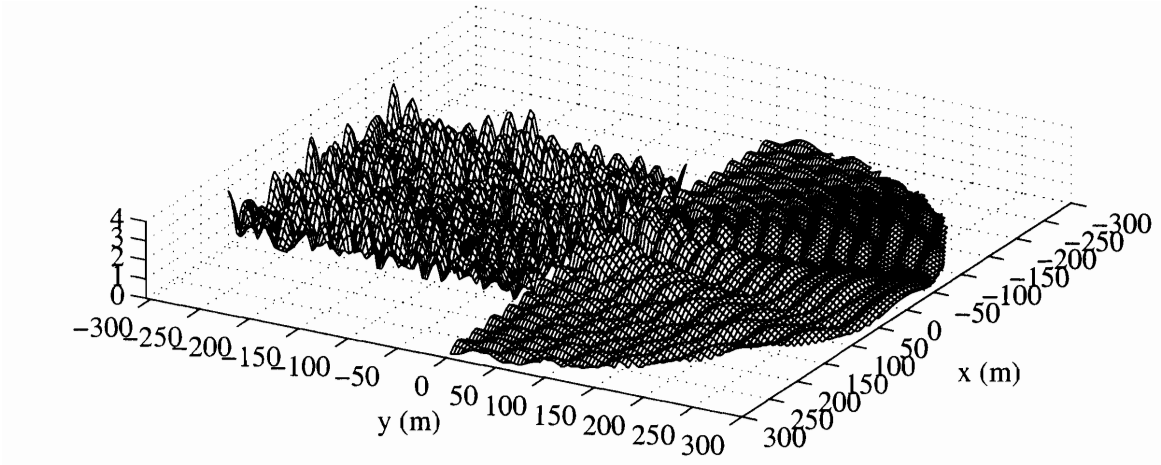

Figure 7-44: The dimensionless second-order amplitude, $|\eta_{2,2}^{(1)} + \eta_{2,2}^{(2)}|/2k_0A^2$,for a square harbor with a semi-circular shoal near a coast. Incident wave frequency $\omega = 0.7$ rad/s. Normal incidence ($\theta_I = 3\pi/2$).

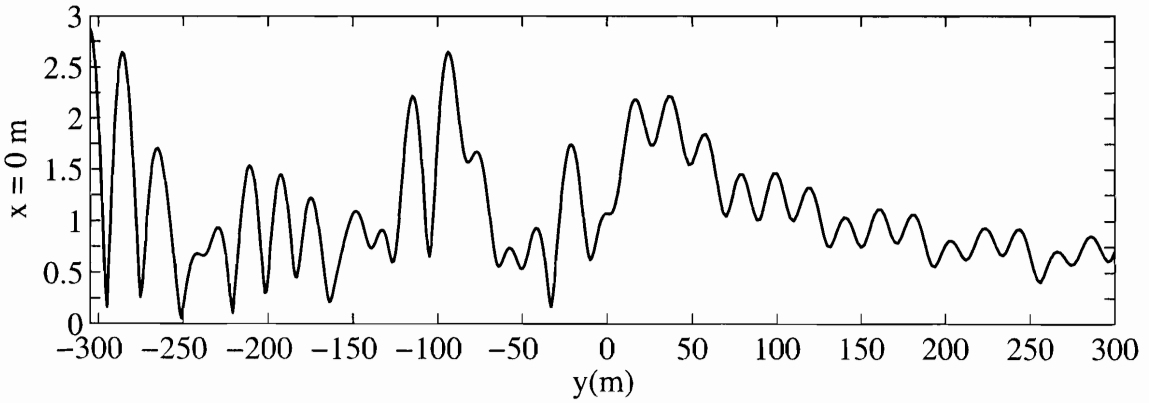

Figure 7-45: Variation of the second-order second-harmonic amplitude $|\eta_{2,2}^{(1)} + \eta_{2,2}^{(2)}|/2k_0A^2$ along the centerline $x = 0\ m$. Incident wave frequency $\omega = 0.7$ rad/s. Normal incidence ($\theta_I = 3\pi/2$).

Part II

Random Incident Waves

Chapter 8

Random Incident Sea

8.1 Incident wave spectrum

In Part II, the incident waves are assumed to be random. In this part, we assume that the first-order incident waves are a stationary and Gaussian stochastic process, long crested and unidirectional. The free surface of the unidirectional incident waves is described by the Fourier-Stieltjes integral

$$\zeta_1^{(I)}(r,\theta,t) = \int_{-\infty}^{\infty} A(\omega)\, e^{ik(\omega)r\cos(\theta-\theta_I)-i\omega t} d\omega, \tag{8.1.1}$$

where θ_I is the incident angle and $A(\omega)$ the random amplitude which satisfies

$$A^*(\omega) = A(-\omega) \tag{8.1.2}$$

since the free-surface elevation is real, with * being the complex conjugate. For each frequency ω, the wave number $k(\omega)$ is given by the dispersion relation

$$\omega^2 = gk\tanh kh.$$

Let us define the covariance function of the incident waves by

$$H_I(r,\theta,t,\tau) = \overline{\zeta_1^{(I)}(r,\theta,t)\,\zeta_1^{(I)^*}(r,\theta,t+\tau)}, \tag{8.1.3}$$

where the overline denotes ensemble averages. Putting Eqn. (8.1.1) into the previous equation, we obtain

$$H_I(r,\theta,t,\tau) = \int_{-\infty}^{\infty} S_I(r,\theta,t,\omega_2)\, e^{-ik(\omega_2)r\cos(\theta-\theta_I)+i\omega_2\tau} d\omega_2 \tag{8.1.4}$$

where S_I is the incident wave spectrum

$$S_I(r,\theta,t,\omega_2) = \int_{-\infty}^{\infty} \overline{A(\omega_1) A^*(\omega_2)} e^{i[k(\omega_1)-k(\omega_2)]r\cos(\theta-\theta_I)-i(\omega_1-\omega_2)t} d\omega_1. \tag{8.1.5}$$

For homogeneous and stationary incident waves, i.e. the incident waves spectrum is independent of space and initial time t, hence $A(\omega)$ obeys the relation

$$\overline{A(\omega_1) A^*(\omega_2)} = \mathbf{S}_A(\omega_1)\,\delta(\omega_1-\omega_2). \tag{8.1.6}$$

with $\mathbf{S}_A$ being the a two-sided frequency spectrum of the amplitudes A

$$\mathbf{S}_A(\omega_1) = \mathbf{S}_A(-\omega_1). \tag{8.1.7}$$

Thus for a spatially homogeneous and temporally stationary incident wave field,

$$S_I(r,\theta,t,\omega_2) = \mathbf{S}_A(\omega_2). \tag{8.1.8}$$

It follows that $H_I(r,\theta,t,\tau) = H_I(r,\theta,\tau)$ with

$$H_I(r,\theta,\tau) = \int_{-\infty}^{\infty} S_A(\omega_2)\, e^{-ik(\omega_2)r\cos(\theta-\theta_I)+i\omega_2\tau} d\omega_2, \tag{8.1.9}$$

or equivalently,

$$H_I(r,\theta,\tau) = \Re\left\{\int_0^{\infty} 2S_A(\omega_2)\, e^{-ik(\omega_2)r\cos(\theta-\theta_I)+i\omega_2\tau} d\omega_2\right\}. \tag{8.1.10}$$

with $\Re\{\}$ being the real part. It is clear that the one-sided spectrum is two times the two-sided spectrum.

We shall take the TMA (a modified JONSWAP) spectrum(one-sided) as being representative of $2S_A(\omega_2)$.

8.2 TMA spectrum

The TMA spectrum formulation is developed as an extension of the well known JONSWAP spectrum(deep water spectrum) so that it can applied to wind-generated seas in finite water depth (Bouws et al.(1985) [7]). Its validity is verified through analysis of three sets of data obtained (a) near *TEXEL* in the North Sea, (b) during the *MARSEN* Project conducted in the North Sea and (c) in the *ARSLOE* Project carried out at Duck, North Carolina, USA. The concept is based on the similarity law shown by Kitaigorodskii et al. (1975) [19], who introduced the factor

$$T = \left(\frac{\omega^2 h}{gkh}\right)^3 \left[\tanh kh + kh\cosh^2 kh\right]^{-1} \tag{8.2.1}$$

with ω and k satisfying the dispersion relation $\omega^2 = gk\tanh kh$, to extend Phillips' spectrum from deep to finite water. The transformation factor T are plotted in Figure 8-1.

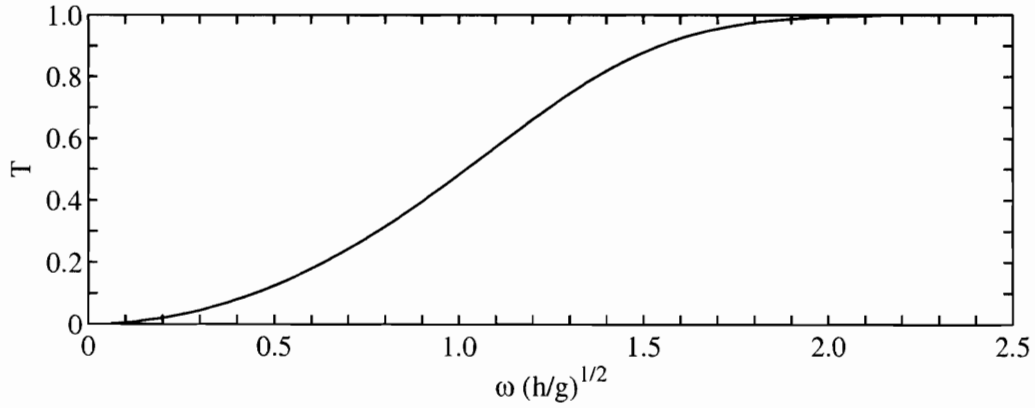

Figure 8-1: Transformation factor T as a function of dimensionless frequency $\omega(h/g)^{1/2}$.

Bouws et al.(1985) [7] applied the same transformation factor T to the JON-

SWAP spectrum. The result is called the TMA spectrum:(Cf. Ochi 1998, pp.48[29])

$$S_{TMA}(\omega) = [S_{JON}(\omega)] \times T \tag{8.2.2}$$

where $S_{JON}(\omega)$ is the JONSWAP spectrum.

$$S_{JON}(\omega) = \alpha \frac{g^2}{\omega^5} \exp\left\{-1.25\left(\omega_p/\omega\right)^4\right\} \gamma^{\exp\left\{-(\omega-\omega_p)^2/2(\sigma\omega_p)^2\right\}} \tag{8.2.3}$$

where $\gamma =$ peak-shape parameter, 3.3 as an average,

$$\omega_p = 2\pi f_p = 7\pi\left(g/\bar{U}\right)\bar{x}^{-0.33}, \tag{8.2.4}$$

$$\alpha = 0.076\bar{x}^{-0.22}, \qquad \sigma = \begin{cases} 0.07 & \text{for } \omega \leq \omega_p, \\ 0.09 & \text{for } \omega \geq \omega_p, \end{cases}$$

with $\bar{x}$ being dimensionless fetch

$$\bar{x} = \frac{gx}{\bar{U}^2},$$

x the fetch length, $\bar{U}$ the mean wind speed and g gravity constant. The formula can be expressed in terms of the frequency f in Hz as

$$S_{JON}(f) = \alpha \frac{g^2}{(2\pi)^4} \frac{1}{f^5} \exp\left\{-1.25\left(f_p/f\right)^4\right\} \gamma^{\exp\left\{-(f-f_p)^2/2(\sigma f_p)^2\right\}} \tag{8.2.5}$$

where $f = \omega/2\pi$ and $f_p = \omega_p/2\pi$. Note that $S(f) = 2\pi S(\omega)$.

Examples of the TMA spectrum and the JONSWAP spectrum are shown in Figure 8-2.

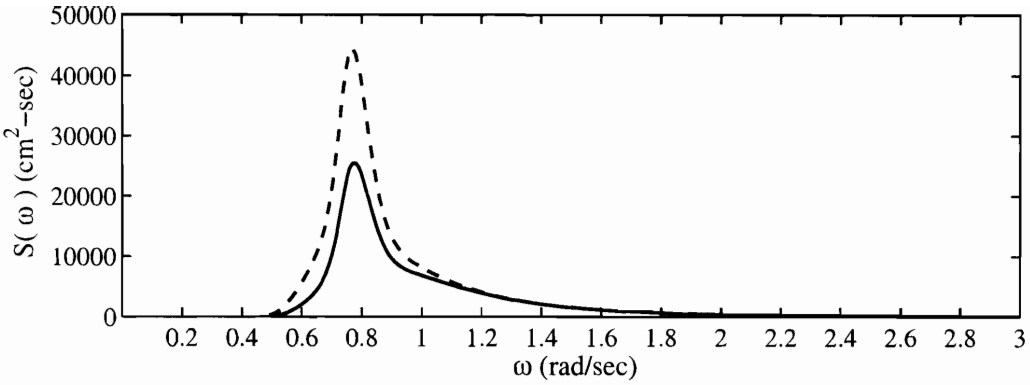

Figure 8-2: Comparison between the TMA and the JONSWAP spectrum with $\gamma = 3.3$, $\bar{U} = 20\ m^2/sec$, $\bar{x} = 3000$. Solid line: S_{TMA} for $h = 20\ m$. Dashed line: S_{JON}.

8.3 First-order Diffraction

Because the first-order incident waves are a homogeneous and stationary random process, the first-order velocity potential is given by

$$\Phi_1(\mathbf{x}, t) = \int_{-\infty}^{\infty} A(\omega)\, \phi_1(\mathbf{x}, \omega)\, e^{-i\omega t} d\omega, \tag{8.3.1}$$

where $\phi_1(\mathbf{x}, \omega)$ is the unit potential which is the deterministic single frequency response.

Putting Eqn. (8.3.1) into the first-order perturbation equations, Eqs. (2.2.3), (2.2.4) and (2.2.6), we find that $\phi_1(\mathbf{x}, \omega)$ satisfies the following equations:

$$\left(\frac{\partial^2}{\partial x} + \frac{\partial^2}{\partial y^2} + \frac{\partial^2}{\partial z^2}\right) \phi_1(\mathbf{x}, \omega) = 0, \quad -h(x, y) < z < 0, \tag{8.3.2}$$

$$\frac{\partial \phi_1(\mathbf{x}, \omega)}{\partial z} = -\nabla \phi_1(\mathbf{x}, \omega) \cdot \nabla h, \quad z = -h(x, y), \tag{8.3.3}$$

$$\frac{\partial \phi_1(\mathbf{x}, \omega)}{\partial z} - \frac{\omega^2}{g} \phi_1(\mathbf{x}, \omega) = 0, \quad z = 0. \tag{8.3.4}$$

Let us assume

$$\phi_1(\mathbf{x}, \omega) = -\frac{ig}{\omega} \frac{\cosh[k(\omega)(z + h)]}{\cosh[k(\omega) h]} \Gamma_1(x, y, \omega), \tag{8.3.5}$$

where ω and $k(\omega)$ satisfy dispersion relation $\omega^2 = gk(\omega)\tanh[k(\omega)h]$, and $\Gamma_1(x,y,\omega)$ is the unit transfer function of the free surface displacement. By applying the similar procedure as in Section 3.1, Γ_1 is governed by the modified mild-slope equation of Chamberlain and Porter(1995)

$$\nabla\cdot[CC_g\nabla\Gamma_1(x,y,\omega)]+\left[k^2CC_g+gU\nabla^2h+gV(\nabla h)^2\right]\Gamma_1(x,y,\omega)=0, \tag{8.3.6}$$

where the coefficients U and V depend on ω through the dispersion relation

$$U(\omega)=\frac{\sinh 2kh-2kh\cosh 2kh}{4\cosh^2(kh)(2kh+\sinh 2kh)}, \tag{8.3.7}$$

$$\begin{aligned}V(\omega)=&\frac{k\left[(2kh)^4+4(2kh)^3\sinh 2kh-9\sinh 2kh\sinh 4kh\right]}{12\cosh^2(kh)(2kh+\sinh 2kh)^3}\\&+\frac{k\left[kh(kh+\sinh 2kh)\left(\cosh^2 2kh-2\cosh 2kh+3\right)\right]}{\cosh^2(kh)(2kh+\sinh 2kh)^3}\end{aligned} \tag{8.3.8}$$

with

$$C(\omega)=\frac{\omega}{k} \tag{8.3.9}$$

being the phase velocity, and

$$C_g(\omega)=\frac{C}{2}\left(1+\frac{2kh}{\sinh 2kh}\right) \tag{8.3.10}$$

the group velocity. In the limit of constant depth, Eqn. (8.3.6) reduces to Helmholtz equation,

$$\nabla^2\Gamma_1(x,y,\omega)+k^2\Gamma_1(x,y,\omega)=0. \tag{8.3.11}$$

By putting Eqs. (8.3.1) and (8.3.5) into Eq. (2.2.7), the first-order free surface displacement is given by

$$\zeta_1(x,y,t)=\int_{-\infty}^{\infty}A(\omega)\Gamma_1(x,y,\omega)e^{-i\omega t}d\omega. \tag{8.3.12}$$

Since the free surface displacement is real,

$$\zeta_1(x,y,t) \equiv \zeta_1^*(x,y,t), \tag{8.3.13}$$

we get by using Eqn. (8.1.2)

$$\Gamma_1^*(x,y,\omega) = \Gamma_1(x,y,-\omega) \tag{8.3.14}$$

8.4 Second-order Diffraction

8.4.1 The potential

At the second order, let us rewrite the inhomogeneous free surface boundary condition

$$\frac{\partial \Phi_2}{\partial z} + \frac{1}{g}\frac{\partial^2 \Phi_2}{\partial t^2} = \mathbf{F} \tag{8.4.1}$$

where

$$\mathbf{F} = \frac{1}{g^2}\frac{\partial \Phi_1}{\partial t}\frac{\partial}{\partial z}\left[g\left(\frac{\partial \Phi_1}{\partial z}\right) + \frac{\partial^2 \Phi_1}{\partial t^2}\right] - \frac{1}{g}\frac{\partial}{\partial t}\left(\nabla_3 \Phi_1\right)^2, \quad z = 0. \tag{8.4.2}$$

With the assumption of Eq. (8.3.1), the random forcing $\mathbf{F}$ becomes

$$\mathbf{F} = \int_{-\infty}^{\infty}\int_{-\infty}^{\infty} A(\omega_1) A(\omega_2) f(x,y,\omega_1,\omega_2) e^{-i(\omega_1+\omega_2)t} d\omega_1 d\omega_2 \tag{8.4.3}$$

where

$$\begin{aligned} f(x,y,\omega_1,\omega_2) = \Bigg\{ &-\frac{i\omega_1}{g}\phi_1(\mathbf{x},\omega_1)\left[\frac{\partial^2 \phi_1(\mathbf{x},\omega_2)}{\partial z^2} - \frac{\omega_2^2}{g}\frac{\partial \phi_1(\mathbf{x},\omega_2)}{\partial z}\right] \\ &+ \frac{i(\omega_1+\omega_2)}{g}\nabla_3\phi_1(\mathbf{x},\omega_1)\cdot\nabla_3\phi_1(\mathbf{x},\omega_2)\Bigg\}_{z=0}. \end{aligned} \tag{8.4.4}$$

Putting Eq. (8.3.5) into the previous equation, we get

$$\begin{aligned} f\left(x,y,\omega_1,\omega_2\right) =& \beta_1\left(\omega_1,\omega_2\right)\Gamma_1\left(x,y,\omega_1\right)\Gamma_1\left(x,y,\omega_2\right) \\ &+ \beta_2\left(\omega_1,\omega_2\right)\nabla_2\Gamma_1\left(x,y,\omega_1\right)\cdot\nabla_2\Gamma_1\left(x,y,\omega_2\right) \end{aligned} \tag{8.4.5}$$

with

$$\beta_1\left(\omega_1,\omega_2\right) = \frac{ig\left[k\left(\omega_2\right)\right]^2}{\omega_2} - \frac{i\omega_2^3}{g} - \frac{i\left(\omega_1+\omega_2\right)\omega_1\omega_2}{g}, \tag{8.4.6}$$

and

$$\beta_2\left(\omega_1,\omega_2\right) = -\frac{i\left(\omega_1+\omega_2\right)g}{\omega_1\omega_2}. \tag{8.4.7}$$

Note if $\omega_1+\omega_2=0$ ($\omega_2=-\omega_1$), we get

$$\beta_1\left(\omega_1,-\omega_1\right) = -\beta_1(-\omega_1,\omega_1), \quad \beta_2(\omega_1,-\omega_1) = \beta_2(-\omega_1,\omega_1) = 0, \tag{8.4.8}$$

which leads to the following expression

$$f(\omega_1,-\omega_1) = -f(-\omega_1,\omega_1). \tag{8.4.9}$$

From the inhomogeneous forcing term on the free surface, Eq. (8.4.3), we expect the second-order potential to be a double integral

$$\Phi_2\left(\mathbf{x},t\right) = \int_{-\infty}^{\infty}\int_{-\infty}^{\infty} A\left(\omega_1\right)A\left(\omega_2\right)\phi_2\left(\mathbf{x},\omega_1,\omega_2\right)e^{-i(\omega_1+\omega_2)t}d\omega_1 d\omega_2. \tag{8.4.10}$$

with $\mathbf{x}=(x,y,z)$ and $\phi_2\left(\mathbf{x},\omega_1,\omega_2\right)$ will be deterministically obtained.

Putting Eq. (8.4.10) into Eqs. (2.2.8), (2.2.9) and (2.2.11), we find that $\phi_2\left(\mathbf{x},\omega_1,\omega_2\right)$ satisfies the Laplace equation

$$\nabla^2\phi_2\left(\mathbf{x},\omega_1,\omega_2\right) + \frac{\partial^2\phi_2\left(\mathbf{x},\omega_1,\omega_2\right)}{\partial z^2} = 0, \quad -h(x,y) < z < 0, \tag{8.4.11}$$

the boundary condition at the sea bottom

$$\frac{\partial\phi_2\left(\mathbf{x},\omega_1,\omega_2\right)}{\partial z} = -\nabla\phi_2\left(\mathbf{x},\omega_1,\omega_2\right)\cdot\nabla h, \quad z=-h(x,y), \tag{8.4.12}$$

and the free surface boundary condition,

$$\frac{\partial \phi_2 (\mathbf{x}, \omega_1, \omega_2)}{\partial z} - \frac{(\omega_1 + \omega_2)^2}{g} \phi_2 (\mathbf{x}, \omega_1, \omega_2) = f (x, y, \omega_1, \omega_2), \ z = 0. \tag{8.4.13}$$

Since ω_1 and ω_2 can be either positive or negative, $(\omega_1 + \omega_2)$ includes the sum $|\omega_1| + |\omega_2|$ and the difference $|\omega_1| - |\omega_2|$. In summary, Eqns. (8.4.11), (8.4.12) and (8.4.13) form the second-order boundary value problem.

Now let us assume that the second-order potential $\phi_2 (\mathbf{x}, \omega_1, \omega_2)$ has the following form

$$\phi_2 (\mathbf{x}, \omega_1, \omega_2) = -\frac{ig}{\omega_1 + \omega_2} \sum_{m=0}^{\infty} \xi_m (x, y, \omega_1, \omega_2) \frac{\cos \kappa_m (z + h)}{\cos \kappa_m h}, \tag{8.4.14}$$

where κ_m, $m = 1, 2, \ldots$ are the real roots of the equation

$$-(\omega_1 + \omega_2)^2 = g \kappa_m \tan \kappa_m h, \quad (m - 1/2)\pi \leq \kappa_m h \leq m\pi, \tag{8.4.15}$$

and κ_0 are

$$\kappa_0 = -i \widehat{\kappa}_0, \tag{8.4.16}$$

with $\widehat{\kappa}_0$ being the real root of the dispersion equation

$$(\omega_1 + \omega_2)^2 = g \widehat{\kappa}_0 \tanh \widehat{\kappa}_0 h. \tag{8.4.17}$$

Note that $m = 0$ represents the propagating mode in which the waves propagates to infinity where the radiation condition must be applied, while $m \geq 1$ represent the evanescent modes in which the waves represent local effects. Applying the similar procedure of using Green's formula as in the first order,we obtain a modi-

fied couple-mode mild-slope equation for ξ_ℓ (see Appendix C for details):

$$\sum_{\ell=0}^{\infty}\left\{\nabla\cdot\left[A_{m,\ell}\nabla\xi_\ell\left(x,y,\omega_1,\omega_2\right)\right]+B_{m,\ell}\nabla\xi_\ell\left(x,y,\omega_1,\omega_2\right)\cdot\nabla h+C_{m,\ell}\xi_\ell\left(x,y,\omega_1,\omega_2\right)\right\}$$
$$=-i\left(\omega_1+\omega_2\right)f\left(x,y,\omega_1,\omega_2\right), \tag{8.4.18}$$

where

$$A_{m,\ell}=\begin{cases}\frac{gh}{2\cos^2\kappa_\ell h}\left(1+\frac{\sin 2\kappa_\ell h}{2\kappa_\ell h}\right) & \text{when, } m=l\\ 0 & \text{when, } m\neq l\end{cases} \tag{8.4.19}$$

$$B_{m,\ell}=\begin{cases}0 & \text{when, } m=l\\ g\left(U_{m,\ell}-U_{\ell,m}\right), & \text{when, } m\neq l\end{cases} \tag{8.4.20}$$

with the $U_{m,\ell}$ being

$$U_{m,\ell}=\begin{cases}\frac{\sin 2\kappa_m h-2\kappa_m h\cos 2\kappa_m h}{4\cos^2(\kappa_m h)(2\kappa_m h+\sin 2\kappa_m h)} & \text{when, } m=l,\\ -\frac{\kappa_\ell^2}{\left(\kappa_\ell^2-\kappa_m^2\right)\cos\kappa_m h\cos\kappa_{n,l}h}, & \text{when, } m\neq l,\end{cases} \tag{8.4.21}$$

and

$$C_{m,\ell}=\begin{cases}-\kappa_m^2A_{m,m}+gU_{m,m}\nabla^2h+gV_{m,m}\left(\nabla h\right)^2, & \text{if, } m=l\\ gU_{m,\ell}\nabla^2h+gV_{m,\ell}\left(\nabla h\right)^2, & \text{if , } m\neq l\end{cases} \tag{8.4.22}$$

with $U_{m,\ell}$ being Eq. (8.4.21) and $V_{m,\ell}$ being the following equations. For $m=l$,

$$V_{m,m}=\frac{-\kappa_m\sec^2\left(\kappa_m h\right)}{12\left(2\kappa_m h+\sin 2\kappa_m h\right)^3}\left[\left(2\kappa_m h\right)^4+4\left(2\kappa_m h\right)^3\sin 2\kappa_m h+9\sin\left(2\kappa_m h\right)\sin 4\kappa_m h\right.$$
$$\left.-12\kappa_m h\left(\kappa_m h+\sin 2\kappa_m h\right)\left(\cos^2 2\kappa_m h-2\cos 2\kappa_m h+3\right)\right], \tag{8.4.23}$$

For $m \neq \ell$,

$$V_{m,\ell} = \frac{-2\kappa_\ell \sec \kappa_m h \sec \kappa_\ell h}{(2\kappa_\ell h + \sin 2\kappa_\ell h)} \frac{\left[4\kappa_\ell^2 \kappa_m^2 + (\kappa_\ell^4 - \kappa_m^4) \sin^2 \kappa_\ell h\right]}{(\kappa_\ell^2 - \kappa_m^2)^2}. \tag{8.4.24}$$

Note that Eq. (8.4.18) forms a matrix equation and $C_{m,\ell}$ contains $O(1)$, $O(\mu)$,and $O(\mu^2)$ terms. In summary, the second order theory is accurate by including terms of $O(1, \epsilon,\ \epsilon\mu,\ \epsilon\mu^2,\ \epsilon^2,$ and $\epsilon^2\mu^2)$. Finally, these are of the same form as these for monochromatic waves with 2ω replaced by $(\omega_1 + \omega_2)$

For constant depth , Eq. (8.4.18) becomes

$$\sum_{\ell=0}^{\infty} \left\{A_{m,\ell} \nabla^2 \xi_\ell + C_{m,\ell} \xi_\ell\right\} = -i\left(\omega_1 + \omega_2\right) f\left(x, y, \omega_1, \omega_2\right), \qquad m = 0, 1, 2, 3 \cdots, \tag{8.4.25}$$

or in matrix form

$$\mathbb{A}\nabla^2 \boldsymbol{\xi} + \mathbb{C}\boldsymbol{\xi} = \mathbb{D} \tag{8.4.26}$$

where

$$\mathbb{A} = diag\left[A_{0,0}, A_{1,1}, \cdots, A_{N,N}, \cdots\right], \tag{8.4.27}$$

$$\mathbb{C} = diag\left[-\kappa_0^2 A_{0,0}, -\kappa_1^2 A_{1,1}, \cdots, -\kappa_N^2 A_{N,N}, \cdots\right], \tag{8.4.28}$$

$$\mathbb{D} = -i\left(\omega_1 + \omega_2\right) f\left[1, 1, 1, \cdots, 1\right], \tag{8.4.29}$$

$$\boldsymbol{\xi} = \left[\xi_0, \xi_1, \cdots, \xi_N, \cdots\right]. \tag{8.4.30}$$

Note that both $\mathbb{A}$ and $\mathbb{C}$ are diagonal matrices. Since $\mathbb{A}$ is nonsingular, we can multiply Eq. (8.4.26) with the inverse of $\mathbb{A}$ on the left. Then we obtain a set of

equations in which each mode is independent to the others

$$\nabla^2\xi_0 - \kappa_0^2\xi_0 = -i\frac{\omega_1+\omega_2}{A_{0,0}}f, \tag{8.4.31}$$

$$\nabla^2\xi_1 - \kappa_1^2\xi_1 = -i\frac{\omega_1+\omega_2}{A_{1,1}}f, \tag{8.4.32}$$

$$\cdots\cdots\cdots\cdots\cdots, \tag{8.4.33}$$

$$\nabla^2\xi_N - \kappa_N^2\xi_N = -i\frac{\omega_1+\omega_2}{A_{N,N}}f \tag{8.4.34}$$

$$\cdots\cdots\cdots\cdots\cdots. \tag{8.4.35}$$

Eq. (8.4.18) and (8.4.31)-(8.4.34) must be solved with the boundary condition on the coastal boundaries andthe radiations condition at infinity.

8.4.2 The free surface displacement

From Eq. (2.2.12), we obtain the second-order free surface elevation

$$\zeta_2(\mathbf{x},t) = \int_{-\infty}^{\infty}\int_{-\infty}^{\infty} A(\omega_1)\,A(\omega_2)\,\Gamma_2(x,y,\omega_1,\omega_2)\,e^{-i(\omega_1+\omega_2)t}d\omega_1 d\omega_2, \tag{8.4.36}$$

where

$$\begin{aligned}\Gamma_2(x,y,\omega_1,\omega_2) = &-\frac{\omega_1\omega_2}{g^2}\phi_1(\mathbf{x},\omega_1)\frac{\partial\phi_1(\mathbf{x},\omega_2)}{\partial z} - \frac{1}{2g}\nabla_3\phi_1(\mathbf{x},\omega_1)\cdot\nabla_3\phi_1(\mathbf{x},\omega_2)\\ &+\frac{i\sigma}{g}\phi_2(\mathbf{x},\omega_1,\omega_2).\end{aligned} \tag{8.4.37}$$

Making use of the expression of ϕ_1 and ϕ_2, we get

$$\begin{aligned}\Gamma_2(x,y,\omega_1,\omega_2) = &\left(\frac{\omega_2^2}{g}+\frac{\omega_1\omega_2}{2g}\right)\Gamma_1(\omega_1)\Gamma_1(\omega_2) + \frac{g}{2\omega_1\omega_2}\nabla_2\Gamma_1(\omega_1)\cdot\nabla_2\Gamma_1(\omega_2)\\ &+\sum_{\ell=0}^{\infty}\xi_\ell(\omega_1,\omega_2)\end{aligned} \tag{8.4.38}$$

The ensemble average of ζ_2 is the second-order mean setup or setdown

$$\begin{aligned}\overline{\zeta_2}(\mathbf{x},t) &= \int_{-\infty}^{\infty}\int_{-\infty}^{\infty}\overline{A(\omega_1)A(\omega_2)}\Gamma_2(x,y,\omega_1,\omega_2)\,e^{-i(\omega_1+\omega_2)t}d\omega_1 d\omega_2 \\ &= \int_{-\infty}^{\infty} S_A(\omega)\,\Gamma_2(x,y,\omega_1,-\omega_1)\,d\omega_1\end{aligned} \quad . \tag{8.4.39}$$

where

$$\begin{aligned}\Gamma_2(x,y,\omega_1,-\omega_1) = \left(\frac{\omega_1^2}{g}-\frac{\omega_1^2}{2g}\right)\Gamma_1(\omega_1)\,\Gamma_1(-\omega_1) - \frac{g}{2\omega_1^2}\nabla_2\Gamma_1(\omega_1)\cdot\nabla_2\Gamma_1(-\omega_1) \\ + \sum_{\ell=0}^{\infty}\xi_\ell(\omega_1,-\omega_1)\end{aligned} \tag{8.4.40}$$

Note that for $\omega_1 = -\omega_2$ all forcing terms in Eqs. (8.4.18) and (8.4.31)-(8.4.34) vanish. Hence $\xi_\ell(\omega_1,-\omega_1) = \xi_\ell(-\omega_1,\omega_1) = 0$. Eq. (8.4.39) can be rewritten as integrated from 0 to ∞

$$\overline{\zeta_2}(\mathbf{x},t) = \int_0^{\infty} S_A(\omega)\left[\Gamma_2(x,y,\omega_1,-\omega_1)+\Gamma_2(x,y,-\omega_1,\omega_1)\right]d\omega_1 \tag{8.4.41}$$

where

$$\Gamma_2(x,y,\omega_1,-\omega_1)+\Gamma_2(x,y,-\omega_1,\omega_1) = \frac{\omega_1^2}{g}\left|\Gamma_1(\omega_1)\right|^2 - \frac{g}{\omega_1^2}\left|\nabla_2\Gamma_1(\omega_1)\right|^2 . \tag{8.4.42}$$

8.5 The Frequency Spectrum

Now we extend the nonlinear stochastic theory of Sclavounos [34]. Let us define the covariance function of the total free-surface height $\zeta(x,y,t)$ by

$$H(x,y,\tau,t) = \overline{\zeta(x,y,t)\,\zeta^*(x,y,t+\tau)}, \tag{8.5.1}$$

and the corresponding frequency spectrum S by

$$S(x,y,\omega,t) = \frac{1}{2\pi}\int_{-\infty}^{\infty} d\tau e^{i\omega\tau} H(x,y,\tau,t). \tag{8.5.2}$$

For simplicity, the spatial coordinates x and y are omitted in the rest of this section. ζ is the total free surface displacement

$$\zeta = \epsilon\zeta_1 + \epsilon^2\zeta_2 + \epsilon^3\zeta_3 + \cdots, \tag{8.5.3}$$

where the ordering parameter ϵ is defined by

$$\epsilon = k_p \frac{H_s}{2}, \tag{8.5.4}$$

with k_p being wave number corresponding to the peak frequency ω_p defined in Eq. (8.2.4) and H_s significant wave height

$$H_s = \sqrt{4\int_0^{\infty} 2S_A(\omega)d\omega}. \tag{8.5.5}$$

Note that significant wave height is the measure most commonly used for representing the severity of sea conditions. Although it is defined as the average of the one-third highest observed wave height, it is commonly evaluated by using the variance computed from a spectrum.(Cf. Ochi, 1998,pp. 81.) For the spectrum in figure 8-2, $\epsilon = 0.063$.

The covariance function of the free surface therefore is given by

$$H(\tau,t) = \overline{\left[\epsilon\zeta_1(t) + \epsilon^2\zeta_2(t) + \epsilon^3\zeta_3(t) + \cdots\right]\left[\epsilon\zeta_1^*(t+\tau) + \epsilon^2\zeta_2^*(t+\tau) + \epsilon^3\zeta_3^*(t+\tau) + \cdots\right]} \tag{8.5.6}$$

Since ζ_2, ζ_3,... involve quadratic, triple and higher products of A, the right-hand side involves ensemble averages of even and odd products of A. Due to the assumption of $A(\omega)$ being a Gaussian random variable, all odd products of random variables gives zero averages, while all even products(e.g., quadratic) can be re-

duced to averages of quadratic products. For convenience of reference, this well known result is derived in Appendix H. It follows that, up to $O(\epsilon^4)$,

$$H(\tau,t) = \epsilon^2 H_2(\tau,t) + \epsilon^4 H_4(\tau,t) + \cdots \tag{8.5.7}$$

where

$$H_2(\tau,t) = \overline{\zeta_1(t)\,\zeta_1^*(t+\tau)}, \tag{8.5.8}$$

$$H_4(\tau,t) = \overline{\zeta_2(t)\,\zeta_2^*(t+\tau)} + \overline{\zeta_1(t)\,\zeta_3^*(t+\tau)} + \overline{\zeta_3(t)\,\zeta_1^*(t+\tau)}. \tag{8.5.9}$$

There is no contributions at $O(\epsilon^3)$. At the leading order, $O(\epsilon^2)$, H_2 depends only on the first-order solution. For a complete analysis of the $O(\epsilon^4)$ correction, $H_4(\tau,t)$, it is necessary to find not only ζ_2 but also ζ_3. Let us decompose $H_4(\tau,t)$ as follows.

$$H_4(\tau,t) = H_{22}(\tau,t) + H_{13}(\tau,t) + H_{31}(\tau,t) \tag{8.5.10}$$

with $H_{22}(\tau,t)$ being the auto-correlation of the ζ_2

$$H_{22}(\tau,t) = \overline{\zeta_2(t)\,\zeta_2^*(t+\tau)}, \tag{8.5.11}$$

and $H_{13}(\tau,t)$ and $H_{31}(\tau,t)$ the cross correlations of the ζ_1 and ζ_3

$$H_{13}(\tau,t) = \overline{\zeta_1(t)\,\zeta_3^*(t+\tau)}, \tag{8.5.12}$$

$$H_{31}(\tau,t) = \overline{\zeta_3(t)\,\zeta_1^*(t+\tau)}. \tag{8.5.13}$$

The corresponding frequency spectrum can also be written

$$S(\omega,t) = \epsilon^2 S_2(\omega,t) + \epsilon^4 S_4(\omega,t). \tag{8.5.14}$$

with

$$S_4(\omega,t) = S_{22}(\omega,t) + S_{13}(\omega,t) + S_{31}(\omega,t). \tag{8.5.15}$$

The first part S_{22} is the self-product of the second-order frequency response , and

the last two parts S_{13} and S_{31} are the quadratic products of the first-order and the third-order frequency response. The spectra S_{22}, S_{13} and S_{31} are respectively the Fourier transforms of H_{22}, H_{13} and H_{31}.

8.5.1 Linear frequency spectrum S_2

By putting Eq. (8.3.12) into Eq. (8.5.8), H_2 becomes

$$\begin{aligned} H_2(x,y,t,\tau) &= \int_{-\infty}^{\infty}\int_{-\infty}^{\infty} \overline{A(\omega_1)A^*(\omega_2)}\Gamma_1(x,y,\omega_1)\,\Gamma_1^*(x,y,\omega_2)\,e^{-i\omega_1 t}e^{i\omega_2(t+\tau)}d\omega_1 d\omega_2 \\ &= \int_{-\infty}^{\infty} S_2(x,y,t,\omega_2)\,e^{i\omega_2\tau}d\omega_2 \end{aligned} \tag{8.5.16}$$

where the linear spectrum $S_2(x,y,t,\omega_2)$ of the first-order free surface elevation is given by

$$S_2(x,y,t,\omega_2) = \int_{-\infty}^{\infty} \overline{A(\omega_1)A^*(\omega_2)}\Gamma_1(x,y,\omega_1)\,\Gamma_1^*(x,y,\omega_2)\,e^{-i(\omega_1-\omega_2)t}d\omega_1. \tag{8.5.17}$$

Since the wave process is stationary in time, the time at which we begin to observe will be immaterial. H_2 depends only on τ and not t. Let us recall Eqn. (8.1.2)

$$\overline{A(\omega_1)A^*(\omega_2)} = S_A(\omega_1)\,\delta(\omega_1-\omega_2). \tag{8.5.18}$$

Therefore, only when $\omega_1 = \omega_2$, the integrand of Eq. (8.5.17) is nonzero. Let us change variable ω_2 to ω. Then Eq. (8.5.16) becomes

$$H_2(x,y,\tau) = \int_{-\infty}^{\infty} S_2(x,y,\omega)\,e^{i\omega\tau}d\omega, \tag{8.5.19}$$

and Eq. (8.5.17) becomes

$$S_2(x,y,\omega) = S_A(\omega)\,|\Gamma_1(x,y,\omega)|^2, \tag{8.5.20}$$

This is the familiar Wiener-Khintchine relation for a linear system and depends only on the linear frequency response $\Gamma_1(x, y, \omega)$.

Since S_A is a two-sided spectrum $S_A(\omega) = S_A(-\omega)$ and

$$\Gamma_1^*(x, y, \omega) = \Gamma_1(x, y, -\omega),$$

$S_2(x, y, \omega)$ is also a two-sided frequency spectrum

$$\begin{aligned} S_2(x, y, -\omega) &= S_A(-\omega) |\Gamma_1(x, y, -\omega)|^2 \\ &= S_A(\omega) |\Gamma_1(x, y, \omega)|^2 \\ &= S_2(x, y, \omega). \end{aligned} \tag{8.5.21}$$

8.5.2 Nonlinear Correction S_{22}

Now let us obtain $H_{22}(x, y, t, \tau)$ first. From Eq. (8.4.36) and Eq.(8.5.11), we get

$$\begin{aligned} H_{22}(x, y, t, \tau) = \iiiint_{-\infty}^{\infty} d\omega_1 d\omega_2 d\omega_3 d\omega_4 \overline{A(\omega_1) A(\omega_2) A^*(\omega_3) A^*(\omega_4)} \times \\ \Gamma_2(x, y, \omega_1, \omega_2) \Gamma_2^*(x, y, \omega_3, \omega_4) e^{-i(\omega_1+\omega_2-\omega_3-\omega_4)t} e^{i(\omega_3+\omega_4)\tau} \end{aligned} \tag{8.5.22}$$

The random variable $A(\omega_i)$, with $i = 1, 2, 3, 4$, is already assumed to be Gaussian, so $A(\omega_i)$, $i = 1, 2, 3, 4$ are jointly normally distributed and independent.

$$\begin{aligned} \overline{A(\omega_1) A(\omega_2) A^*(\omega_3) A^*(\omega_4)} = \overline{A(\omega_1) A(\omega_2)} \quad \overline{A^*(\omega_3) A^*(\omega_4)} \\ + \overline{A(\omega_1) A^*(\omega_3)} \quad \overline{A(\omega_2) A^*(\omega_4)} + \overline{A(\omega_1) A^*(\omega_4)} \quad \overline{A(\omega_2) A^*(\omega_3)}. \end{aligned} \tag{8.5.23}$$

It follows that

$$\begin{aligned} H_{22}(x, y, t, \tau) = \iiiint_{-\infty}^{\infty} d\omega_1 d\omega_2 d\omega_3 d\omega_4 \left\{ \overline{A(\omega_1) A(\omega_2)} \quad \overline{A^*(\omega_3) A^*(\omega_4)} \right. \\ \left. + \overline{A(\omega_1) A^*(\omega_3)} \quad \overline{A(\omega_2) A^*(\omega_4)} + \overline{A(\omega_1) A^*(\omega_4)} \quad \overline{A(\omega_2) A^*(\omega_3)} \right\} \times \\ \Gamma_2(x, y, \omega_1, \omega_2) \Gamma_2^*(x, y, \omega_3, \omega_4) e^{-i(\omega_1+\omega_2-\omega_3-\omega_4)t} e^{i(\omega_3+\omega_4)\tau}. \end{aligned} \tag{8.5.24}$$

By making use of $A(\omega) = A^*(-\omega)$ and Eqn. (8.1.2), we get

$$\overline{A(\omega_1)\,A(\omega_2)} = \overline{A(\omega_1)\,A^*(-\omega_2)} = S_A(\omega_1)\,\delta(\omega_1+\omega_2)\,, \tag{8.5.25}$$

$$\overline{A^*(\omega_3)\,A^*(\omega_4)} = \overline{A(-\omega_3)\,A^*(\omega_4)} = S_A(-\omega_3)\,\delta(-\omega_3-\omega_4) = S_A(\omega_3)\,\delta(\omega_3+\omega_4)\,. \tag{8.5.26}$$

Similarly for the remaining terms in Eq. (8.5.23), we have

$$\overline{A(\omega_1)\,A(\omega_2)}\quad\overline{A^*(\omega_3)\,A^*(\omega_4)} = S_A(\omega_1)\,\delta(\omega_1+\omega_2)\,S_A(\omega_3)\,\delta(\omega_3+\omega_4)\,, \tag{8.5.27}$$

$$\overline{A(\omega_1)\,A^*(\omega_3)}\quad\overline{A(\omega_2)\,A^*(\omega_4)} = S_A(\omega_1)\,\delta(\omega_1-\omega_3)\,S_A(\omega_2)\,\delta(\omega_2-\omega_4)\,, \tag{8.5.28}$$

$$\overline{A(\omega_1)\,A^*(\omega_4)}\quad\overline{A(\omega_2)\,A^*(\omega_3)} = S_A(\omega_1)\,\delta(\omega_1-\omega_4)\,S_A(\omega_2)\,\delta(\omega_2-\omega_3)\,. \tag{8.5.29}$$

In summary,

$$\begin{aligned}
&\overline{A(\omega_1)\,A(\omega_2)\,A^*(\omega_3)\,A^*(\omega_4)} \\
&\quad= S_A(\omega_1)\,\delta(\omega_1+\omega_2)\,S_A(\omega_3)\,\delta(\omega_3+\omega_4) + S_A(\omega_1)\,\delta(\omega_1-\omega_3)\,S_A(\omega_2)\,\delta(\omega_2-\omega_4) \\
&\qquad+ S_A(\omega_1)\,\delta(\omega_1-\omega_4)\,S_A(\omega_2)\,\delta(\omega_2-\omega_3)\,.
\end{aligned} \tag{8.5.30}$$

The first integral in Eqn. (8.5.24) then becomes

$$\begin{aligned}
\text{term } 1 &= \iiiint_{-\infty}^{\infty} d\omega_1 d\omega_2 d\omega_3 d\omega_4 \left\{\overline{A(\omega_1)\,A(\omega_2)}\quad\overline{A^*(\omega_3)\,A^*(\omega_4)}\times\right. \\
&\qquad\left.\Gamma_2(x,y,\omega_1,\omega_2)\,\Gamma_2^*(x,y,\omega_3,\omega_4)\,e^{-i(\omega_1+\omega_2-\omega_3-\omega_4)t}e^{i(\omega_3+\omega_4)\tau}\right\} \\
&= \iiiint_{-\infty}^{\infty} d\omega_1 d\omega_2 d\omega_3 d\omega_4 \left\{S_A(\omega_1)\,\delta(\omega_1+\omega_2)\,S_A(\omega_3)\,\delta(\omega_3+\omega_4)\times\right. \\
&\qquad\left.\Gamma_2(x,y,\omega_1,\omega_2)\,\Gamma_2^*(x,y,\omega_3,\omega_4)\,e^{-i(\omega_1+\omega_2-\omega_3-\omega_4)t}e^{i(\omega_3+\omega_4)\tau}\right\}.
\end{aligned} \tag{8.5.31}$$

Because of $\delta(\omega_1+\omega_2)$ and $\delta(\omega_3+\omega_4)$, Term 1 becomes

$$\text{term } 1 = \left[\int_{-\infty}^{\infty} S_A(\omega_1)\,\Gamma_2(x,y,\omega_1,-\omega_1)\,d\omega_1\right]\times\left[\int_{-\infty}^{\infty} S_A(\omega_3)\,\Gamma_2^*(x,y,\omega_3,-\omega_3)\,d\omega_3\right], \tag{8.5.32}$$

which is independent of τ and is the square of the mean sea level

$$\overline{\zeta_2(t)} = \int_{-\infty}^{\infty} S_A \Gamma_2(x, y, \omega_1, -\omega_1) d\omega_1 = \int_{-\infty}^{\infty} S_A \Gamma_2^*(x, y, \omega_1, -\omega_1) d\omega_1. \tag{8.5.33}$$

The second integral in Eqn. (8.5.24) is

$$\begin{aligned} \text{term 2} = & \iiiint_{-\infty}^{\infty} d\omega_1 d\omega_2 d\omega_3 d\omega_4 \left\{ \overline{A(\omega_1) A^*(\omega_3)} \quad \overline{A(\omega_2) A^*(\omega_4)} \times \right. \\ & \left. \Gamma_2(x, y, \omega_1, \omega_2) \Gamma_2^*(x, y, \omega_3, \omega_4) e^{-i(\omega_1+\omega_2-\omega_3-\omega_4)t} e^{i(\omega_3+\omega_4)\tau} \right\} \\ = & \iiiint_{-\infty}^{\infty} d\omega_1 d\omega_2 d\omega_3 d\omega_4 \left\{ S_A(\omega_1) \delta(\omega_1 - \omega_3) S_A(\omega_2) \delta(\omega_2 - \omega_4) \times \right. \\ & \left. \Gamma_2(x, y, \omega_1, \omega_2) \Gamma_2^*(x, y, \omega_3, \omega_4) e^{-i(\omega_1+\omega_2-\omega_3-\omega_4)t} e^{i(\omega_3+\omega_4)\tau} \right\}. \end{aligned} \tag{8.5.34}$$

Because of $\delta(\omega_1 - \omega_3)$ and $\delta(\omega_2 - \omega_4)$, Term 2 becomes

$$\text{term 2} = \iint_{-\infty}^{\infty} S_A(\omega_1) S_A(\omega_2) \Gamma_2(x, y, \omega_1, \omega_2) \Gamma_2^*(x, y, \omega_1, \omega_2) e^{i(\omega_1+\omega_2)\tau} d\omega_1 d\omega_2, \tag{8.5.35}$$

which is a function of τ. The third integral in Eqn. (8.5.24) is

$$\begin{aligned} \text{term 3} = & \iiiint_{-\infty}^{\infty} d\omega_1 d\omega_2 d\omega_3 d\omega_4 \left\{ \overline{A(\omega_1) A^*(\omega_4)} \quad \overline{A(\omega_2) A^*(\omega_3)} \times \right. \\ & \left. \Gamma_2(x, y, \omega_1, \omega_2) \Gamma_2^*(x, y, \omega_3, \omega_4) e^{-i(\omega_1+\omega_2-\omega_3-\omega_4)t} e^{i(\omega_3+\omega_4)\tau} \right\} \\ = & \iiiint_{-\infty}^{\infty} d\omega_1 d\omega_2 d\omega_3 d\omega_4 \left\{ S_A(\omega_1) \delta(\omega_1 - \omega_4) S_A(\omega_2) \delta(\omega_2 - \omega_3) \times \right. \\ & \left. \Gamma_2(x, y, \omega_1, \omega_2) \Gamma_2^*(x, y, \omega_3, \omega_4) e^{-i(\omega_1+\omega_2-\omega_3-\omega_4)t} e^{i(\omega_3+\omega_4)\tau} \right\}. \end{aligned} \tag{8.5.36}$$

Because of $\delta(\omega_1 - \omega_4)$ and $\delta(\omega_2 - \omega_3)$, Term 3 then becomes

$$\text{term 3} = \iint_{-\infty}^{\infty} S_A(\omega_1) S_A(\omega_2) \Gamma_2(x, y, \omega_1, \omega_2) \Gamma_2^*(x, y, \omega_2, \omega_1) e^{i(\omega_1+\omega_2)\tau} d\omega_1 d\omega_2, \tag{8.5.37}$$

which is also a function of τ. Finally, H_{22} is given by

$$H_{22}(x,y,\tau) = \left[\overline{\zeta_2}\right]^2 + \iint_{-\infty}^{\infty} S_A(\omega_1) S_A(\omega_2) \{\Gamma_2(x,y,\omega_1,\omega_2) \Gamma_2^*(x,y,\omega_1,\omega_2) + \Gamma_2(x,y,\omega_1,\omega_2) \Gamma_2^*(x,y,\omega_2,\omega_1)\} e^{i(\omega_1+\omega_2)\tau} d\omega_1 d\omega_2. \tag{8.5.38}$$

Note that the first integral in H_{22} is independent of τ, while the second integral is a function of τ.

Now let us denote

$$\sigma = \omega_1 + \omega_2, \tag{8.5.39}$$

and rewrite the first term of equation (8.5.38) as

$$\left[\overline{\zeta_2}(t)\right]^2 = \int_{-\infty}^{\infty} d\sigma e^{i\sigma\tau} \delta(\sigma) \left[\overline{\zeta_2}\right]^2. \tag{8.5.40}$$

It follows that

$$\begin{aligned} H_{22}(t,\tau) &= \int_{-\infty}^{\infty} d\sigma e^{i\sigma\tau} \delta(\sigma) \left[\overline{\zeta_2}\right]^2 \\ &\quad + \int_{-\infty}^{\infty} d\sigma e^{i\sigma\tau} \int_{-\infty}^{\infty} S_A(\omega_1) S_A(\sigma-\omega_1) \Gamma_2(x,y,\omega_1,\sigma-\omega_1) \\ &\qquad [\Gamma_2^*(x,y,\omega_1,\sigma-\omega_1) \Gamma_2^*(x,y,\sigma-\omega_1,\omega_1)] d\omega_1 \\ &= \int_{-\infty}^{\infty} S_{22}(\sigma) e^{i\sigma\tau} d\sigma, \end{aligned} \tag{8.5.41}$$

Thus the corresponding frequency spectrum $S_{22}(\sigma)$ is

$$S_{22}(\sigma) = \delta(\sigma) \left[\overline{\zeta_2}\right]^2 + \int_{-\infty}^{\infty} S_A(\omega_1) S_A(x,y,\sigma-\omega_1) \Gamma_2(x,y,\omega_1,\sigma-\omega_1) \times [\Gamma_2^*(x,y,\omega_1,\sigma-\omega_1) + \Gamma_2^*(x,y,\sigma-\omega_1,\omega_1)] d\omega_1. \tag{8.5.42}$$

Let us change the notation and replace σ by ω so that

$$S_{22}(\omega) = \delta(\omega)\left[\overline{\zeta_2}\right]^2 + \int_{-\infty}^{\infty} S_A(\omega_1) S_A(x, y, \omega - \omega_1) \Gamma_2(x, y, \omega_1, \omega - \omega_1) \times \left[\Gamma_2^*(x, y, \omega_1, \omega - \omega_1) + \Gamma_2^*(x, y, \omega - \omega_1, \omega_1)\right] d\omega_1. \tag{8.5.43}$$

Note that since $H_{22}(\tau)$ is real, $S_{22}(\omega) = S_{22}(-\omega)$.

The first term in Eq. (8.5.43) is the spectral part of the mean sea-level squared. Reliable field data near zero frequency is likely hard to find in view of the possible importance of tide and other long-periods events, and instrumentation limit. Only the remaining integral, $\omega \neq 0$, is included in the existing field data.

Although in principle the second term in Eq. (8.5.43) is integrated over the entired frequency range of ω_1, the sum of the two arguments of $\Gamma_2(\omega_1, \omega - \omega_1)$ $\Gamma_2^*(\omega_1, \omega - \omega_1)$ and $\Gamma_2^*(\omega - \omega_1, \omega_1)$ is always

$$\omega_1 + (\omega - \omega_1) = \omega, \tag{8.5.44}$$

If we only interested in the low frequencies part of spectrum $\mathbf{S}_{22}(\omega)$, we only need to compute $\Gamma_2(\omega_1, \omega_2)$ in a narrow strip near the limit $\omega_1 + \omega_2 = 0$ instead of the entire plane of (ω_1, ω_2). Similar savings are possible for the second-order $\xi_\ell(\omega_1, \omega - \omega_1)$, $\xi_\ell^*(\omega_1, \omega - \omega_1)$ and $\xi_\ell^*(\omega - \omega_1, \omega_1)$.

8.5.3 Nonlinear Corrections S_{13} and S_{31}

Now let us get S_{13} and S_{31}. By inspecting the third-order perturbation equations, we expect the third-order free surface elevation to take the following form

$$\zeta_3(\mathbf{x}, t) = \iiint_{-\infty}^{\infty} A(\omega_1) A(\omega_2) A(\omega_3) \Gamma_3(x, y, \omega_1, \omega_2, \omega_3) e^{-i(\omega_1+\omega_2+\omega_3)t} d\omega_1 d\omega_2 d\omega_3. \tag{8.5.45}$$

with $\Gamma_3(x, y, \omega_1, \omega_2, \omega_3)$ being the transfer function of the third-order wave elevation. By putting the above equation into Eq. (8.5.12), $H_{13}(t, \tau)$ is given by

$$\begin{aligned} H_{13}(t,\tau) &= \overline{\zeta_1(t)\,\zeta_3^*(t+\tau)} \\ &= \iiiint_{-\infty}^{\infty} d\omega_1 d\omega_2 d\omega_3 d\omega_4 \overline{A(\omega_1)\,A^*(\omega_2)\,A^*(\omega_3)\,A^*(\omega_4)} \times \\ &\qquad \Gamma_1(x,y,\omega_1)\,\Gamma_3^*(x,y,\omega_2,\omega_3,\omega_4)\,e^{-i(\omega_1-\omega_2-\omega_3-\omega_4)t} e^{i(\omega_2+\omega_3+\omega_4)\tau}. \end{aligned} \tag{8.5.46}$$

Since the random variable $A(\omega_i)$,with $i = 1, 2, 3, 4$, is Gaussian, so $A(\omega_i)$ are jointly normally distributed and independent.

$$\begin{aligned} \overline{A(\omega_1)\,A^*(\omega_2)\,A^*(\omega_3)\,A^*(\omega_4)} &= \overline{A(\omega_1)\,A^*(\omega_2)}\quad\overline{A^*(\omega_3)\,A^*(\omega_4)} \\ &+ \overline{A(\omega_1)\,A^*(\omega_3)}\quad\overline{A^*(\omega_2)\,A^*(\omega_4)} + \overline{A(\omega_1)\,A^*(\omega_4)}\quad\overline{A^*(\omega_2)\,A^*(\omega_3)}. \end{aligned} \tag{8.5.47}$$

Hence, we obtain

$$\begin{aligned} H_{13}(t,\tau) = \iiiint_{-\infty}^{\infty} d\omega_1 d\omega_2 d\omega_3 d\omega_4 \Big[&\overline{A(\omega_1)\,A^*(\omega_2)}\quad\overline{A^*(\omega_3)\,A^*(\omega_4)} \\ &+\overline{A(\omega_1)\,A^*(\omega_3)}\quad\overline{A^*(\omega_2)\,A^*(\omega_4)} + \overline{A(\omega_1)\,A^*(\omega_4)}\quad\overline{A^*(\omega_2)\,A^*(\omega_3)}\Big] \times \\ &\Gamma_1(x,y,\omega_1)\,\Gamma_3^*(x,y,\omega_2,\omega_3,\omega_4)\,e^{-i(\omega_1-\omega_2-\omega_3-\omega_4)t} e^{i(\omega_2+\omega_3+\omega_4)\tau}. \end{aligned} \tag{8.5.48}$$

Each ensemble average in Eqn. (8.5.47) is given as follows.

$$\overline{A(\omega_1)\,A^*(\omega_2)}\quad\overline{A^*(\omega_3)\,A^*(\omega_4)} = S_A(\omega_1)\,\delta(\omega_1-\omega_2)\,S_A(\omega_3)\,\delta(\omega_3+\omega_4), \tag{8.5.49}$$

$$\overline{A(\omega_1)\,A^*(\omega_3)}\quad\overline{A^*(\omega_2)\,A^*(\omega_4)} = S_A(\omega_1)\,\delta(\omega_1-\omega_3)\,S_A(\omega_2)\,\delta(\omega_2+\omega_4), \tag{8.5.50}$$

$$\overline{A(\omega_1)\,A^*(\omega_4)}\quad\overline{A^*(\omega_2)\,A^*(\omega_3)} = S_A(\omega_1)\,\delta(\omega_1-\omega_4)\,S_A(\omega_2)\,\delta(\omega_2+\omega_3). \tag{8.5.51}$$

Therefore, Eq. (8.5.47) becomes

$$\begin{aligned}
&\overline{A(\omega_1)A^*(\omega_2)A^*(\omega_3)A^*(\omega_4)} \\
&\quad = S_A(\omega_1)\delta(\omega_1-\omega_2)S_A(\omega_3)\delta(\omega_3+\omega_4) + S_A(\omega_1)\delta(\omega_1-\omega_3)S_A(\omega_2)\delta(\omega_2+\omega_4) \\
&\qquad + S_A(\omega_1)\delta(\omega_1-\omega_4)S_A(\omega_2)\delta(\omega_2+\omega_3).
\end{aligned} \tag{8.5.52}$$

Thus the first integral in Eqn. (8.5.48) becomes

$$\begin{aligned}
\text{term } 1 &= \iiiint_{-\infty}^{\infty} d\omega_1 d\omega_2 d\omega_3 d\omega_4 \left\{ \overline{A(\omega_1)A^*(\omega_2)} \quad \overline{A^*(\omega_3)A^*(\omega_4)} \times \right. \\
&\qquad \left. \Gamma_1(x,y,\omega_1)\Gamma_3^*(x,y,\omega_2,\omega_3,\omega_4)e^{-i(\omega_1-\omega_2-\omega_3-\omega_4)t}e^{i(\omega_2+\omega_3+\omega_4)\tau} \right\} \\
&= \iiiint_{-\infty}^{\infty} d\omega_1 d\omega_2 d\omega_3 d\omega_4 \left\{ S_A(\omega_1)\delta(\omega_1-\omega_2)S_A(\omega_3)\delta(\omega_3+\omega_4) \times \right. \\
&\qquad \left. \Gamma_1(x,y,\omega_1)\Gamma_3^*(x,y,\omega_2,\omega_3,\omega_4)e^{-i(\omega_1-\omega_2-\omega_3-\omega_4)t}e^{i(\omega_2+\omega_3+\omega_4)\tau} \right\}
\end{aligned} \tag{8.5.53}$$

Because of $\delta(\omega_1-\omega_2)$ and $\delta(\omega_3+\omega_4)$, Term 1 becomes

$$\text{term } 1 = \int_{-\infty}^{\infty}\int_{-\infty}^{\infty} S_A(\omega_1)S_A(\omega_3)\Gamma_1(x,y,\omega_1)\Gamma_3^*(x,y,\omega_1,\omega_3,-\omega_3)e^{i\omega_1\tau}d\omega_1 d\omega_3. \tag{8.5.54}$$

Let us change the notation and replace variable ω_3 by ω_2

$$\text{term } 1 = \int_{-\infty}^{\infty}\int_{-\infty}^{\infty} S_A(\omega_1)S_A(\omega_2)\Gamma_1(x,y,\omega_1)\Gamma_3^*(x,y,\omega_1,\omega_2,-\omega_2)e^{i\omega_1\tau}d\omega_1 d\omega_2. \tag{8.5.55}$$

The second integral in Eqn. (8.5.48) is

$$\begin{aligned}
\text{term } 2 &= \iiiint_{-\infty}^{\infty} d\omega_1 d\omega_2 d\omega_3 d\omega_4 \left\{ \overline{A(\omega_1)A^*(\omega_3)} \quad \overline{A^*(\omega_2)A^*(\omega_4)} \times \right. \\
&\qquad \left. \Gamma_1(x,y,\omega_1)\Gamma_3^*(x,y,\omega_2,\omega_3,\omega_4)e^{-i(\omega_1-\omega_2-\omega_3-\omega_4)t}e^{i(\omega_2+\omega_3+\omega_4)\tau} \right\} \\
&= \iiiint_{-\infty}^{\infty} d\omega_1 d\omega_2 d\omega_3 d\omega_4 \left\{ S_A(\omega_1)\delta(\omega_1-\omega_3)S_A(\omega_2)\delta(\omega_2+\omega_4) \times \right. \\
&\qquad \left. \Gamma_1(x,y,\omega_1)\Gamma_3^*(x,y,\omega_2,\omega_3,\omega_4)e^{-i(\omega_1-\omega_2-\omega_3-\omega_4)t}e^{i(\omega_2+\omega_3+\omega_4)\tau} \right\}.
\end{aligned} \tag{8.5.56}$$

Because of $\delta(\omega_1 - \omega_3)$ and $\delta(\omega_2 + \omega_4)$, Term 2 becomes

$$\text{term } 2 = \int_{-\infty}^{\infty}\int_{-\infty}^{\infty} S_A(\omega_1) S_A(\omega_2) \Gamma_1(x,y,\omega_1) \Gamma_3^*(x,y,\omega_2,\omega_1,-\omega_2) e^{i\omega_1\tau} d\omega_1 d\omega_2 \tag{8.5.57}$$

The third integral in Eqn. (8.5.48) is

$$\begin{aligned}\text{term } 3 = \iiiint_{-\infty}^{\infty} d\omega_1 d\omega_2 d\omega_3 d\omega_4 \Big\{ &\overline{A(\omega_1) A^*(\omega_4)} \quad \overline{A^*(\omega_2) A^*(\omega_3)} \times \\ &\Gamma_1(x,y,\omega_1) \Gamma_3^*(x,y,\omega_2,\omega_3,\omega_4) e^{-i(\omega_1-\omega_2-\omega_3-\omega_4)t} e^{i(\omega_2+\omega_3+\omega_4)\tau} \Big\} \\ = \iiiint_{-\infty}^{\infty} d\omega_1 d\omega_2 d\omega_3 d\omega_4 \Big\{ &S_A(\omega_1) \delta(\omega_1 - \omega_4) S_A(\omega_2) \delta(\omega_2 + \omega_3) \times \\ &\Gamma_1(x,y,\omega_1) \Gamma_3^*(x,y,\omega_2,\omega_3,\omega_4) e^{-i(\omega_1-\omega_2-\omega_3-\omega_4)t} e^{i(\omega_2+\omega_3+\omega_4)\tau} \Big\}.\end{aligned} \tag{8.5.58}$$

Because of $\delta(\omega_1 - \omega_4)$ and $\delta(\omega_2 + \omega_3)$, Term 3 becomes

$$\text{term } 3 = \int_{-\infty}^{\infty}\int_{-\infty}^{\infty} S_A(\omega_1) S_A(\omega_2) \Gamma_1(x,y,\omega_1) \Gamma_3^*(x,y,\omega_2,-\omega_2,\omega_1) e^{i\omega_1\tau} d\omega_1 d\omega_2. \tag{8.5.59}$$

In summary, we get

$$\begin{aligned}H_{13}(x,y,\tau) &= \int_{-\infty}^{\infty} d\omega_1 e^{i\omega_1\tau} S_A(\omega_1) \Gamma_1(x,y,\omega_1) \Big\{ \int_{-\infty}^{\infty} S_A(\omega_2) \left[\Gamma_3^*(x,y,\omega_1,\omega_2,-\omega_2)\right. \\ &\qquad \left. + \Gamma_3^*(x,y,\omega_2,\omega_1,-\omega_2) + \Gamma_3^*(x,y,\omega_2,-\omega_2,\omega_1)\right] d\omega_2 \Big\} \\ &= \int_{-\infty}^{\infty} S_{13}(\omega_1) e^{i\omega_1\tau} d\omega_1.\end{aligned} \tag{8.5.60}$$

where

$$\begin{aligned}\mathbf{S}_{13}(\omega_1) = S_A(\omega_1) \Gamma_1(x,y,\omega_1) \int_{-\infty}^{\infty} S_A(\omega_2) &\left[\Gamma_3^*(x,y,\omega_1,\omega_2,-\omega_2)\right. \\ &\left. + \Gamma_3^*(x,y,\omega_2,\omega_1,-\omega_2) + \Gamma_3^*(x,y,\omega_2,-\omega_2,\omega_1)\right] d\omega_2.\end{aligned} \tag{8.5.61}$$

Again, let us change the notation and replace variable ω_1 by ω and ω_2 by ω_1

$$S_{13}(\omega) = S_A(\omega)\Gamma_1(x,y,\omega)\int_{-\infty}^{\infty} S_A(x,y,\omega_1)\left[\Gamma_3^*(x,y,\omega,\omega_1,-\omega_1)\right. \\ \left.+\Gamma_3^*(x,y,\omega_1,\omega,-\omega_1)+\Gamma_3^*(x,y,\omega_1,-\omega_1,\omega)\right]d\omega_1. \tag{8.5.62}$$

Now $H_{31}(t,\tau)$

$$H_{31}(t,\tau) = \overline{\zeta_3(t)\,\zeta_1^*(t+\tau)} \\ = \iiiint_{-\infty}^{\infty} d\omega_1 d\omega_2 d\omega_3 d\omega_4 \overline{A^*(\omega_1)\,A(\omega_2)\,A(\omega_3)\,A(\omega_4)}\times \\ \Gamma_1^*(x,y,\omega_1)\,\Gamma_3(x,y,\omega_2,\omega_3,\omega_4)\,e^{-i(-\omega_1+\omega_2+\omega_3+\omega_4)t}e^{i\omega_1\tau}, \tag{8.5.63}$$

can be computed similarly. Details are given in the Appendix J. The result is

$$H_{31}(x,y,\tau) = \int_{-\infty}^{\infty} d\omega_1 e^{i\omega_1\tau}\left\{S_A(\omega_1)\,\Gamma_1^*(\omega_1)\int_{-\infty}^{\infty} S_A(\omega_2)\left[\Gamma_3(\omega_1,\omega_2,-\omega_2)\right.\right. \\ \left.\left.+\Gamma_3(\omega_2,\omega_1,-\omega_2)+\Gamma_3(\omega_2,-\omega_2,\omega_1)\right]d\omega_2\right\} \\ = \int_{-\infty}^{\infty} S_{31}(\omega_1)\,e^{i\omega_1\tau}d\omega_1. \tag{8.5.64}$$

The corresponding frequency spectrum is

$$S_{31}(\omega_1) = S_A(\omega_1)\,\Gamma_1^*(\omega_1)\int_{-\infty}^{\infty} S_A(\omega_2)\left[\Gamma_3(\omega_1,\omega_2,-\omega_2)\right. \\ \left.+\Gamma_3(\omega_2,\omega_1,-\omega_2)+\Gamma_3(\omega_2,-\omega_2,\omega_1)\right]d\omega_2. \tag{8.5.65}$$

Let us change the notation and replace variable ω_1 by ω and ω_2 by ω_2 get

$$S_{31}(\omega) = S_A(\omega)\,\Gamma_1^*(\omega)\int_{-\infty}^{\infty} S_A(\omega_1)\left[\Gamma_3(\omega,\omega_1,-\omega_1)\right. \\ \left.+\Gamma_3(\omega_1,\omega,-\omega_1)+\Gamma_3(\omega_1,-\omega_1,\omega)\right]d\omega_2. \tag{8.5.66}$$

The extension of Sclavounos is formally complete. The nonlinear spectral correction S_4 is the sum of Eq. (8.5.66), Eq. (8.5.62) and Eq. (8.5.43).

For simple plane progressive or standing waves in deep water, Scalvounos derived explicitly the transfer function for ζ_1, ζ_2 and ζ_3, calculated S_{22} and S_{13}, by using Pierson-Moskowitz spectrum for S_A.

In the remainder of this thesis, focus is on the low-frequency harbor resonance. Since in the range of low frequencies, $S_A(\omega)$ is practical zero for typical sea spectra such as JONSWAP, as can be seen in figure 8-2 $S_{13}(\omega)$ and $S_{31}(\omega)$ which are proportional to $S_A(\omega)$ can be neglected. This fortunate result makes it unnecessary to compute Γ_3 and simplifies the task for the harbor problem. In the computation of the integral in S_{22} the main task is to compute the transfer function Γ_2 for many pairs of frequencies. For this purpose it is necessary to solve the second-order diffraction problem for ξ_ℓ for all pairs of frequencies in a narrow strip near the diagonal $\omega_1 + \omega_2 = 0$ of the (ω_1, ω_2)[1]. Hence the numerical task is limited.

[1]The same advantage applies to the slow-drift motion of an offshore platforms.

Chapter 9

Calculations of nonlinear transfer functions and spectra

9.1 Hybrid-element Method

Numerical analysis for the first-order problem is similar to that in Part I. Therefore, we only focus on the second-order analysis in this chapter.

Let us divide the domain into two regions (Fig. 4-1) with a varying depth region inside where the finite element method is applied, and a constant depth region where the analytic solution is applied.

We require the matching condition at $r = a$ for the finite element solution and the analytic solution

$$[\xi_\ell(x, y, \omega_1, \omega_2)]_{\Omega_A} = [\xi_\ell(x, y, \omega_1, \omega_2)]_{\Omega_F}, \qquad r = a, \ \ \ell = 0, 1, 2, 3, \cdots, \tag{9.1.1}$$

$$\left[\frac{\partial \xi_\ell(x, y, \omega_1, \omega_2)}{\partial r}\right]_{\Omega_A} = \left[\frac{\partial \xi_\ell(x, y, \omega_1, \omega_2)}{\partial r}\right]_{\Omega_F}, \qquad r = a, \ \ \ell = 0, 1, 2, 3, \cdots, \tag{9.1.2}$$

where $()_{\Omega_A}$ denotes the solution in Ω_A, $()_{\Omega_F}$ denotes the solution in Ω_F, ∂A is the boundary between Ω_A and Ω_F where $r = a$. Now, the argument (x, y) will be omitted throughout this chapter.

9.2 Second-order analytic solution in the Far-field

The analytic solutions in $()_{\Omega_F}$ are obtained as follows. As will be shown in the next section, $f(\omega_1, \omega_2)$ can be split into two parts

$$f(\omega_1, \omega_2) = \mathcal{P}(\omega_1, \omega_2) + \mathcal{Q}(\omega_1, \omega_2), \tag{9.2.1}$$

representing respectively self interaction of progressive waves, and quadratic interactions involving scattered waves (progressive-scattered and scattered-scattered). In accordance with the form of the forcing term, we can separate the second-order response, $(\xi_\ell(\omega_1, \omega_2))_{\Omega_F}$, defined by Eqn. (8.4.14) into three parts

$$[\xi_\ell(\omega_1, \omega_2)]_{\Omega_F} = \xi_\ell^P(\omega_1, \omega_2) + \xi_\ell^Q(\omega_1, \omega_2) + \xi_\ell^H(\omega_1, \omega_2), \quad \ell = 0, 1, 2, 3, \cdots. \tag{9.2.2}$$

Let the first part $\xi_\ell^P(\omega_1, \omega_2)$ satisfy the following inhomogeneous equation and zero normal flux on the entire coast

$$\left(\nabla^2 - \kappa_\ell^2\right) \xi_\ell^P(\omega_1, \omega_2) = -i\frac{(\omega_1 + \omega_2)}{A_{\ell,\ell}} \mathcal{P}(\omega_1, \omega_2), \quad \ell = 0, 1, 2, 3 \cdots, \tag{9.2.3}$$

and

$$\frac{\partial \xi_\ell^P}{\partial \theta} = 0, \quad r > a; \quad \theta = 0 \text{ and } \theta = \pi, \quad \ell = 0, 1, 2, 3, \cdots \tag{9.2.4}$$

along the coast. No conditions are imposed elsewhere. It will be solved in section 9.4.1. The second part $\xi_\ell^P(\omega_1, \omega_2)$ represents the second-order progressive waves which responds to forcing $\mathcal{P}(\omega_1, \omega_2)$ due to the interaction of first-order incident and reflected waves.

In addition, let $\xi_\ell^Q(\omega_1, \omega_2)$ satisfy inhomogeneous equation

$$\left(\nabla^2 - \kappa_\ell^2\right) \xi_\ell^Q(\omega_1, \omega_2) = -i\frac{\omega_1 + \omega_2}{A_{\ell,\ell}} \mathcal{Q}(\omega_1, \omega_2), \quad \ell = 0, 1, 2, 3, \cdots, \tag{9.2.5}$$

the no-flux condition along the straight coast

$$\frac{\partial \xi_\ell^Q(\omega_1,\omega_2)}{\partial \theta} = 0, \quad \theta = 0 \text{ and } \theta = \pi, \quad \ell = 0,1,2,3,\cdots, \tag{9.2.6}$$

and along the semi-circle $r = a$

$$\frac{\partial \xi_\ell^Q(\omega_1,\omega_2)}{\partial r} = 0, \quad r = a \quad \ell = 0,1,2,3,\cdots. \tag{9.2.7}$$

$\xi_\ell^Q(\omega_1,\omega_2)$ is the response to the scattered forcing due to the interaction between the first-order scattered waves and the first-order progressive waves. For the evanescent modes, $\ell = 1,2,3,\cdots$, $\xi_\ell^Q(\omega_1,\omega_2)$ diminishes to zero at large enough r. For the propagating mode, $\ell = 0$, $\xi_\ell^Q(\omega_1,\omega_2)$ must satisfy the weak (integral) radiation condition at infinity due to the slow attenuation of $\mathcal{Q}(\omega_1,\omega_2)$. We shall call both $\xi_\ell^P(\omega_1,\omega_2)$ and $\xi_\ell^Q(\omega_1,\omega_2)$ both *forced waves*.

Furthermore, let the *free wave* $\xi_\ell^H(\omega_1,\omega_2)$ satisfy the homogeneous Helmholtz equation

$$\left(\nabla^2 - \kappa_\ell^2\right)\xi_\ell^H(\omega_1,\omega_2) = 0, \quad \ell = 0,1,2,3,\cdots, \tag{9.2.8}$$

the boundary conditions at $r = a$

$$\xi_\ell^H(\omega_1,\omega_2) = 0, \quad \theta = 0 \text{ and } \theta = \pi, \quad \ell = 0,1,2,3\cdots. \tag{9.2.9}$$

In addition, $\xi_\ell^H(\omega_1,\omega_2)$ must satisfy the usual (strong) radiation condition at infinity. The formal solution to the free wave $\xi_\ell^H(\omega_1,\omega_2)$ is immediate

$$\xi_\ell^H(\omega_1,\omega_2) = \sum_{m=0}^{\infty} \widehat{\alpha}_{\ell,m}(\omega_1,\omega_2) K_m(\kappa_\ell r)\cos m\theta \tag{9.2.10}$$

where K_m is the modified Bessel function of the second kind of order m. For $\ell = 0$, $\kappa_0 = -i\widehat{\kappa}_0$ is pure imaginary and $K_m(\kappa_0 r)$ is proportional to $H_m^{(1)}(\widehat{\kappa}_0 r)$. The unknown coefficients $\widehat{\alpha}_{\ell,m}(\omega_1,\omega_2)$ will be found jointly with the discrete solution in the near field by the hybrid-element analysis(in section 5.2), which requires the

continuity of the near and far fields and their radial derivatives along $r = a$

$$\xi_\ell^H(\omega_1,\omega_2) = [\xi_\ell(\omega_1,\omega_2)]_{\Omega_A} - \xi_\ell^Q(\omega_1,\omega_2) - \xi_\ell^P(\omega_1,\omega_2) \tag{9.2.11}$$

$$\frac{\partial \xi_\ell^H(\omega_1,\omega_2)}{\partial r} = \left[\frac{\partial \xi_\ell(\omega_1,\omega_2)}{\partial r}\right]_{\Omega_A} - \frac{\partial \xi_\ell^Q(\omega_1,\omega_2)}{\partial r} - \frac{\partial \xi_\ell^P(\omega_1,\omega_2)}{\partial r}, \quad r = a, \tag{9.2.12}$$

The solutions for $\xi_\ell^P(\omega_1,\omega_2)$ and $\xi_\ell^Q(\omega_1,\omega_2)$ can be obtained explicitly, as shown in section 9.4.

9.3 Expression of $f(x, y, \omega_1, \omega_2)$ in the far-field Ω_F

For the case of a infinite straight coastline and in the constant depth region, the first-order free surface elevation for frequency ω consists of the incident, reflected and scattered waves as

$$\Gamma_1(\omega_1) = \Gamma_1^{(T)}(\omega_1) + \Gamma_1^{(S)}(\omega_1) \tag{9.3.1}$$

where

$$\Gamma_1^{(T)}(\omega) = \Gamma_1^{(I)}(\omega) + \Gamma_1^{(R)}(\omega), \tag{9.3.2}$$

$\Gamma_1^{(I)}(\omega)$ is the first-order incident wave with frequency ω

$$\Gamma_1^{(I)}(\omega) = e^{ik(\omega)r\cos(\theta-\theta_I)}, \tag{9.3.3}$$

$\Gamma_1^{(R)}(\omega)$ is the first-order reflected wave with frequency ω

$$\Gamma_1^{(R)}(\omega) = e^{ik(\omega)r\cos(\theta+\theta_I)}, \tag{9.3.4}$$

with θ_I being the incident angle. $\Gamma_1^{(S)}(\omega)$ is the first-order scattered wave

$$\Gamma_1^{(S)}(\omega) = \sum_{n=0}^{\infty} \epsilon_n \cos n\theta \begin{cases} i^n B_n(\omega) H_n^{(1)}[k(\omega) r], & \omega > 0 \\ (-i)^n B_n^*(\omega) H_n^{(2)}[-k(\omega) r], & \omega < 0 \end{cases} \tag{9.3.5}$$

with the Jacobi symbol ϵ_n

$$\epsilon_0 = 1, \quad \epsilon_n = 2, \quad n = 1, 2, 3, \cdots . \tag{9.3.6}$$

The coefficients $B_n(\omega)$ are obtained from the hybrid-element method for the first-order problem.

Let us recall Eq. (8.4.5)

$$f(\omega_1, \omega_2) = \beta_1(\omega_1, \omega_2)\,\Gamma_1(\omega_1)\,\Gamma_1(\omega_2) + \beta_2(\omega_1, \omega_2)\,\nabla_2\Gamma_1(\omega_1)\cdot\nabla_2\Gamma_1(\omega_2) \tag{9.3.7}$$

with $\beta_1(\omega_1, \omega_2)$ given by Eqn. (8.4.6) and $\beta_2(\omega_1, \omega_2)$by Eqn. (8.4.7). Clearly, $f(\omega_1, \omega_2)$ contains quadratic products of the first-order waves and they are of the form

$$\Gamma_1(\omega_1)\,\Gamma_1(\omega_2) = \left[\Gamma_1^{(T)}(\omega_1) + \Gamma_1^{(S)}(\omega_2)\right]\left[\Gamma_1^{(T)}(\omega_1) + \Gamma_1^{(S)}(\omega_2)\right]. \tag{9.3.8}$$

There are the self products, like $\Gamma_1^{(T)}(\omega_1)\,\Gamma_1^{(T)}(\omega_2)$, and the cross products, like $\Gamma_1^{(T)}(\omega_1)\,\Gamma_1^{(S)}(\omega_2)$, of the component waves. Therefore, the forcing term can be written as

$$f(\omega_1, \omega_2) = \mathcal{P}(\omega_1, \omega_2) + \mathcal{Q}(\omega_1, \omega_2), \tag{9.3.9}$$

where $\mathcal{P}$ involves only the incident and reflected waves

$$\mathcal{P}(\omega_1, \omega_2) = \beta_1(\omega_1, \omega_2)\,\Gamma_1^{(T)}(\omega_1)\,\Gamma_1^{(T)}(\omega_2) + \beta_2(\omega_1, \omega_2)\,\nabla_2\Gamma_1^{(T)}(\omega_1)\cdot\nabla_2\Gamma_1^{(T)}(\omega_2), \tag{9.3.10}$$

and $\mathcal{Q}$ involves the scattered wave

$$\begin{aligned}\mathcal{Q}(\omega_1, \omega_2) =& \beta_1(\omega_1, \omega_2)\left[\Gamma_1^{(T)}(\omega_1)\,\Gamma_1^{(S)}(\omega_2) + \Gamma_1^{(S)}(\omega_1)\,\Gamma_1^{(T)}(\omega_2) + \Gamma_1^{(S)}(\omega_1)\,\Gamma_1^{(S)}(\omega_2)\right] \\ &+ \beta_2(\omega_1, \widetilde{\omega})\left[\nabla_2\Gamma_1^{(T)}(\omega_1)\cdot\nabla_2\Gamma_1^{(S)}(\omega_2) + \nabla_2\Gamma_1^{(S)}(\omega_1)\cdot\nabla_2\Gamma_1^{(T)}(\omega_2)\right. \\ &\left.+\nabla_2\Gamma_1^{(S)}(\omega_1)\cdot\nabla_2\Gamma_1^{(S)}(\omega_2)\right]\end{aligned} \tag{9.3.11}$$

9.3.1 Explicit Expression for $\mathcal{P}(\omega_1, \omega_2)$ in Ω_F

Let us recall $\mathcal{P}(\omega_1, \omega_2)$ to be defined as Eqn. (9.3.10)

$$\mathcal{P}(\omega_1, \omega_2) = \beta_1(\omega_1, \omega_2)\,\Gamma_1^{(T)}(\omega_1)\,\Gamma_1^{(T)}(\omega_2) + \beta_2(\omega_1, \omega_2)\,\nabla_2\Gamma_1^{(T)}(\omega_1)\cdot\nabla_2\Gamma_1^{(T)}(\omega_2), \tag{9.3.12}$$

with

$$\Gamma_1^{(T)}(\omega_1) = e^{ik(\omega_1)r\cos(\theta-\theta_I)} + e^{ik(\omega_1)r\cos(\theta+\theta_I)}, \tag{9.3.13}$$

$$\Gamma_1^{(T)}(\omega_2) = e^{ik(\omega_2)r\cos(\theta-\theta_I)} + e^{ik(\omega_2)r\cos(\theta+\theta_I)}, \tag{9.3.14}$$

To get $\mathcal{P}(\omega_1, \omega_2)$, we must obtain $\Gamma_1^{(T)}(\omega_1)\,\Gamma_1^{(T)}(\omega_2)$ and $\nabla_2\Gamma_1^{(T)}(\omega_1)\cdot\nabla_2\Gamma_1^{(T)}(\omega_2)$

$$\begin{aligned}\Gamma_1^{(T)}(\omega_1)\,\Gamma_1^{(T)}(\omega_2) =& e^{i[k(\omega_1)+k(\omega_2)]r\cos(\theta-\theta_I)} + e^{i[k(\omega_1)+k(\omega_2)]r\cos(\theta+\theta_I)} \\ & e^{ik(\omega_1)r\cos(\theta-\theta_I)+ik(\omega_2)r\cos(\theta+\theta_I)} + e^{ik(\omega_1)r\cos(\theta+\theta_I)+ik(\omega_2)r\cos(\theta-\theta_I)},\end{aligned} \tag{9.3.15}$$

and

$$\begin{aligned}&\nabla_2\Gamma_1^{(T)}(\omega_1)\cdot\nabla_2\Gamma_1^{(T)}(\omega_2) = \frac{\partial\Gamma_1^{(T)}(\omega_1)}{\partial r}\frac{\partial\Gamma_1^{(T)}}{\partial r} + \frac{1}{r^2}\frac{\partial\Gamma_1^{(T)}(\omega_1)}{\partial\theta}\frac{\partial\Gamma_1^{(T)}(\omega_2)}{\partial\theta} \\ &= -k(\omega_1)\,k(\omega_2)\left\{e^{i[k(\omega_1)+k(\omega_2)]r\cos(\theta-\theta_I)} + e^{i[k(\omega_1)+k(\omega_2)]r\cos(\theta+\theta_I)}\right. \\ &\quad \left. + \cos 2\theta_I\left[e^{ik(\omega_2)r\cos(\theta-\theta_I)+ik(\omega_1)r\cos(\theta+\theta_I)} + e^{ik(\omega_1)r\cos(\theta+\theta_I)+ik(\omega_2)r\cos(\theta-\theta_I)}\right]\right\}.\end{aligned} \tag{9.3.16}$$

Putting Eqs. (9.3.15) and (9.3.16) into Eq. (9.3.12), we obtain

$$\begin{aligned}\mathcal{P}(\omega_1, \omega_2) =& \left[\beta_1(\omega_1, \omega_2) - \beta_2(\omega_1, \omega_2)\,k(\omega_1)\,k(\omega_2)\right]\left\{e^{i[k(\omega_1)+k(\omega_2)]r\cos(\theta-\theta_I)}\right. \\ & \left. + e^{i[k(\omega_1)+k(\omega_2)]r\cos(\theta+\theta_I)}\right\} + \left[\beta_1(\omega_1, \omega_2) - \beta_2(\omega_1, \omega_2)\,k(\omega_1)\,k(\omega_2)\cos 2\theta_I\right]\times \\ & \left\{e^{ik(\widetilde{\omega})r\cos(\theta-\theta_I)+ik(\omega_1)r\cos(\theta+\theta_I)} + e^{ik(\omega_1)r\cos(\theta+\theta_I)+ik(\omega_2)r\cos(\theta-\theta_I)}\right\}.\end{aligned} \tag{9.3.17}$$

As a check, we take $\omega_1 = \omega_2$, $\mathcal{P}(\omega_1, \omega_2)$ becomes

$$\mathcal{P}(\omega_1, \omega_1) = [\beta_1(\omega_1, \omega_1) - \beta_2(\omega_1, \omega_1) k(\omega_1) k(\omega_1)] \left\{ e^{i2k(\omega_1) r \cos(\theta - \theta_I)} + e^{i2k(\omega_1) r \cos(\theta + \theta_I)} \right\}$$
$$+ 2[\beta_1(\omega_1, \omega_1) - \beta_2(\omega_1, \omega_1) k(\omega_1) k(\omega_1) \cos 2\theta_I] e^{ik(\omega_1) r [\cos(\theta + \theta_I) + \cos(\theta - \theta_I)]}. \tag{9.3.18}$$

which is same as Eq. (4.3.8) for monochramatic incident waves.

9.3.2 Fourier expression for $\mathcal{Q}(\omega_1, \omega_2)$ in Ω_F

Let us rewrite $\Gamma_1^{(T)}(\omega)$, Eqn. (9.3.13) as

$$\Gamma_1^{(T)}(\omega) = \sum_{m=-\infty}^{\infty} T_m(r, \omega) e^{im\theta} \tag{9.3.19}$$

with

$$T_m(r, \omega) = 2 \cos m\theta_I \begin{cases} (i)^m J_m[k(\omega) r], & \omega > 0 \\ (-i)^m J_m[-k(\omega) r], & \omega < 0 \end{cases}. \tag{9.3.20}$$

From the first-order scattered waves can be written as

$$\Gamma_1^{(S)}(r, \theta, \omega) = \sum_{m=-\infty}^{\infty} \widehat{S}_m(r, \omega) e^{im\theta} \tag{9.3.21}$$

where

$$\widehat{S}_m(r, \omega) = \begin{cases} i^m B_m(\omega) H_m^{(1)}[k(\omega) r], & \omega > 0 \\ (-i)^m B_m^*(\omega) H_m^{(2)}[-k(\omega) r], & \omega < 0 \end{cases} \tag{9.3.22}$$

Note that all $B_m(\omega)$, $T_m(r, \omega)$ and $\widehat{S}_m(r, \omega)$ are even with respect to m, i.e. $B_m(\omega) = B_{-m}(\omega)$, $T_m(r, \omega) = T_{-m}(r, \omega)$ and $\widehat{S}_m(r, \omega) = \widehat{S}_{-m}(r, \omega)$.

In Eq. (9.3.11), there are quadratic products of the first-order progressive waves

and the first-order scattered waves and their derivatives. They are of the form

$$\begin{aligned}\Gamma_1^{(T)}(r,\theta,\omega_1)\,\Gamma_1^{(S)}(r,\theta,\omega_2) &= \sum_{m=-\infty}^{\infty} T_m(r,\omega_1)\,e^{im\theta}\sum_{q=-\infty}^{\infty}\widehat{S}_q(r,\omega_2)\,e^{iq\theta}\\ &= \sum_{m=-\infty}^{\infty}\left[\sum_{q=-\infty}^{\infty} T_{m-q}(r,\omega_1)\,\widehat{S}_q(r,\omega_2)\right]e^{im\theta}\end{aligned} \tag{9.3.23}$$

Therefore, $\mathcal{Q}(\omega_1,\omega_2)$ can be expressed in Fourier series

$$\mathcal{Q}(\omega,\widetilde{\omega}) = \sum_{m=-\infty}^{\infty}\widehat{\mathcal{Q}}_m(\omega,\widetilde{\omega})\,e^{im\theta}, \tag{9.3.24}$$

or equivalently

$$\mathcal{Q}(\omega_1,\omega_2) = \sum_{m=0}^{\infty}\epsilon_m\widehat{\mathcal{Q}}_m(\omega_1,\omega_2)\cos m\theta, \tag{9.3.25}$$

with

$$\begin{aligned}\widehat{\mathcal{Q}}_m(\omega_1,\omega_2) = \sum_{q=-\infty}^{\infty}\Bigg\{&\left[\beta_1(\omega_1,\omega_2) - \frac{q(m-q)}{r^2}\beta_2(\omega_1,\omega_2)\right]\Big[T_{m-q}(\omega_1)\,\widehat{S}_q(\omega_2)\\ &+\widehat{S}_{m-q}(\omega_1)\,T_q(\omega_2) + \widehat{S}_{m-q}(\omega_1)\,\widehat{S}_q(\omega_2)\Big] + \beta_2(\omega_1,\omega_2)\left[\frac{\partial T_{m-q}(\omega_1)}{\partial r}\frac{\partial\widehat{S}_q(\omega_2)}{\partial r}\right.\\ &\left.+\frac{\partial\widehat{S}_{m-q}(\omega_1)}{\partial r}\frac{\partial T_q(\omega_2)}{\partial r} + \frac{\partial\widehat{S}_{m-q}(\omega_1)}{\partial r}\frac{\partial\widehat{S}_q(\omega_2)}{\partial r}\right]\Bigg\}\end{aligned} \tag{9.3.26}$$

where the argument r in $T_m(r,\omega)$ and $\widehat{S}_m(r,\omega)$ are omitted.

9.4 $\xi_\ell^P(\omega_1,\omega_2)$ and $\xi_\ell^Q(\omega_1,\omega_2)$ in the far field Ω_F

The analytical solution for $\xi_\ell^P(\omega_1,\omega_2)$ and $\xi_\ell^Q(\omega_1,\omega_2)$ are obtained in the following sections

9.4.1 Exact solution for $\xi_\ell^P(\omega_1,\omega_2)$

Let us recall Eqn. (9.2.3), $\xi_\ell^P(\omega_1,\omega_2)$ satisfies,

$$\left[\nabla^2-\kappa_\ell^2\right]\xi_\ell^P(\omega_1,\omega_2)=-i\frac{\omega_1+\omega_2}{A_{\ell,\ell}}\mathcal{P}(\omega_1,\omega_2) \tag{9.4.1}$$

with $\mathcal{P}(\omega_1,\omega_2)$ given by (9.3.17). After inspecting the form of $\mathcal{P}(\omega_1,\omega_2)$ we expect $\xi_\ell^P(\omega_1,\omega_2)$ also has the same form,

$$\begin{aligned}\xi_\ell^P(\omega_1,\omega_2)&=L(\omega_1,\omega_2)\left\{e^{i[k(\omega_1)+k(\omega_2)]r\cos(\theta-\theta_I)}+e^{i[k(\omega_1)+k(\omega_2)]r\cos(\theta+\theta_I)}\right\}\\&+\widehat{L}(\omega_1,\omega_2)\left\{e^{ik(\omega_2)r\cos(\theta-\theta_I)+ik(\omega_1)r\cos(\theta+\theta_I)}+e^{ik(\omega_1)r\cos(\theta-\theta_I)+ik(\omega_2)r\cos(\theta+\theta_I)}\right\}\end{aligned} \tag{9.4.2}$$

Putting the above equation into Eqn. (9.4.1), we obtain

$$L(\omega_1,\omega_2)=\frac{i(\omega_1+\omega_2)}{A_{\ell,\ell}}\frac{\left[\beta_1(\omega_1,\omega_2)-\beta_2(\omega_1,\omega_2)k(\omega_1)k(\omega_2)\right]}{\left[k(\omega_1)+k(\omega_2)\right]^2+\kappa_\ell^2(\sigma)}, \tag{9.4.3}$$

$$\widehat{L}(\omega_1,\omega_2)=\frac{i(\omega_1+\omega_2)}{A_{\ell,\ell}}\frac{\left[\beta_1(\omega_1,\omega_2)-\beta_2(\omega_1,\omega_2)k(\omega_1)k(\omega_2)\cos 2\theta_I\right]}{\left[k(\omega_1)-k(\omega_2)\right]^2+4k(\omega_1)k(\omega_2)\cos^2\theta_I+\kappa_\ell^2(\sigma)}, \tag{9.4.4}$$

In summary,

$$\begin{aligned}\xi_\ell^P(\omega_1,\omega_2)=&\frac{i(\omega_1+\omega_2)}{A_{\ell,\ell}}\frac{\left[\beta_1(\omega_1,\omega_2)-\beta_2(\omega_1,\omega_2)k(\omega_1)k(\omega_2)\right]}{\left[k(\omega_1)+k(\omega_2)\right]^2+\kappa_\ell^2(\sigma)}\times\\&\left\{e^{i[k(\omega_1)+k(\omega_2)]r\cos(\theta-\theta_I)}+e^{i[k(\omega_1)+k(\omega_2)]r\cos(\theta+\theta_I)}\right\}\\&+\frac{i(\omega_1+\omega_2)}{A_{\ell,\ell}}\frac{\left[\beta_1(\omega_1,\omega_2)-\beta_2(\omega_1,\omega_2)k(\omega_1)k(\omega_2)\cos 2\theta_I\right]}{\left[k(\omega_1)-k(\omega_2)\right]^2+4k(\omega_1)k(\omega_2)\cos^2\theta_I+\kappa_\ell^2(\sigma)}\times\\&\left[e^{ik(\omega_2)r\cos(\theta-\theta_I)+ik(\omega_1)r\cos(\theta+\theta_I)}+e^{ik(\omega_1)r\cos(\theta+\theta_I)+ik(\omega_2)r\cos(\theta-\theta_I)}\right]\end{aligned} \tag{9.4.5}$$

9.4.2 Exact solution for $\xi_\ell^Q(\omega_1,\omega_2)$ by Green's theorem

To solve the inhomogeneous equations, we shall employ the method of Green's function, $G_\ell(\omega_1,\omega_2)$, defined here by the following equations

$$\nabla^2G_\ell(\omega_1,\omega_2)-\kappa_\ell^2G_\ell(\omega_1,\omega_2)=\frac{1}{r}\delta(r-r_0)\left[\delta(\theta-\theta_0)+\delta(\theta+\theta_0)\right]\quad\text{in }\Omega_F, \tag{9.4.6}$$

$$\frac{\partial G_\ell\left(\omega_1,\omega_2\right)}{\partial\theta}=0,\quad \theta=0 \text{ and } \theta=\pi, \tag{9.4.7}$$

$$\frac{\partial G_\ell\left(\omega_1,\omega_2\right)}{\partial r}=0,\quad r=a, \tag{9.4.8}$$

with $\ell=0,1,2,3\cdots$.

For $\ell=0$, the usual(strong) radiation condition is required, i.e., at infinity, G_0 behaves as an outgoing waves,

$$\sqrt{r}\left[\frac{\partial G_0\left(\omega_1,\omega_2\right)}{\partial r}-\widehat{\kappa}_0 G_0\left(\omega_1,\omega_2\right)\right]\to 0,\quad r\to\infty, \tag{9.4.9}$$

For $\ell=1,2,3,\cdots$, we require that the evanescent modes die out at infinity

$$G_\ell\left(\omega_1,\omega_2\right)\to 0,\quad r\to\infty,\quad \ell=1,2,3\cdots. \tag{9.4.10}$$

The Green's function $G_\ell(r,\theta;r_0,\theta_0)$ is then obtained (see section 4.4.2 for details)

$$\begin{aligned} G_\ell\left(r,\theta;r_0,\theta_0\right)=&\sum_{m=0}^{\infty}\frac{\epsilon_m}{\pi}\left[\frac{I_m'\left(\kappa_\ell a\right)}{K_m'\left(\kappa_\ell a\right)}K_m\left(\kappa_\ell r_>\right)K_m\left(\kappa_\ell r_<\right)\right]\cos m\theta\cos m\theta_0\\ &-\sum_{m=0}^{\infty}\frac{\epsilon_m}{\pi}\left[K_m\left(\kappa_\ell r_>\right)I_m\left(\kappa_\ell r_<\right)\right]\cos m\theta\cos m\theta_0 \end{aligned} \tag{9.4.11}$$

with

$$r_>=Max\left\{r,r_0\right\},\quad r_<=Min\left\{r,r_0\right\}. \tag{9.4.12}$$

Note that Eq. (9.4.11) is equivalent to Eq. (4.4.41) when $\omega_1=\omega_2$. Also, it is clear that the arguments in G_ℓ are interchangeable, i.e.

$$G_\ell\left(r,\theta;r_0,\theta_0\right)=G_\ell\left(r_0,\theta_0;r,\theta\right). \tag{9.4.13}$$

After obtaining Green's function, we can solve $\xi_\ell^Q(r,\theta)$ by making use of Green's theorem

$$\int_0^\pi\int_a^\infty\left(\xi_\ell^Q\nabla^2 G_\ell-G_\ell\nabla^2\xi_\ell^Q\right)rd\theta dr=\oint_{\partial\Omega_F}\left(\xi_\ell^Q\frac{\partial G_\ell}{\partial n}-G_\ell\frac{\partial\xi_\ell^Q}{\partial n}\right)dS \tag{9.4.14}$$

where $\partial\Omega_F$ is the boundary of Ω_F,

$$\partial\Omega_F = \partial A + \partial B + \partial F, \tag{9.4.15}$$

with ∂A being the boundary between Ω_A and Ω_F, ∂B is the coastline and ∂F being the semi-circle boundary with a infinite radius.

By making use of Eqns. (9.2.7), and (9.4.8), Eqn. (9.4.14) becomes

$$\int_0^{\pi}\int_a^{\infty}\left(\xi_\ell^Q\nabla^2 G_\ell - G_\ell\nabla^2\xi_\ell^Q\right) r d\theta dr = \int_{\partial F}\left(\xi_\ell^Q\frac{\partial G_\ell}{\partial n} - G_\ell\frac{\partial \xi_\ell^Q}{\partial n}\right) dS \tag{9.4.16}$$

The line integral along the infinite boundary

$$I_{\partial F} = \int_{\partial F}\left(\xi_\ell^Q\frac{\partial G_\ell}{\partial n} - G_\ell\frac{\partial \xi_\ell^Q}{\partial n}\right) dS \tag{9.4.17}$$

is evaluated in Appendix I.2, where it is shown that $I_{\partial F}$ approximates to zero

$$I_{\partial F} = \int_{\partial F}\left(\xi_\ell^Q\frac{\partial G_\ell}{\partial n} - G_\ell\frac{\partial \xi_\ell^Q}{\partial n}\right) dS \approx O\left(\frac{1}{\sqrt{R_\infty}}\right) \to 0. \tag{9.4.18}$$

Therefore, Eqn. (9.4.16) becomes

$$\int_0^{\pi}\int_a^{\infty}\left(\xi_\ell^Q\nabla^2 G_\ell - G_\ell\nabla^2\xi_\ell^Q\right) r d\theta dr = 0. \tag{9.4.19}$$

Putting Eqn. (9.2.5) and (9.4.6) into Eqn. (9.4.19), we finally get

$$\xi_\ell^Q\left(r_0,\theta_0,\omega_1,\omega_2\right) = \int_0^{\pi}\int_a^{\infty} -i\frac{\omega_1+\omega_2}{A_{\ell,\ell}}\mathcal{Q}\left(\omega_1,\omega_2\right) G_\ell\left(\omega_1,\omega_2\right) r d\theta dr. \tag{9.4.20}$$

Due to the symmetry of the obtained Green's function, the preceding equation can be further rewritten as

$$\xi_\ell^Q\left(r,\theta,\omega_1,\omega_2\right) = \int_0^{\pi}\int_a^{\infty} -i\frac{\omega_1+\omega_2}{A_{\ell,\ell}}\mathcal{Q}\left(\omega_1,\omega_2\right) G_\ell\left(\omega_1,\omega_2\right) r_0 d\theta_0 dr. \tag{9.4.21}$$

The above integral which involves the infinite integration will be evaluated by using the similar approach as Chau and Eatock Taylor (1992). Putting Green function Eqn. (9.4.11) into Eqn. (9.4.21), we obtain

$$\xi_\ell^Q(r,\theta,\omega_1,\omega_2) = \int_a^\infty r_0 dr_0 \int_0^\pi d\theta_0 \left[-i\frac{\omega_1+\omega_2}{A_{\ell,\ell}}\mathcal{Q}(\omega_1,\omega_2)\right] \times \sum_{m=0}^{\infty}\frac{\epsilon_m}{\pi}\cos m\theta\cos m\theta_0 K_m(\kappa_\ell r_>)\left[\frac{I_m'(\kappa_\ell a)}{K_m'(\kappa_\ell a)}K_m(\kappa_\ell r_<) - I_m(\kappa_\ell r_<)\right]. \tag{9.4.22}$$

From Eqn. (9.3.25), $\mathcal{Q}(\omega_1,\omega_2)$ is written in terms of a Fourier series

$$\mathcal{Q}(\omega_1,\omega_2) = \sum_{m=0}^{\infty}\epsilon_m\widehat{\mathcal{Q}}_m(\omega_1,\omega_2)\cos m\theta, \tag{9.4.23}$$

with

$$\widehat{\mathcal{Q}}_m(\omega_1,\omega_2) = \sum_{q=-\infty}^{\infty}\left\{\left[\beta_1(\omega_1,\omega_2) - \frac{q(m-q)}{r^2}\beta_2(\omega_1,\omega_2)\right]\left[T_{m-q}(\omega_1)\widehat{S}_q(\omega_2) + \widehat{S}_{m-q}(\omega_1)T_q(\omega_2) + \widehat{S}_{m-q}(\omega_1)\widehat{S}_q(\omega_2)\right] + \beta_2(\omega_1,\omega_2)\left[\frac{\partial T_{m-q}(\omega_1)}{\partial r}\frac{\partial\widehat{S}_q(\omega_2)}{\partial r} + \frac{\partial\widehat{S}_{m-q}(\omega_1)}{\partial r}\frac{\partial T_q(\omega_2)}{\partial r} + \frac{\widehat{S}_{m-q}(\omega_1)}{\partial r}\frac{\partial\widehat{S}_q(\omega_2)}{\partial r}\right]\right\}. \tag{9.4.24}$$

Making use of Eq. (4.4.56) , Eqn. (9.4.22) becomes

$$\xi_\ell^Q(r,\theta) = \sum_{m=0}^{\infty}\epsilon_m\cos(m\theta)\int_a^\infty r_0 dr_0\left[-i\frac{\omega_1+\omega_2}{A_{\ell,\ell}}\right]\widehat{\mathcal{Q}}_m(\omega_1,\omega_2)K_m(\kappa_\ell r_>)\times \left[\frac{I_m'(\kappa_\ell a)}{K_m'(\kappa_\ell a)}K_m(\kappa_\ell r_<) - I_m(\kappa_\ell r_<)\right]. \tag{9.4.25}$$

In particular, for $r = a$ (i.e. on the boundary between Ω_A and Ω_F):

$$\xi_\ell^Q(a,\theta) = \sum_{m=0}^{\infty} \epsilon_m \cos(m\theta) \int_a^\infty r_0 dr_0 \left[-i\frac{\omega_1+\omega_2}{A_{\ell,\ell}}\right] \widehat{\mathcal{Q}}_m(\omega_1,\omega_2) K_m(\kappa_\ell r) \times \left[\frac{I_m'(\kappa_{n,l}a)}{K_m'(\kappa_\ell a)} K_m(\kappa_\ell a) - I_m(\kappa_\ell a)\right]. \tag{9.4.26}$$

Making use of Eqn. (4.4.34), the previous equation can be reduced as

$$\xi_\ell^Q(a,\theta) = \sum_{m=0}^{\infty} \frac{\epsilon_m}{\kappa_\ell a} \cos(m\theta) \int_a^\infty r_0 dr_0 \left[-i\frac{\omega_1+\omega_2}{A_{\ell,\ell}}\right] \widehat{\mathcal{Q}}_m(\omega_1,\omega_2) \frac{K_m(\kappa_\ell r)}{K_m'(\kappa_\ell a)}. \tag{9.4.27}$$

Now the analytical solutions in the far-field are obtained. In the near field of complex bathymetry and coastline, discrete finite elemets are used. The finite element analysis is same as chapter 5.2 by simply replacing the analytic solutions of ξ_ℓ^P, ξ_ℓ^Q by Eqs. (9.4.5) and (9.4.27) and is therefore omitted.

9.5 Evaluation of spectrum S_{22}

Let us recall Eq. (8.5.43) and rewrite it as

$$S_{22}(\omega) = \delta(\omega) \left[\overline{\zeta_2}\right]^2 + \mathcal{I}(\omega) \tag{9.5.1}$$

where

$$\mathcal{I}(\omega) = \int_{-\infty}^{\infty} S_A(\omega_1) S_A(\omega-\omega_1) \Gamma_2(\omega_1,\omega-\omega_1) \left[\Gamma_2^*(\omega_1,\omega-\omega_1) + \Gamma_2^*(\omega-\omega_1,\omega_1)\right] d\omega_1, \tag{9.5.2}$$

By dividing the interval $[-\infty,\infty]$ into two subintervals, $[-\infty,0]$ and $[0,\infty]$, the above integral can be written as

$$I(\omega) = \int_0^{\infty} S_A(\omega_1) S_A(\omega-\omega_1) \Gamma_2(\omega_1,\omega-\omega_1) \left[\Gamma_2^*(\omega_1,\omega-\omega_1) + \Gamma_2^*(\omega-\omega_1,\omega_1)\right] d\omega_1 + \int_{-\infty}^{0} S_A(\omega_1) S_A(\omega-\omega_1) \Gamma_2(\omega_1,\omega-\omega_1) \left[\Gamma_2^*(\omega_1,\omega-\omega_1) + \Gamma_2^*(\omega-\omega_1,\omega_1)\right] d\omega_1. \tag{9.5.3}$$

Now for the integral of the preceding equation, let us change ω_1 by $-\omega_1$, so the upper and lower limits of the integral becomes $[\infty, 0]$. Making use of the fact that

$$\int_{\infty}^{0} d(-\omega_1) = \int_{0}^{\infty} d\omega_1,$$

we get

$$\begin{aligned}\mathcal{I}(\omega) = &\int_0^{\infty} S_A(\omega_1) S_A(\omega-\omega_1) \Gamma_2(\omega_1, \omega-\omega_1) \left[\Gamma_2^*(\omega_1, \omega-\omega_1) + \Gamma_2^*(\omega-\omega_1, \omega_1)\right] d\omega_1 \\ &+ \int_0^{\infty} S_A(-\omega_1) S_A(\omega+\omega_1) \Gamma_2(-\omega_1, \omega+\omega_1) \left[\Gamma_2^*(-\omega_1, \omega+\omega_1) + \Gamma_2^*(\omega+\omega_1, -\omega_1)\right] d\omega_1.\end{aligned} \tag{9.5.4}$$

Since $S_A(\omega)$ is two-sided, i.e. $S_A(\omega_1) = S(-\omega_1)$, Eq. (9.5.4) can further be written as

$$\begin{aligned}\mathcal{I}(\omega) = &\int_0^{\infty} S_A(\omega_1) S_A(\omega-\omega_1) \Gamma_2(\omega_1, \omega-\omega_1) \left[\Gamma_2^*(\omega_1, \omega-\omega_1) + \Gamma_2^*(\omega-\omega_1, \omega_1)\right] d\omega_1 \\ &+ \int_0^{\infty} S_A(\omega_1) S_A(\omega+\omega_1) \Gamma_2(-\omega_1, \omega+\omega_1) \left[\Gamma_2^*(-\omega_1, \omega+\omega_1) + \Gamma_2^*(\omega+\omega_1, -\omega_1)\right] d\omega_1,\end{aligned} \tag{9.5.5}$$

As mention in section 8.1, we take the TMA spectrum to represent $2S_A(\omega_1)$ and from section 8.2, S_{TMA} is nonzero only in the range of $[\omega_a, \omega_b]$, Eq. (9.5.5) can further be rewritten as

$$\begin{aligned}\mathcal{I}(\omega) = &\int_{\omega_a}^{\omega_b} S_A(\omega_1) S_A(\omega-\omega_1) \Gamma_2(\omega_1, \omega-\omega_1) \left[\Gamma_2^*(\omega_1, \omega-\omega_1) + \Gamma_2^*(\omega-\omega_1, \omega_1)\right] d\omega_1 \\ &+ \int_{\omega_a}^{\omega_b} S_A(\omega_1) S_A(\omega+\omega_1) \Gamma_2(-\omega_1, \omega+\omega_1) \left[\Gamma_2^*(-\omega_1, \omega+\omega_1) + \Gamma_2^*(\omega+\omega_1, -\omega_1)\right] d\omega_1.\end{aligned} \tag{9.5.6}$$

The trapezoid rule is used in the numerical integration of $\mathcal{I}(\omega)$, which is approached by first dividing the interval $[\omega_a, \omega_b]$ into N subintervals according to the partition : $\{\omega_a < \omega_a + \Delta\omega < \omega_a + 2\Delta\omega < \omega_a + 3\Delta\omega < \cdots < \omega_b\}$ so we can write Eq.

(9.5.6) in series form by

$$\begin{aligned}\mathcal{I}(\omega) = &\sum_{n_1=0}^{N} S_A(\omega_a + n_1\Delta\omega)\, S_A(\omega - \omega_a - n_1\Delta\omega)\, \Gamma_2(\omega_a + n_1\Delta\omega, \omega - \omega_a - n_1\Delta\omega) \times \\ &\left[\Gamma_2^*(\omega_a + n_1\Delta\omega, \omega - \omega_a - n_1\Delta\omega) + \Gamma_2^*(\omega - \omega_a - n_1\Delta\omega, \omega_a + n_1\Delta\omega)\right]\Delta\omega \\ + &\sum_{n_2=0}^{N} S_A(\omega_a + n_2\Delta\omega)\, S_A(\omega + \omega_a + n_2\Delta\omega)\, \Gamma_2(-\omega_a - n_2\Delta\omega, \omega + \omega_a + n_2\Delta\omega) \times \\ &\left[\Gamma_2^*(-\omega_a - n_2\Delta\omega, \omega + \omega_a + n_2\Delta\omega) + \Gamma_2^*(\omega + \omega_a + n_2\Delta\omega, -\omega_a - n_2\Delta\omega)\right]\Delta\omega.\end{aligned} \tag{9.5.7}$$

Since: (1) we are only interested in low frequency , $0 < \omega < \omega_a$, (2) $0 < (n_1, n_2) < N$ and (3)

$$S_A(\omega - \omega_a - n_1\Delta\omega) \neq 0, \quad \text{only when } \omega_a < \omega_a + n_1\Delta\omega - \omega < \omega_b,$$

$$S_A(\omega + \omega_a + n_2\Delta\omega) \neq 0, \quad \text{only when } \omega_a < \omega + \omega_a + n_2\Delta\omega < \omega_b,$$

we get the range of integers n_1 and n_2

$$\frac{\omega}{\Delta\omega} < n_1 < \frac{\omega_b - \omega_a + \omega}{\Delta\omega},$$

$$0 < n_2 < \frac{\omega_b - \omega_a - \omega}{\Delta\omega}.$$

Therefore Eq. (9.5.7) becomes

$$\begin{aligned}\mathcal{I}(\omega) = &\sum_{n=n_3}^{n_4} S_A(\omega_a + n\Delta\omega)\, S_A(\omega - \omega_a - n\Delta\omega)\, \Gamma_2(\omega_a + n\Delta\omega, \omega - \omega_a - n\Delta\omega) \times \\ &\left[\Gamma_2^*(\omega_a + n\Delta\omega, \omega - \omega_a - n\Delta\omega) + \Gamma_2^*(\omega - \omega_a - n\Delta\omega, \omega_a + n\Delta\omega)\right]\Delta\omega \\ + &\sum_{n=1}^{n_5} S_A(\omega_a + n\Delta\omega)\, S_A(\omega + \omega_a + n_2\Delta\omega)\, \Gamma_2(-\omega_a - n\Delta\omega, \omega + \omega_a + n\Delta\omega) \times \\ &\left[\Gamma_2^*(-\omega_a - n\Delta\omega, \omega + \omega_a + n\Delta\omega) + \Gamma_2^*(\omega + \omega_a + n\Delta\omega, -\omega_a - n\Delta\omega)\right]\Delta\omega\end{aligned} \tag{9.5.8}$$

where

$$n_3 = \text{ the smallest integer } \geq \omega/\Delta\omega,$$

$$n_4 = \text{ the largest integer } \leq (\omega_b - \omega_a + \omega)/\Delta\omega,$$

$$n_5 = \text{ the largest integer } \leq (\omega_b - \omega_a - \omega)/\Delta\omega.$$

In the computation of the integral in S_{22} the main task is to compute the transfer function $\Gamma_2(\omega_1, \omega_2)$ for many pairs of frequencies. According to Eq. (9.5.8), the pairs for $S_{22}(\omega)$ needed in the $\Gamma_2(\omega_1, \omega_2)$ are shown in the shaded portions of the narrow strip shown in Figure 9-1 and are tabulated in Table 9.1 and Table 9.2. All $\Gamma_2(\omega_1, \omega_2)$ are computed by the hybrid element method.

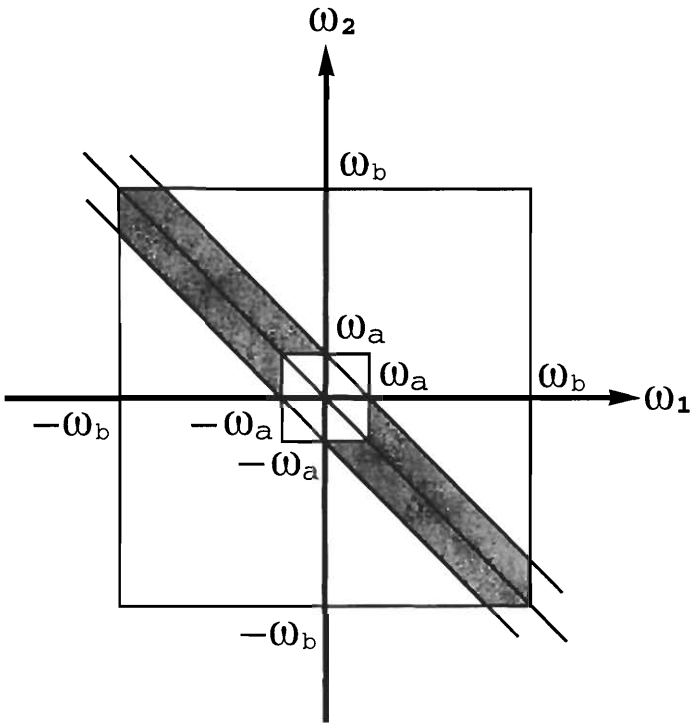

Figure 9-1: Plane of (ω_1, ω_2). Γ_2 is computed for frequency pairs inside the shaded strips. Frequencies ω_a and ω_b are the truncated limits of the incident sea spectrum.

$[\omega_a + n_3\Delta\omega, \omega - \omega_a - n_3\Delta\omega]$	$[\omega - \omega_a - n_3\Delta\omega, \omega_a + n_3\Delta\omega]$
$[\omega_a + (n_3+1)\Delta\omega, \omega - \omega_a - (n_3+1)\Delta\omega]$	$[\omega - \omega_a - (n_3+1)\Delta\omega, \omega_a + (n_3+1)\Delta\omega]$
$[\omega_a + (n_3+2)\Delta\omega, \omega - \omega_a - (n_3+2)\Delta\omega]$	$[\omega - \omega_a - (n_3+2)\Delta\omega, \omega_a + (n_3+2)\Delta\omega]$
$[\omega_a + (n_3+3)\Delta\omega, \omega - \omega_a - (n_3+3)\Delta\omega]$	$[\omega - \omega_a - (n_3+3)\Delta\omega, \omega_a + (n_3+3)\Delta\omega]$
$\vdots$	$\vdots$
$[\omega_a + n_4\Delta\omega, \omega - \omega_a - n_4\Delta\omega]$	$[\omega - \omega_a - n_4\Delta\omega, \omega_a + n_4\Delta\omega]$

Table 9.1: Pairs of (ω_1, ω_2) for computing the first series of $\mathcal{I}(\omega)$

$(\omega + \omega_a + \Delta\omega, -\omega_a - \Delta\omega)$	$(-\omega_a - \Delta\omega, \omega + \omega_a + \Delta\omega)$
$(\omega + \omega_a + 2\Delta\omega, -\omega_a - 2\Delta\omega)$	$(-\omega_a - 2\Delta\omega, \omega + \omega_a + 2\Delta\omega)$
$(\omega + \omega_a + 3\Delta\omega, -\omega_a - 3\Delta\omega)$	$(-\omega_a - 3\Delta\omega, \omega + \omega_a + 3\Delta\omega)$
$(\omega + \omega_a + 4\Delta\omega, -\omega_a - 4\Delta\omega)$	$(-\omega_a - 4\Delta\omega, \omega + \omega_a + 4\Delta\omega)$
$\vdots$	$\vdots$
$(\omega + \omega_a + n_5\Delta\omega, -\omega_a - n_5\Delta\omega)$	$(-\omega_a - n_5\Delta\omega, \omega + \omega_a + n_5\Delta\omega)$

Table 9.2: Pairs of (ω_1, ω_2) for computing the second series of $\mathcal{I}(\omega)$

Chapter 10

Numerical Solution for a Square Harbor in constant depth

10.1 Square Harbor in constant depth

In general, the theory presented here can deal with variable depth, which has already been demonstrated for monochromatic incident waves in Part I. Since here our focus is on the stochastic theory, only the cases involving constant depth $h = 20\ m$ are considered in order to reduce the numerical burden . Now let us consider a square harbor behind the straight coast in constant depth. The width and length of the basin is $300\ m$. Three entrances are considered (as shown in Figure 10-1): (Case 1) centered harbor entrance of width $60\ m$ and open to the sea, (Case 2) centered harbor entrance of width $30\ m$ and open to the sea, and (Case 3) centered harbor entrance of width $30\ m$ and protected by a detached breakwater ($100\ m$ length, $5\ m$ thickness and $30\ m$ from the main breakwaters). In these three geometries, the opening is formed by a pair of breakwaters of $5\ m$ thickness. Only normal incidence angle ($\theta_I = 3\pi/2$) is considered.

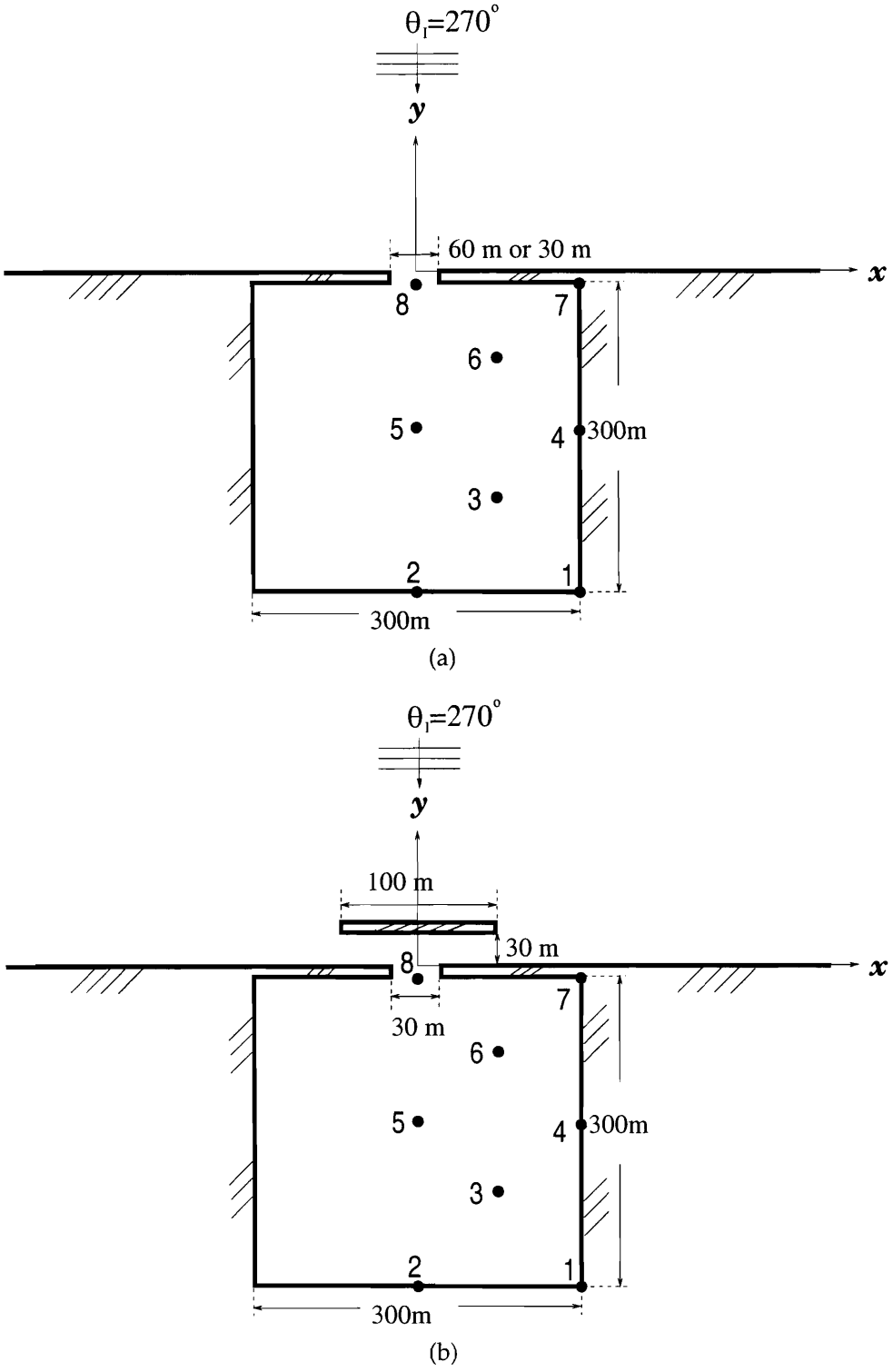

Figure 10-1: Plane view of the square basin and locations of St. $1-8$. (a): without protection. Case 1: $60\ m$ opening . Case 2: $30\ m$ opening . (b): Case 3 with protection.

10.2 Incident wave spectrum

In the numerical computation, we have made use of the TMA spectrum (see section 8.2) with $\gamma = 3.3$, $\bar{x} = 3000$ and $\bar{U} = 20\ m/s$. We find from Eq. (8.2.4), $\omega_p = 0.767\ rad/s$. The corresponding modal wavenumber is $k_p = 0.068\ (1/m)$ We further truncate the range of this TMA spectrum from $\omega = 0.6$ to $\omega = 1.8$. Figure 10-2 shows both the TMA spectrum and $2S_A$ in frequency ω and f space. According to Eqs. (8.5.5) and (8.5.4), we get the significant wave height $H_s = 1.85\ m$ and ordering parameter $\epsilon = 0.063$.

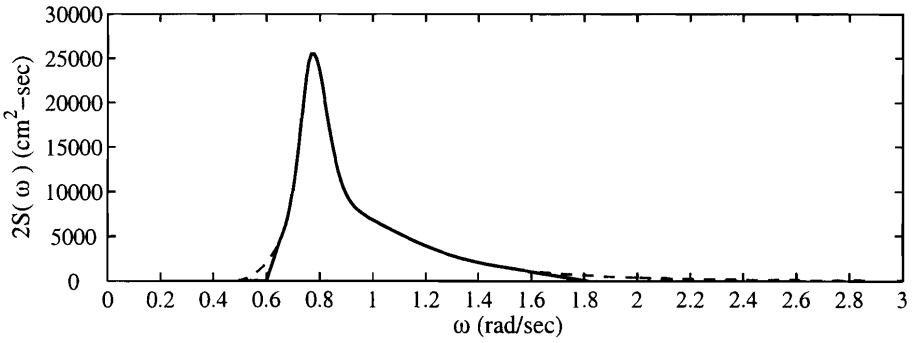

(a)

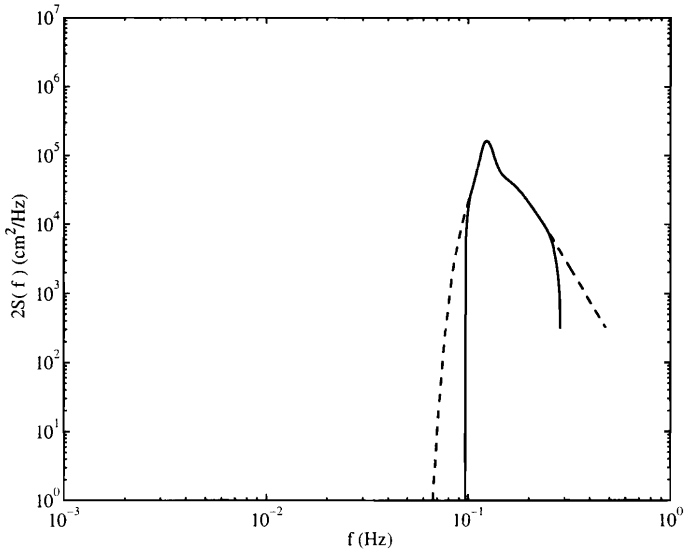

(b)

Figure 10-2: Comparison between TMA spectrum and our incident spectrum in frequency (a) ω (b) f space . Solid line: the incident spectrum $2S_A(\omega)$. Dashed line: TMA spectrum $S_{TMA}(\omega)$. Input parameters $\gamma = 3.3$, $\bar{x} = 3000$ and $\bar{U} = 20\ m/s$.

10.3 Pairs of frequencies

In the computation of the integral in S_{22} the main task is to compute the transfer function $\Gamma_2(\omega_1, \omega_2)$ for many pairs of frequencies as shown in Section 9.5. For each pair, the hybrid-element method is needed and finite element matrix has to be solved numerically. We choose $\Delta\omega = 0.01\ rad/sec$ and let $\omega = m\Delta\omega$. With the assumed incident wave spectrum, the frequency of the incident waves ranges from $0.6\ rad/s$ to $1.8\ rad/s$the according to Eq. (9.5.8), examples of the pairs that needed in computing $\Gamma_2(\omega_1, \omega_2)$ are shown in Table 10.1 and 10.2. It is clearly that for each ω, the total number of pairs is at least 100. We have computed the solutions from $\omega = 0.01\ rad/s$ to $0.6\ rad/s$. The total number of pairs needed for each mode is 10620. The time for solving each pair with FEM is around 15 minutes, therefore, the time required to compute the total pairs is around 100 days if only ONE computer is used. The required computational time is reduced greatly by using 20-25 parallel computers at the same time. The total computational time for one case is around two weeks.

$\omega = 0.01$	$\omega = 0.02$
(ω_1, ω_2)	(ω_1, ω_2)
$(0.62, -0.61), (-0.61, 0.62)$	$- - -$
$(0.63, -0.62), (-0.62, 0.63)$	$(0.63, -0.61), (-0.61, 0.63)$
$(0.64, -0.63), (-0.63, 0.64)$	$(0.64, -0.62), (-0.62, 0.64)$
$(0.65, -0.64), (-0.64, 0.65)$	$(0.65, -0.63), (-0.63, 0.65)$
$\vdots$	$\vdots$
$(1.79, -1.78), (-1.78, 1.79)$	$(1.79, -1.78), (-1.78, 1.79)$
total $= 238$	236

Table 10.1: Pairs of (ω_1, ω_2) for computing $S(\omega = 0.01)$ and $S(\omega = 0.02)$.

10.4 Numerical result

In the hybrid-element scheme, finite elements are used to discretize the basin ($-150\ m < x < 150\ m$ and $0 < y < 305\ m$) and the neighborhood near the entrance : (Case 1)

$\omega = 0.59$	$\omega = 0.60$
(ω_1, ω_2)	(ω_1, ω_2)
$(1.2, -0.61), (-0.61, 1.2)$	$- - -$
$(1.21, -0.62), (-0.62, 1.21)$	$(1.21, -0.61), (-0.61, 1.21)$
$(1.22, -0.63), (-0.63, 1.22)$	$(1.22, -0.62), (-0.62, 1.22)$
$(1.23, -0.64), (-0.64, 1.23)$	$(1.23, -0.63), (-0.63, 1.23)$
$\vdots$	$\vdots$
$(1.79, -1.20), (-1.20, 1.79)$	$(1.79, -1.59), (-1.59, 1.79)$
total = 118	116

Table 10.2: Pairs of (ω_1, ω_2) for computing $S(\omega = 0.59)$ and $S(\omega = 0.6)$.

$r < 30\ m$, (Case 2) $r < 15\ m$, (Case 3) $r < 62\ m$. In the region (Ω_F: (Case 1) $r > 30\ m$, (Case 2) $r > 15\ m$, (Case 3) $r > 62\ m$) the solution is analytical. The maximum element size L_e is $1\ m$, small compared with the shortest wave length $\lambda = 19\ m$. The total number of nodes is (Case 1) $N_P = 164062$, (Case 2) $N_P = 162935$ and (Case 3) $N_P = 171209$.

As a convenient measure of the overall response, we define the spatially averaged response over the entire area of the basin,

$$\text{Spatially averaged response} = \left(\frac{1}{A_b} \iint_{\Omega_{A_b}} |\Gamma_1|^2 d\Omega \right)^{1/2} \tag{10.4.1}$$

with Ω_{A_b} being the domain inside the basin and $A_b = 300 \times 300\, m^2$ the area of the basin.

The spatially averaged response of Γ_1 is plotted as a function of ω for three entrances in Figure 10-3. Table 10.3 compares the first 18 resonated peaks observed from Figure 10-3 with the natural modes of the closed basin, $\omega_{n,m}$(Cf. Eq. (7.3.3)). From Table 10.3, the first resonated peaks for three cases are at frequency $\omega = 0.032\ rad/s$, $\omega = 0.028\ rad/s$ and $\omega = 0.027\ rad/s$ for Case 1, 2 and 3 respectively. The first peak corresponds to the Helmholtz mode or pumping mode where the free surface with the harbor rises and falls in unison. In addition, the remaining non-Helmholtz modes are also identified by comparing the pattern of the free surface. The free-surface contours of first four natural modes of a closed

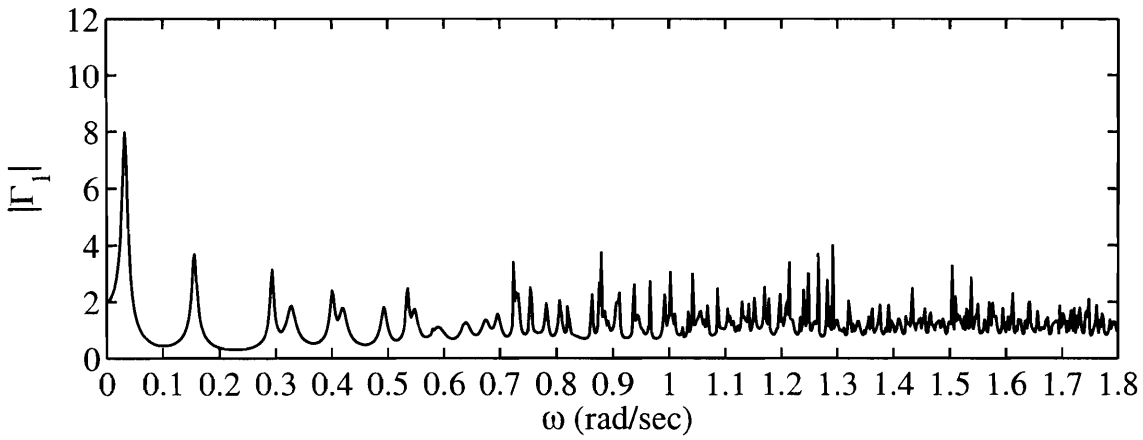

(a)

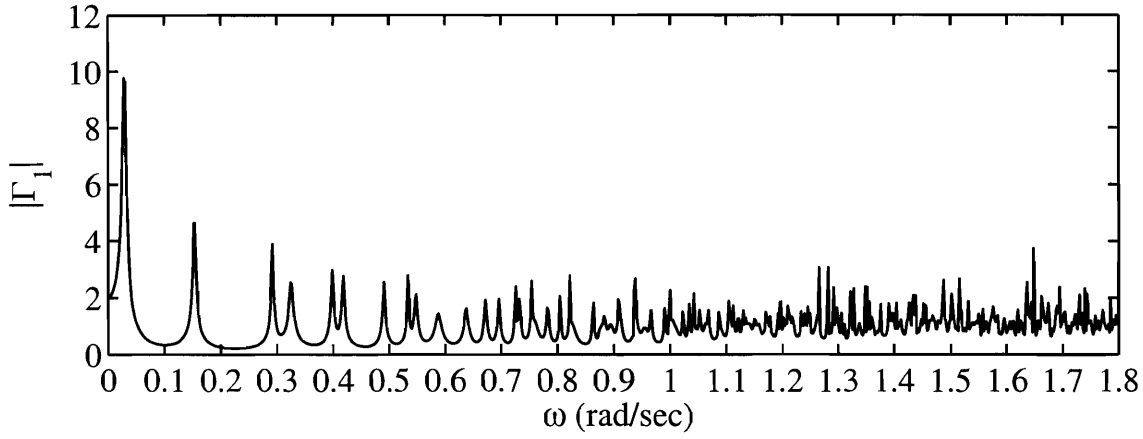

(b)

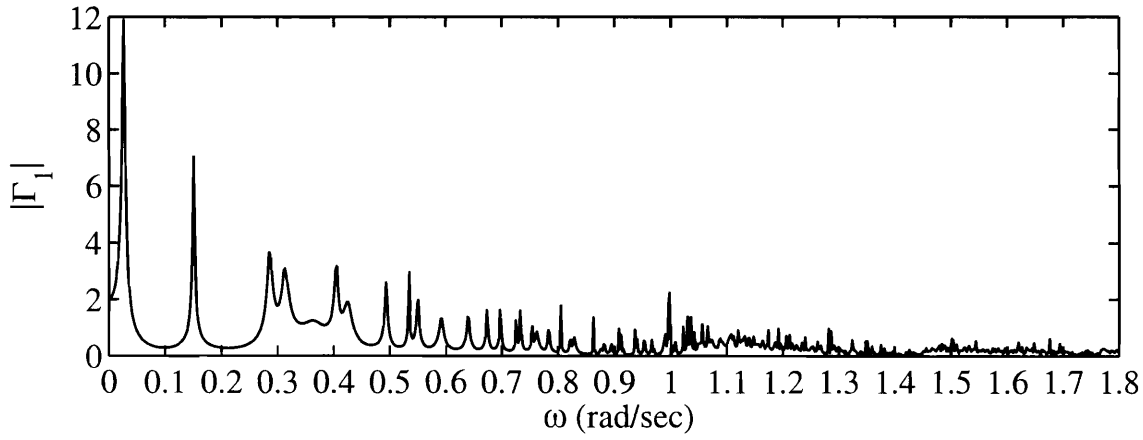

(c)

Figure 10-3: Spatial-averaged response Γ_1 for (a): 60 m opening (Case 1) , (b): 30m opening without protection (Case 2) , (c): 30 m opening with protection (Case 3).

peak no.	(n,m)	(1) $\omega_{n,m}$	(2)	(3)	(4)
1	(0,0)		0.032	0.028	0.027
2	(0,1)	0.146	0.156	0.154	0.15
3	(0,2)	0.285	0.294	0.292	0.285
4	(2,1)	0.316	0.328	0.324	0.312
5	(2,2)	0.392	0.4	0.398	0.405
6	(0,3)	0.414	0.42	0.418	0.425
7	(2,3)	0.485	0.492	0.49	0.493
8	(0,4)	0.530	0.536	0.534	0.535
9	(4,1)	0.544	0.548	0.548	0.55
10	(2,4)	0.58	0.59	0.588	0.592
11	(0,5)	0.632	0.64	0.638	0.64
12	(2,5)	0.669	0.674	0.672	0.672
13	(4,4)	0.693	0.696	0.696	0.696
14	(0,6)	0.723	0.724	0.726	0.726
15	(6,1)	0.731	0.73	0.732	0.732
16	(4,5)	0.756	0.754	0.754	0.754
17	(6,3)	0.78	0.782	0.782	0.782
18	(0,7)	0.8	0.806	0.804	0.804

Table 10.3: The resonant frequencies for (1) closed basin (2) opening 60 m (Case 1) (3) 30 m opening without protection (Case 2) (4) 30 m opening with protection (Case 3).

basin are shown in Figure 10-4. It is clear that odd modes in n are not resonated due to the symmetry of the harbor and normal incidence. From Table 10.3, the peak frequency is slightly shifted and Γ_1 is finite at resonance. For the first three modes, the peak frequencies of Case 3 are the smallest and closest to the natural frequencies of the closed basin among the three cases.

From Figure 10-3, the response curves look qualitatively the same in cases 1 and 2 with the peaks occurring at the expected places. However, the height of the peaks differ quantitatively for different entrances. The greatest spatial-averaged response for each case occurs at the first peak. By comparing Case 1, Case 2 and Case 3, it is clear that when the incident frequency is high (short waves, $\omega > 0.6$), the narrower entrance has the smaller response. Moreover, by putting a breakwater in front of the entrance, the response decreases tremendously. On the contrary, when the incident frequency is low (long waves, $\omega < 0.6$), the narrower entrance

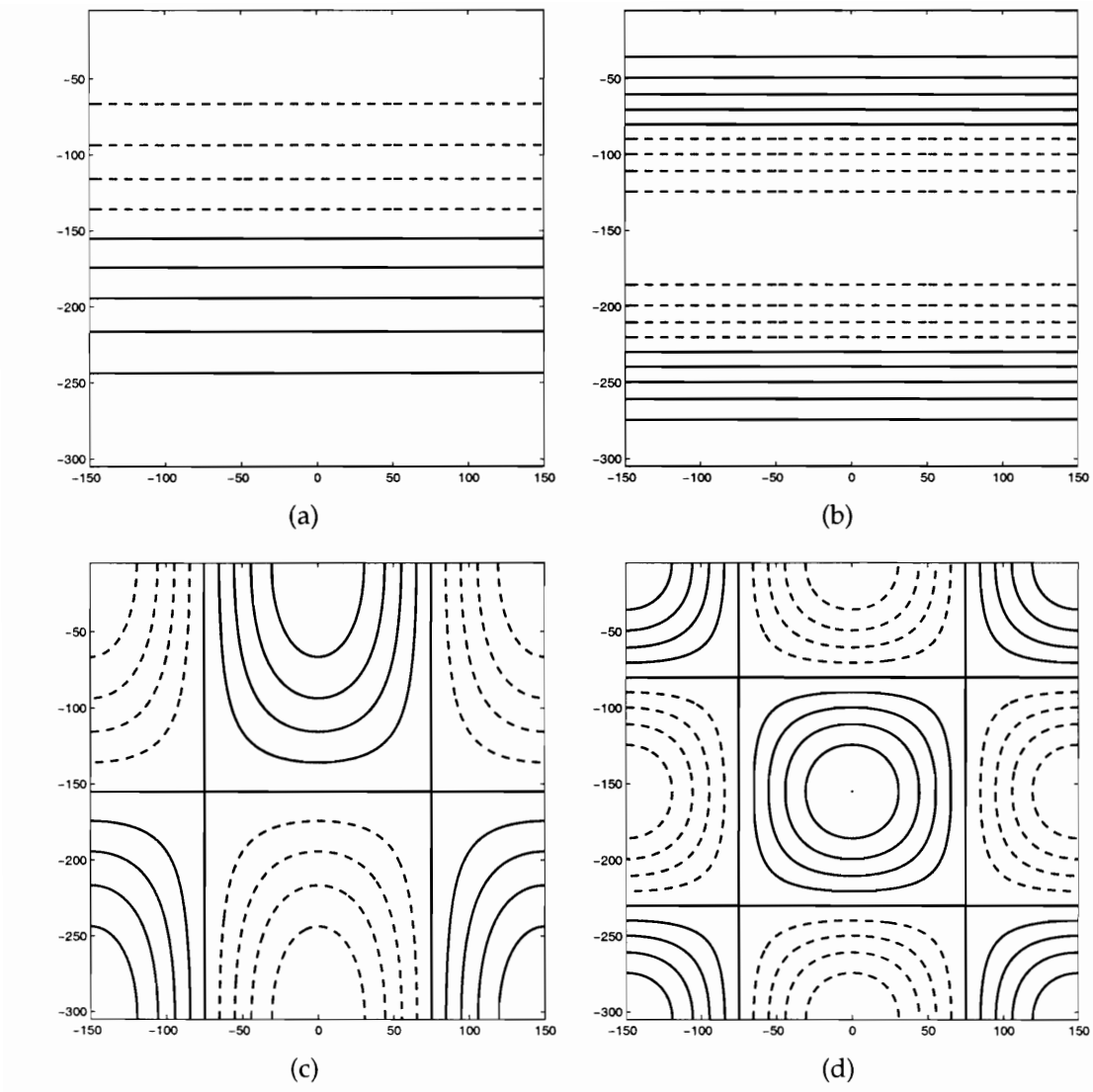

Figure 10-4: Free-surface contours of natural mode in a closed basin. (a) mode $(n, m) = (0, 1)$. (b) mode $(n, m) = (0, 2)$. (c)mode $(n, m) = (2, 1)$. (d) mode $(n, m) = (2, 2)$. Solid line: positive value. Dash line: negative.

has the smaller response and smaller width of the peak. In particular, the height of the first peak increases from 8 (Case 1) to 12 (Case 3) , and the second peak increases from 4 (Case 1) to 7 (Case 3). Since with small entrance or with protection, it is harder for energy to escape the harbor, therefore the response is greater. The feature that the resonant response increases with narrowing entrance does not always agree with practical experience and is one aspect of the harbor paradox named by Miles and Munk (1961). This indicates the friction loss at the entrance may play important role in reducing the resonant peaks.

The local responses at stations 1-8 for three entrances are also plotted in Figures 10-5 – 10-10. The location of each station shown in Figure 10-1 is $1 : (x, y) = (150\ m, -305\ m)$, $2 : (0\ m, -305\ m)$, $3 : (75\ m, -230\ m)$, $4 : (150\ m, -155\ m)$, $5 : (0\ m, -155\ m)$, $6 : (75\ m, -80\ m)$, $7 : (-150\ m, -5\ m)$ and 8: $(0\ m, -5\ m)$. Some of the peaks observed from the spatial-averaged response do not appear in the local response curve because some stations coincide with the nodal points of the standing wave mode. In particular, at St. 4 and 5 the peak for mode $(0, 1)$and at St. 3, 6 the peak for mode $(0, 2)$ disappear. The height of the peak differ quantitatively for different location. Among all, St. 8 in general has the smallest response. In comparison with the spatial-averaged response, the height of the peak at the corners (St. 1 and 7) and the inner end St. 2 are much greater then the spatial-averaged response. This can be understood since according to the natural modes of the closed basin, the corners and st 2 are the antinodes. It can also be seen at each station (except for St. 4 and 5), that the responses of the first two peaks increase due to narrowing the entrance and Case 3 is the greastest. However, the height of the Helmholtz mode does not differ much at 8 locations in each case.

The spatially-averaged linear spectrum $S_2(\omega)$ for three different entrances are shown in Figure 10-11. Recall that $S_2(\omega)$ is proportional to the incident wave spectrum and the square of $|\Gamma_1|$. Since the incident waves contains no energy at low frequency ($\omega < 0.6$) and for higher frequency the spatial-averaged $|\Gamma_1|$ is small , $S_2(\omega)$ is mainly in the range from $\omega = 0.6\ rad/s$ to $1.2\ rad/s$. Despite the large value of the height, the width of the peak is more important since in the spectral

analysis, the area under the curve represents wave energy and is of interest mostly. It can been seen that the areas under $S_2(\omega)$ decreases greatly for Case 3. By making use of Eq. (8.5.5), the significant wave heights H_s for Case 1, 2 and 3 are obtained by calculating the area under the curve as $1.2\ m$, $0.8\ m$ and $0.5\ m$ respectively. In comparison with $H_s = 1.85\ m$ of the incident waves, Cases 3 has reduced the incident wave energy by almost 73% ($(1.85 - 0.5)/1.85$). The linear spectrum $S_2(\omega)$ at station 1-8 for three entrance are also plotted in Figures 10-12– 10-17. St. 1, 2 and 7 again have the greatest spectra.

The mean-sea-level setup/setdown $\overline{\zeta_2}$ within the square basin are shown in Figures 10-18– 10-20 for three entrances. According to Eq. (8.4.39), the mean-sea-level setup/setdown is an ensemble of various frequencies. To better understand the computed mean sea-level, it is useful to examine the limiting result under a simple standing waves at the natural modes of the closed basin

$$\begin{aligned}\frac{\eta_{20}}{a_{n,m}^2} =& \frac{\omega_{n,m}^2}{g}\left|\cos\left[\frac{n\pi}{300}(x+150)\right]\cos\left[\frac{m\pi}{300}(y+305)\right]\right|^2 \\ &- \frac{g}{\omega_{n,m}^2}\frac{n\pi}{300}\left\{\sin\left[\frac{n\pi}{300}(x+150)\right]\cos\left[\frac{m\pi}{300}(y+305)\right]\right\}^2 \\ &- \frac{g}{\omega_{n,m}^2}\frac{m\pi}{300}\left\{\cos\left[\frac{n\pi}{300}(x+150)\right]\sin\left[\frac{m\pi}{300}(y+305)\right]\right\}^2,\end{aligned} \tag{10.4.2}$$

which follows from Eqs. and (3.1.12) and (7.3.1). Spatial variation of η_{20} are plotted in Figures 10-21–10-24 for eight modes: $(n,m) = (0,5)$, $(2,5)$, $(4,4)$, $(0,6)$, $(6,1)$, $(4,5)$,$(6,3)$ and $(0,7)$. The eight corresponding frequencies, $\omega_{n,m}$, are in the range of $[0.6\ rad/s, 0.8\ rad/s]$ which contains most energy. Therefore, these modes should dominate in the assemble average of ζ_2. Due to the staggering of the nodal lines and antinodal lines, the assemble of all the frequencies response with the corresponding incident wave spectral $S_A(\omega_1)$ renders a more complicated free surface. Figures 10-18– 10-20, it can been seen that on the wall and along the centerline($x = 0\ m$) the setup are the greatest. Again, with a narrower opening and a breakwater in front of the entrance , the setup is reduced tremendously especially in the neighborhood of the centerline ($x = 0\ m$).

The low-frequency wave spectra are obtained from the nonlinear correction $S_{22}(\omega)$. The spatial-averaged response are shown in Figure 10-25 for three entrances. The first two peaks in S_{22} coincide with Helmholtz mode and the first non-Helmoholtz mode observed from the first-order response curves with the similar dependence on the opening. The feature of the harbor paradox mentioned in the first-order result is again observed. It can be seen that most of the low-frequency energy concentrates in the neighborhood of the first two modes. $S_{22}(\omega)$ at eight stations for three entrances are also plotted in Figures 10-26-10-31. It can been seen that in comparison with Case 1 and Case 2, the second peak for Case 3 is much larger. However, for Case 3 almost all the energy concentrates under the first two peaks while for Case 1 it still have some energy spreading though out the entire range of low- frequency domain. Among all, the nonlinear effect at St. 8 is the smallest while at St. 7 is the greatest.

For qualitative comparison with field data, let us first see the spectrum during Typhoon Tim in Hualien Harbor at several stations both in side and outside the harbor, as shownin Figures 10-33 and 10-32. Figure 10-33 shows that inside the harbor high frequency energy component was blocked by the breakerwater, but the low frequency energy was increased by resonace hundred times.

In order to compare further the computed result with the spectra during Typhoon Tim in Hualien Harbor, shown in figure 10-33, we presented in Figures 10-34 – 10-60 the total spectrum $S(f) = S_2(f) \cup S_{22}(f)$ for the spatial-averaged spectrum as well as the local spectra at eight station. Note that the relation between $S(f)$ and $S(\omega)$ is

$$S(f) = 2\pi S(\omega).$$

Among the three cases, Case 3, which has a narrower entrance and a breakwater in front of the entrance, is the most relevant to Hualien Harbor. The computed spectrum of Case 3 resembles the spectrum of Typhoon Tim at St. 22 (Outer Basin). From Figure 10-36 and 10-33, it can be seen that the height of the peak of the short wave and long wave are about the same order in each figures. Also by compar-

ing $S_{22}(f)$ with the incident spectrum, the height of the peak at Helmoltz modes is arout 1/50-1/100 times of the peak of the incident waves spectrum. As mentioned previously, frictional loss at the entrance may play an important role in reducing the resonant peaks. This, as well as the effects of variable depth inside and outside the harbour, are of considerable practical importance and deserve further study. The present method in principle can be applied to a slow-drift motion of an offshore tethered platform. Although the third-order solution is not needed in this type of problems, for high-frequency response of a floating structure, it is still necessary to include the third-order solution to get a complete spectrum up to $O(\epsilon^4)$.

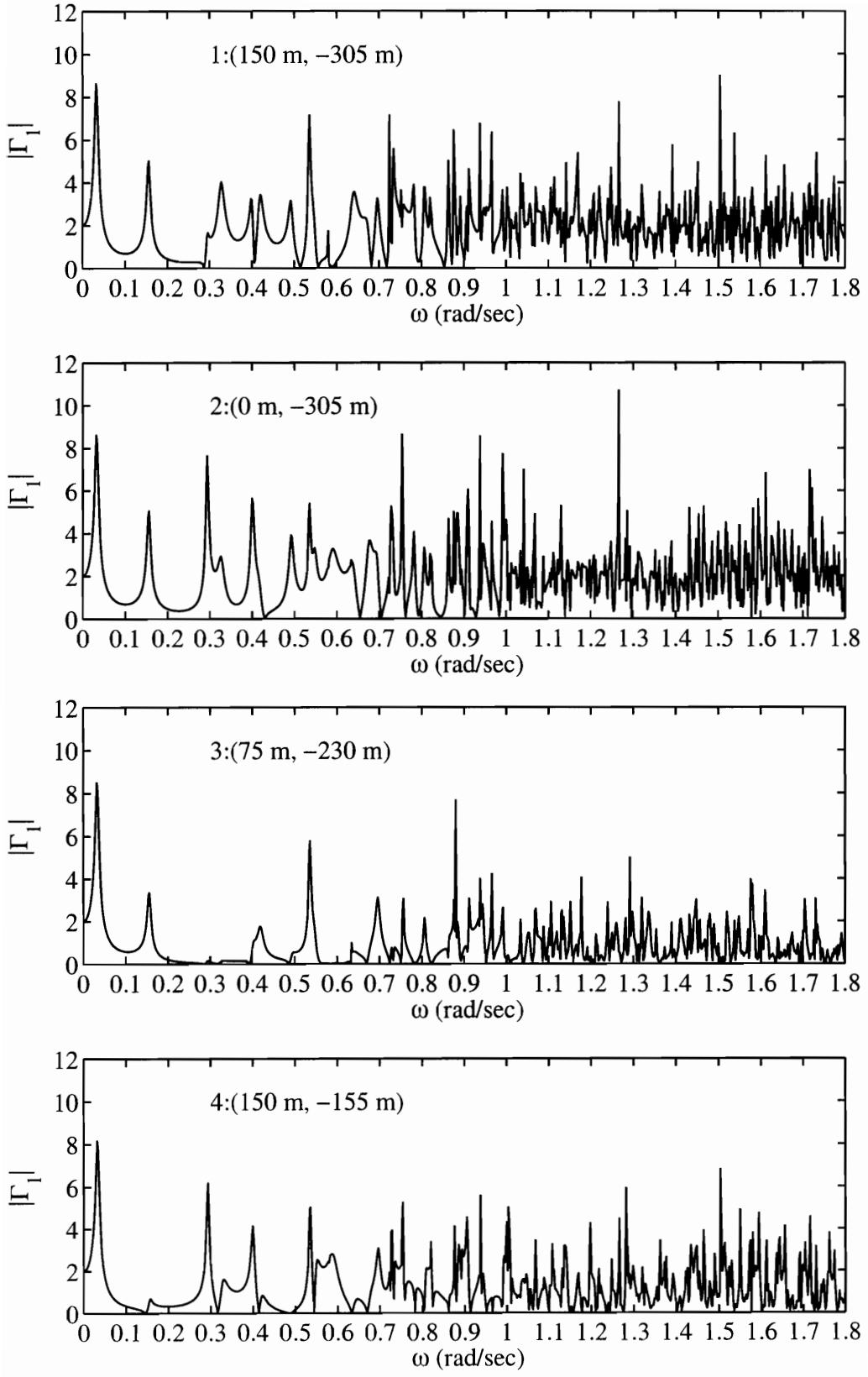

Figure 10-5: Free surface response Γ_1 at St. 1-4 for opening 60 m (Case 1)

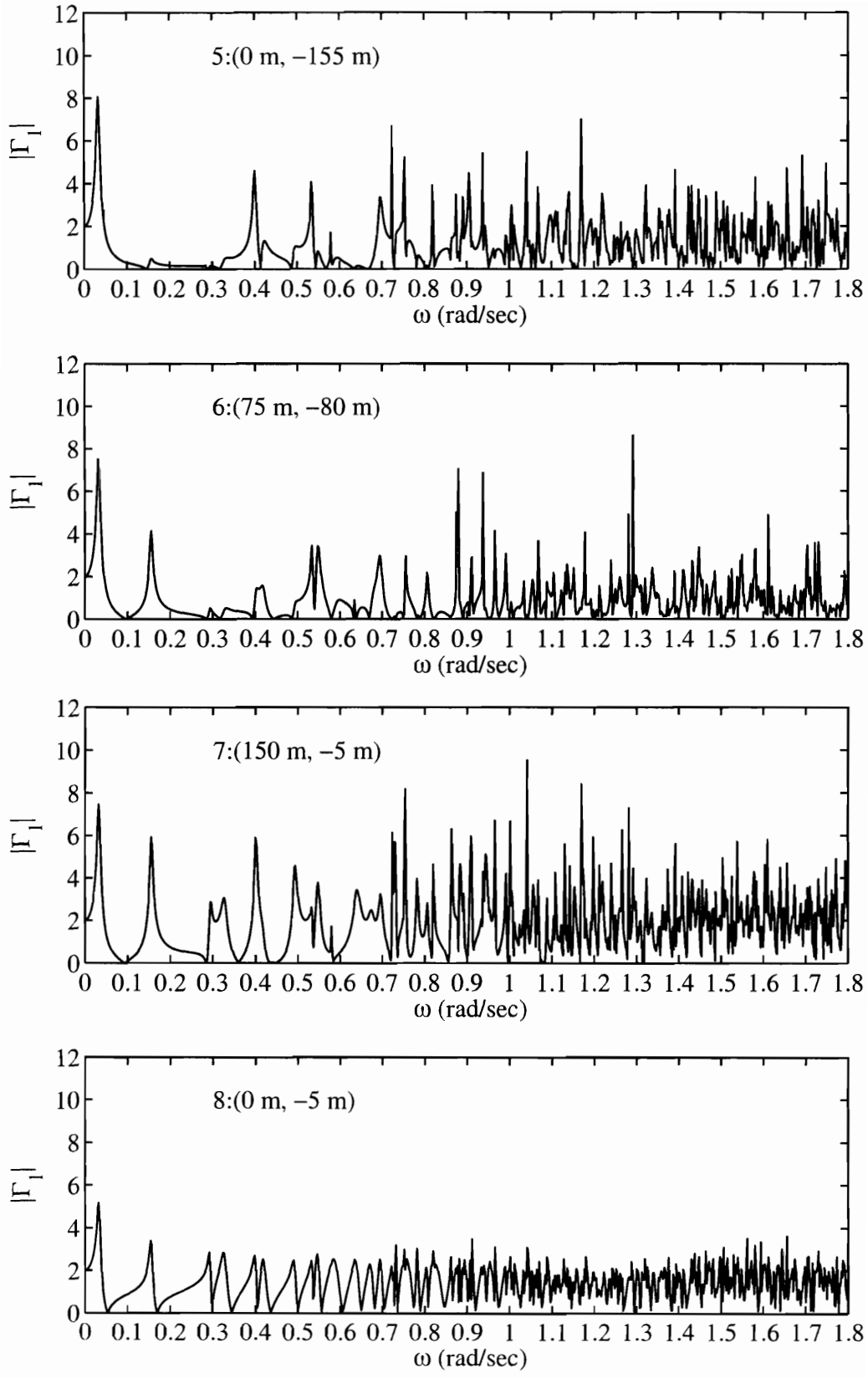

Figure 10-6: Free surface response Γ_1 at St. 5-8 for opening 60 m (Case 1)

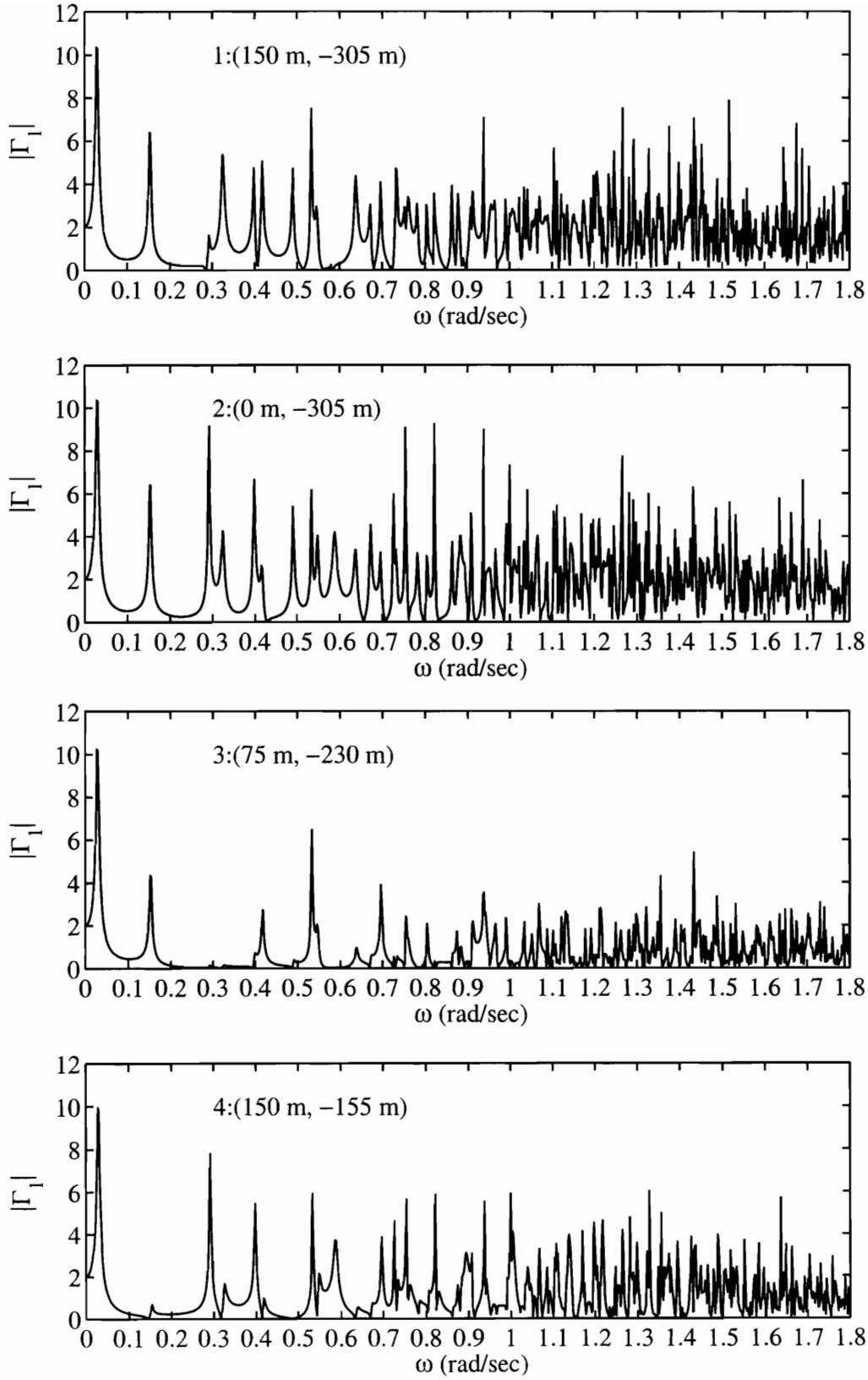

Figure 10-7: Free surface response Γ_1 at St. 1-4 for opening 30 m (Case 2)

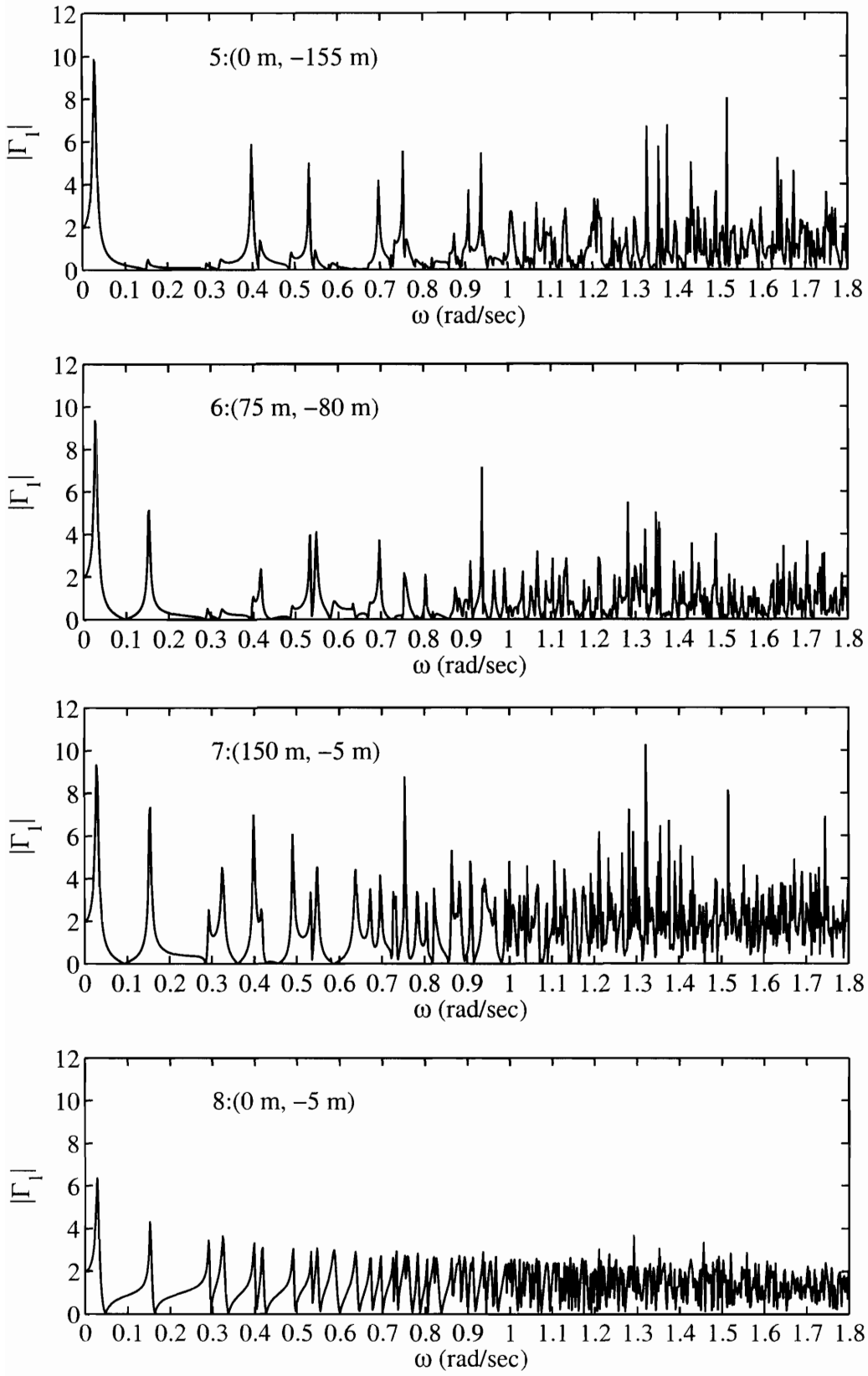

Figure 10-8: Free surface response Γ_1 at St. 5-8 for opening 30 m (Case 2)

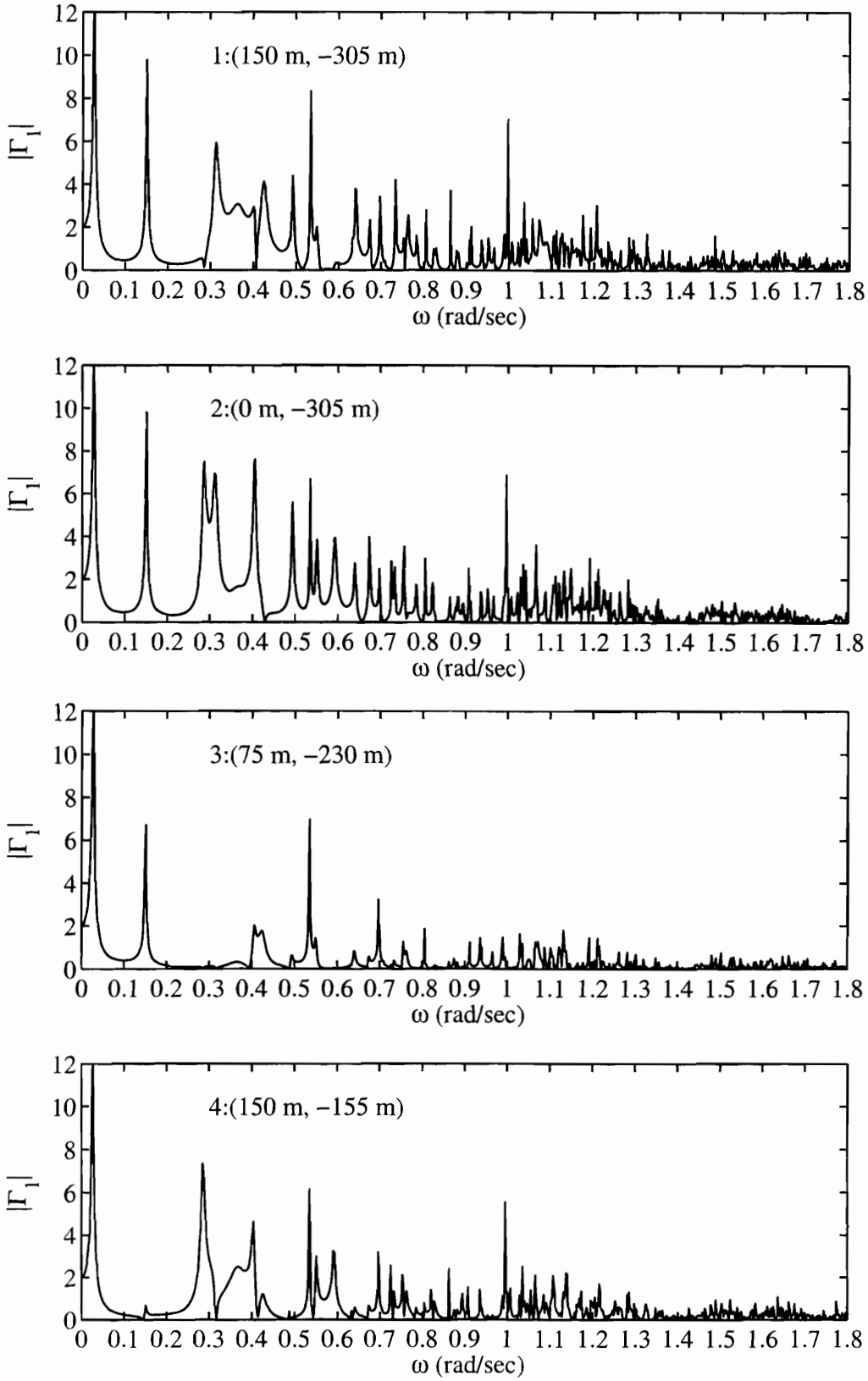

Figure 10-9: Free surface response Γ_1 at St. 1-4 for opening 30 m with breakwater (Case 3)

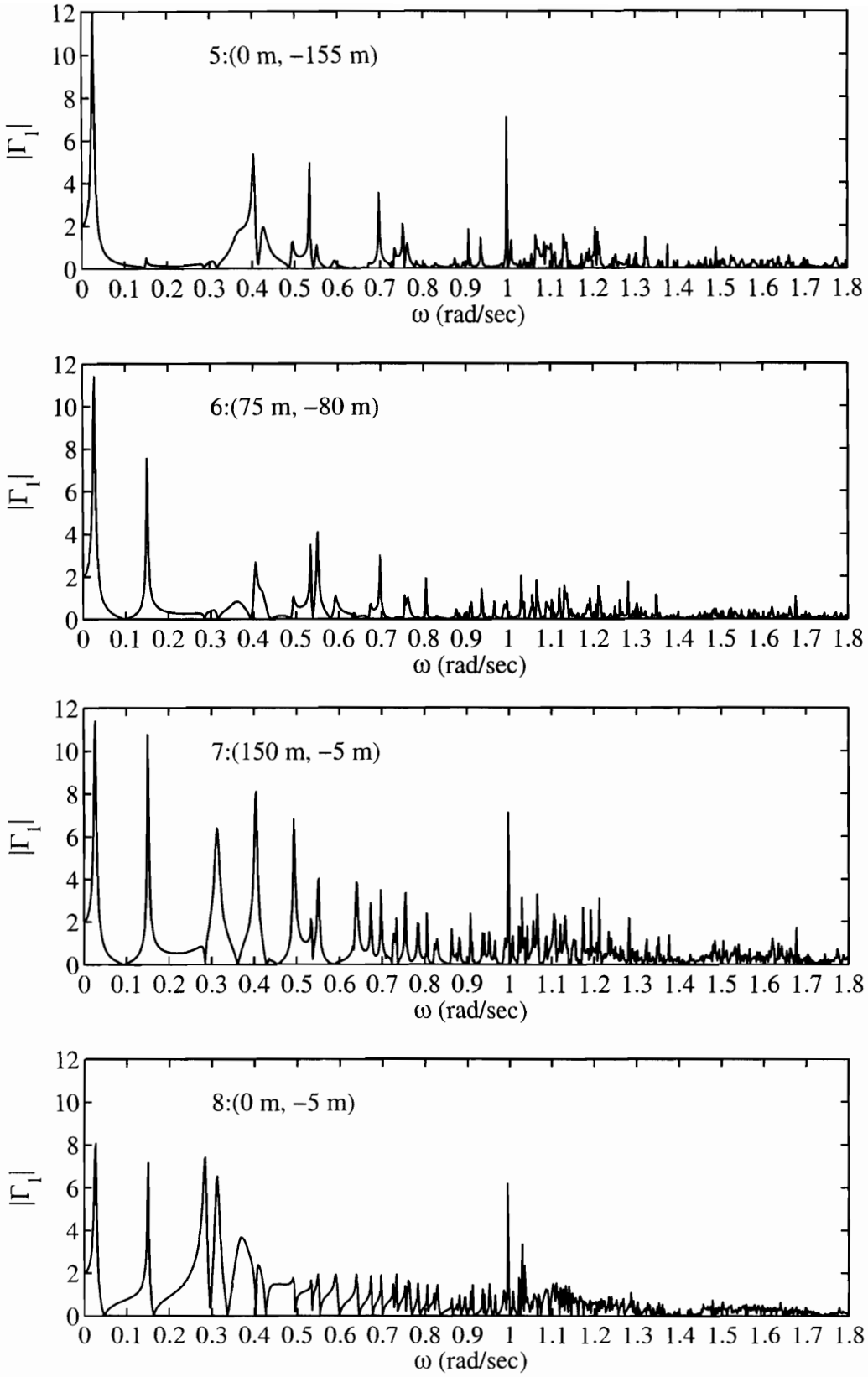

Figure 10-10: Free surface response Γ_1 at St. 5-8 for opening 30 m with breakwater (Case 3)

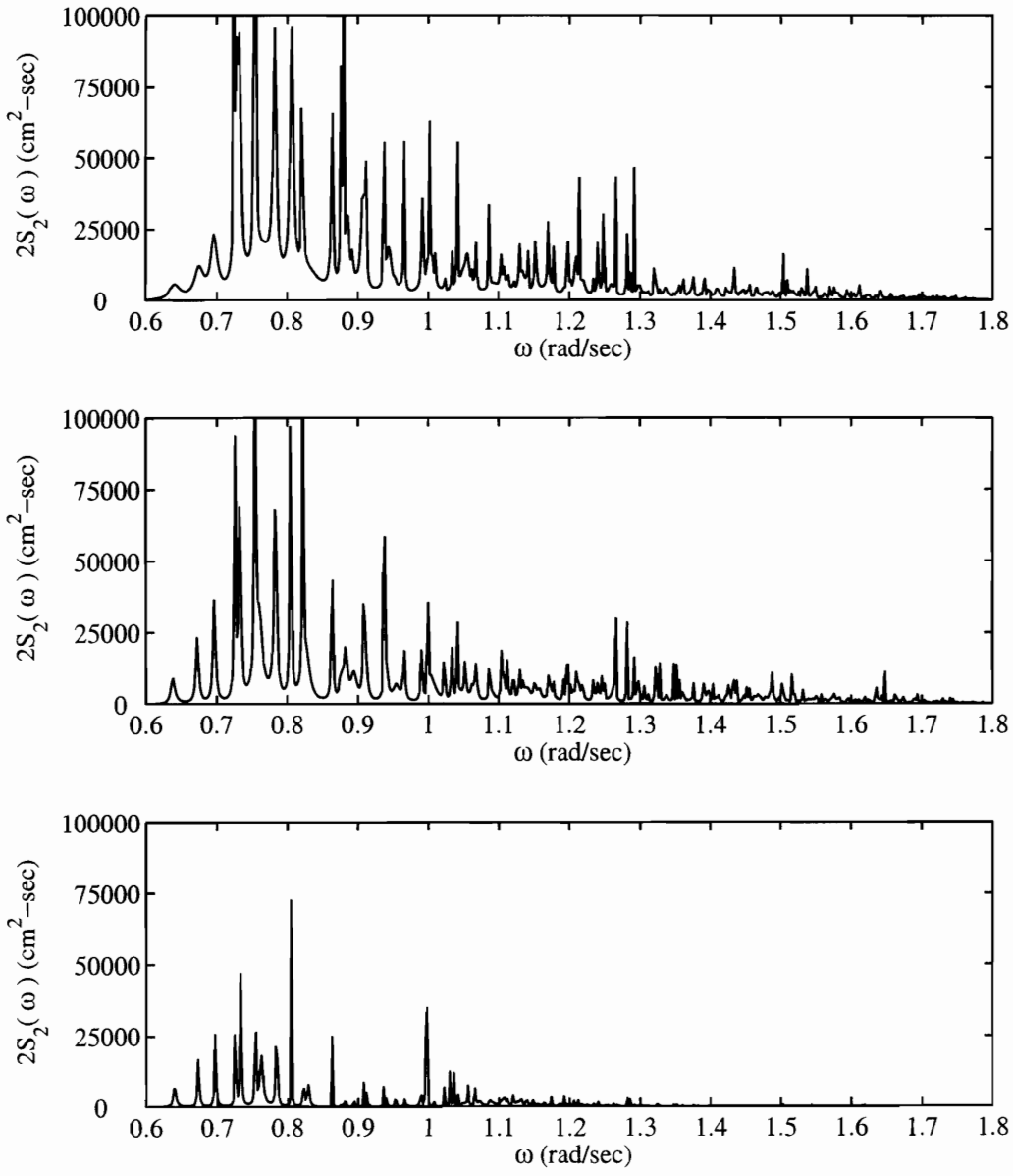

Figure 10-11: Spatial-averaged spectrum $2S_2(\omega)$. Top : opening 60 m (Case 1). Middle: 30m (Case 2). Bottom: 30 m with protection (Case 3).

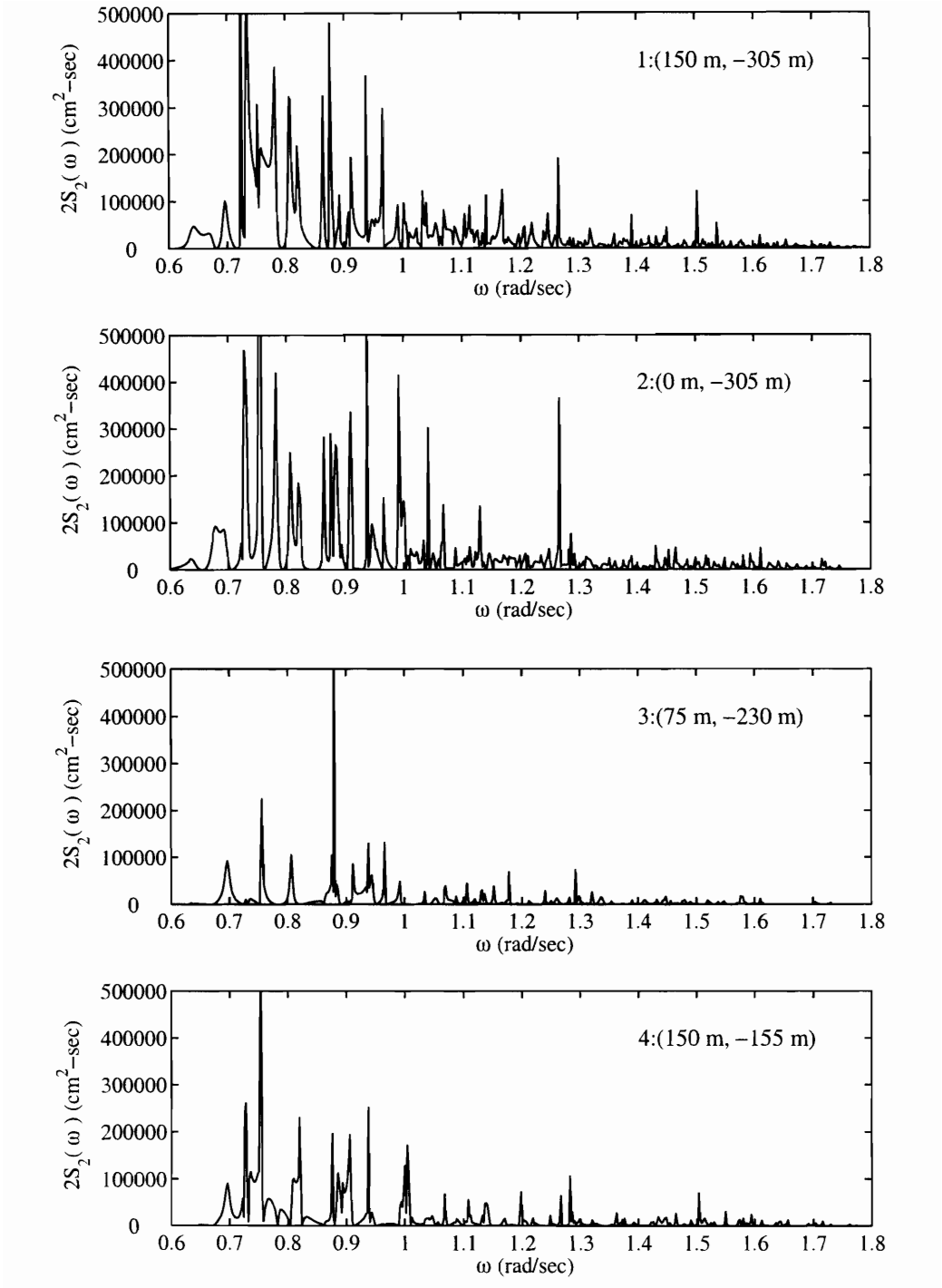

Figure 10-12: Linear spectrum $2S_2(\omega)$ at St. 1-4 for opening 60 m (Case 1)

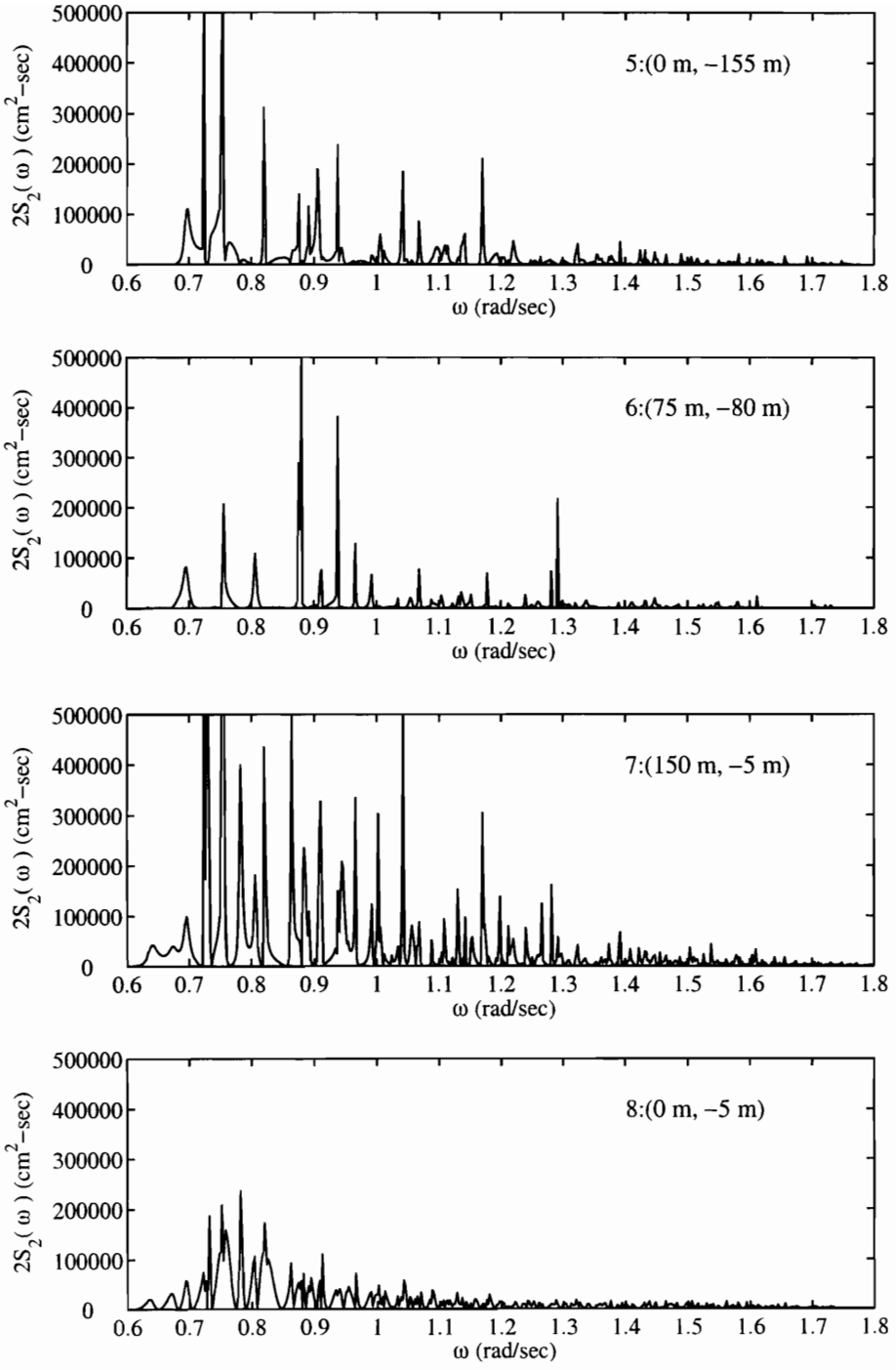

Figure 10-13: Linear spectrum $2S_2(\omega)$ at St. 5-8 for opening 60 m (Case 1)

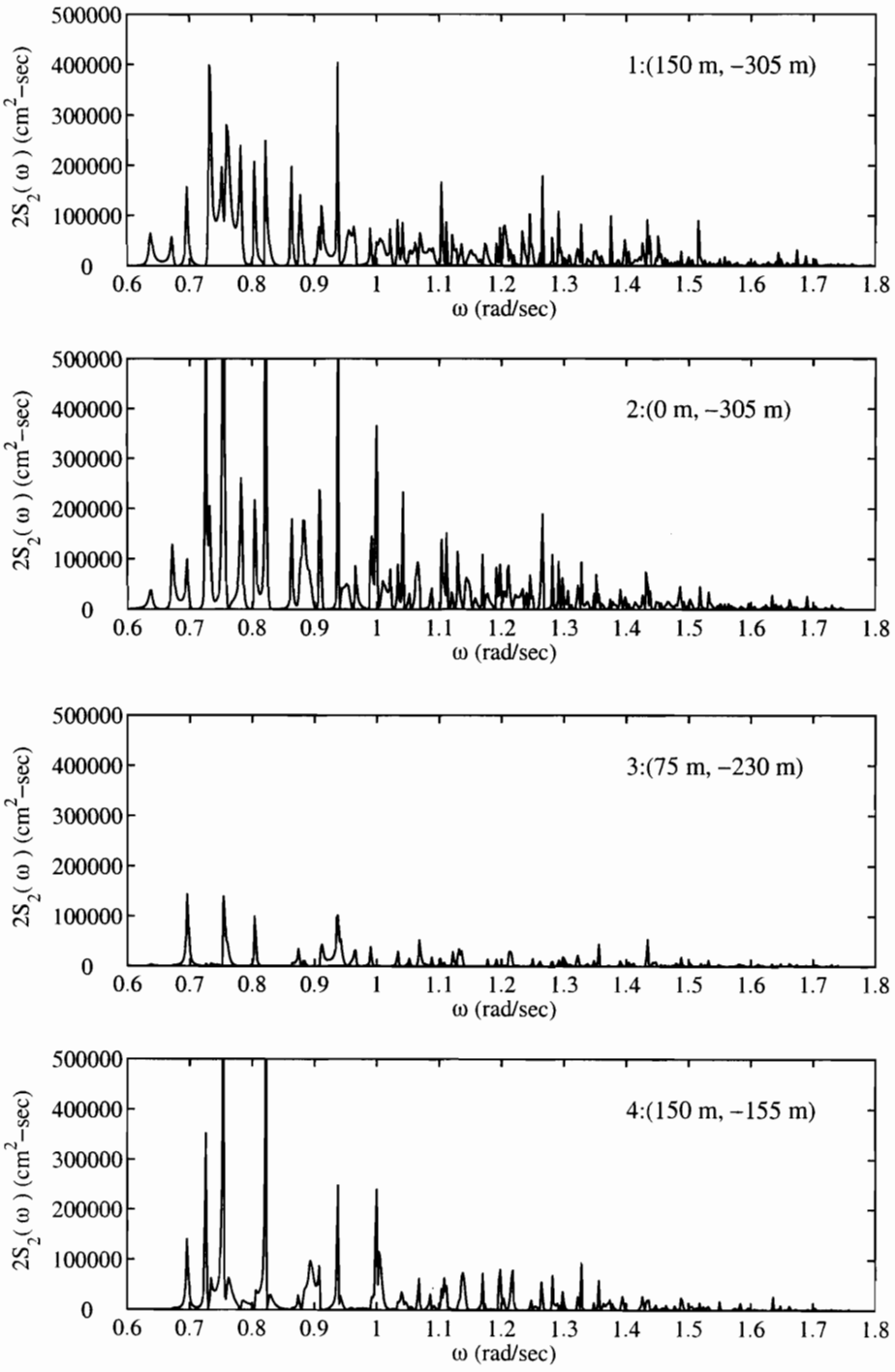

Figure 10-14: Linear spectrum $2S_2(\omega)$ at St. 1-4 for opening 30 m (Case 2)

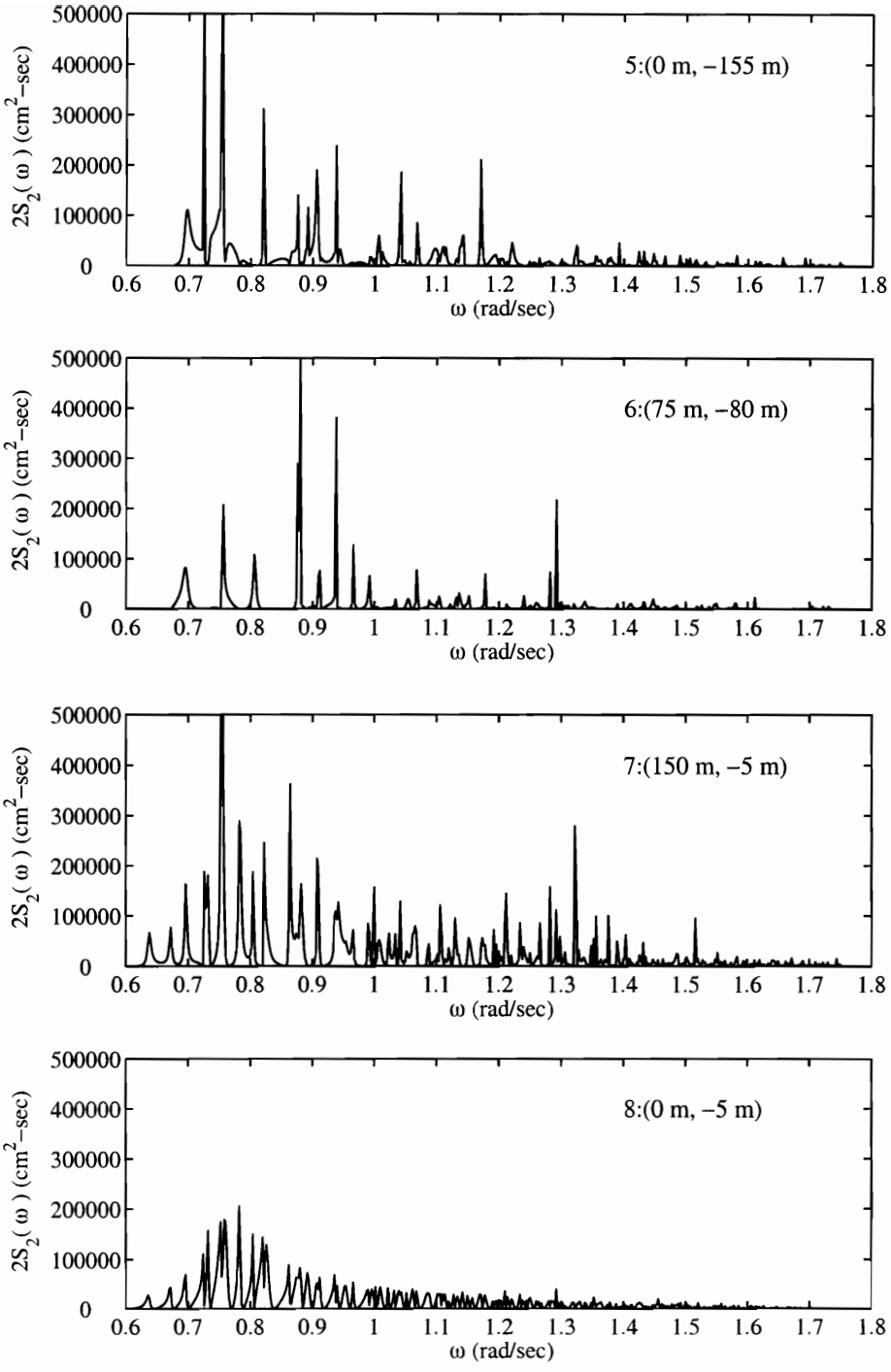

Figure 10-15: Linear spectrum $2\mathcal{S}_2(\omega)$ at St. 5-8 for opening 30 m (Case 2)

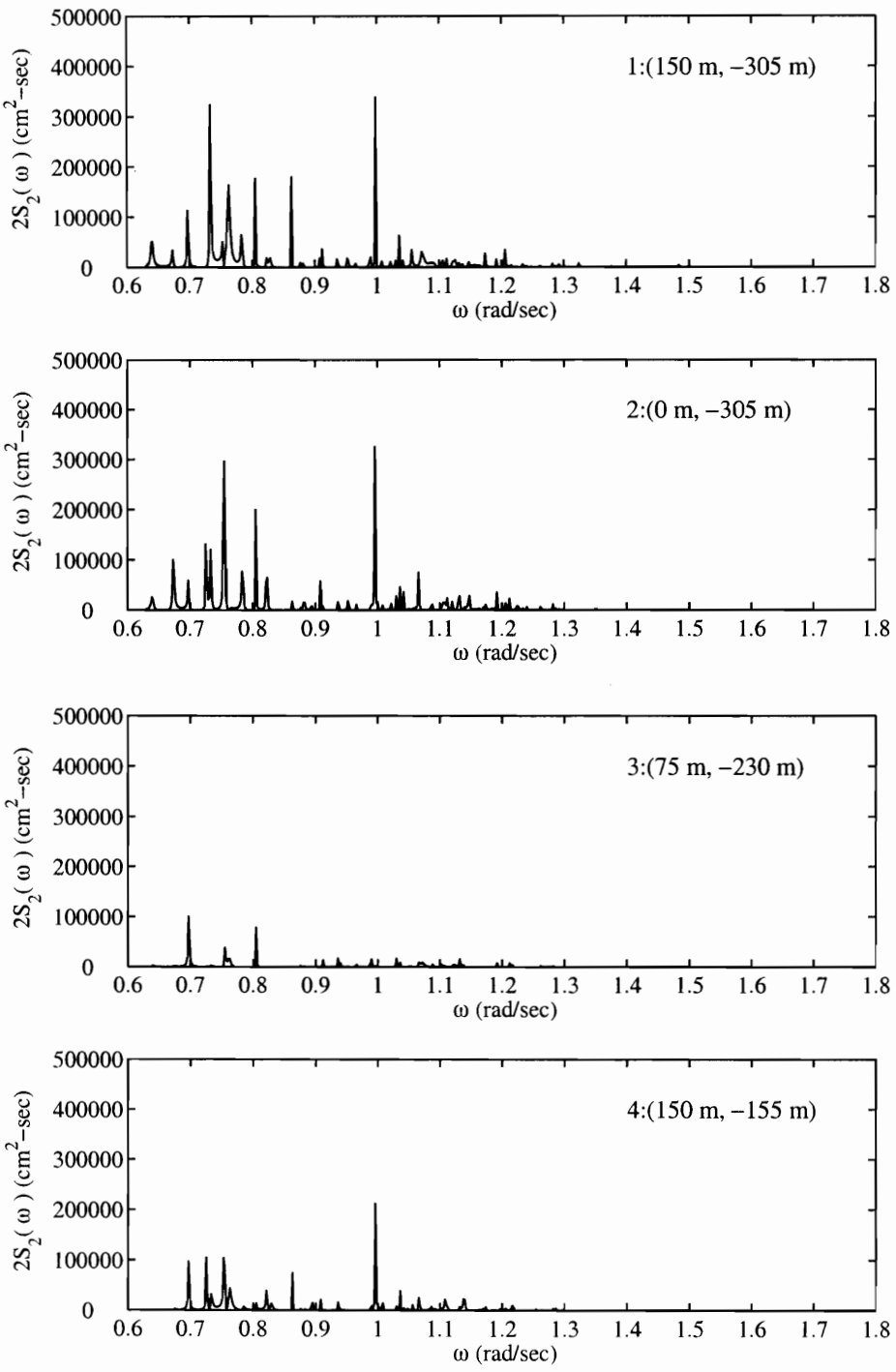

Figure 10-16: Linear spectrum $2\mathcal{S}_2(\omega)$ at St. 1-4 for opening 30 m with breakwater(Case 3)

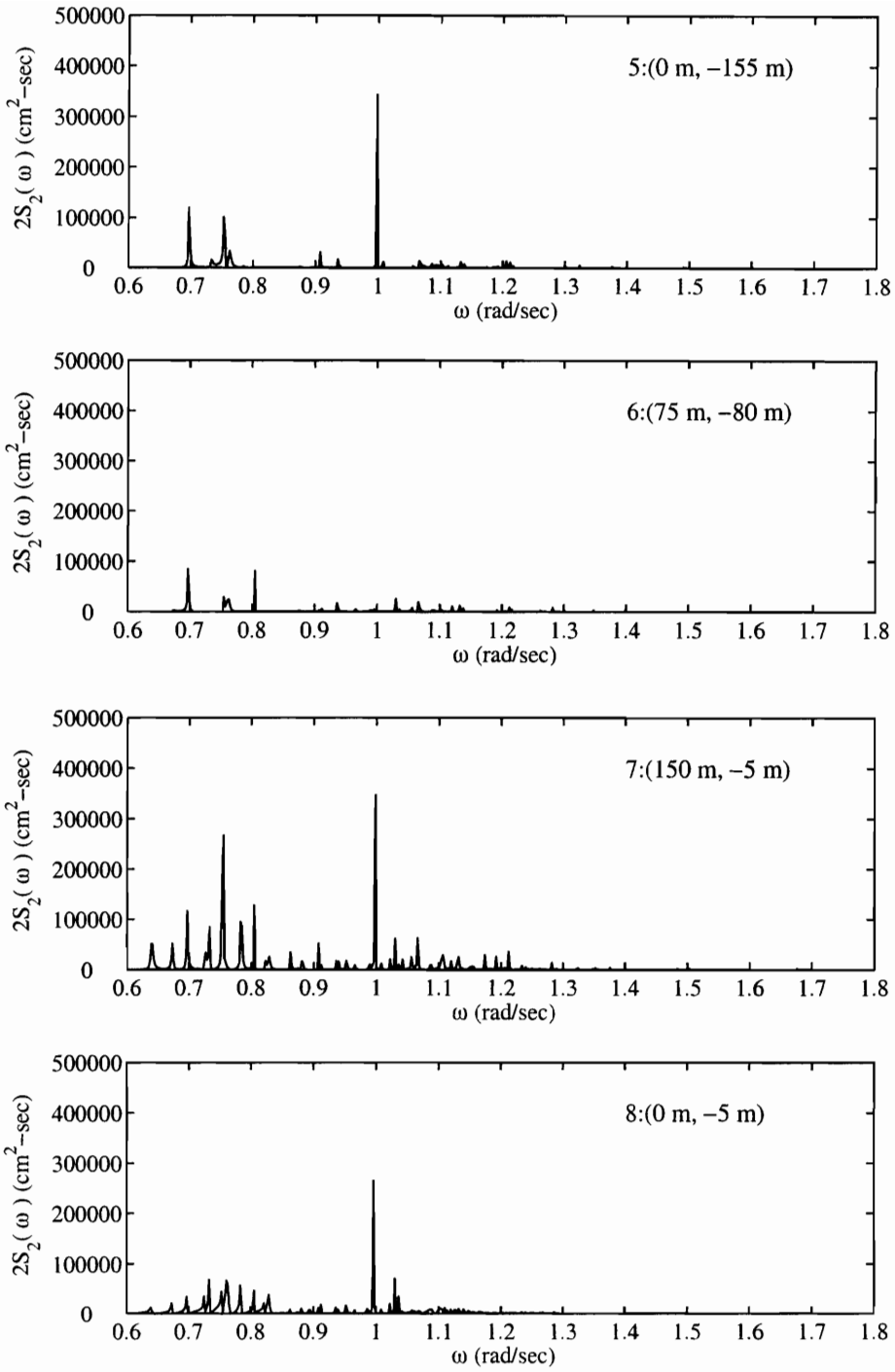

Figure 10-17: Linear spectrum $2\mathcal{S}_2(\omega)$ at St. 5-8 for opening 30 m with breakwater (Case 3)

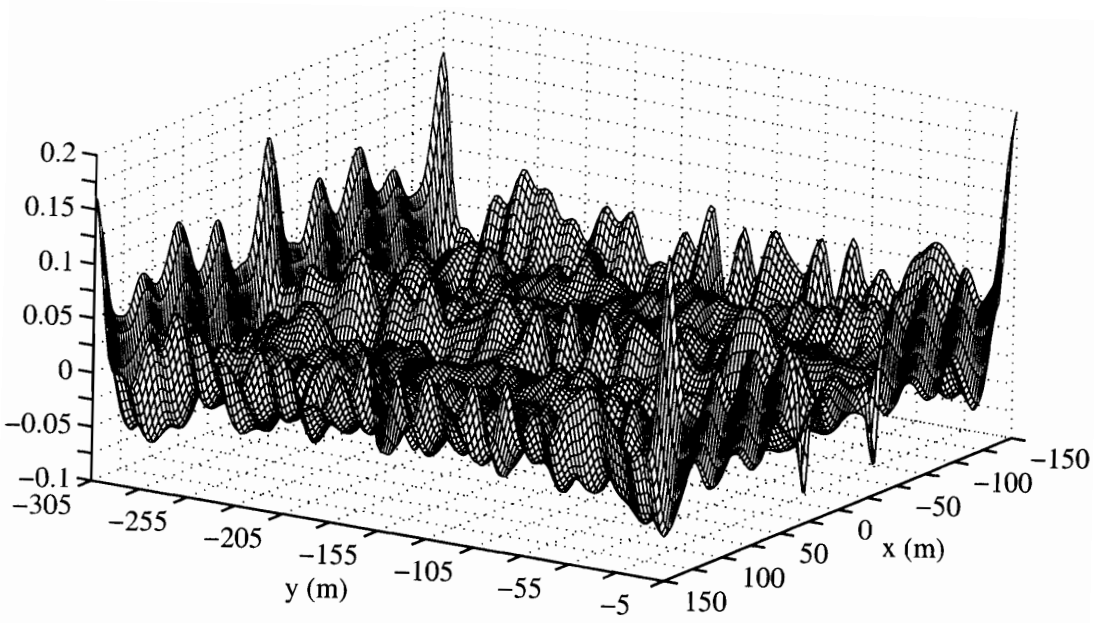

Figure 10-18: The second-order setup/down for opening 60 m (Case 1).

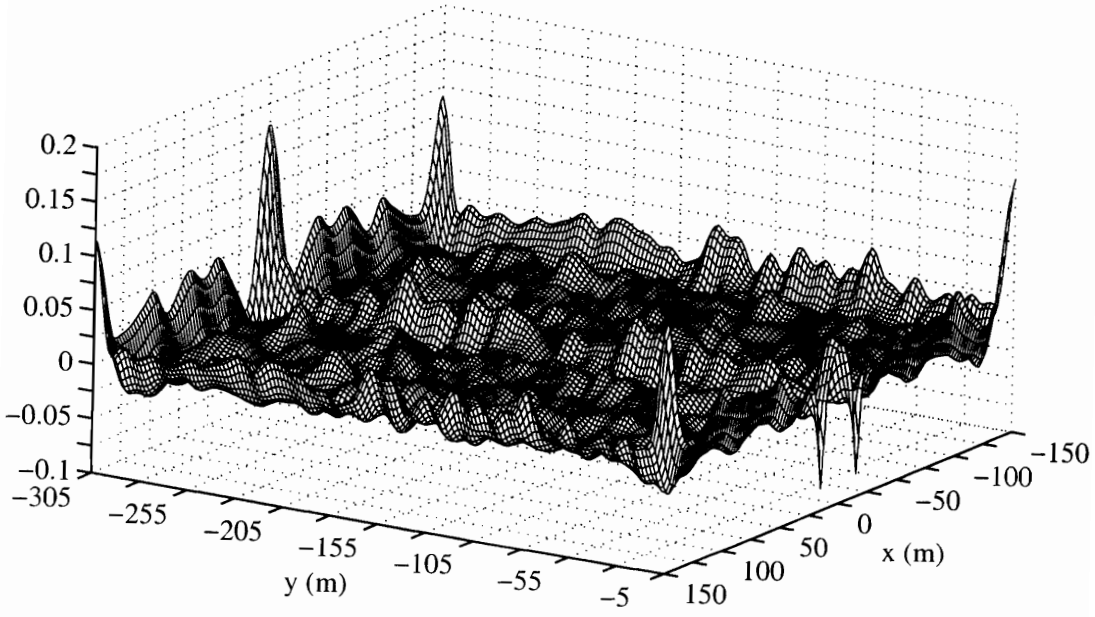

Figure 10-19: The second-order setup/down for opening 30 m (Case 2).

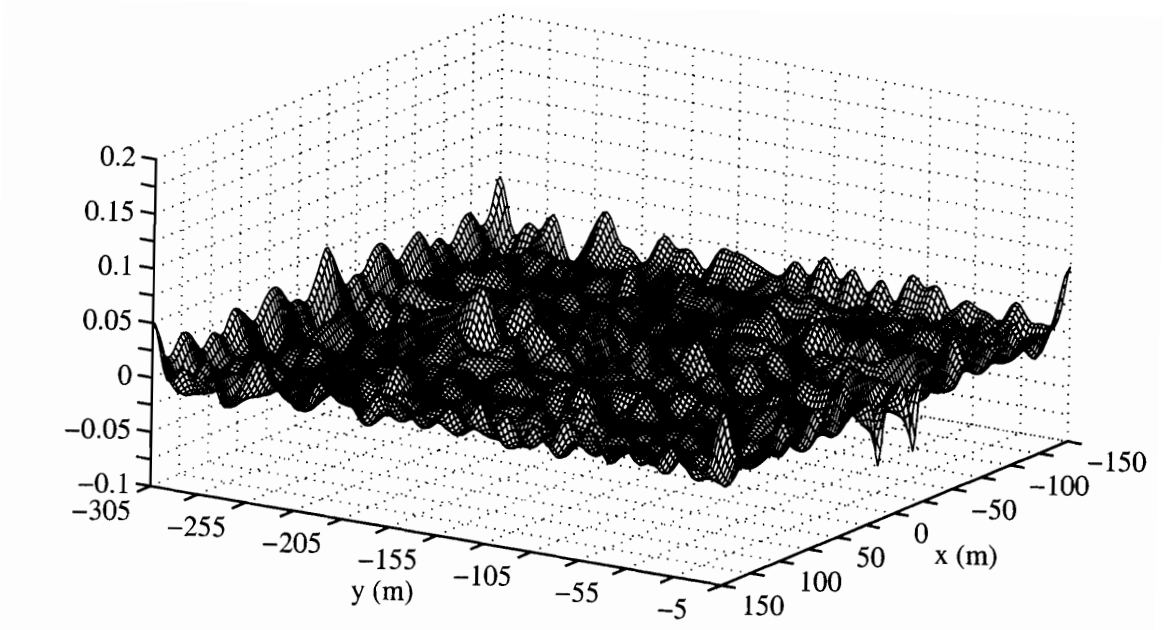

Figure 10-20: The second-order setup/down for opening 30 m with breakwater (Case 3).

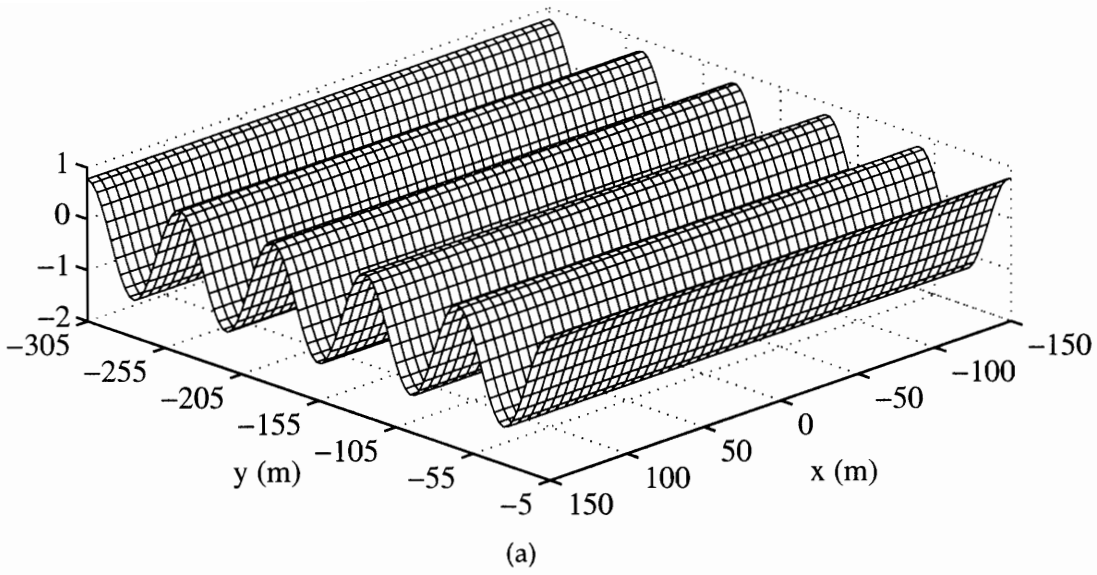

(a)

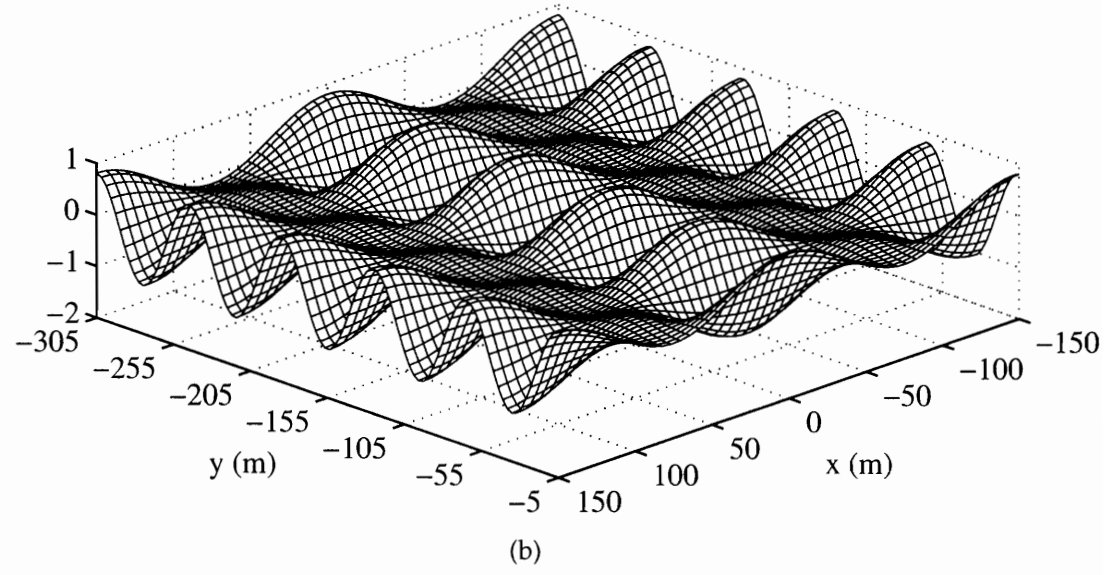

(b)

Figure 10-21: Setup/setdown $\eta_{20}/ka_{n,m}^2$ of standing wave in closed basin at mode (a) $(n, m) = (0, 5)$ and (b) $(n, m) = (2, 5)$

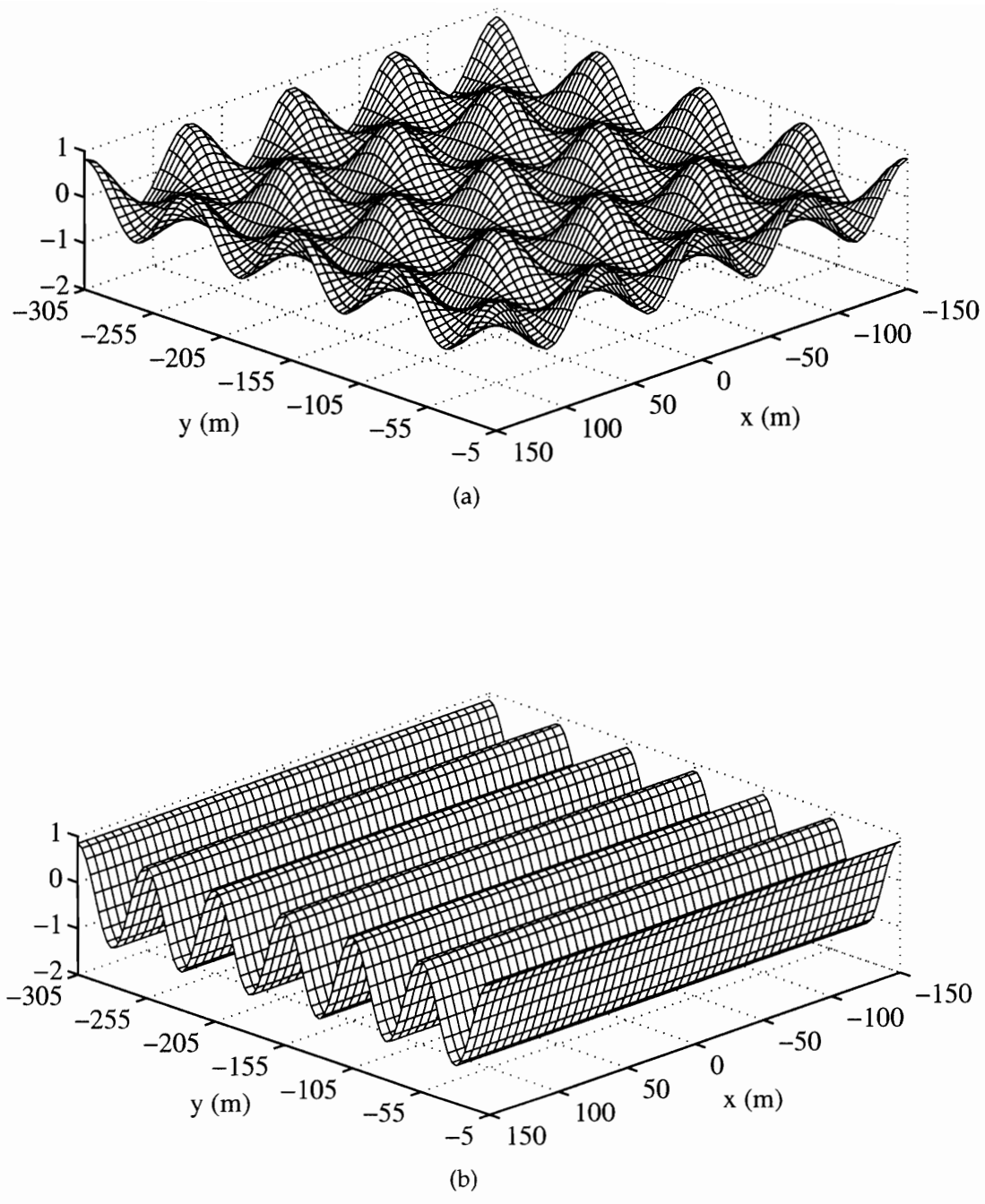

Figure 10-22: Setup/setdown $\eta_{20}/ka_{n,m}^2$ of standing wave in closed basin at mode (a) $(n, m) = (4, 4)$ and (b) $(n, m) = (0, 6)$

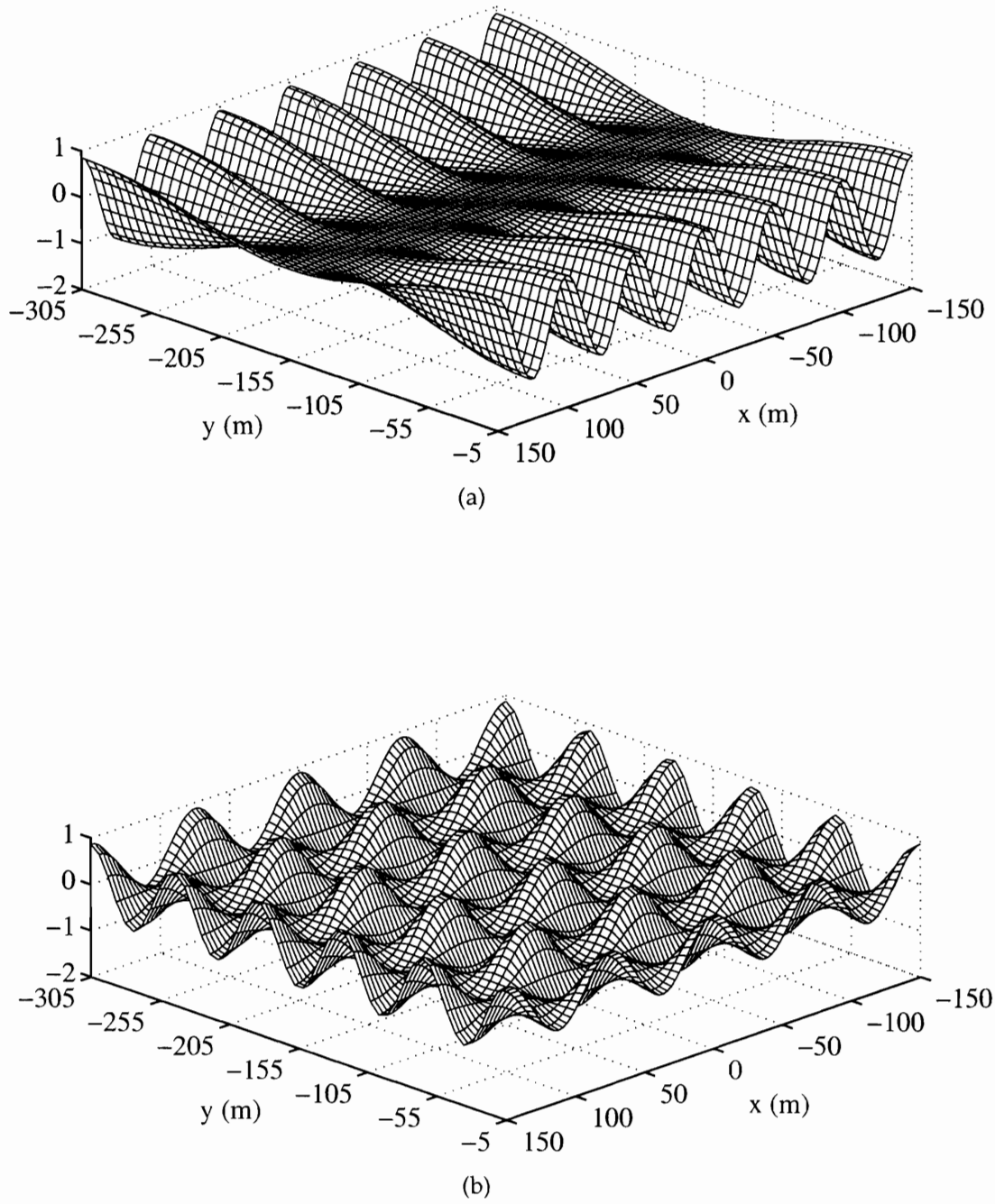

Figure 10-23: Setup/setdown $\eta_{20}/ka_{n,m}^2$ of standing wave in closed basin at mode (a) $(n, m) = (6, 1)$ and (b) $(n, m) = (4, 5)$

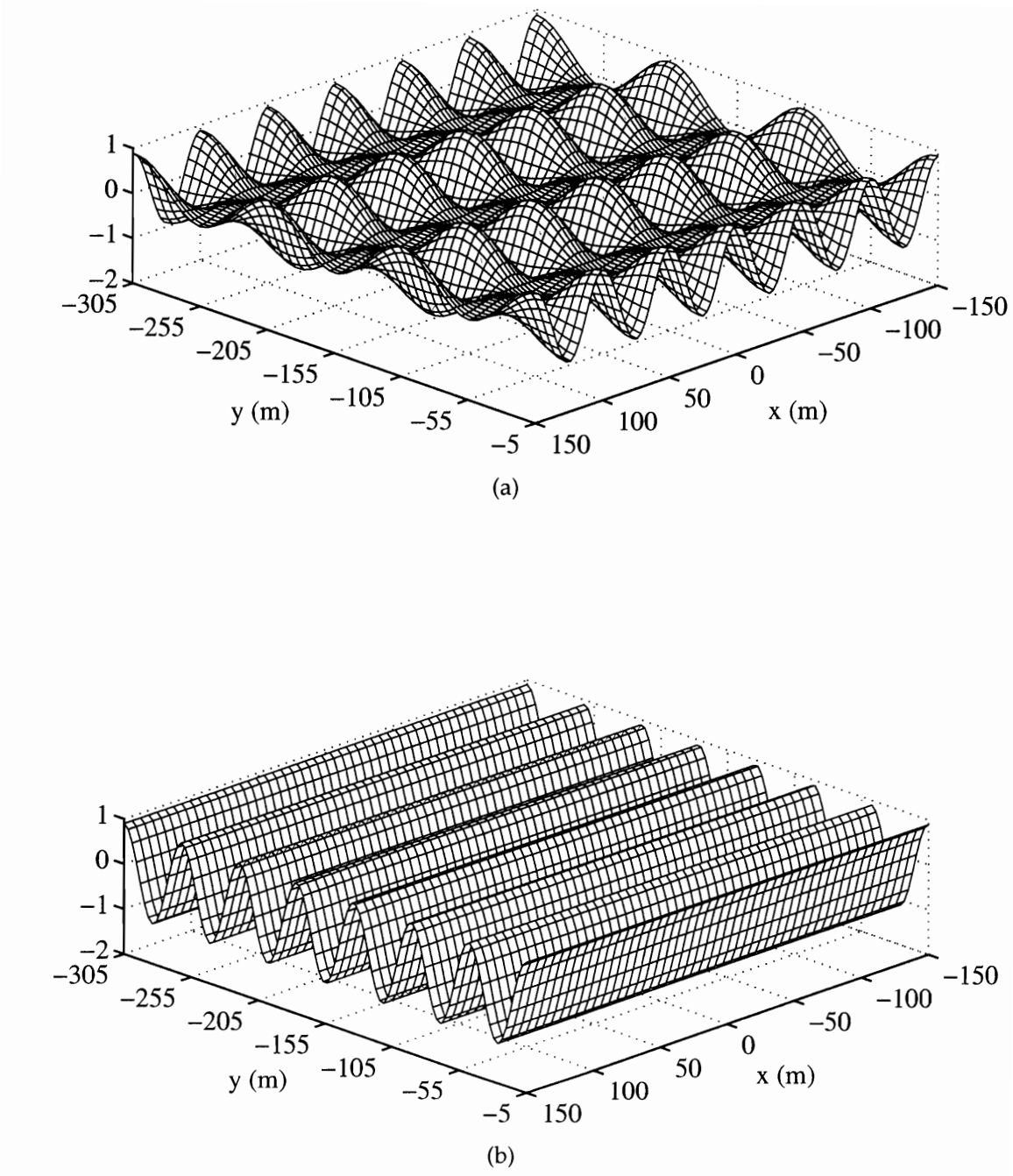

Figure 10-24: Setup/setdown $\eta_{20}/ka_{n,m}^2$ of standing wave in closed basin at mode (a) $(n, m) = (6, 3)$ and (b) $(n, m) = (0, 7)$

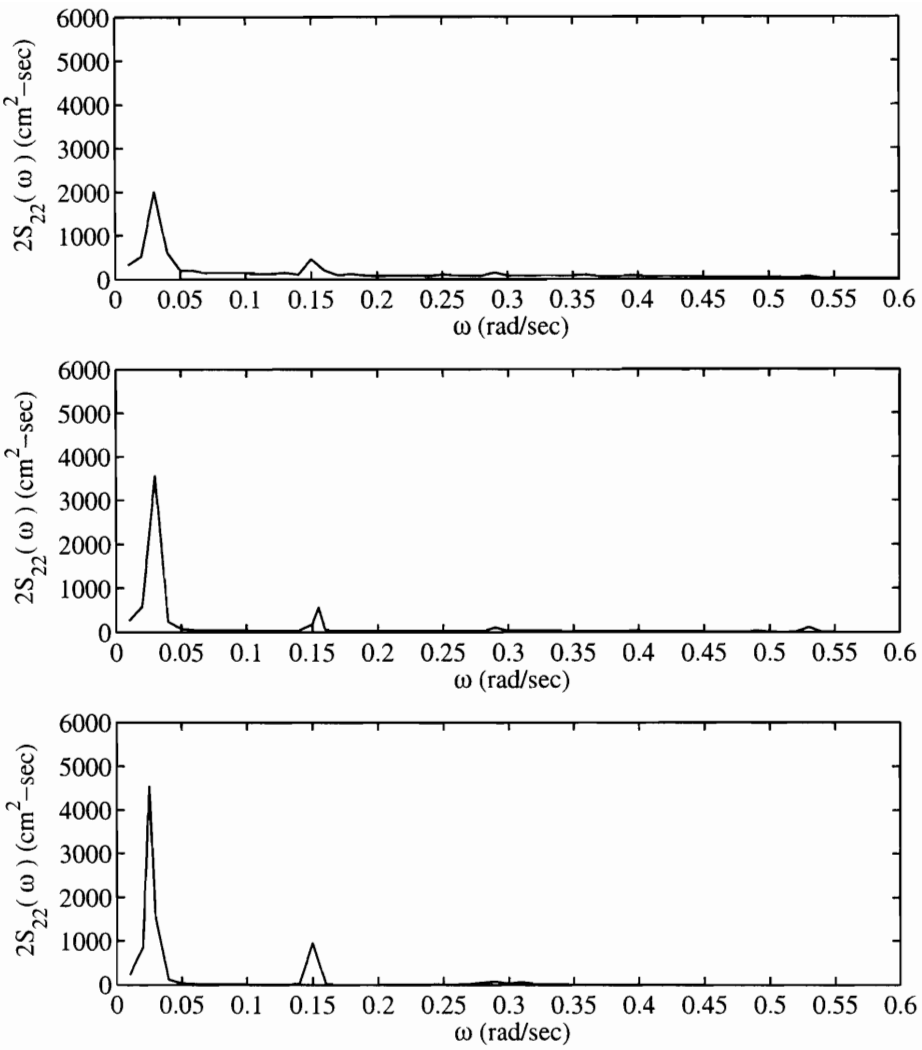

Figure 10-25: Spatial-averaged nonlinear correction $2\mathcal{S}_{22}(\omega)$. Top : opening 60 m, Middle: 30m. Bottom: 30 m with protection

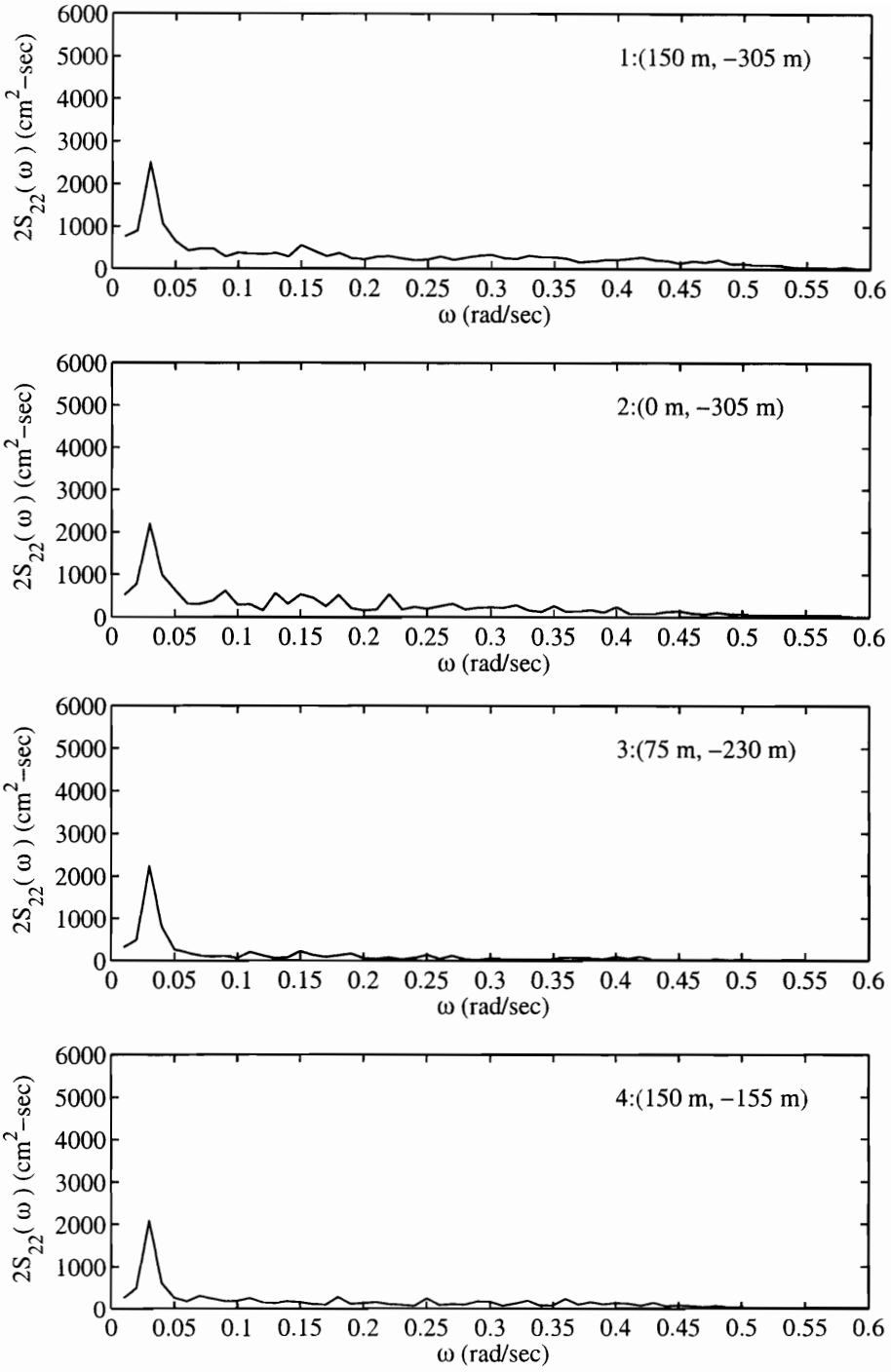

Figure 10-26: Nonlinear correction $2S_{22}(\omega)$ at St. 1-4 for 60 m opening (Case 1).

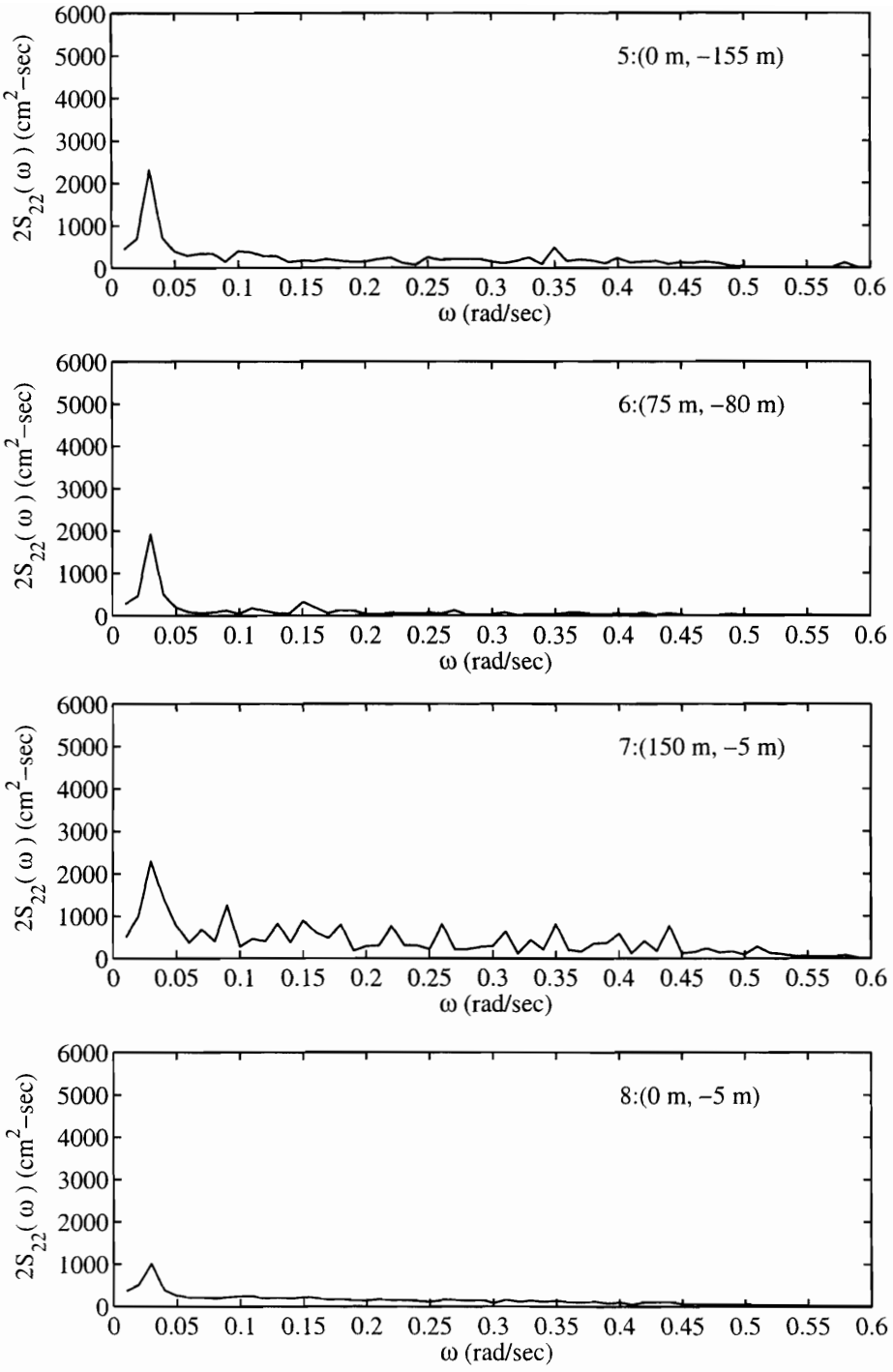

Figure 10-27: Nonlinear correction $2S_{22}(\omega)$ at St. 5-8 for 60 m opening (Case 1).

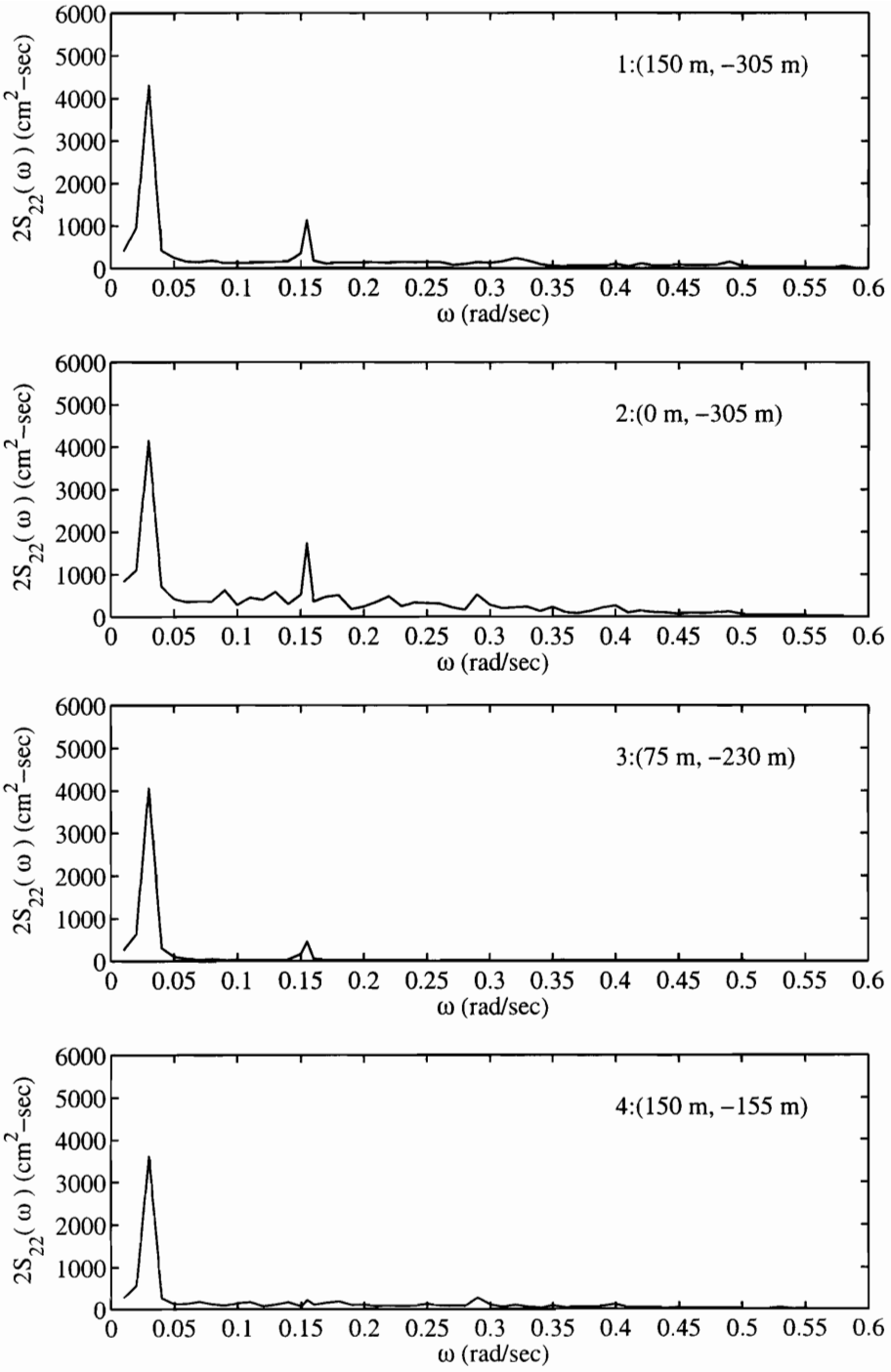

Figure 10-28: Nonlinear correction $2\mathcal{S}_{22}(\omega)$ at St. 1-4 for 30 m opening (Case 2).

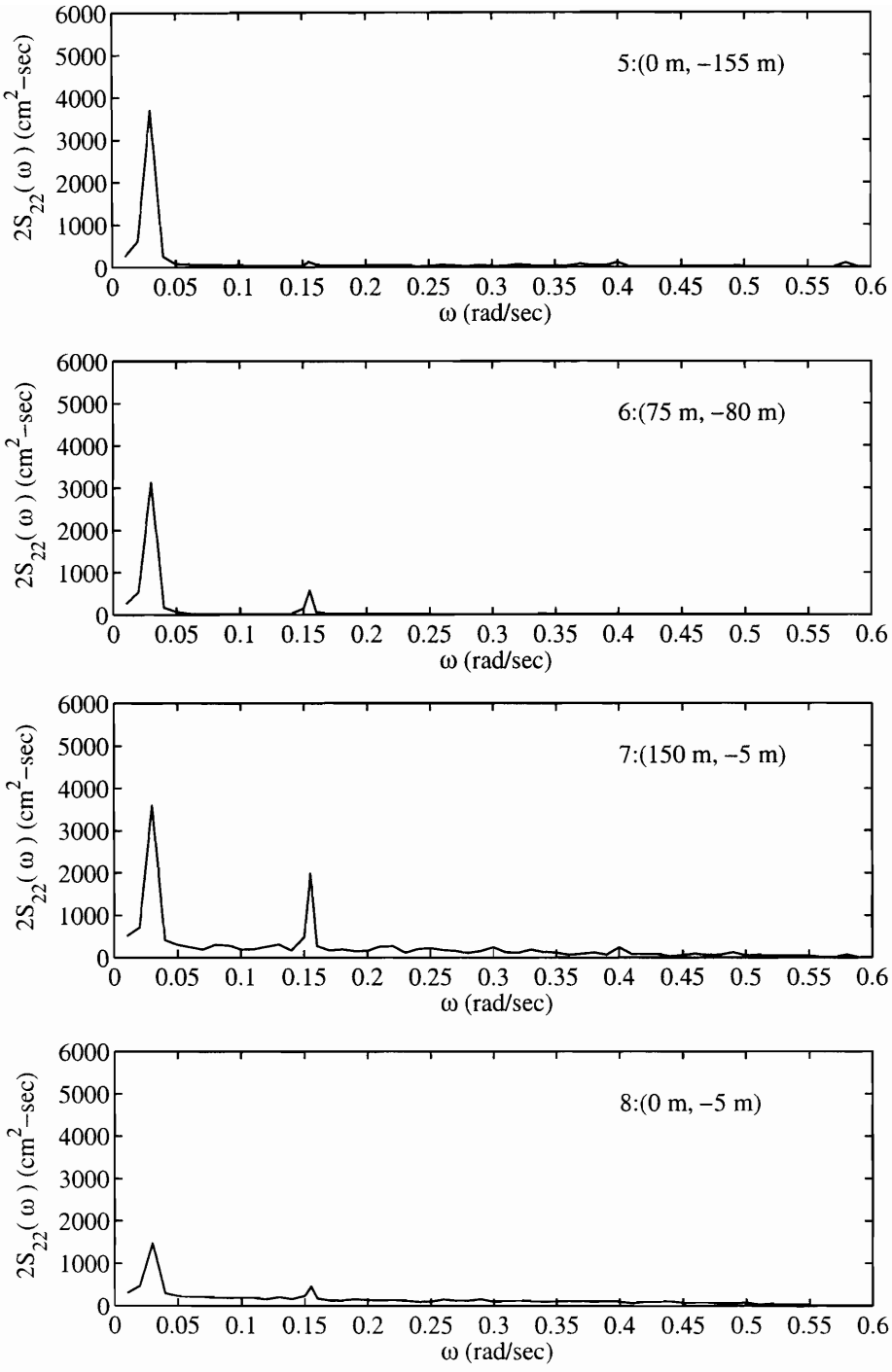

Figure 10-29: Nonlinear correction $2S_{22}(\omega)$ at St. 5-8 for 30 m opening (Case 2).

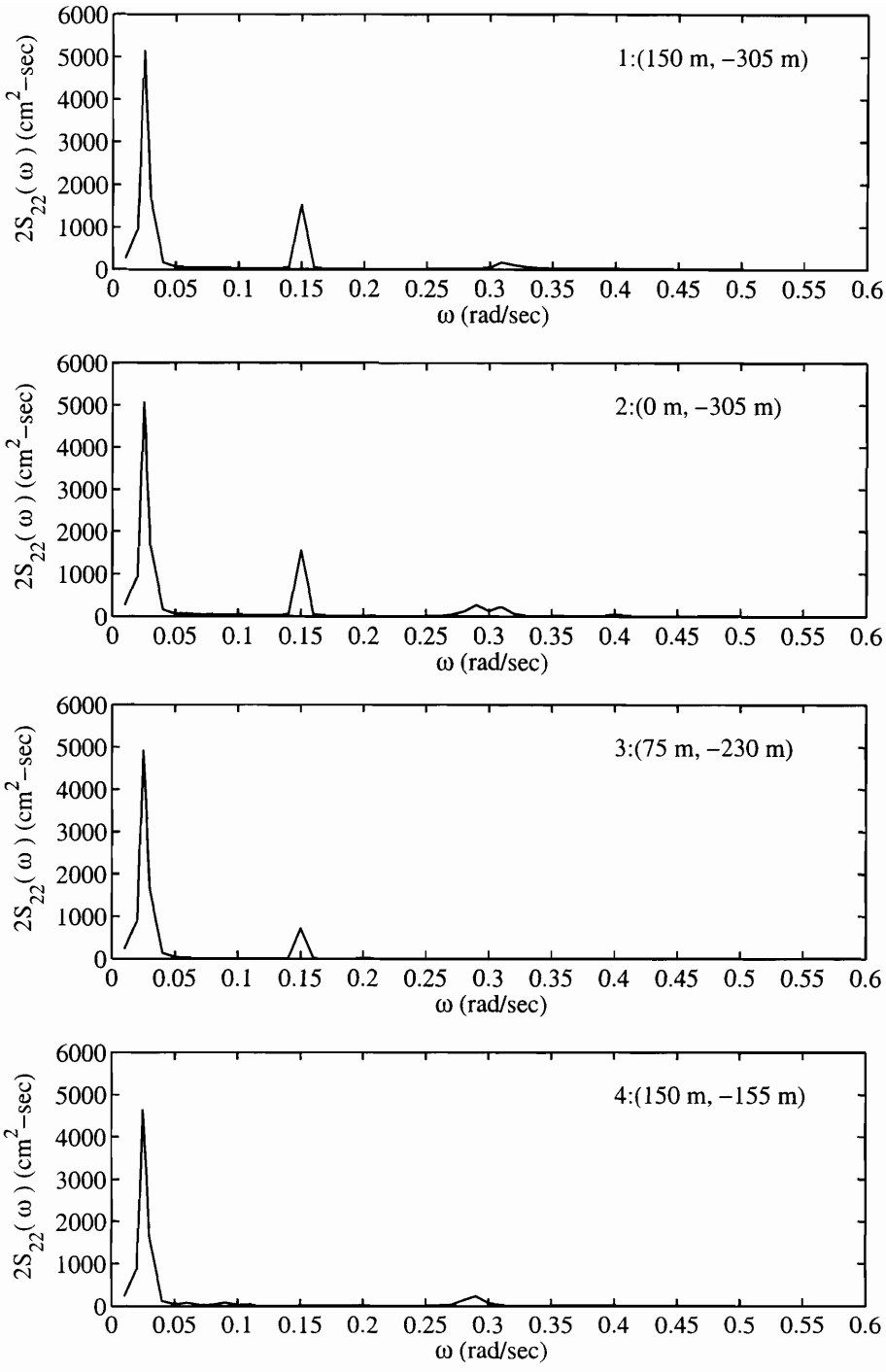

Figure 10-30: Nonlinear correction $2\mathcal{S}_{22}(\omega)$ at St. 1-4 for 30 m opening with breakwater (Case 3).

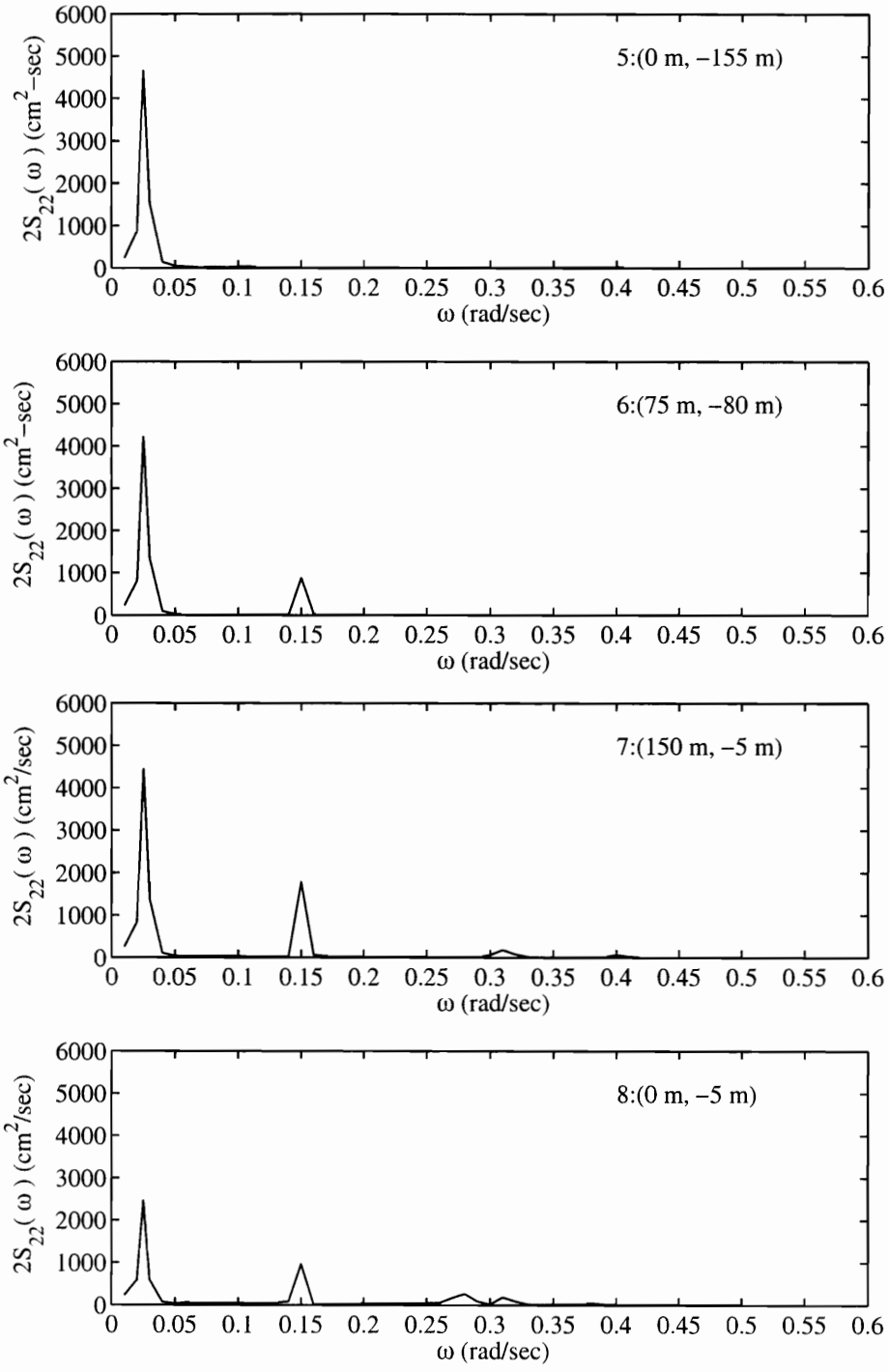

Figure 10-31: Nonlinear correction $2\mathcal{S}_{22}(\omega)$ at St. 5-8 for $30\ m$ opening with breakwater (Case 3).

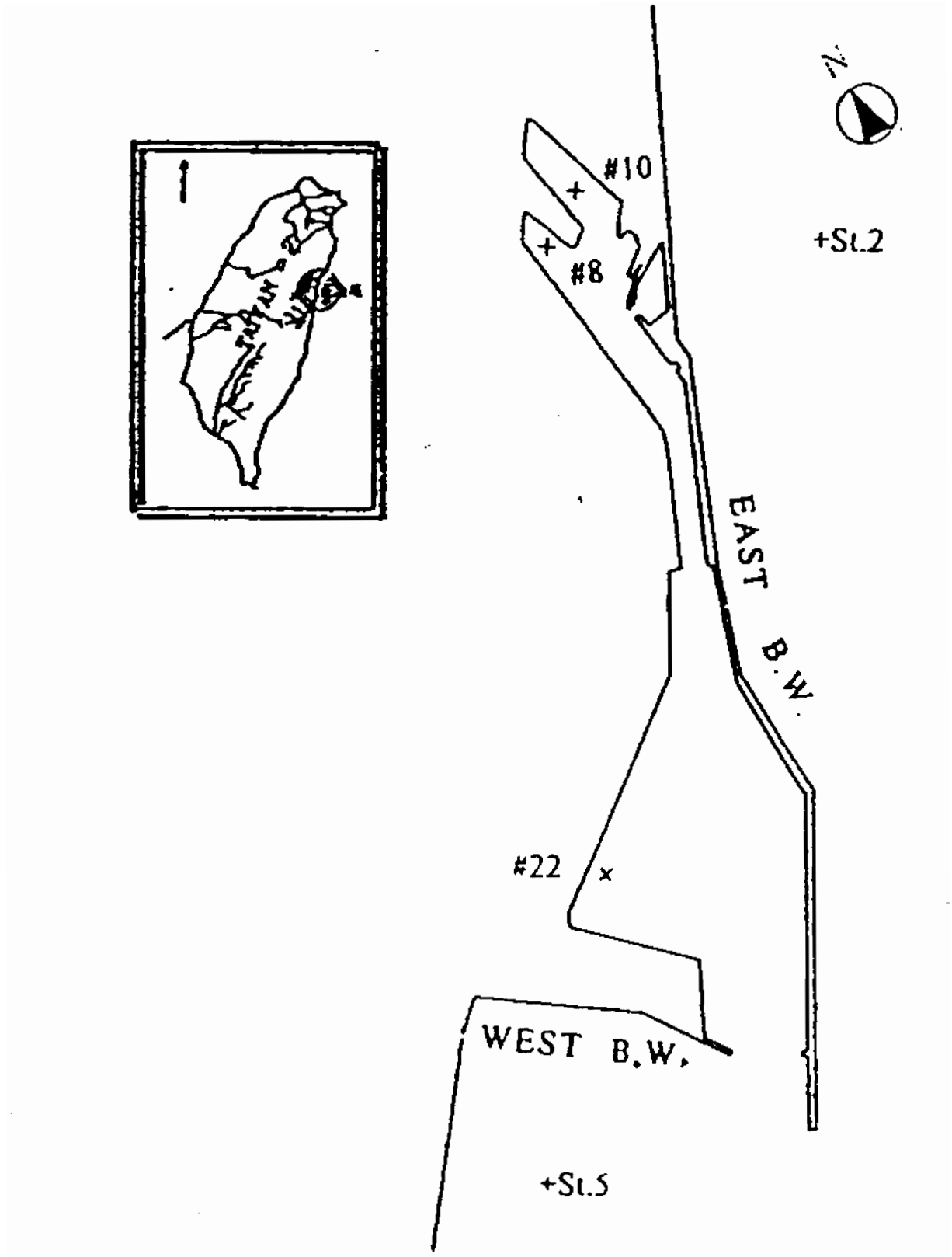

Figure 10-32: Layout of Hualien Harbor

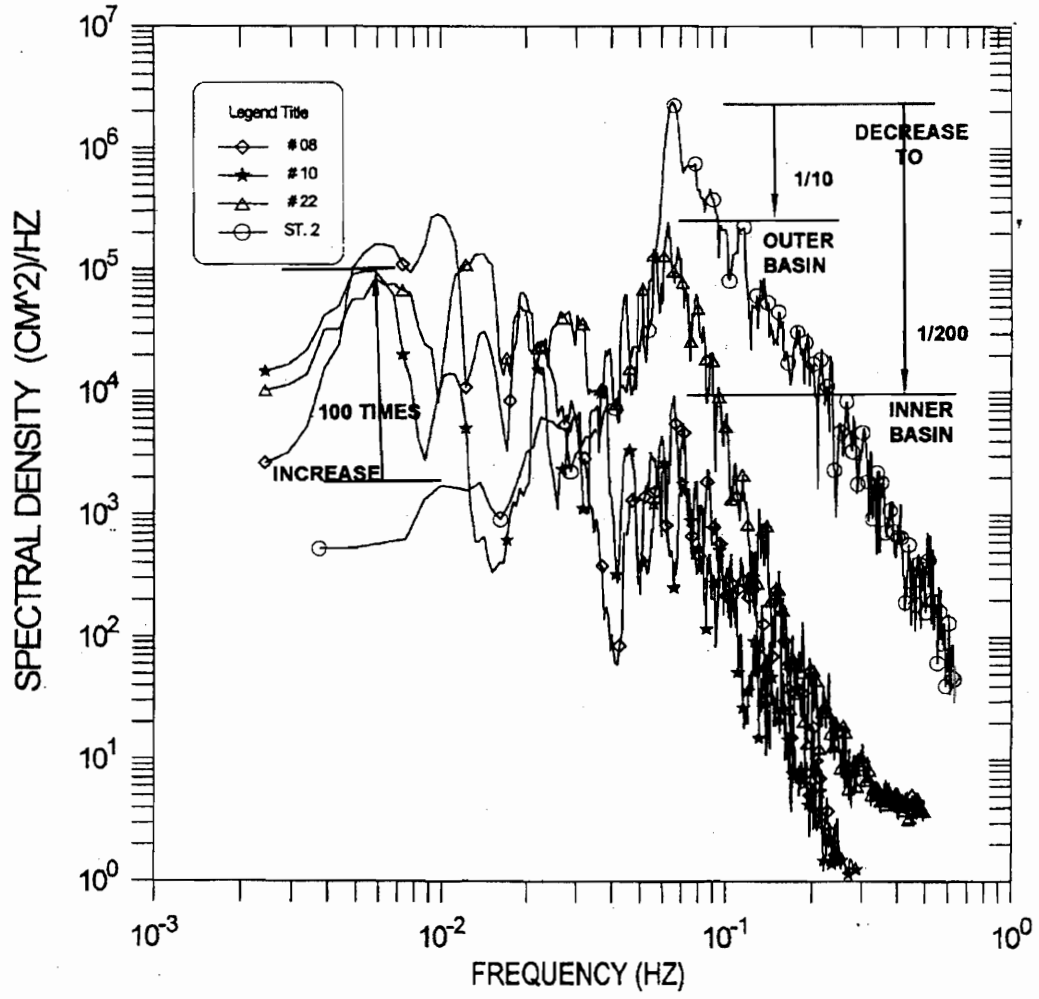

Figure 10-33: Spectrum during Typhoon Tim of Hualien Harbor

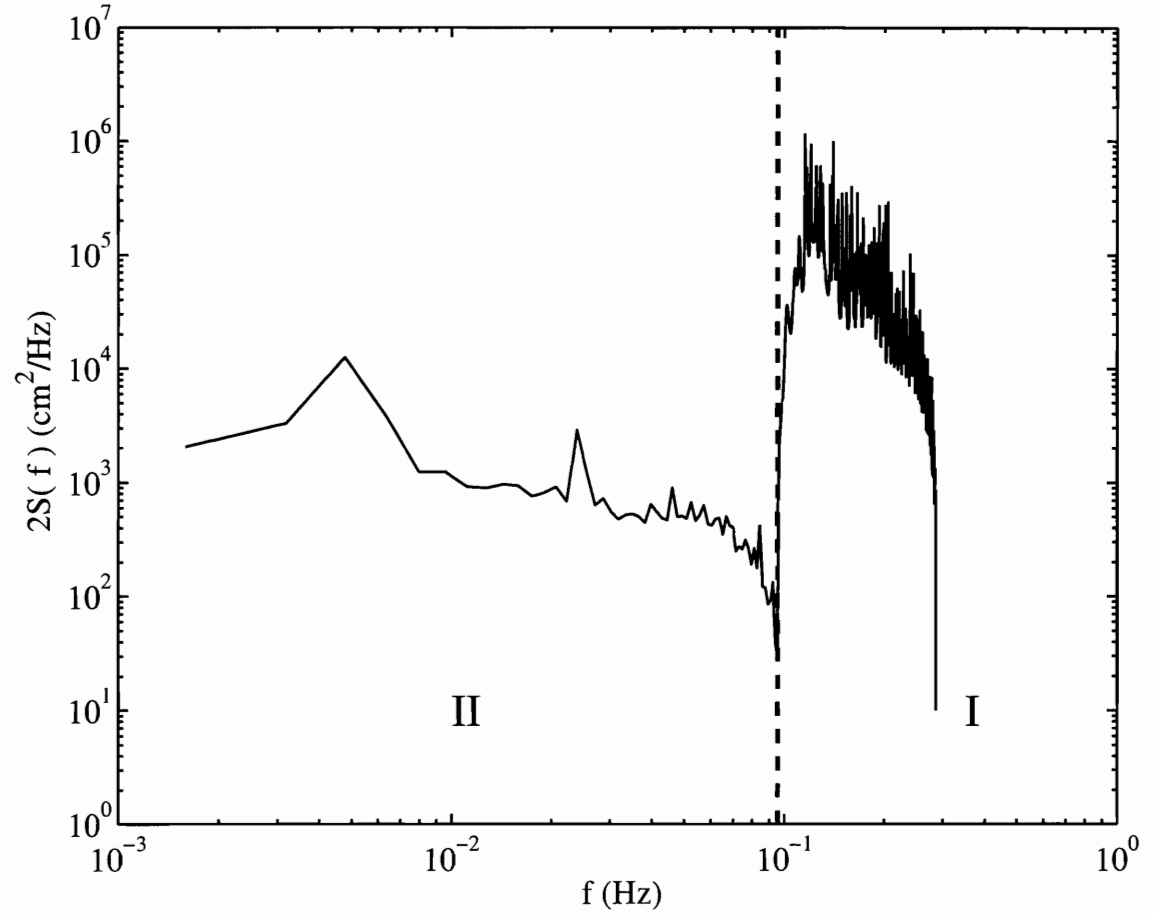

Figure 10-34: Spatial-averaged spectrum $2\mathcal{S}(f)$ for 60 m opening (Case 1). Region I: $2\mathcal{S}_2(f)$. Region II: $2\mathcal{S}_{22}(f)$.

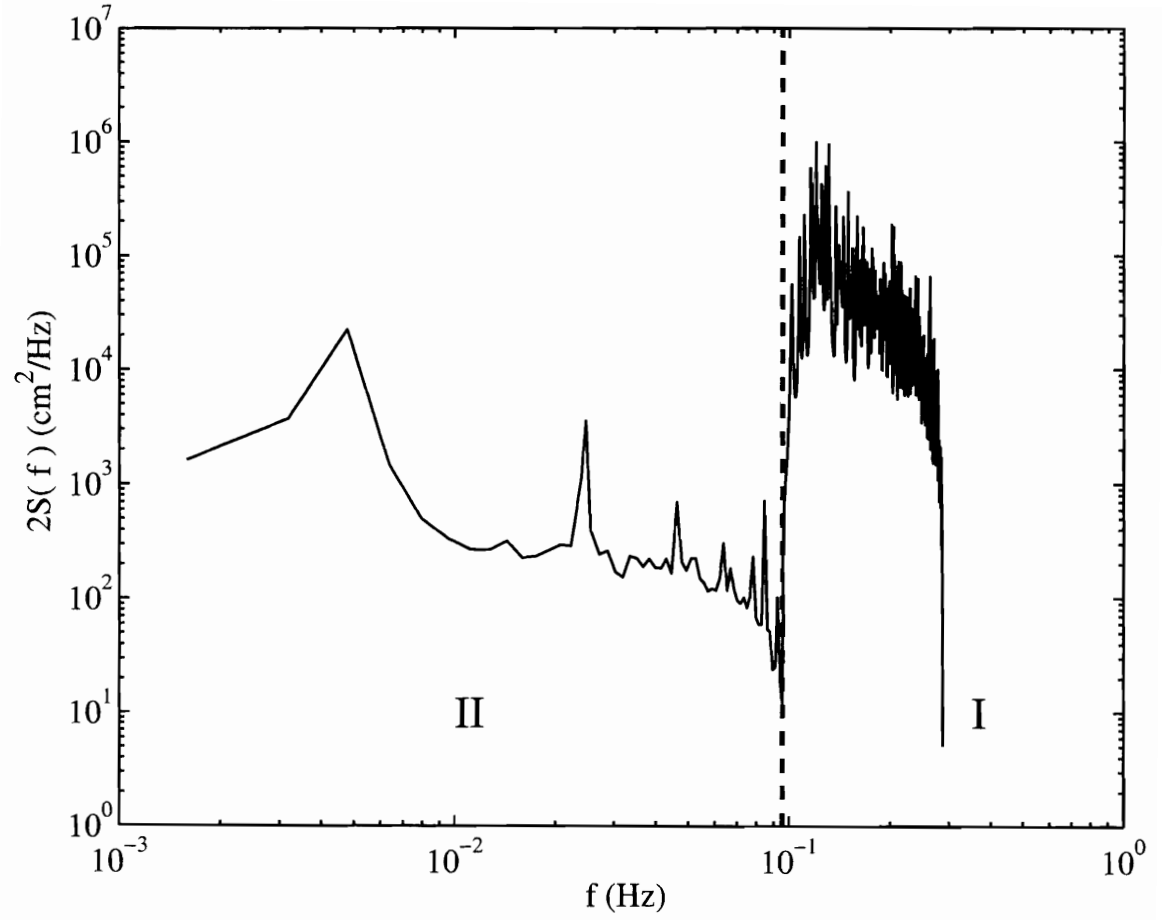

Figure 10-35: Spatial-averaged spectrum $2\mathcal{S}(f)$ for 30 m opening (Case 2). Region I: $2\mathcal{S}_2(f)$. Region II: $2\mathcal{S}_{22}(f)$.

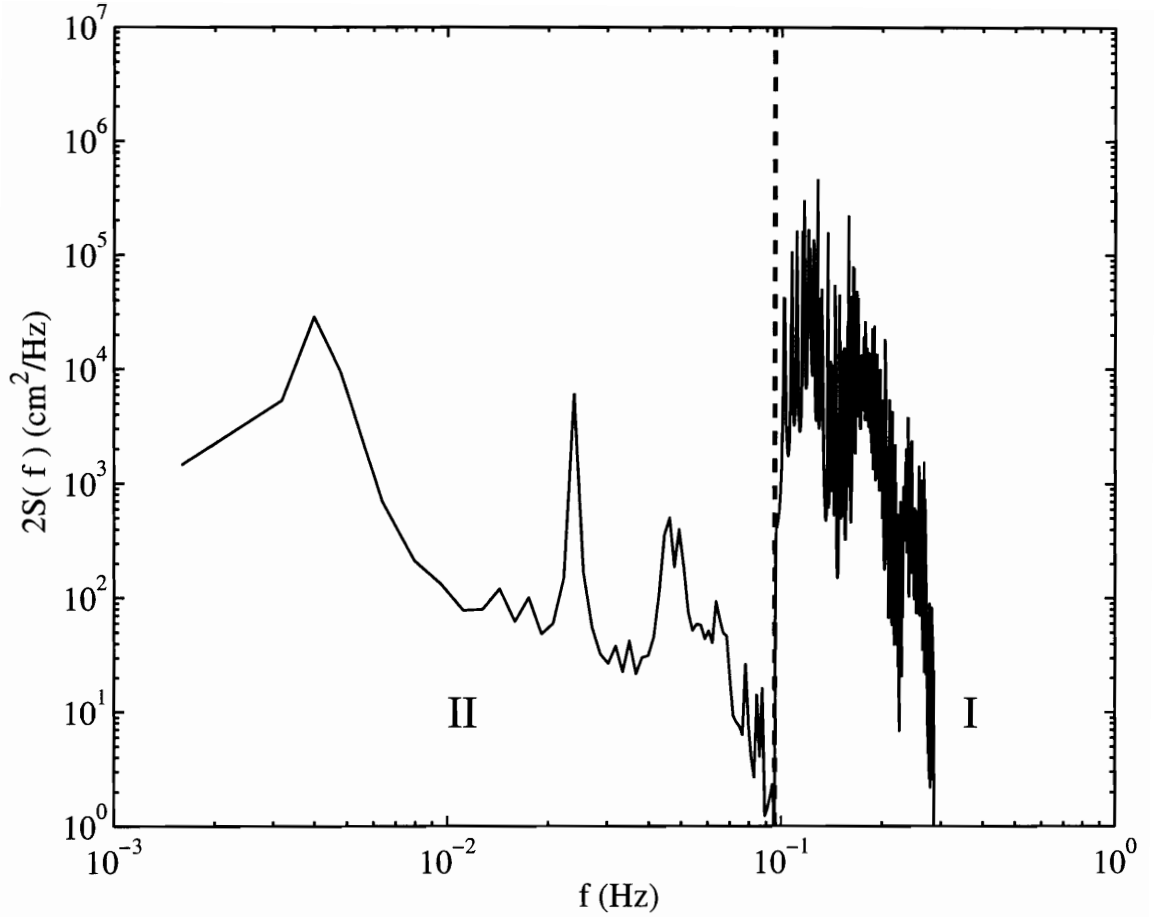

Figure 10-36: Spatial-averaged spectrum $2\mathcal{S}(f)$ for 30 m opening with breakwater (Case 3). Region I: $2\mathcal{S}_2(f)$. Region II: $2\mathcal{S}_{22}(f)$.

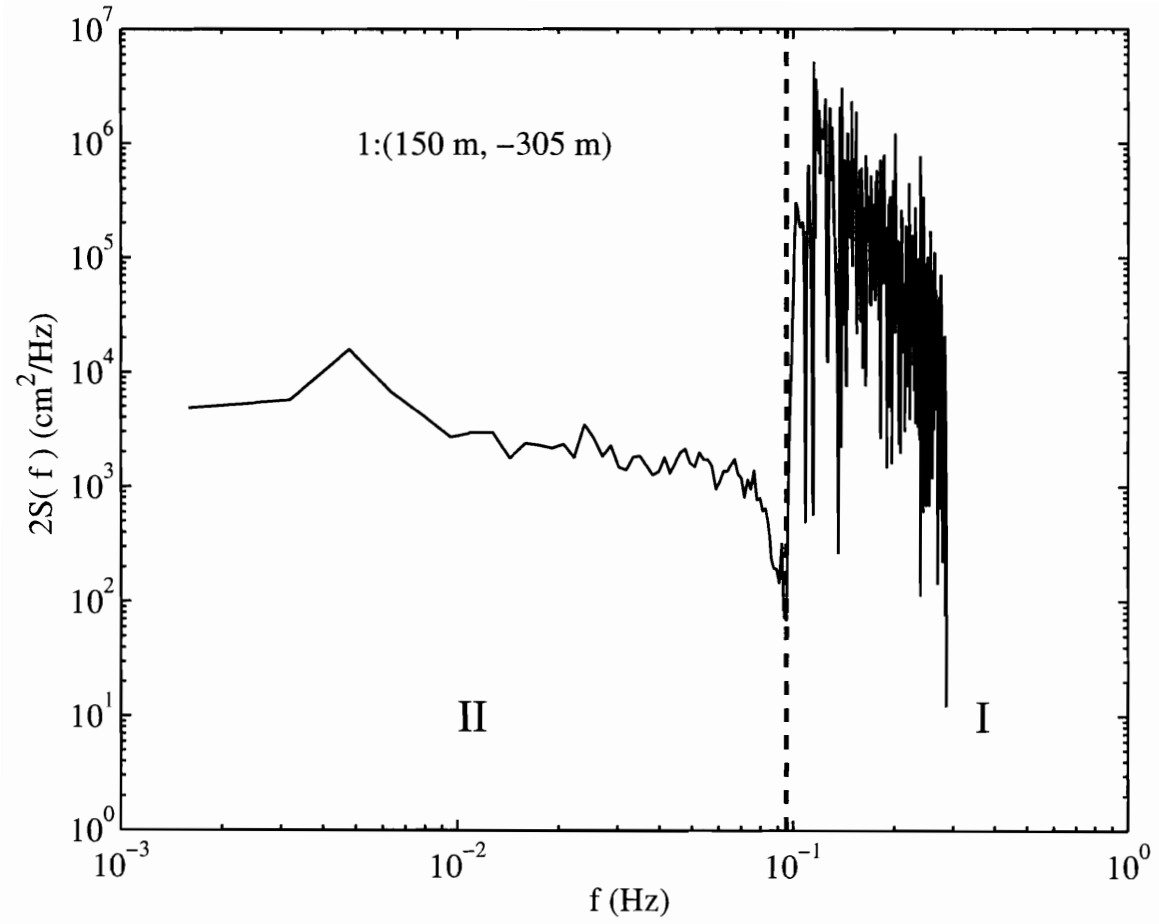

Figure 10-37: $2\mathcal{S}(f)$ at St. 1 for 60 m opening (Case 1). Region I: $2\mathcal{S}_2(f)$. Region II: $2\mathcal{S}_{22}(f)$.

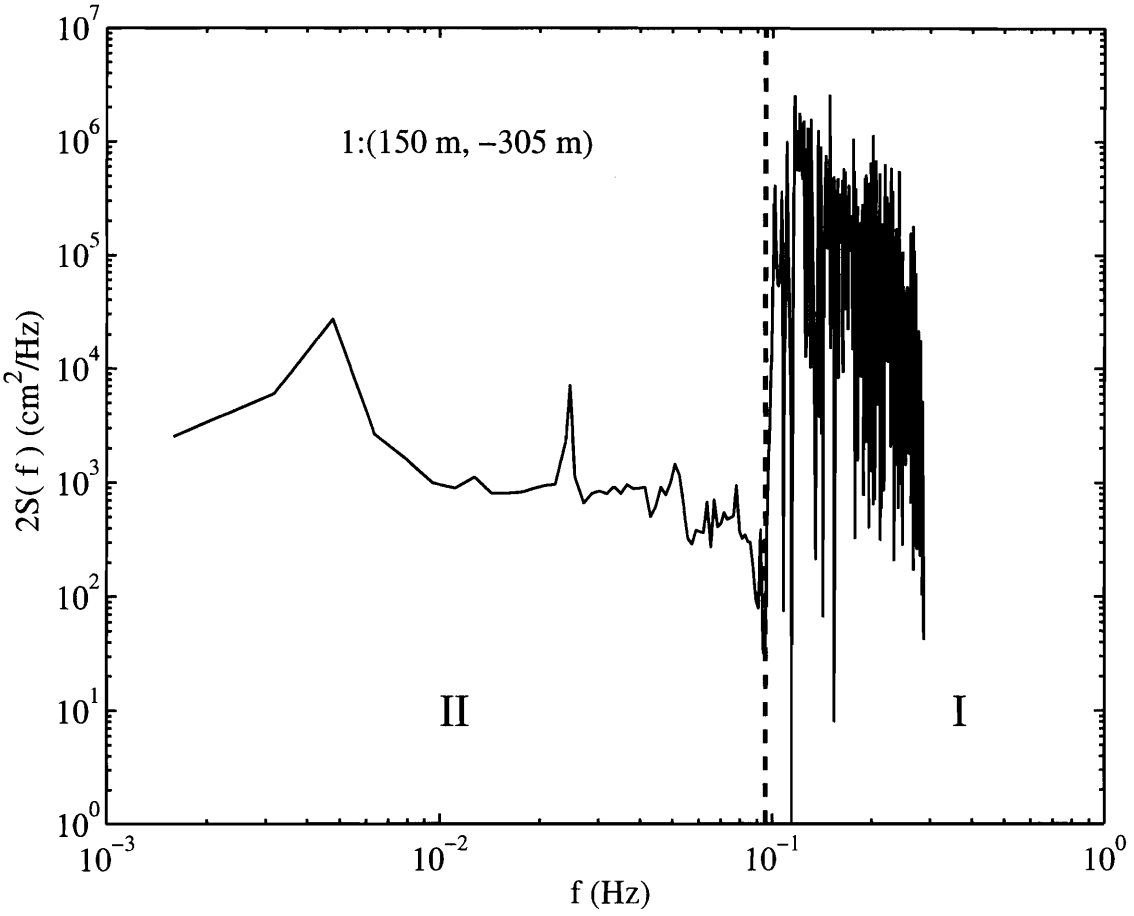

Figure 10-38: $2\mathcal{S}(f)$ at St. 1 for 30 m opening (Case 2). Region I: $\mathcal{S}_2(f)$. Region II: $2\mathcal{S}_{22}(f)$.

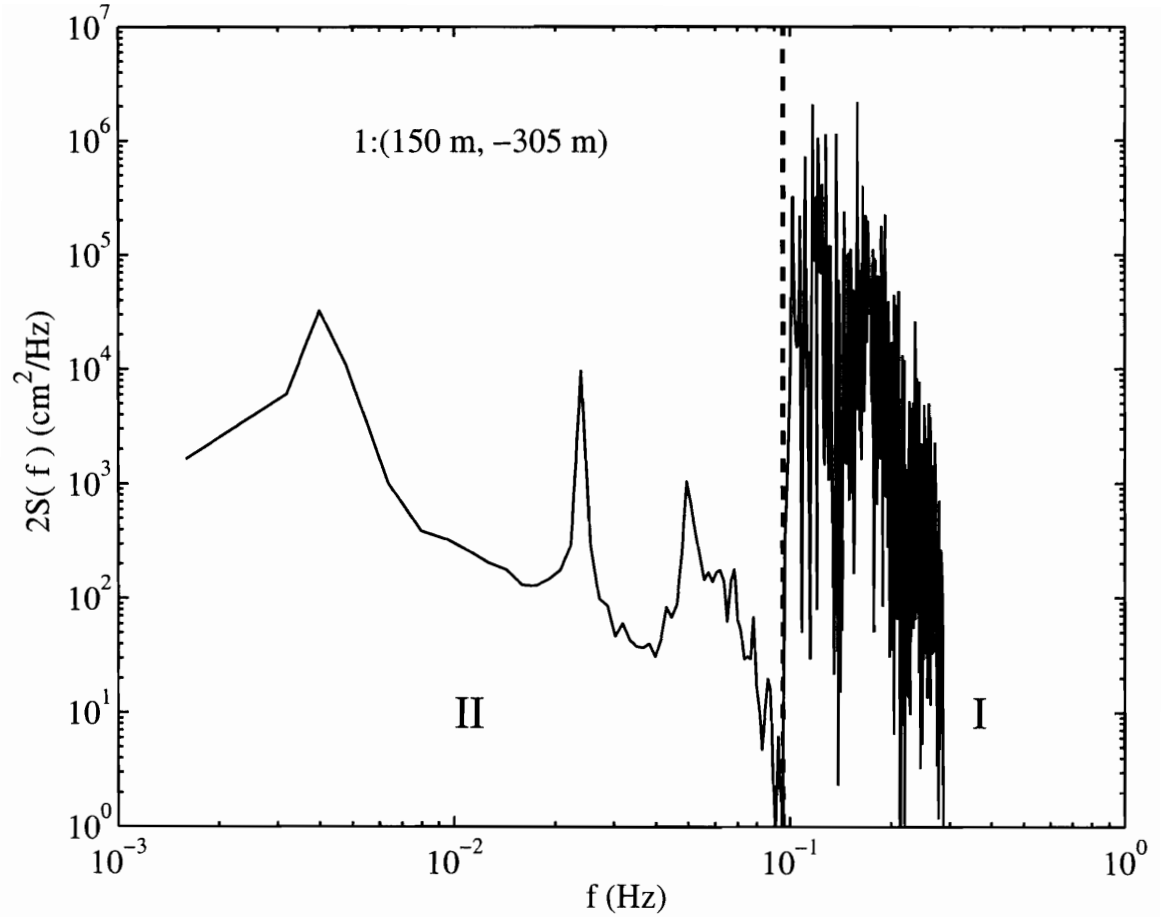

Figure 10-39: $2\mathcal{S}(f)$ at St.1 for 30 m opening with breakwater (Case 3). Region I: $\mathcal{S}_2(f)$. Region II: $2\mathcal{S}_{22}(f)$.

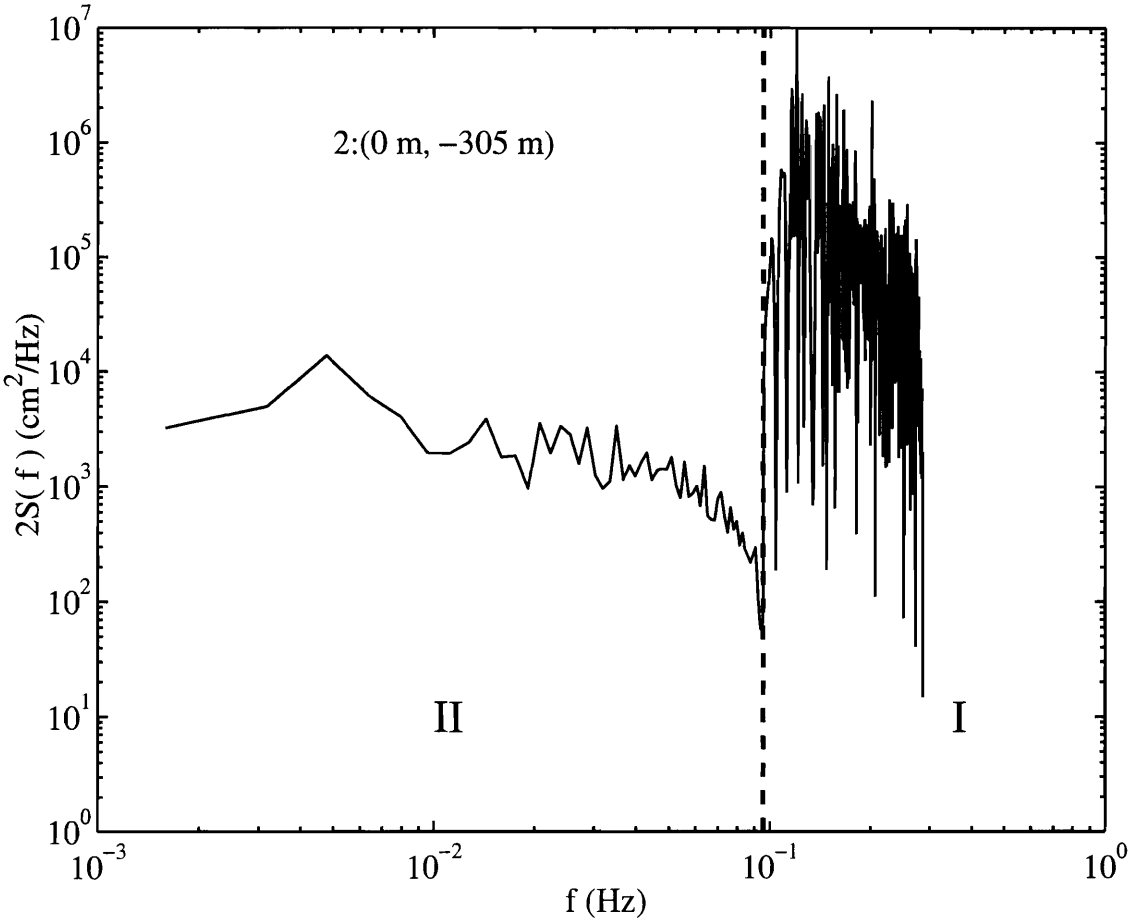

Figure 10-40: $2\mathcal{S}(f)$ at St.2 for 60 m opening (Case 1). Region I: $2\mathcal{S}_2(f)$. Region II: $2\mathcal{S}_{22}(f)$.

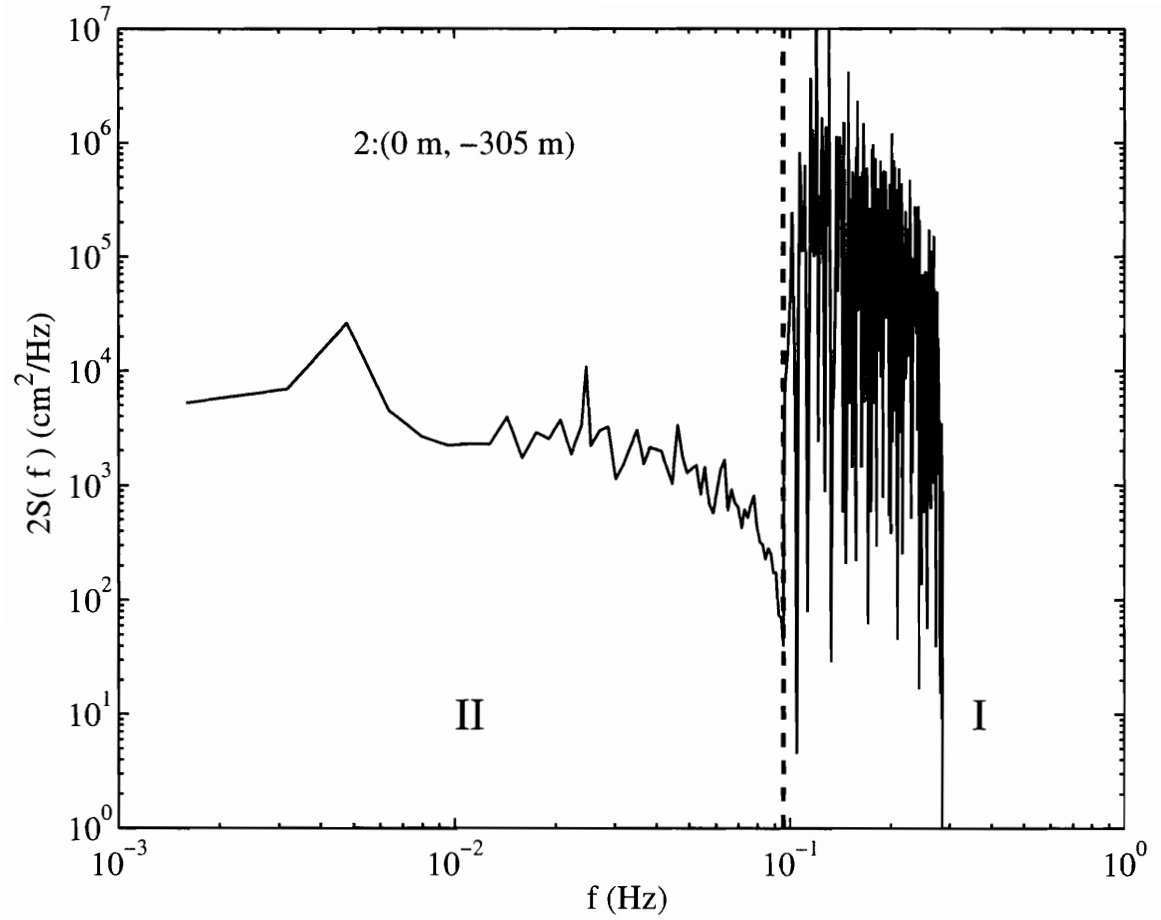

Figure 10-41: $2\mathcal{S}(f)$ at St. 2 for $30\ m$ opening (Case 2). Region I: $2\mathcal{S}_2(f)$. Region II: $2\mathcal{S}_{22}(f)$.

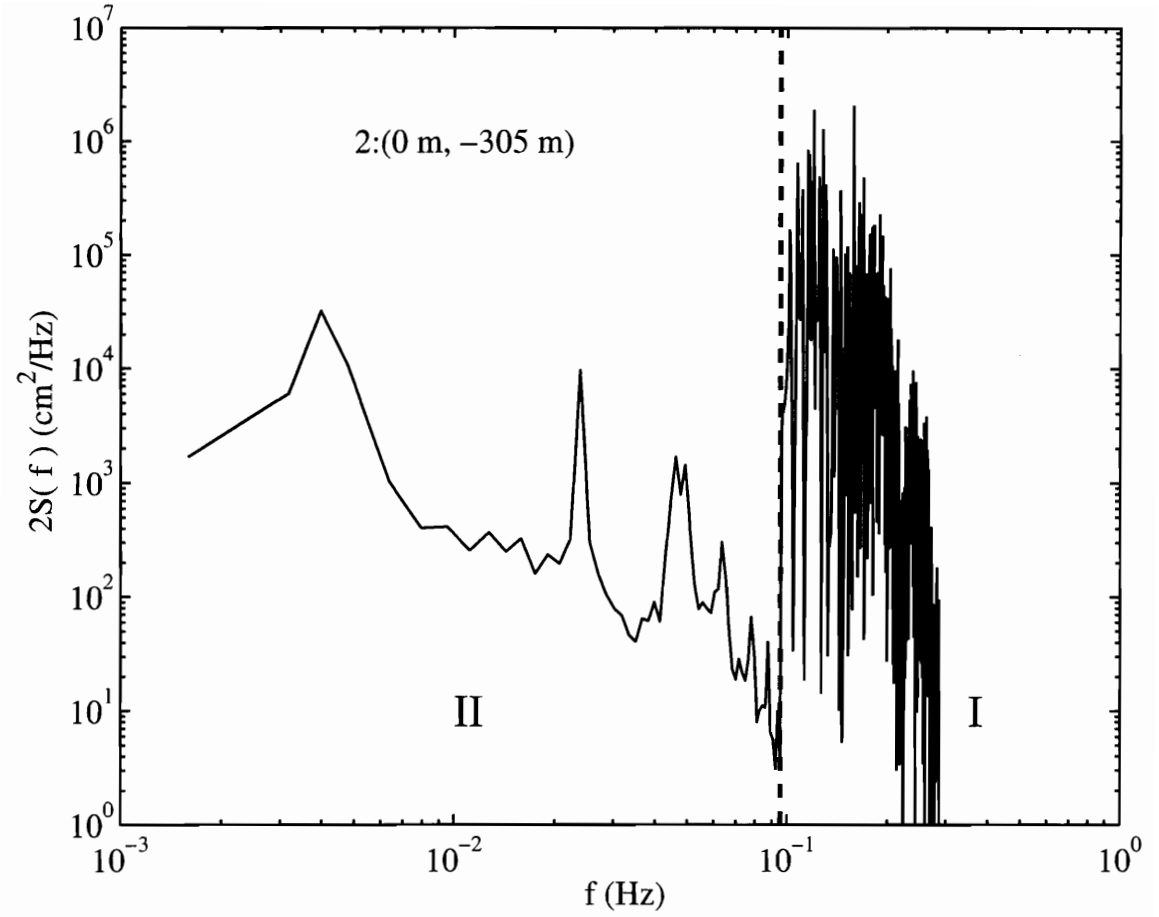

Figure 10-42: $2\mathcal{S}(f)$ at St. 2 for 30 m opening with breakwater (Case 3). Region I: $2\mathcal{S}_2(f)$. Region II: $2\mathcal{S}_{22}(f)$.

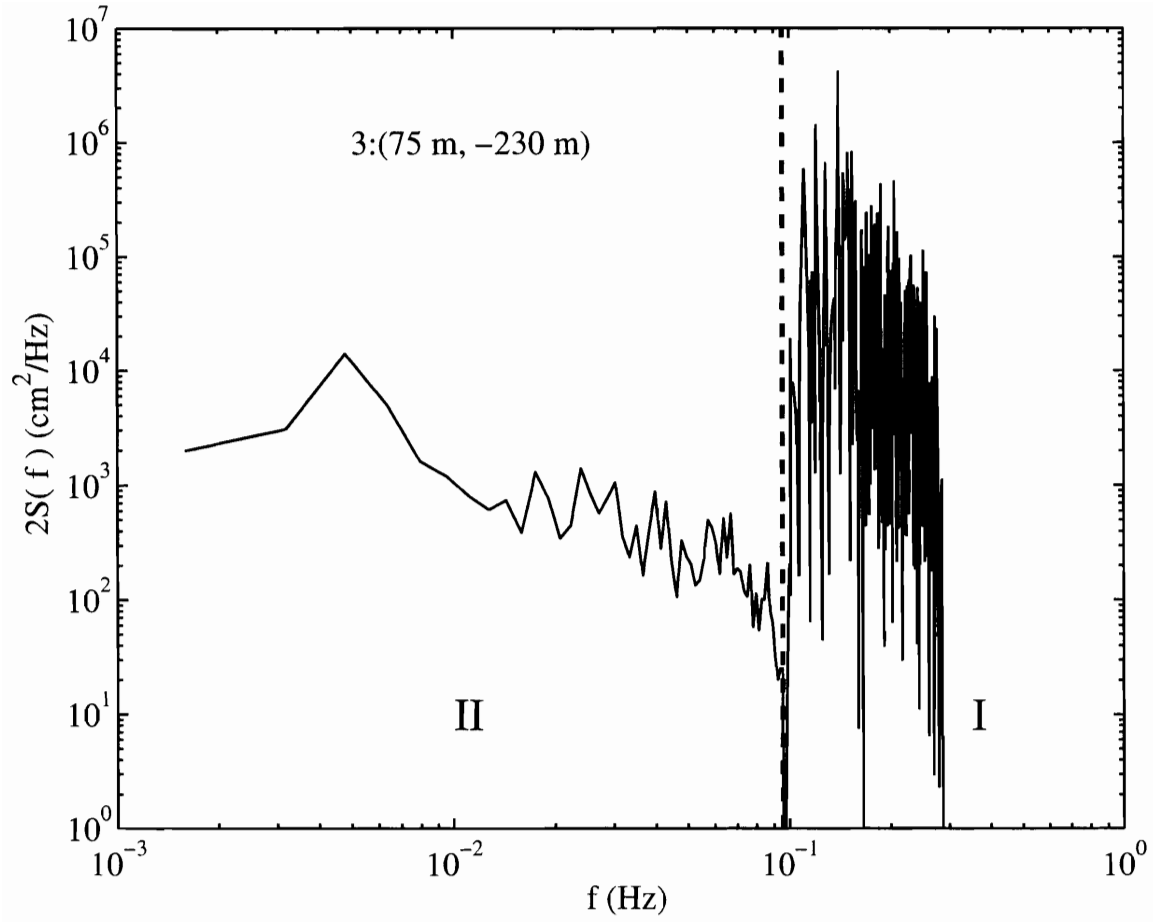

Figure 10-43: $2\mathcal{S}(f)$ at St. 3 for 60 m opening (Case 1). Region I: $2\mathcal{S}_2(f)$. Region II: $2\mathcal{S}_{22}(f)$.

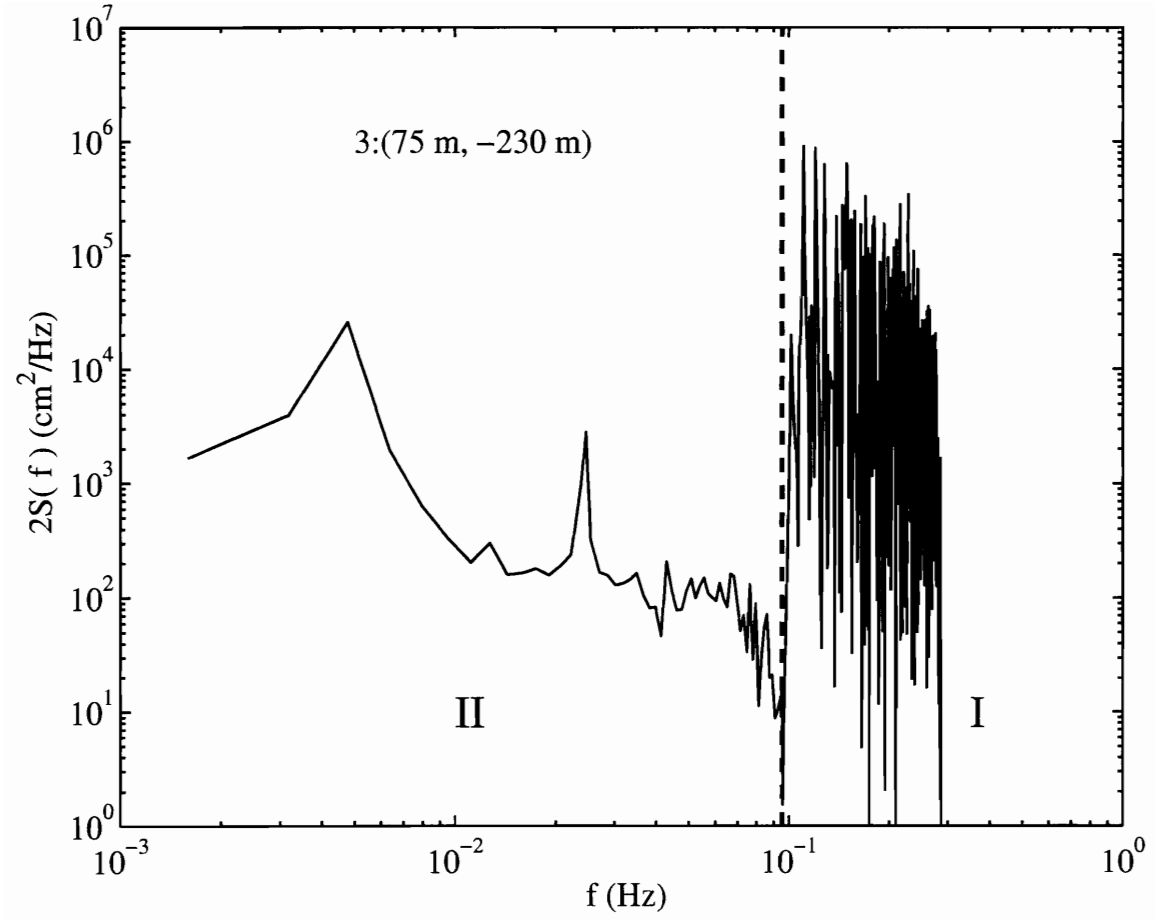

Figure 10-44: $2\mathcal{S}(f)$ at St. 3 for 30 m opening (Case 2). Region I: $2\mathcal{S}_2(f)$. Region II: $2\mathcal{S}_{22}(f)$.

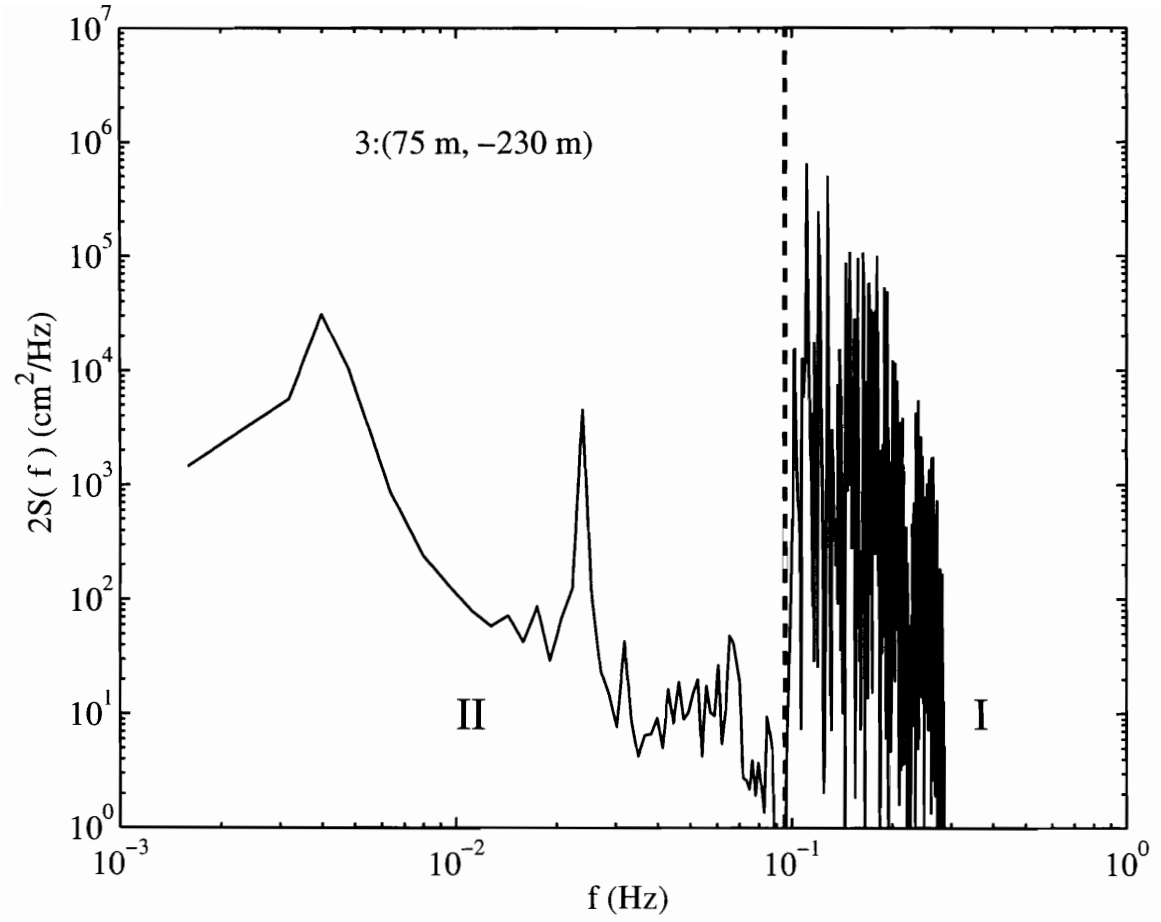

Figure 10-45: $2\mathcal{S}(f)$ at St. 3 for 30 m opening with breakwater (Case 3). Region I: $2\mathcal{S}_2(f)$. Region II: $2\mathcal{S}_{22}(f)$.

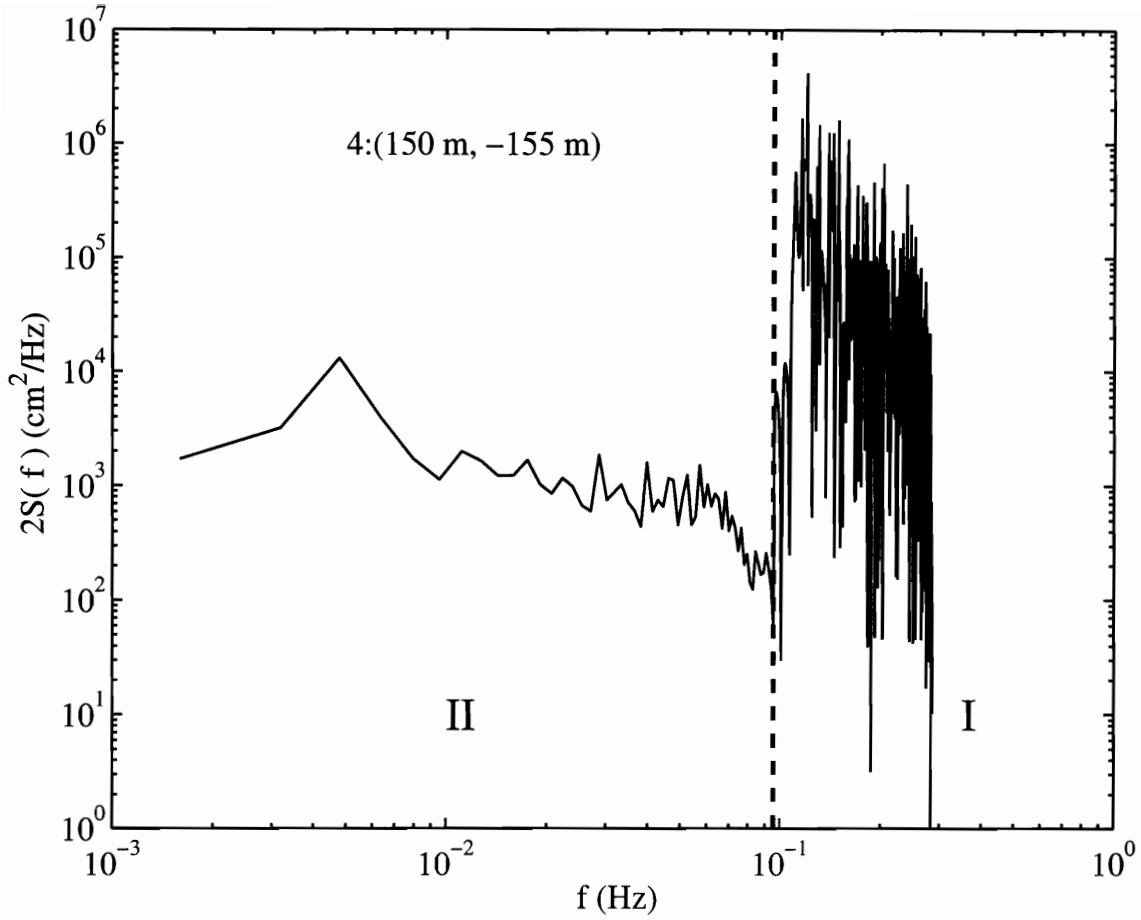

Figure 10-46: $2\mathcal{S}(f)$ at St. 4 for 60 m opening (Case 1). Region I: $2\mathcal{S}_2(f)$. Region II: $2\mathcal{S}_{22}(f)$.

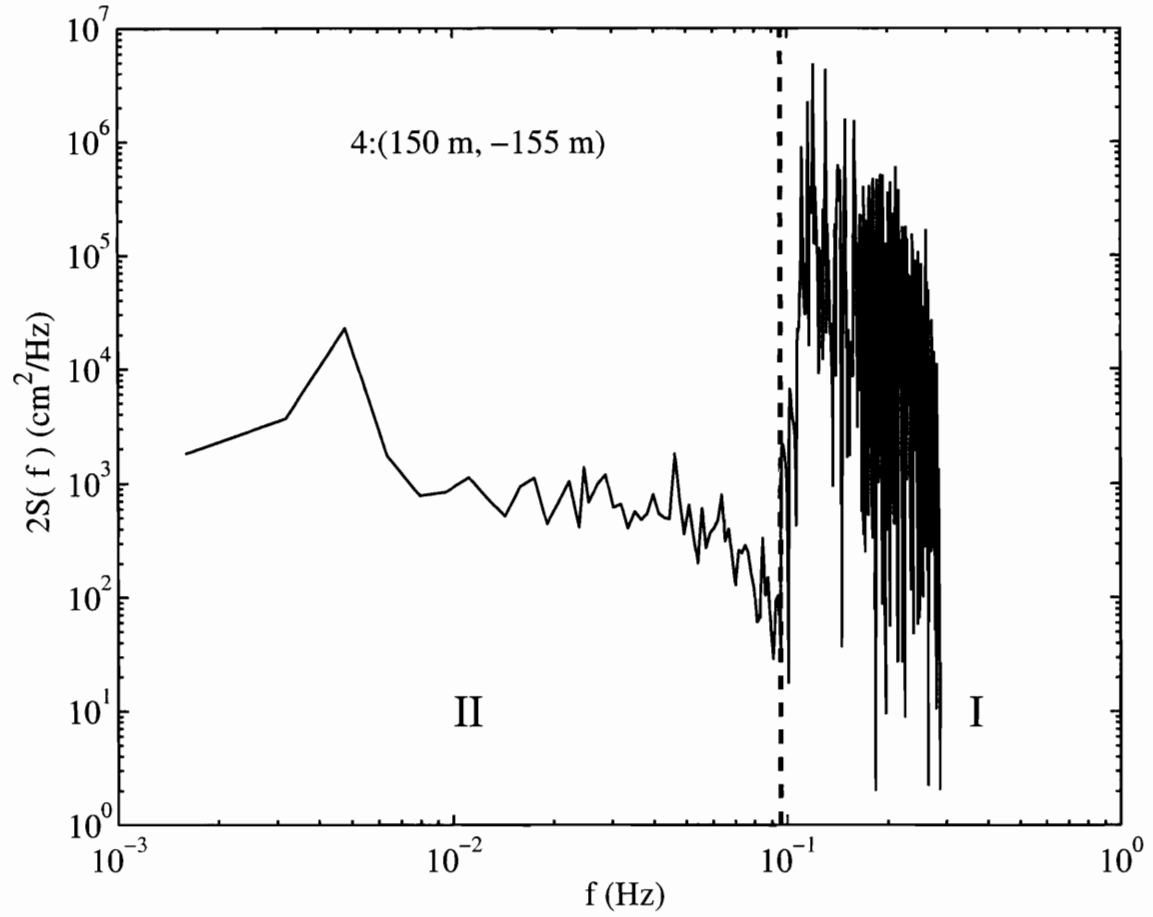

Figure 10-47: $2\mathcal{S}(f)$ at St. 4 for $30\ m$ opening (Case 2). Region I: $2\mathcal{S}_2(f)$. Region II: $2\mathcal{S}_{22}(f)$.

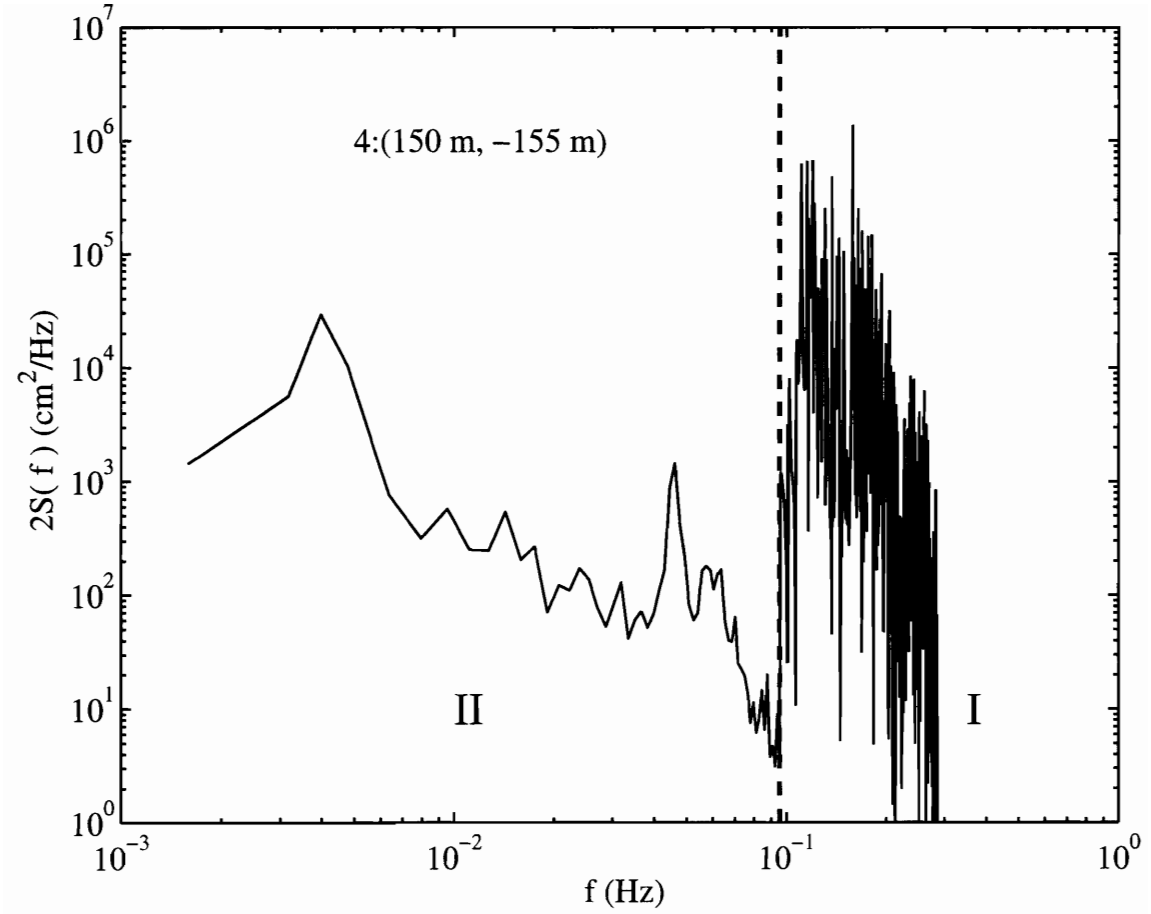

Figure 10-48: $2\mathcal{S}(f)$ at St.4 for 30 m opening with breakwater (Case 3). Region I: $2\mathcal{S}_2(f)$. Region II: $2\mathcal{S}_{22}(f)$.

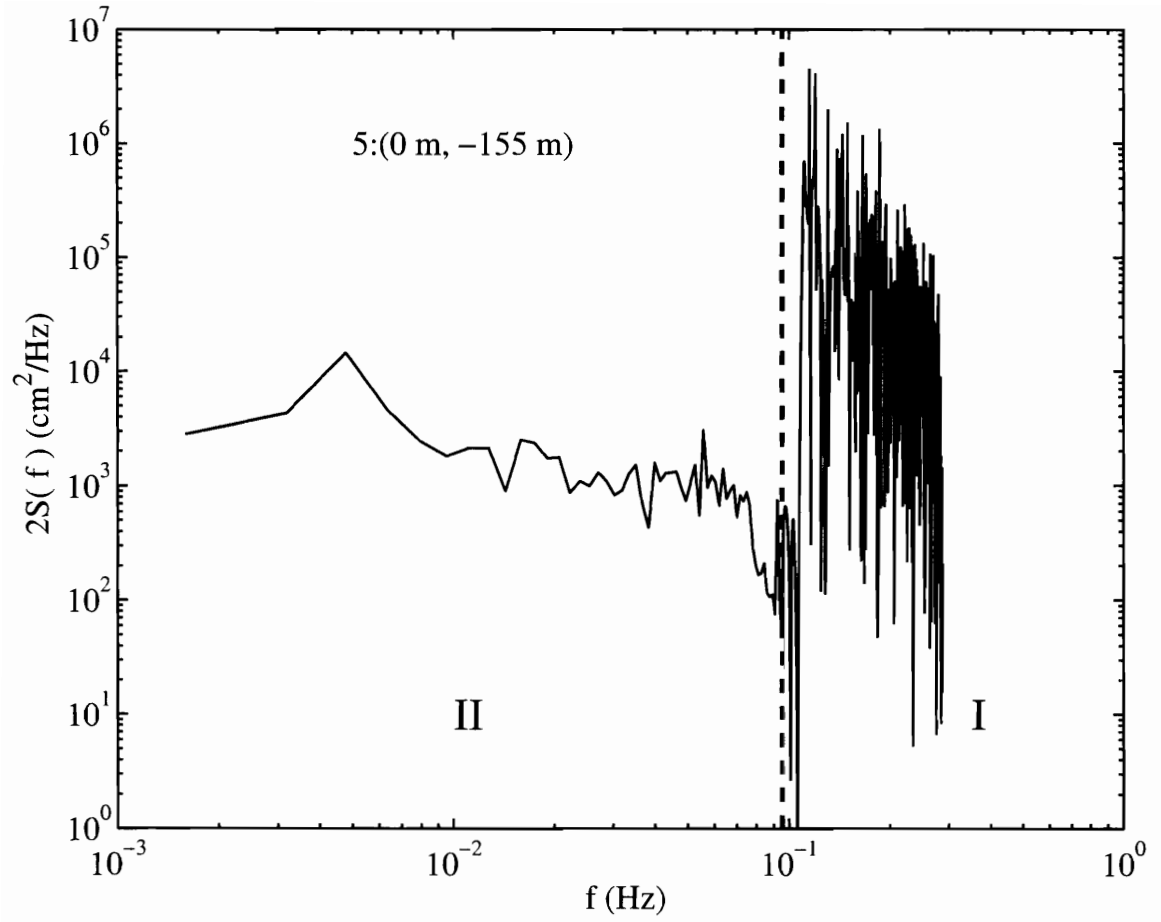

Figure 10-49: $2\mathcal{S}(f)$ at St.5 for $60\ m$ opening (Case 1). Region I: $2\mathcal{S}_2(f)$. Region II: $2\mathcal{S}_{22}(f)$.

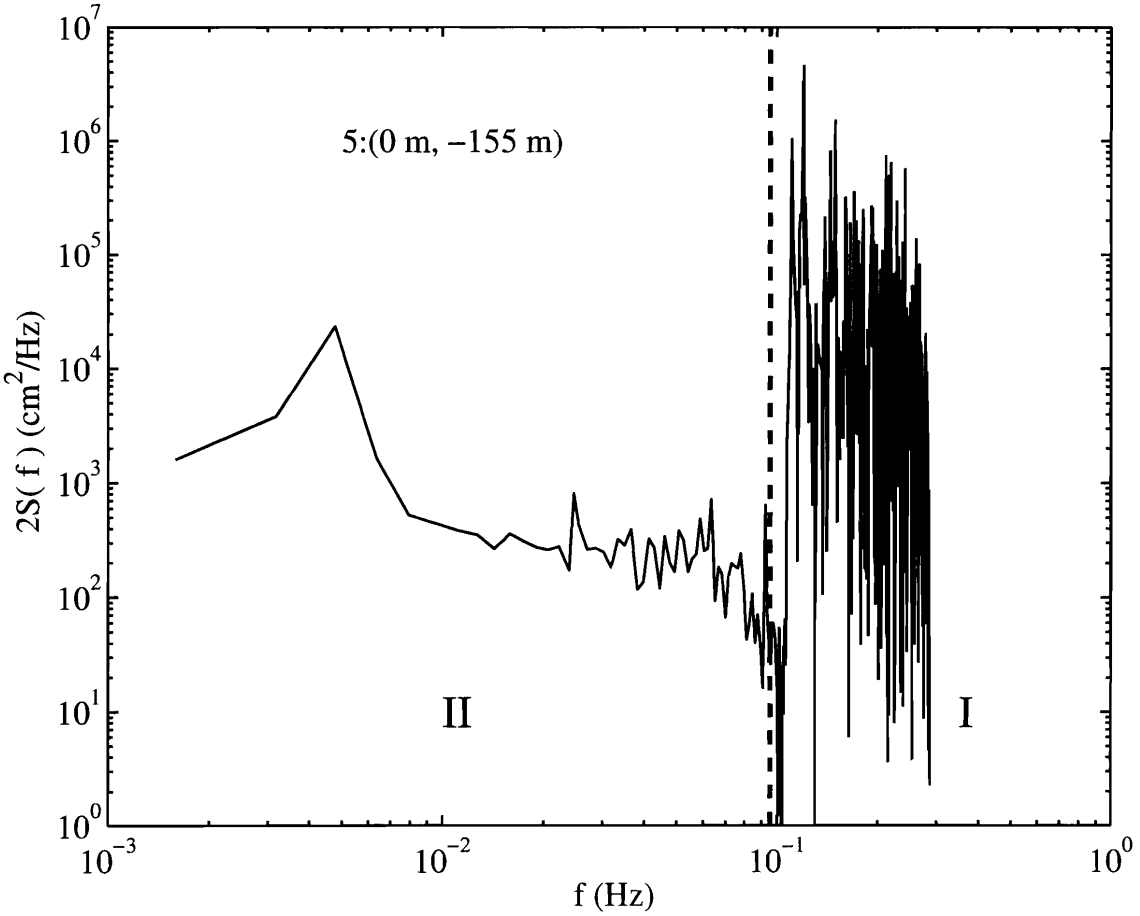

Figure 10-50: $2\mathcal{S}(f)$ at St.5 for 30 m opening (Case 2). Region I: $2\mathcal{S}_2(f)$. Region II: $2\mathcal{S}_{22}(f)$.

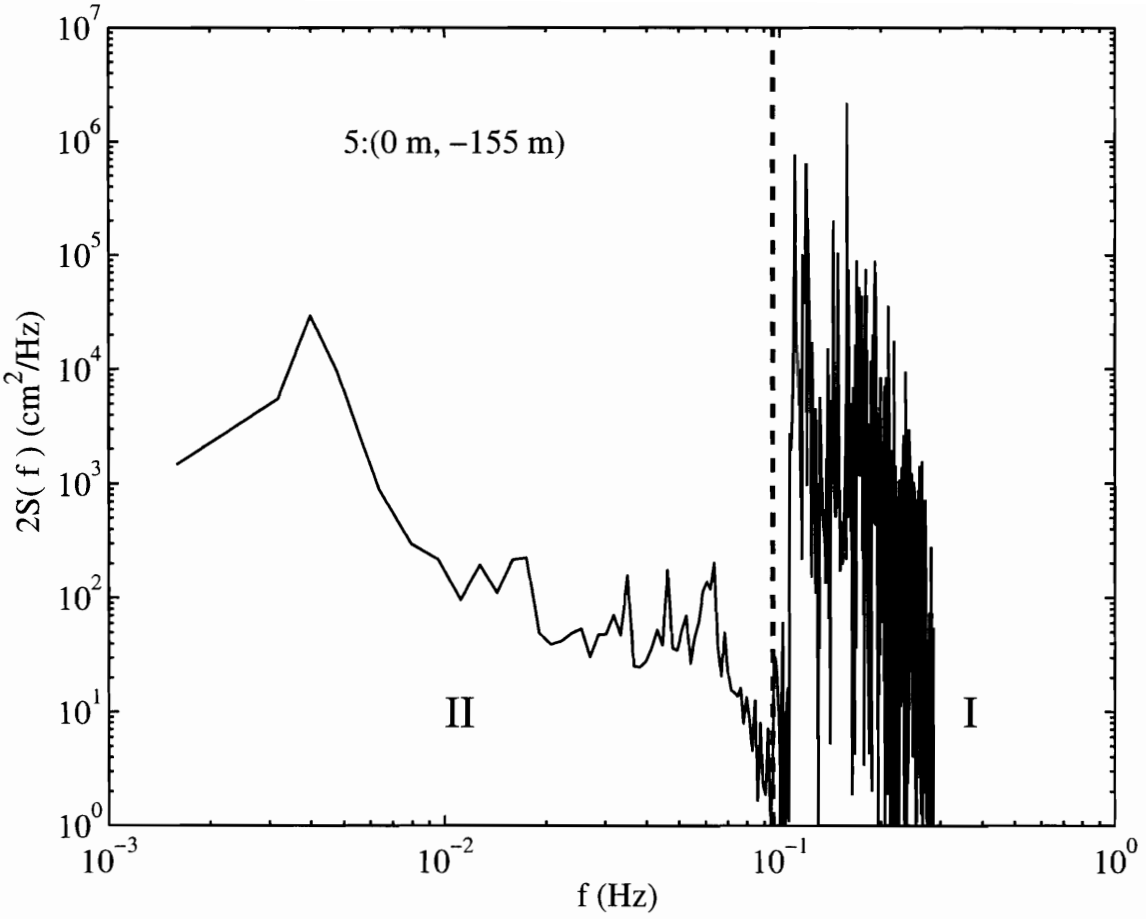

Figure 10-51: $2\mathcal{S}(f)$ at St.5 for 30 m opening with breakwater (Case 3). Region I: $2\mathcal{S}_2(f)$. Region II: $2\mathcal{S}_{22}(f)$.

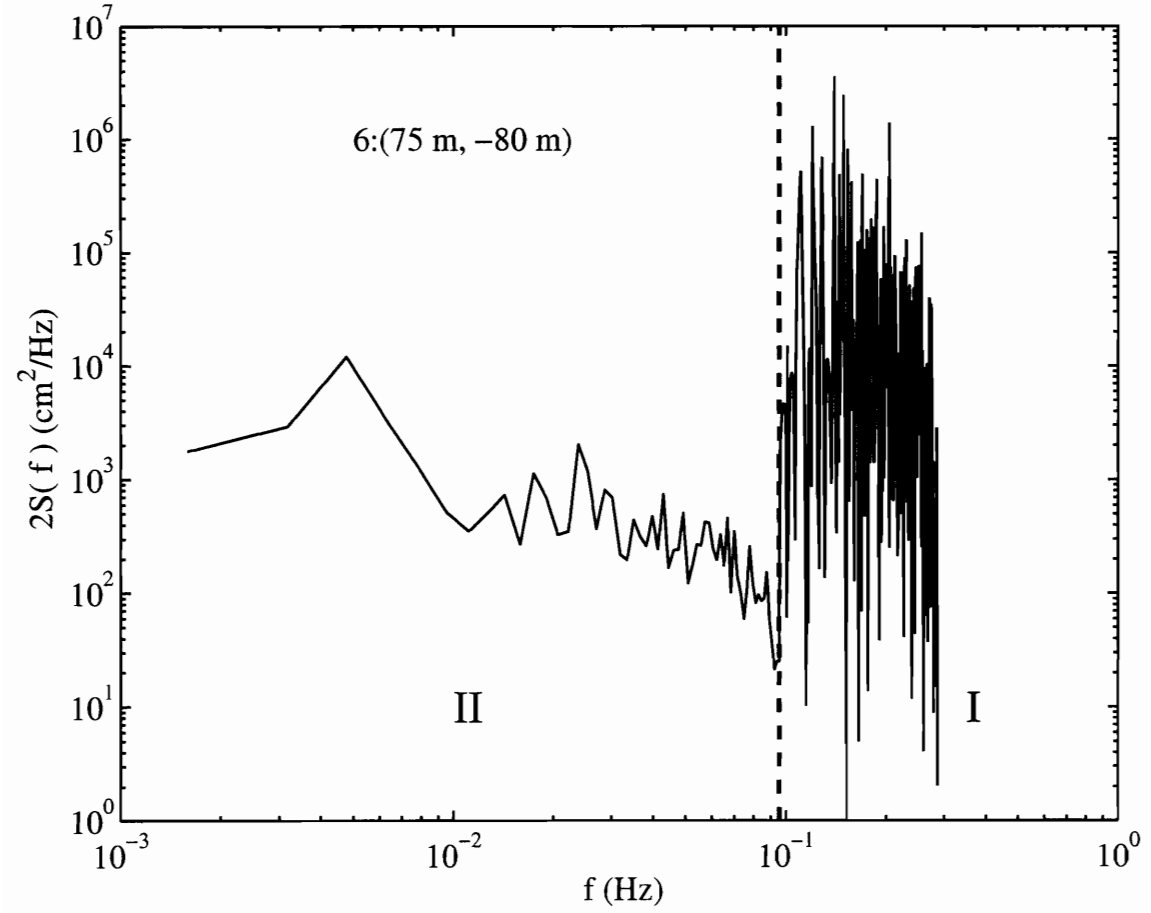

Figure 10-52: $2\mathcal{S}(f)$ at St.6 for 60 m opening (Case 1). Region I: $2\mathcal{S}_2(f)$. Region II: $2\mathcal{S}_{22}(f)$.

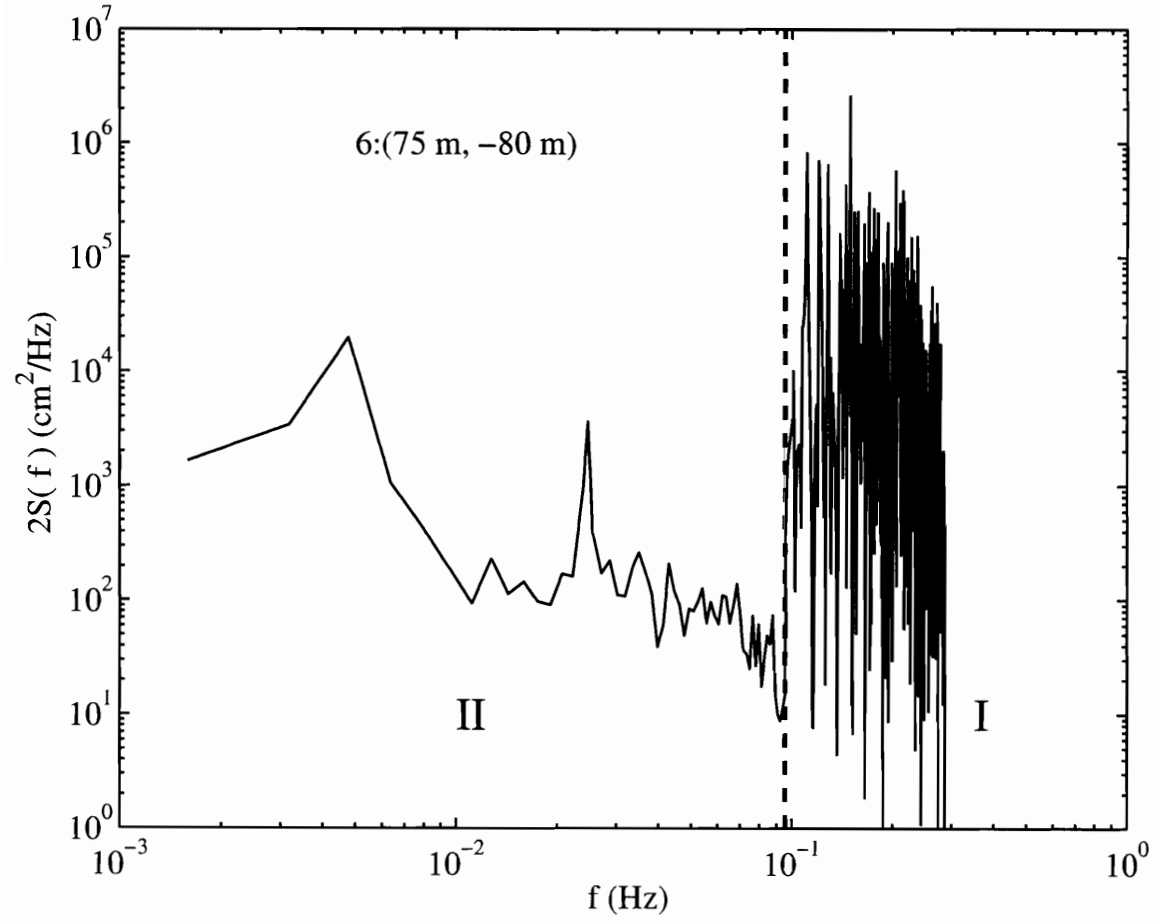

Figure 10-53: $2\mathcal{S}(f)$ at St.6 for 30 m opening (Case 2). Region I: $2\mathcal{S}_2(f)$. Region II: $2\mathcal{S}_{22}(f)$.

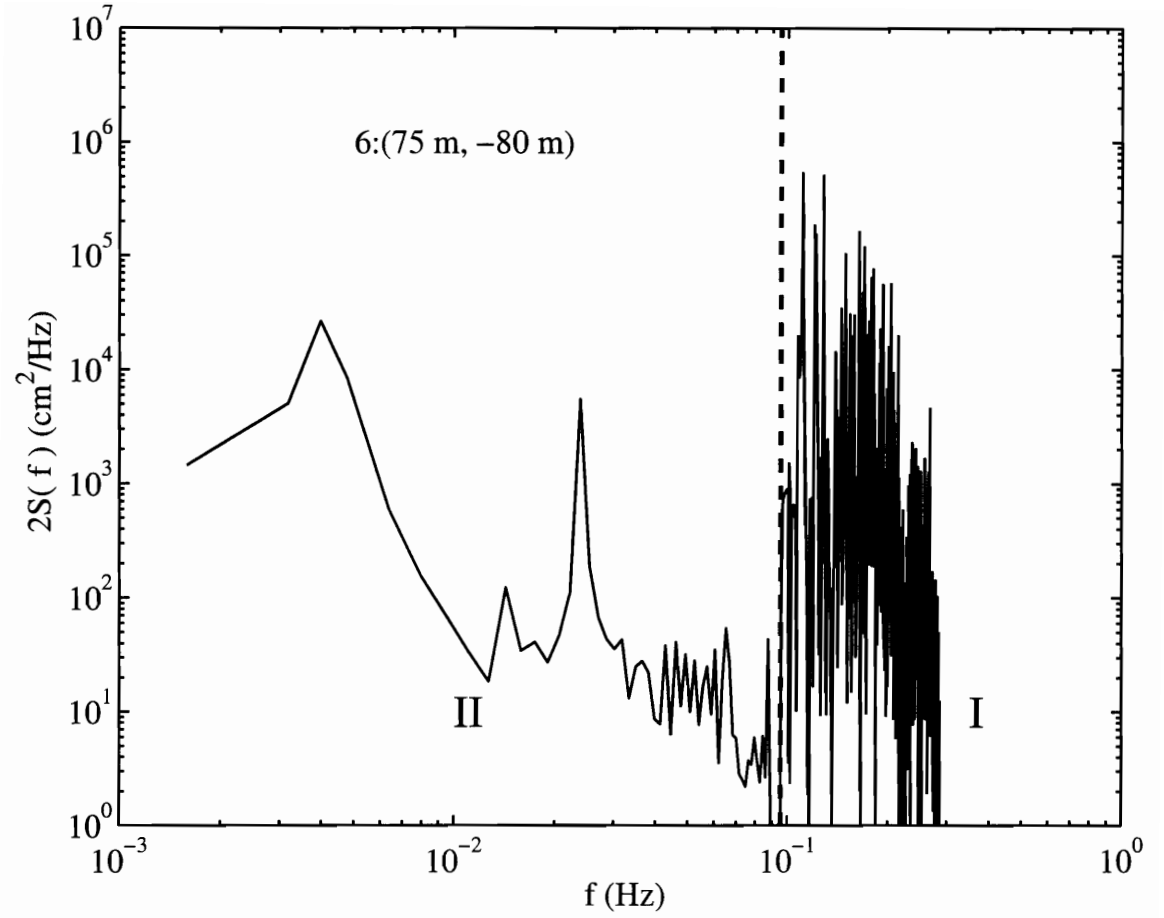

Figure 10-54: $2\mathcal{S}(f)$ at St.6 for 30 m opening with breakwater (Case 3). Region I: $2\mathcal{S}_2(f)$. Region II: $2\mathcal{S}_{22}(f)$.

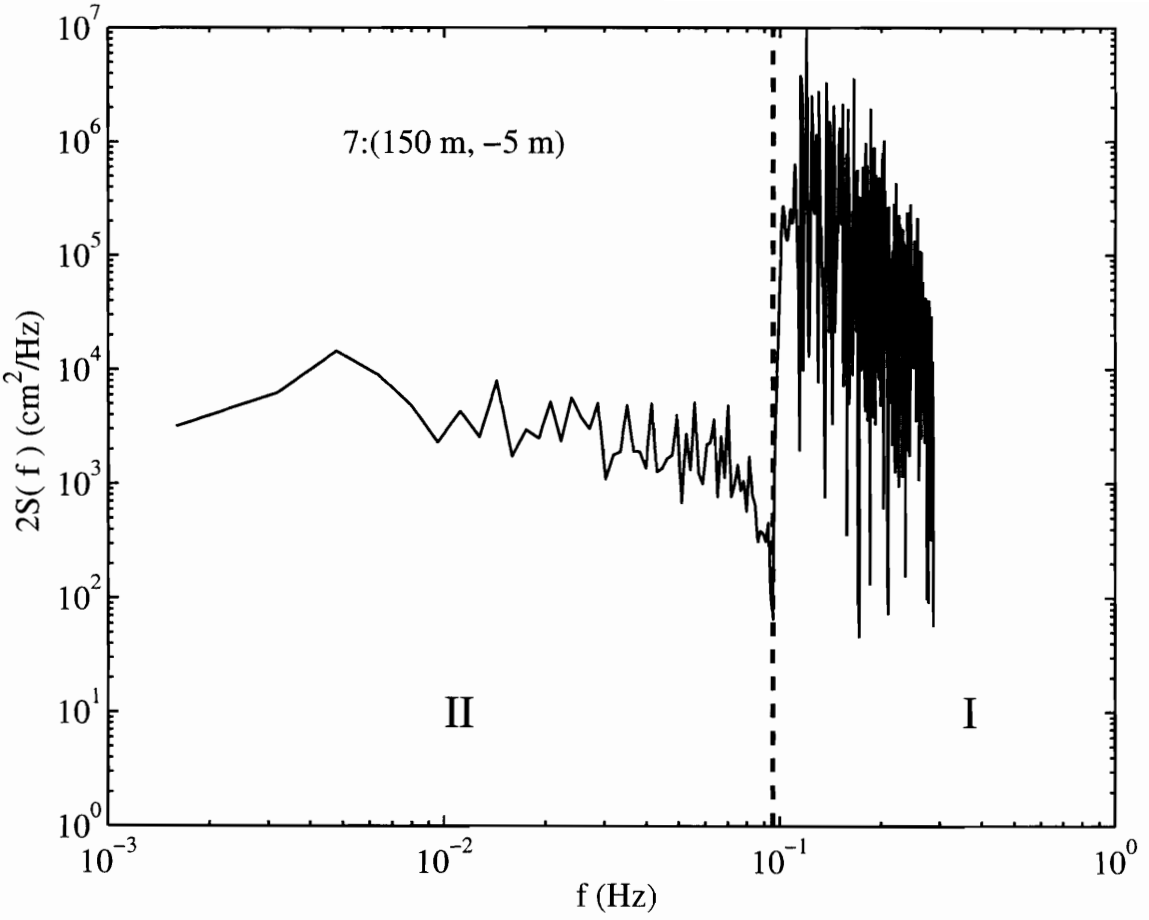

Figure 10-55: $2\mathcal{S}(f)$ at St.7 for 60 m opening (Case 1). Region I: $2\mathcal{S}_2(f)$. Region II: $2\mathcal{S}_{22}(f)$.

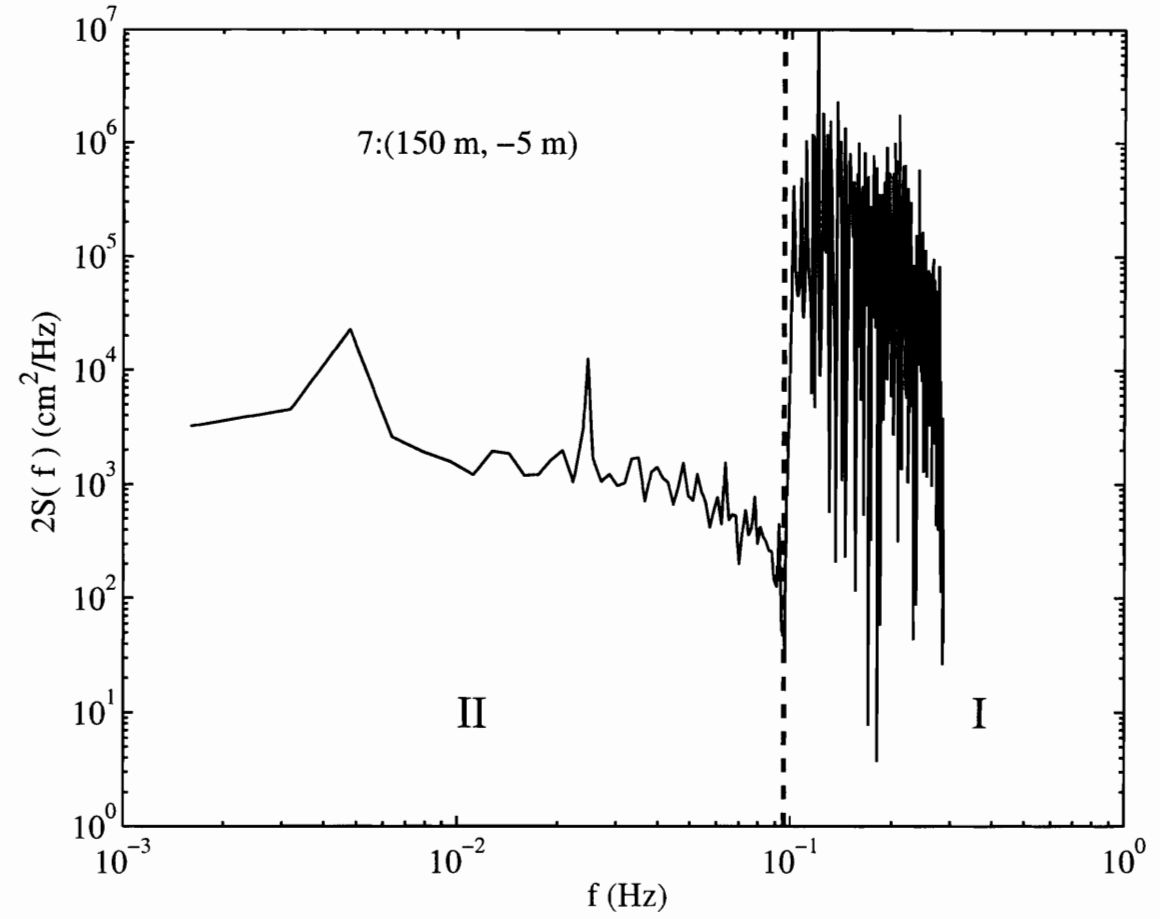

Figure 10-56: $\mathcal{S}(f)$ at St.7 for 30 m opening (Case 2). Region I: $\mathcal{S}_2(f)$. Region II: $\mathcal{S}_{22}(f)$.

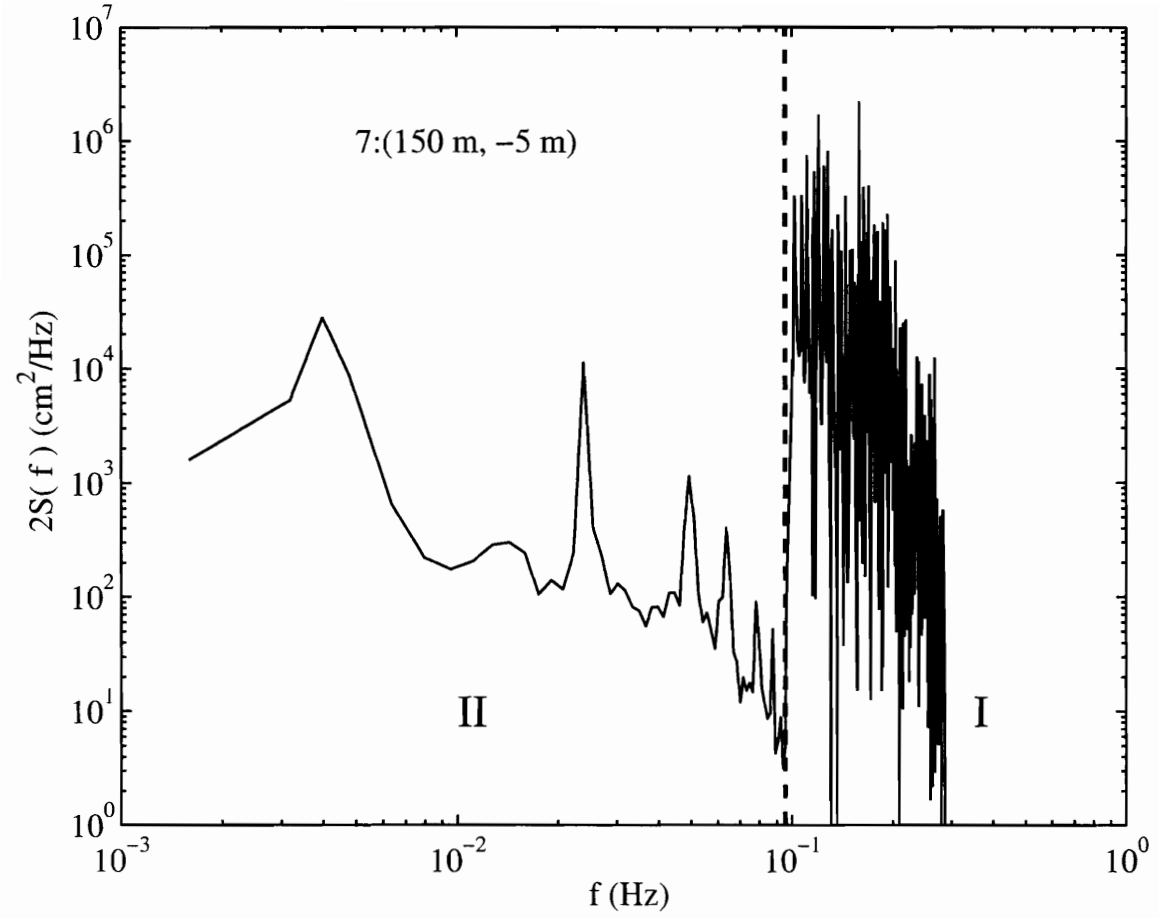

Figure 10-57: $2\mathcal{S}(f)$ at St.7 for 30 m opening with breakwater (Case 3). Region I: $2\mathcal{S}_2(f)$. Region II: $\mathcal{S}_{22}(f)$.

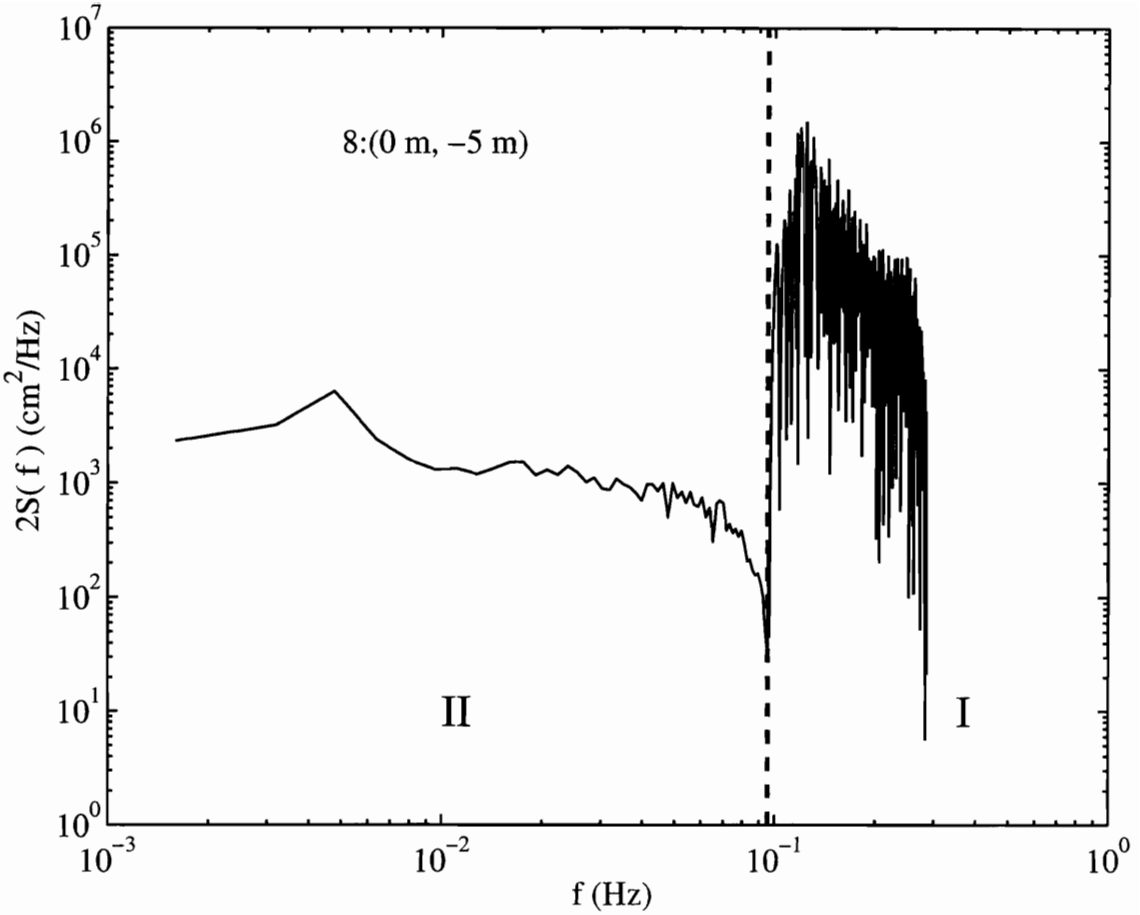

Figure 10-58: $2\mathcal{S}(f)$ at St.8 for 60 m opening (Case 1). Region I: $2\mathcal{S}_2(f)$. Region II: $2\mathcal{S}_{22}(f)$.

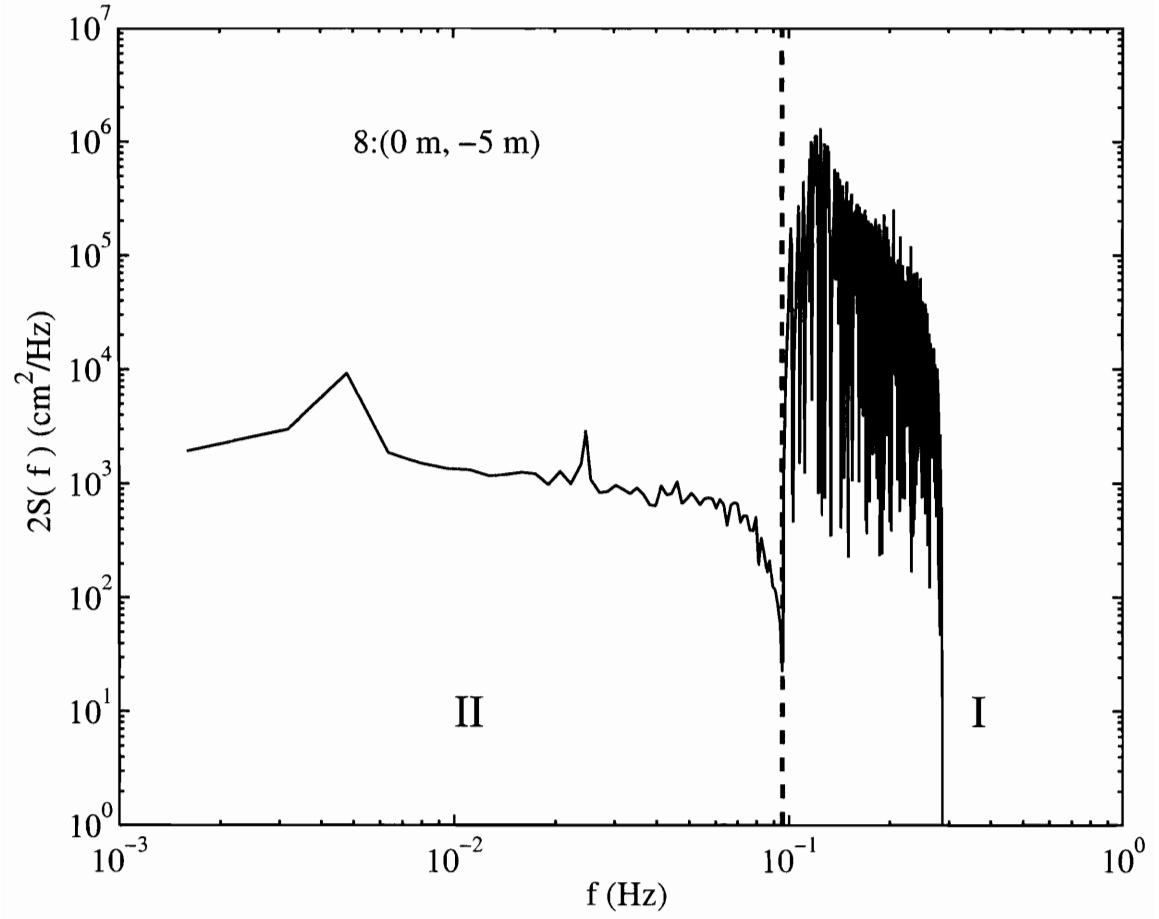

Figure 10-59: $2\mathcal{S}(f)$ at St.8 for 30 m opening (Case2). Region I: $2\mathcal{S}_2(f)$. Region II: $2\mathcal{S}_{22}(f)$.

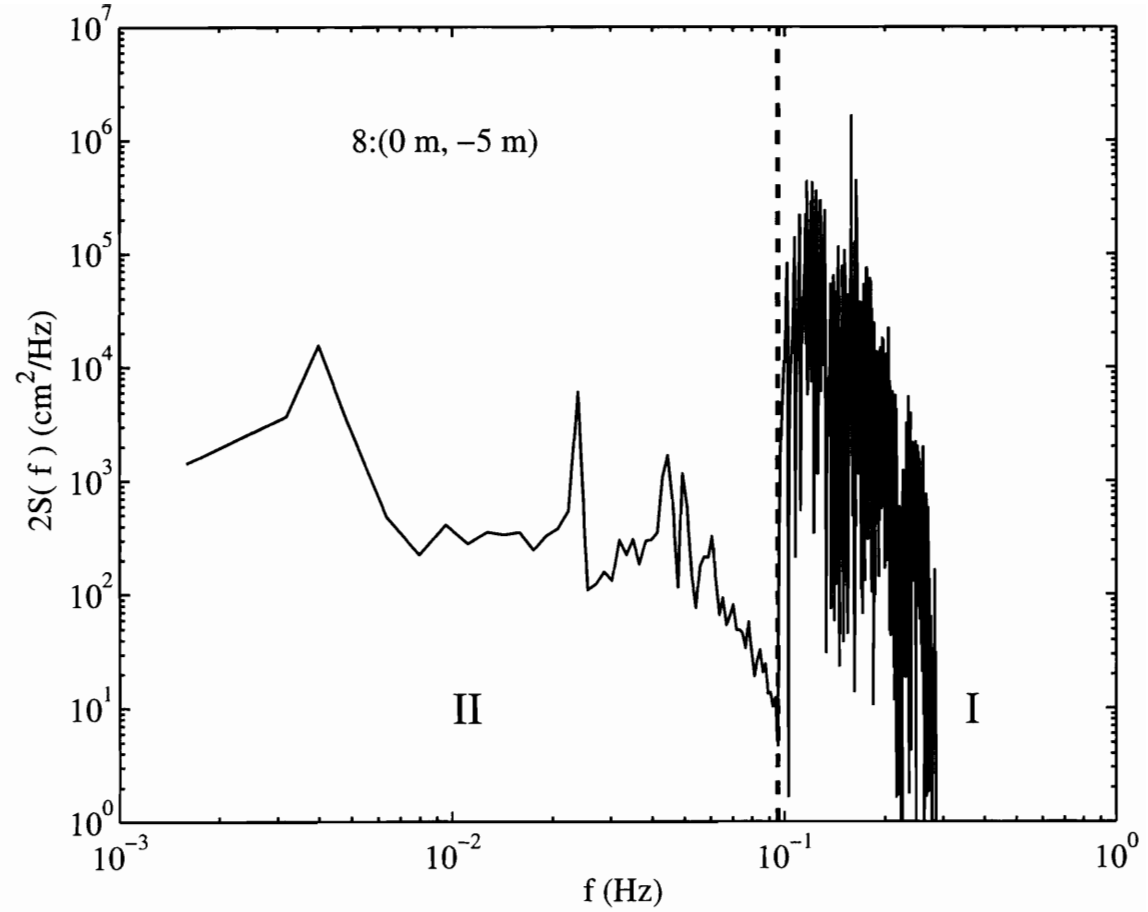

Figure 10-60: $2\mathcal{S}(f)$ at St.8 for 30 m opening with breakwater(Case 3). Region I: $2\mathcal{S}_2(f)$. Region II: $\mathcal{S}_{22}(f)$.

Chapter 11

Conclusion

In this thesis, we have studied the combined second-order nonlinear diffraction and refraction with the following two types of incident waves:

1. Monochromatic waves,

2. Random wave with broad frequency spectrum.

The theory is based on the mild-slope approximation, whose special feature is that it reduces the boundary value problem from three dimensions to two, hence, facilitates numerical computations.

In Part I, the incident waves are monochromatic. We have extended the ideas behind the mild-slope equation, developed previously for linearized problems of water-wave diffraction and refraction, to account for nonlinearity up to second order in wave steepness. For the first-order problem, we get the modified mild-slope equation by including only the propagating wave and keeping all terms proportional to $\nabla h, \nabla^2 h$ and $(\nabla h)^2$(Chamberlain and Porter [9]). For the second-order problem, a coupled mild-slope equation with forcing is derived for a slowly varying bathymetry. In the case of uniform depth, the second-order diffraction is governed by a set of uncoupled two-dimensional Helmholtz equations with forcing. For a semi-circular peninsula in constant depth, the solution is exact and can be obtained analytically. A hybrid-element method is described for the second-order refraction/diffraction over a slowly varying bathymetry. A two-dimensional Green's

function including the propagating waves and all the evanecent waves and the weak radiation condition for propagating waves are used to get the analytic solution in the far field where depth is constant and coastline is straight.

Numerical results are demonstrated for three geometries, (1) pure shoaling without a scatterer , (2) a semi-circular cylinder resting on top of a semi-circular shoal and (3) a harbor behind a semi-circular shoal. Effects of incidence angles are studied. In past studies the phenomenon of ringing near an offshore tower has been attributed to third-order effects (Faltinsen et al 1995 [30]). The ideas here can in principle be extended to third-order analysis for a tower on a slowly varying seabed, with of course increased algebraic and numerical complexity. Nevertheless the advantage of this approach that discrete computations are needed only for two horizontal coordinates would likely be even more preferable since refraction usually involves a large domain extending over many wavelengths in all horizontal directions. The fully three-dimensional alternative via either boundary elements or finite elements covering the entire region of variable boundary and bathymetry would appear to be extremely cumbersome and demanding. On the other hand, extending the three-dimensional treatment of Yue et al (1978) and Kim & Yue (1989) only near the structure, and matching with the quasi-two-dimensional mild-slope approximation for the much larger zone of variable depth, may simplify the numerical task considerably.

We point out that the present theory is an extension of Stokes approximation, which is inherently limited to small Ursell-Stokes parameter ($A/k^2h^3 \ll 1$) (see (E.1.5) where $\sinh^4 kh$ appears in the denominator). For very shallow water waves propagating over long distances one must use Boussinesq or other appropriate approximations expressly devised for small kh.

In Part II, the incident waves are random and broad-banded. For treating slow-drift motions of floating platforms or long-period oscillations in harbors, it is necessary to consider nonlinear effects due to random incident waves of broad frequency band. In this part, we have generalize the stochastic approach of Sclavounos, and, for calculating the nonlinear transfer function, the second-order mild-slope

approximation by modifying the mild-slope equation for monochromatic incident waves described in Part I. At the leading order $O(\epsilon^2)$ spectrum $S_2(\omega)$ is in the Wiener-Khintchine relation. The complete nonlinear spectral correction S_4 is the sum of S_{22}, S_{13} and S_{31} and consists of the transfer functions Γ_1, Γ_2 and Γ_3 which are associated with the first, second and third-order diffraction, and if the sea depth is slowly varying, refraction also. For simple plane waves in deep water, Sclavounos derived explicitly the transfer functions for ζ_1, ζ_2, and ζ_3, and calculated S_{22}, S_{13} and S_{31}, by using Pierson-Moskowitz spectrum for S_A. Strictly speaking, if one is interested in the $O(\epsilon^4)$ corrections for the entire frequency range, or for the mean-square amplitude(or the correlation function), it is necessary to complex the analysis of ζ_3 and solve the second-order problems for all pairs of frequencies in the ω_1 and ω_2 plane. The compuational task involving diffraction is a dauntingly complex task.

In typical sea spectra such as JONSWAP and its extension to finite water depth (TMA), the incident spectrum $S_A(\omega)$ is practically zero for small ω. In view of the Wiener-Khintchine relation, the leading-order spectrum $S_2(\omega)$ of the harbor response is virtually zero in the low frequency range, where the total spectrum is dominated by the nonlinear correction S_4. For the prediction of long-period oscillations in a harbor, due to the coincidence of the following two special features:

1. The typical wind-generated incident spectrum $S_A(\omega)$ is practically zero for small ω,

2. The nonlinear corrections $S_{13}(\omega)$ and $S_{31}(\omega)$ are proportional to $S_A(\omega)$,

S_{13} and S_{31} must also be negligibly small at low frequencies. This fortunate result makes it unnecessary to compute ζ_3 to get S_4, for small ω. In the computation of the integrals in S_{22}, it is necessary to solve the second-order diffraction/refraction problems for Γ_2 for many (in principle, infinite) pairs of frequencies only in a narrow strip near the diagonal $\omega_1 + \omega_2 = 0$ of the (ω_1, ω_2) plane. Furthermore, because the incident sea spectrum $S_A(\omega)$ is effectively nonzero only in a finite range $\omega_a < \omega < \omega_b$, only the pairs in the shaded portions of the narrow strip shown

in Figure 9-1 are relevant. These two advantages are particularly suited for the harbor resonance problem (and to slow-drift problems of ships and floating platforms). In the range of high frequencies, contributions by S_{22}, S_{13} and S_{31} are of $O(\epsilon^4)$ importance but are all much smaller than S_2, hence they are not pursued here.

Numerical examples are given for a simple square harbor of constant depth with normal incidence. As the Helmholtz mode or the pumping mode is known to strongly affected by the entrance geometry, we have studied three different entrances. The short waves spectrum is dominated by the leading order response by the linearized theory. The long wave spectral response is dominated by the second-order response. Harbor paradox is observed and the resemblance of the numerical results to the field data of Hualien harbor is also shown. We have shown that for the analysis of long-period oscillations in harbors the third-order solution can be omitted. However, for high-frequency response of structure like the oil platform, it is still necessary to include the third-order solution to get a complete spectrum up to $O(\epsilon^4)$.

In principle the present method for random waves can be applied or extended to study slow-drift motions of moored ships or tethered offshore platforms. Near the scatters, three-dimensional computations are needed, and be matched with the mild-slope theory away from the scatterer. For harbors, friction loss at the entrance must play an important role in reducing the resonant peaks. This, as well as the effects of variable depth inside and outside the harbour, require further modifications as well as streamlining of the computational efficiency.

Appendix A

First-order MSE

A.1 Derivation of the first-order MSE

From Eqns. (2.2.3)-(2.2.6) and (3.1.1), ϕ satisfies

$$\nabla^2\phi + \frac{\partial^2\phi}{\partial z^2} = 0, \quad -h(x,y) < z < 0, \tag{A.1.1}$$

$$\frac{\partial\phi}{\partial z} = -\nabla\phi\cdot\nabla h, \quad z = -h(x,y), \tag{A.1.2}$$

$$\frac{\partial\phi}{\partial z} - \frac{\omega^2}{g}\phi = 0, \quad z = 0, \tag{A.1.3}$$

Let us recall the procedure of Smith and Spinks[35], and introduce

$$f = \frac{\cosh k(z+h)}{\cosh kh} \tag{A.1.4}$$

with

$$\omega^2 = gk\tanh kh.$$

Note that f is a homogeneous solution which satisfies

$$\frac{\partial^2 f}{\partial z^2} - k^2 f = 0, \quad -h < z < 0, \tag{A.1.5}$$

$$\frac{\partial f}{\partial z} = 0, \quad z = -h, \tag{A.1.6}$$

$$\frac{\partial f}{\partial z} - \frac{\omega^2}{g} f = 0, \quad z = 0. \tag{A.1.7}$$

Applying Green's formula to f and ϕ, we obtain

$$\int_{-h}^{0} \left(\phi \frac{\partial^2 f}{\partial z^2} - f \frac{\partial^2 \phi}{\partial z^2} \right) dz = \left(\phi \frac{\partial f}{\partial z} - f \frac{\partial \phi}{\partial z} \right)_{z=-h}^{z=0}, \tag{A.1.8}$$

Putting Eqns. (A.1.1)-(A.1.3) and (A.1.5)-(A.1.7) into Eqn.(A.1.8), the preceding equation becomes

$$\int_{-h}^{0} \left(\phi k^2 f + f \nabla^2 \phi \right) dz = - \left(f \nabla \phi \cdot \nabla h \right)_{z=-h}. \tag{A.1.9}$$

We then assume

$$\phi = -\frac{ig}{\omega} \eta(x, y) f(x, y, z). \tag{A.1.10}$$

Note that h is a function of x, y, so f is function of x, y and z. Taking the derivative of ϕ, we obtain $\nabla\phi$ and $\nabla^2\phi$

$$\nabla \phi = -\frac{ig}{\omega} \left(\eta \frac{\partial f}{\partial h} \nabla h + f \nabla \eta \right) \tag{A.1.11}$$

$$\nabla^2 \phi = -\frac{ig}{\omega} \left[\eta \frac{\partial f}{\partial h} \nabla^2 h + \eta \frac{\partial^2 f}{\partial h^2} (\nabla h)^2 + f \nabla^2 \eta + 2 \frac{\partial f}{\partial h} \nabla \eta \cdot \nabla h \right]. \tag{A.1.12}$$

Putting ϕ, $\nabla\phi$ and $\nabla^2\phi$ into Eqn. (A.1.9), we get

$$\begin{aligned} g \int_{-h}^{0} \left[\eta k^2 f^2 + f \eta \frac{\partial f}{\partial h} \nabla^2 h + f \eta \frac{\partial^2 f}{\partial h^2} (\nabla h)^2 + f^2 \nabla^2 \eta \right] dz \\ + g \int_{-h}^{0} 2 f \frac{\partial f}{\partial h} \nabla \eta \cdot \nabla h dz = -g \left[f \eta \frac{\partial f}{\partial h} (\nabla h)^2 + f^2 \nabla \eta \cdot \nabla h \right]_{z=-h}. \end{aligned} \tag{A.1.13}$$

By Leibniz's rule,

$$\nabla \cdot \int_{-h}^{0} f^2 \nabla \eta dz = \int_{-h}^{0} \left\{ f^2 \nabla^2 \eta + 2 f \frac{\partial f}{\partial h} \nabla h \cdot \nabla \eta \right\} dz + \left(f^2 \nabla \eta \cdot \nabla h \right)_{z=-h},$$

we can combine the last two terms on the left hand side of Eqn. (A.1.13) and the last term on the right hand side of the Eqn. (A.1.13). We then get

$$\begin{aligned} g\nabla\cdot\int_{-h}^{0}f^2\nabla\eta dz+\eta\left(gk^2\int_{-h}^{0}f^2dz\right)+\eta\left[\left(\nabla^2h\right)g\int_{-h}^{0}f\frac{\partial f}{\partial h}dz\right] \\ +\eta\left[(\nabla h)^2g\int_{-h}^{0}f\frac{\partial^2 f}{\partial h^2}dz\right]+\eta\left[(\nabla h)^2g\left(f\frac{\partial f}{\partial h}\right)_{z=-h}\right]=0. \end{aligned} \tag{A.1.14}$$

We can denote the preceding equation as

$$\nabla\cdot(a\nabla\eta)+b\eta=0 \tag{A.1.15}$$

where

$$a=g\int_{-h}^{0}f^2dz, \tag{A.1.16}$$

$$b=k^2a+gU\nabla^2h+gV\left(\nabla h\right)^2, \tag{A.1.17}$$

$$U=\int_{-h}^{0}f\frac{\partial f}{\partial h}dz, \tag{A.1.18}$$

and

$$V=\int_{-h}^{0}f\frac{\partial^2 f}{\partial h^2}dz+\left[f\frac{\partial f}{\partial h}\right]_{z=-h}. \tag{A.1.19}$$

Using Leibniz's rule, we can rewrite V as

$$\begin{aligned} V&=\frac{\partial}{\partial h}\int_{-h}^{0}f\frac{\partial f}{\partial h}dz-\int_{-h}^{0}\left(\frac{\partial f}{\partial h}\right)^2dz \\ &=\frac{\partial U}{\partial h}-\int_{-h}^{0}\left(\frac{\partial f}{\partial h}\right)^2dz. \end{aligned} \tag{A.1.20}$$

Let us calculate each integral separately. By using Eqn. (A.1.4),

$$\frac{\partial f}{\partial h}=\frac{1}{\cosh kh}\left(\frac{\partial k}{\partial h}\right)\left[z\sinh k\left(z+h\right)-\frac{\sinh kh\sinh kz}{k}\right], \tag{A.1.21}$$

and

$$\frac{\partial k}{\partial h}=-\frac{2k^2}{2kh+\sinh 2kh} \tag{A.1.22}$$

in each integral, we obtain

$$\begin{aligned} a &= g\int_{-h}^{0} f^2 dz \\ &= \frac{g}{\cosh^2 kh}\int_{-h}^{0} \cosh^2 k(z+h)dz \\ &= \frac{g}{2\cosh^2 kh}\left(\frac{\sinh 2kh + 2kh}{2k}\right) \\ &= CC_g, \end{aligned} \tag{A.1.23}$$

U in the second term of b

$$\begin{aligned} U &= \int_{-h}^{0} f\frac{\partial f}{\partial h}dz \\ &= \frac{\sinh 2kh - 2kh\cosh 2kh}{4\cosh^2(kh)(2kh+\sinh 2kh)}, \end{aligned} \tag{A.1.24}$$

and V in the third term of b

$$\begin{aligned} V = &\frac{k\left[(2kh)^4 + 4(2kh)^3\sinh 2kh - 9\sinh(2kh)\sinh 4kh\right]}{12\cosh^2(kh)(2kh+\sinh 2kh)^3} \\ &+ \frac{k\left[kh(kh+\sinh 2kh)\left(\cosh^2 2kh - 2\cosh 2kh + 3\right)\right]}{\cosh^2(kh)(2kh+\sinh 2kh)^3}. \end{aligned} \tag{A.1.25}$$

Therefore, we obtain the modified mild-slope equation

$$\nabla\cdot(a\nabla\eta) + b\eta = 0, \tag{A.1.26}$$

where

$$a = CC_g,$$

$$b = k^2 CC_g + gU\nabla^2 h + gV(\nabla h)^2,$$

$$U = \frac{\sinh 2kh - 2kh\cosh 2kh}{4\cosh^2(kh)(2kh+\sinh 2kh)},$$

$$V = \frac{k\left[(2kh)^4 + 4(2kh)^3 \sinh 2kh - 9\sinh 2kh \sinh 4kh\right]}{12\cosh^2(kh)(2kh + \sinh 2kh)^3} + \frac{k\left[kh(kh + \sinh 2kh)\left(\cosh^2 2kh - 2\cosh 2kh + 3\right)\right]}{\cosh^2(kh)(2kh + \sinh 2kh)^3}$$

with

$$\omega^2 = gk \tanh kh,$$

$$C = \frac{\omega}{k},$$

$$C_g = \frac{C}{2}(1 + \frac{2kh}{\sinh 2kh}).$$

A.2 Derivation of $\frac{\partial k}{\partial h}$

k satisfies

$$\frac{\omega^2}{g} = k \tanh kh. \tag{A.2.1}$$

Taking the derivative of the preceding equation in respect with h, we obtain

$$\begin{aligned} 0 &= \frac{\partial k}{\partial h}\tanh kh + k\left(h\frac{\partial k}{\partial h} + k\right)\frac{1}{\cosh^2 kh} \\ &= \frac{\partial k}{\partial h}\left[\frac{kh}{\cosh^2 kh} + \tanh kh\right] + \frac{k^2}{\cosh^2 kh} \end{aligned}. \tag{A.2.2}$$

Therefore

$$\frac{\partial k}{\partial h} = -\frac{2k^2}{2kh + \sinh 2kh}. \tag{A.2.3}$$

A.3 Derivation of $\frac{\partial f}{\partial h}$

f is defined as

$$f = \frac{\cosh k(z + h)}{\cosh kh}. \tag{A.3.1}$$

Taking the derivative of the preceding equation in respect with h, we obtain

$$\begin{aligned}\frac{\partial f}{\partial h} &= \left[\frac{\partial k}{\partial h}(z+h)+k\right]\frac{\sinh k(z+h)}{\cosh kh} - \left(\frac{\partial k}{\partial h}h+k\right)\frac{\cosh k(z+h)}{\cosh^2 kh}\sinh kh \\ &= \frac{1}{\cosh kh}\frac{\partial k}{\partial h}\left[(z+h)\sinh k(z+h) - h\sinh kh\frac{\cosh k(z+h)}{\cosh kh}\right] \\ &\quad + \frac{1}{\cosh kh}\frac{\partial k}{\partial h}\frac{k}{(\partial k/\partial h)}\left[\sinh k(z+h) - \sinh kh\frac{\cosh k(z+h)}{\cosh kh}\right].\end{aligned} \tag{A.3.2}$$

Making use of Eqn. (A.2.3), we obtain

$$\frac{k}{(\partial k/\partial h)} = -\left(\frac{\sinh kh\cosh kh}{k}+h\right). \tag{A.3.3}$$

Putting the preceding equation into Eqn. (A.3.2), we get

$$\begin{aligned}\frac{\partial f}{\partial h} = \frac{1}{\cosh kh}\frac{\partial k}{\partial h}\Big\{&z\sinh k(z+h) + \frac{\sinh kh}{k}\left[\cosh k(z+h)\sinh kh\right. \\ &\left. - \cosh kh\sinh k(z+h)\right]\Big\}\end{aligned}. \tag{A.3.4}$$

Since

$$\sinh(z_1 - z_2) = \sinh z_1\cosh z_2 - \cosh z_1\sinh z_2, \tag{A.3.5}$$

we obtain

$$\frac{\partial f}{\partial h} = \frac{1}{\cosh kh}\frac{\partial k}{\partial h}\left[z\sinh k(z+h) - \frac{\sinh kh\sinh kz}{k}\right]. \tag{A.3.6}$$

A.4 Derivation of U

By putting Eq. (A.3.6) into Eq. (A.1.18), U becomes

$$\begin{aligned}U &= \int_{-h}^{0} f\frac{\partial f}{\partial h}dz \\ &= \frac{1}{\cosh^2 kh}\left(\frac{\partial k}{\partial h}\right)\int_{-h}^{0} z\sinh k(z+h)\cosh k(z+h)\,dz \\ &\quad - \frac{1}{\cosh^2 kh}\left(\frac{\partial k}{\partial h}\right)\frac{\sinh kh}{k}\int_{-h}^{0}\sinh kz\cosh k(z+h)\,dz.\end{aligned} \tag{A.4.1}$$

Making use of the following equation,

$$\begin{aligned} & z \sinh k(z+h) \cosh k(z+h) \\ &= \frac{1}{2} z \sinh 2k(z+h) \\ &= \frac{1}{4k}\left\{\frac{\partial}{\partial z}[z \cosh 2k(z+h)] - \cosh 2k(z+h)\right\}, \end{aligned} \tag{A.4.2}$$

and

$$\sinh kz \cosh k(z+h) = \frac{1}{2}[\sinh(2kz+kh) - \sinh kh], \tag{A.4.3}$$

Eq. (A.4.1) becomes

$$\begin{aligned} U &= \int_{-h}^{0} f \frac{\partial f}{\partial h} dz \\ &= \frac{1}{\cosh^2 kh} \frac{\partial k}{\partial h} \int_{-h}^{0} \frac{1}{4k}\left\{\frac{\partial}{\partial z}[z \cosh 2k(z+h)] - \cosh 2k(z+h)\right\} dz \\ &- \frac{1}{\cosh^2 kh} \frac{\partial k}{\partial h} \frac{\sinh kh}{k} \int_{-h}^{0} \frac{1}{2}[\sinh(2kz+kh) - \sinh kh]\, dz. \end{aligned} \tag{A.4.4}$$

Carrying out the integrals, we obtain

$$\begin{aligned} U = & \frac{1}{\cosh^2 kh} \frac{\partial k}{\partial h} \frac{1}{4k}\left\{z \cosh 2k(z+h) - \frac{1}{2k} \sinh 2k(z+h)\right\}_{z=-h}^{z=0} \\ & - \frac{1}{\cosh^2 kh} \frac{\partial k}{\partial h} \frac{\sinh kh}{k} \frac{1}{2}\left[\frac{1}{2k} \cosh(2kz+kh) - z \sinh kh\right]_{z=-h}^{z=0}. \end{aligned} \tag{A.4.5}$$

or equivalently,

$$\begin{aligned} U &= \frac{1}{\cosh^2 kh} \frac{\partial k}{\partial h} \frac{1}{4k}\left[h - \frac{1}{2k} \sinh 2kh + 2h \sinh^2 kh\right] \\ &= \frac{1}{\cosh^2 kh} \frac{\partial k}{\partial h} \frac{1}{4k}\left[-\frac{1}{2k} \sinh 2kh + h \cosh 2kh\right], \end{aligned} \tag{A.4.6}$$

where

$$\sinh^2 kh = \frac{1}{2}(\cosh 2kh - 1) \tag{A.4.7}$$

is applied. Moreover, by making use of Eq. (A.2.3), Eq. (A.4.6) becomes

$$U = \frac{\sinh 2kh - 2kh\cosh 2kh}{4\left(2kh + \sinh 2kh\right)\cosh^2 kh}. \tag{A.4.8}$$

A.5 Derivation of V

V is defined as

$$V = \frac{\partial U}{\partial h} - \int_{-h}^{0} \left(\frac{\partial f}{\partial h}\right)^2 dz. \tag{A.5.1}$$

Let us obtain the first and second term of the previous equation, separately. The first term in Eq. (A.5.1) is obtained as follows.

$$\begin{aligned}
\frac{\partial U}{\partial h} &= \frac{\partial}{\partial h}\left[\frac{\sinh 2kh - 2kh\cosh 2kh}{4\left(2kh + \sinh 2kh\right)\cosh^2 kh}\right] \\
&= \frac{\cosh^{-2} kh}{4\left(2kh + \sinh 2kh\right)}\frac{\partial}{\partial h}\left(\sinh 2kh - 2kh\cosh 2kh\right) \\
&\quad + \left(\sinh 2kh - 2kh\cosh 2kh\right)\frac{\partial}{\partial h}\left[\frac{\cosh^{-2} kh}{4\left(2kh + \sinh 2kh\right)}\right] \\
&= \frac{\cosh^{-2} kh}{4\left(2kh + \sinh 2kh\right)^2}\left(h\frac{\partial k}{\partial h} + k\right)\left\{-4kh\sinh 2kh\left(2kh + \sinh 2kh\right)\right. \\
&\quad \left. - \left(\sinh 2kh - 2kh\cosh 2kh\right)\left[2\frac{\sinh kh}{\cosh kh}\left(2kh + \sinh 2kh\right) + 2\left(1 + \cosh 2kh\right)\right]\right\}.
\end{aligned} \tag{A.5.2}$$

Making use of the following equation

$$\begin{aligned}
\frac{\partial k}{\partial h}\left[h + \frac{k}{\left(\partial k/\partial h\right)}\right] &= -\frac{\sinh 2kh}{2k}\frac{\partial k}{\partial h} \\
&= \frac{k\sinh 2kh}{\left(2kh + \sinh 2kh\right)},
\end{aligned} \tag{A.5.3}$$

we obtain

$$\frac{\partial U}{\partial h} = -\frac{k \sinh 2kh}{4\cosh^2 kh\,(2kh + \sinh 2kh)^3}\left\{4kh \sinh 2kh\,(2kh + \sinh 2kh)\right.$$
$$\left. + 2\,(\sinh 2kh - 2kh\cosh 2kh)\left[\frac{\sinh kh}{\cosh kh}\,(2kh + \sinh 2kh) + (1 + \cosh 2kh)\right]\right\}. \tag{A.5.4}$$

In addition, the second term in Eq. (A.5.1) is obtained as follows.

$$-\int_{-h}^{0}\left(\frac{\partial f}{\partial h}\right)^2 dz = -\frac{1}{\cosh^2 kh}\left(\frac{\partial k}{\partial h}\right)^2 \int_{-h}^{0}\left[z\sinh k\,(z+h) - \frac{\sinh kh \sinh kz}{k}\right]^2 dz$$
$$= -\frac{1}{\cosh^2 kh}\left(\frac{\partial k}{\partial h}\right)^2 \int_{-h}^{0}\left\{z^2 \sinh^2 k\,(z+h) + \frac{\sinh^2 kh}{k^2}\sinh^2 kz\right.$$
$$\left. -2\frac{\sinh kh}{k} z \sinh k\,(z+h)\sinh kz\right\} dz. \tag{A.5.5}$$

Making use of the following equations

$$\sinh^2 k\,(z+h) = \frac{1}{2}\left[\cosh 2k\,(z+h) - 1\right], \tag{A.5.6}$$
$$\sinh^2 kz = \frac{1}{2}\left(\cosh 2kz - 1\right), \tag{A.5.7}$$
$$\sinh k\,(z+h)\sinh kz = \frac{1}{2}\left[\cosh kh - \cosh\,(2kz + kh)\right], \tag{A.5.8}$$
$$\sinh 2kh = 2\sinh kh \cosh kh, \tag{A.5.9}$$

we can rewrite Eq. (A.5.5) as

$$-\int_{-h}^{0}\left(\frac{\partial f}{\partial h}\right)^2 dz = \frac{-\left(\partial k/\partial h\right)^2}{2\cosh^2 kh}\int_{-h}^{0}\left\{z^2\cosh 2k\,(z+h) - z^2 + \frac{\sinh^2 kh}{k^2}\cosh 2kz\right.$$
$$\left. -\frac{\sinh^2 kh}{k^2} - 2\frac{\sinh kh}{k} z\cosh\,(2kz + kh) + \frac{\sinh 2kh}{k} z\right\} dz. \tag{A.5.10}$$

Making use of the following equation

$$\begin{aligned} z^2 \cosh 2k\,(z+h) &= \frac{1}{2k}\left\{\frac{\partial}{\partial z}\left[z^2 \sinh 2k\,(z+h)\right] - 2z \sinh 2k\,(z+h)\right\} \\ &= \frac{1}{2k}\frac{\partial}{\partial z}\left[z^2 \sinh 2k\,(z+h)\right] - \frac{2}{4k^2}\frac{\partial}{\partial z}\left[z \cosh 2k\,(z+h)\right] \\ &\quad + \frac{2}{4k^2}\cosh 2k\,(z+h)\,, \end{aligned} \tag{A.5.11}$$

$$z \cosh\,(2kz+kh) = \frac{1}{2k}\left\{\frac{\partial}{\partial z}\left[z \sinh\,(2kz+kh)\right] - \sinh\,(2kz+kh)\right\}, \tag{A.5.12}$$

and carrying out the integrals in Eq. (A.5.10), we obtain

$$\begin{aligned} -\int_{-h}^{0}\left(\frac{\partial f}{\partial h}\right)^2 dz = \frac{-\left(\partial k/\partial h\right)^2}{2\cosh^2 kh}\Bigg\{ & \frac{1}{2k}\left[z^2 \sinh 2k\,(z+h)\right] - \frac{2}{4k^2}\left[z \cosh 2k\,(z+h)\right] \\ & + \frac{2}{8k^3}\sinh 2k\,(z+h) - \frac{z^3}{3} + \frac{\sinh^2 kh}{2k^3}\sinh 2kz - \frac{\sinh^2 kh}{k^2}z \\ & - \frac{2}{2k}\frac{\sinh kh}{k}\left[z \sinh\,(2kz+kh)\right] + \frac{2}{4k^2}\frac{\sinh kh}{k}\cosh\,(2kz+kh) \\ & + \frac{\sinh 2kh}{k}\frac{z^2}{2}\Bigg\}_{z=-h}^{z=0}. \end{aligned} \tag{A.5.13}$$

Therefore,

$$\begin{aligned} -\int_{-h}^{0}\left(\frac{\partial f}{\partial h}\right)^2 dz = \frac{-\left(\partial k/\partial h\right)^2}{\cosh^2 kh}\Bigg\{ & -\frac{h}{4k^2} + \frac{1}{8k^3}\sinh 2kh - \frac{h^3}{6} \\ & + \frac{\sinh^2 kh}{4k^3}\sinh 2kh - \frac{h^2 \sinh 2kh}{4k}\Bigg\}. \end{aligned} \tag{A.5.14}$$

Putting Eq. (A.2.3) and

$$\sinh^2 kh = \frac{1}{2}\left(\cosh 2kh - 1\right) \tag{A.5.15}$$

into Eq. (A.5.14) ,we obtain

$$\begin{aligned} -\int_{-h}^{0}\left(\frac{\partial f}{\partial h}\right)^2 dz = \frac{k}{\cosh^2 kh\,(2kh+\sinh 2kh)^2}\Bigg\{ & kh + \frac{2\,(kh)^3}{3} \\ & - \frac{\cosh 2kh}{2}\sinh 2kh + (kh)^2 \sinh 2kh\Bigg\}. \end{aligned} \tag{A.5.16}$$

Finally, by combining Eqns. (A.5.4) and (A.5.16), V is found to be

$$V = \frac{k\left[(2kh)^4 + 4(2kh)^3 \sinh 2kh - 9\sinh(2kh)\sinh 4kh\right]}{12\cosh^2(kh)(2kh + \sinh 2kh)^3} + \frac{k\left[kh(kh + \sinh 2kh)\left(\cosh^2 2kh - 2\cosh 2kh + 3\right)\right]}{\cosh^2(kh)(2kh + \sinh 2kh)^3}. \tag{A.5.17}$$

Appendix B

Derivation of F

B.1 Free surface boundary condition

Let us recall Eq. (2.2.11), the free surface boundary condition at $z = 0$,

$$\frac{\partial \Phi_2}{\partial z} + \frac{1}{g}\frac{\partial^2 \Phi_2}{\partial t^2} = Q, \tag{B.1.1}$$

where

$$Q = \frac{1}{g^2}\frac{\partial \Phi_1}{\partial t}\frac{\partial}{\partial z}\left[g\left(\frac{\partial \Phi_1}{\partial z}\right) + \frac{\partial^2 \Phi_1}{\partial t^2}\right] - \frac{1}{g}\frac{\partial}{\partial t}\left(\nabla_3 \Phi_1\right)^2, \quad z = 0. \tag{B.1.2}$$

We assume the first-order potential is

$$\Phi_1 = \phi e^{-i\omega t} + *, \tag{B.1.3}$$

where

$$\phi = -\frac{ig\eta(x,y)f}{\omega}, \tag{B.1.4}$$

and

$$f = \frac{\cosh k(z+h)}{\cosh kh}. \tag{B.1.5}$$

Note that the water depth h is a function of x and y, so f is a function of x, y and z.

Now let us rewrite Eq. (B.1.2) as

$$Q = Q_1 + Q_2 + Q_3 + Q_4 \tag{B.1.6}$$

where

$$Q_1 = \left[\frac{1}{g}\frac{\partial\Phi_1}{\partial t}\frac{\partial^2\Phi_1}{\partial z^2}\right]_{z=0} \tag{B.1.7}$$

$$Q_2 = \left[\frac{1}{g^2}\frac{\partial\Phi_1}{\partial t}\frac{\partial^3\Phi_1}{\partial z\partial t^2}\right]_{z=0} \tag{B.1.8}$$

$$Q_3 = \left[-\frac{1}{g}\frac{\partial}{\partial t}\left(\nabla\Phi_1\right)^2\right]_{z=0} \tag{B.1.9}$$

$$Q_4 = \left[-\frac{1}{g}\frac{\partial}{\partial t}\left(\frac{\partial\Phi_1}{\partial z}\right)^2\right]_{z=0} \tag{B.1.10}$$

By putting Eq. (B.1.3)-(B.1.5) into Eq. (B.1.6), each term in Q is obtained as follows.

B.2 First term (Q_1) in Q

For the first term (Q_1) in Q,

$$\begin{aligned} Q_1 &= \frac{1}{g}\frac{\partial\Phi_1}{\partial t}\left(\frac{\partial^2\Phi_1}{\partial z^2}\right) \\ &= \frac{1}{g}\left\{-i\omega\phi e^{-i\omega t} + *\right\}\left\{\frac{\partial^2\phi}{\partial z^2}e^{-i\omega t} + *\right\} \\ &= \frac{1}{g}\left\{-i\omega\phi\frac{\partial^2\phi}{\partial z^2}e^{-2i\omega t} + * - i\omega\phi\frac{\partial^2\phi^*}{\partial z^2} + i\omega\phi^*\frac{\partial^2\phi}{\partial z^2}\right\}. \end{aligned} \tag{B.2.1}$$

Making use of Eq. (B.1.4) and (B.1.5), the above equation becomes

$$\begin{aligned} Q_1 &= -\frac{i\omega}{g}\left(-\frac{ig}{\omega}k\right)^2\eta^2 e^{-i2\omega t} + * \\ &= \frac{igk^2}{\omega}\eta^2 e^{-i2\omega t} + *. \end{aligned} \tag{B.2.2}$$

Note that there is no zeroth harmonic in Q_1.

B.3 Second term (Q_2) in Q

For the second term (Q_2) in Q

$$\begin{aligned} Q_2 &= \frac{1}{g^2}\frac{\partial \Phi_1}{\partial t}\frac{\partial}{\partial z}\left(\frac{\partial^2 \Phi_1}{\partial t^2}\right) \\ &= \frac{1}{g^2}\left\{-i\omega\phi e^{-i\omega t} + *\right\}\left\{(-i\omega)^2\frac{\partial \phi}{\partial z}e^{-i\omega t} + *\right\} \\ &= \frac{1}{g}\left\{(-i\omega)^3\phi\frac{\partial \phi}{\partial z}e^{-i2\omega t} + * + i\omega^3\phi\frac{\partial \phi^*}{\partial z} - i\omega^3\phi^*\frac{\partial \phi}{\partial z}\right\}. \end{aligned} \tag{B.3.1}$$

Making use of Eq. (B.1.4) and (B.1.5), the above equation becomes

$$\begin{aligned} Q_2 &= (-i\omega k\tanh kh)\,\eta^2 e^{-i2\omega t} + * \\ &= \left(-\frac{i\omega^3}{g}\right)\eta^2 e^{-i2\omega t} + *. \end{aligned} \tag{B.3.2}$$

Note that there is no zeroth harmonic in Q_2.

B.4 Third Term (Q_3) in Q

For the third term (Q_3) in Q

$$\begin{aligned} Q_3 &= -\frac{1}{g}\frac{\partial}{\partial t}\left(\nabla\Phi_1\right)^2 \\ &= -\frac{1}{g}\frac{\partial}{\partial t}\left(\nabla\phi e^{-i\omega t} + *\right)^2 \\ &= -\frac{1}{g}\left\{(-i2\omega)\left(\nabla\phi\right)^2 e^{-i2\omega t} + *\right\} \end{aligned} \tag{B.4.1}$$

Making use of Eq. (B.1.4) and (B.1.5), the above equation becomes

$$\begin{aligned} Q_3 &= \frac{2i\omega}{g}\left[\left(\frac{-ig}{\omega}\right)^2\left(\nabla\eta\right)^2 e^{-i2\omega t} + *\right] \\ &= -\frac{2ig}{\omega}\left(\nabla\eta\right)^2 e^{-i2\omega t} + *. \end{aligned} \tag{B.4.2}$$

Note that there is no zeroth harmonic in Q_3

B.5 Fourth term (Q_4) in Q

For the fourth term (Q_4) in Q

$$\begin{aligned} Q_4 &= -\frac{1}{g}\frac{\partial}{\partial t}\left(\frac{\partial \Phi_1}{\partial z}\right)^2 \\ &= -\frac{1}{g}\frac{\partial}{\partial t}\left[\frac{\partial \phi}{\partial z}e^{-i\omega t} + *\right]^2 \\ &= -\frac{1}{g}\left[(-i2\omega)\left(\frac{\partial \phi}{\partial z}\right)^2 e^{-i2\omega t} + *\right]. \end{aligned} \tag{B.5.1}$$

Making use of Eq. (B.1.4) and (B.1.5), the above equation becomes

$$\begin{aligned} Q_4 &= \frac{2i\omega}{g}\left(\frac{-ig}{\omega}k\tanh kh\right)^2 \eta^2 e^{-i2\omega t} + * \\ &= \left(-\frac{2i\omega^3}{g}\right)\eta^2 e^{-i2\omega t} + * \end{aligned} \tag{B.5.2}$$

Note that there is no zeroth harmonic in Q_3

Finally, combining Eqs. (B.2.2), (B.3.2), (B.4.2) and (B.5.2), we get

$$\begin{aligned} Q &= Q_1 + Q_2 + Q_3 + Q_4 \\ &= Fe^{-i2\omega t} + * \end{aligned} \tag{B.5.3}$$

where

$$F = \widehat{\beta}\eta^2 + \bar{\beta}\left(\nabla\eta\right)^2, \tag{B.5.4}$$

with

$$\widehat{\beta} = \frac{igk^2}{\omega} - \frac{3i\omega^3}{g}, \tag{B.5.5}$$

$$\bar{\beta} = -\frac{2ig}{\omega}. \tag{B.5.6}$$

Appendix C

Second-order MSE

C.1 Derivation of the second-order MSE

ψ satisfies

$$\nabla^2\psi + \frac{\partial^2\psi}{\partial z^2} = 0, \quad -h(x,y) < z < 0, \tag{C.1.1}$$

$$\frac{\partial\psi}{\partial z} = -\nabla\psi\cdot\nabla h, \quad z = -h(x,y), \tag{C.1.2}$$

$$\frac{\partial\psi}{\partial z} - \frac{4\omega^2}{g}\psi = F, \quad z = 0, \tag{C.1.3}$$

Let us introduce

$$f_m = \frac{\cos\kappa_m(z+h)}{\cos\kappa_m h} \tag{C.1.4}$$

which satisfies

$$\frac{\partial^2 f_m}{\partial z^2} + \kappa_m^2 f_m = 0, \quad -h < z < 0, \tag{C.1.5}$$

$$\frac{\partial f_m}{\partial z} = 0, \quad z = -h, \tag{C.1.6}$$

$$\frac{\partial f_m}{\partial z} - \frac{4\omega^2}{g} f_m = 0, \quad z = 0. \tag{C.1.7}$$

where κ_m, $m = 1, 2, \ldots$ are the real roots of the equation

$$-4\omega^2 = g\kappa_m \tan\kappa_m h, \quad (m - 1/2)\,\pi \le \kappa_m h \le m\pi, \tag{C.1.8}$$

and κ_0 are

$$\kappa_0 = i\widehat{k}, \tag{C.1.9}$$

with $\widehat{\kappa}_0$ being the real root of the dispersion equation

$$4\omega^2 = g\widehat{\kappa}_0 \tanh \widehat{\kappa}_0 h. \tag{C.1.10}$$

Applying Green's formula to f_m and ψ, we obtain

$$\int_{-h}^{0} \left(\psi \frac{\partial^2 f_m}{\partial z^2} - f_m \frac{\partial^2 \psi}{\partial z^2} \right) dz = \left(\psi \frac{\partial f_m}{\partial z} - f_m \frac{\partial \psi}{\partial z} \right)_{z=-h}^{z=0}, \tag{C.1.11}$$

Putting Eqns. (C.1.1)-(C.1.7) into Eqn.(C.1.11), the preceding equation becomes

$$\int_{-h}^{0} \left(-\psi \kappa_m^2 f_m + f_m \nabla^2 \psi \right) dz = -\left(f_m \right)_{z=0} F - \left(f_m \nabla \psi \cdot \nabla h \right)_{z=-h}. \tag{C.1.12}$$

We then assume

$$\psi = -\frac{ig}{2\omega} \sum_{\ell=0}^{\infty} \xi_\ell(x,y) f_\ell(x,y,z). \tag{C.1.13}$$

Note that h is a function of x, y, so f_m is function of x, y and z. Taking the derivative of Ψ, we obtain $\nabla\psi$ and $\nabla^2\psi$

$$\nabla \psi = -\frac{ig}{2\omega} \sum_{\ell=0}^{\infty} \left(\xi_\ell \frac{\partial f_\ell}{\partial h} \nabla h + f_\ell \nabla \xi_\ell \right), \tag{C.1.14}$$

$$\nabla^2 \psi = -\frac{ig}{2\omega} \sum_{\ell=0}^{\infty} \left[\xi_\ell \frac{\partial f_\ell}{\partial h} \nabla^2 h + \xi_\ell \frac{\partial^2 f_\ell}{\partial h^2} (\nabla h)^2 + f_\ell \nabla^2 \xi_\ell + 2 \nabla \xi_\ell \frac{\partial f_\ell}{\partial h} \nabla h \right]. \tag{C.1.15}$$

Putting ψ, $\nabla\psi$ and $\nabla^2\psi$ into Eqn. (C.1.12), we get

$$\begin{aligned} \sum_{\ell=0}^{\infty} \Bigg\{ & -\xi_\ell \kappa_m^2 g \int_{-h}^{0} f_m f_\ell dz + \xi_\ell g \int_{-h}^{0} f_m \frac{\partial f_\ell}{\partial h} \nabla^2 h dz + \xi_\ell g \int_{-h}^{0} f_m \frac{\partial^2 f_\ell}{\partial h^2} (\nabla h)^2 dz \\ & + \left(\nabla^2 \xi_\ell \right) g \int_{-h}^{0} f_m f_\ell dz + \left(\nabla \xi_\ell \right) \cdot \left(g \int_{-h}^{0} 2 f_m \frac{\partial f_\ell}{\partial h} \nabla h dz \right) \Bigg\} \\ = & -2i\omega F - \sum_{\ell=0}^{\infty} \left\{ \left[\xi_\ell g f_m \frac{\partial f_\ell}{\partial h} (\nabla h)^2 + \left(\nabla \xi_\ell \right) \cdot \left(g f_m f_\ell \nabla h \right) \right]_{z=-h} \right\}. \end{aligned} \tag{C.1.16}$$

By Leibniz's rule,

$$\begin{aligned}\nabla\cdot\left(\int_{-h}^{0}f_mf_\ell\nabla\xi_\ell dz\right)=&\int_{-h}^{0}f_mf_\ell\nabla^2\xi_\ell dz+\int_{-h}^{0}f_m\frac{\partial f_\ell}{\partial h}\nabla h\cdot\nabla\xi_\ell dz\\&++\int_{-h}^{0}f_\ell\frac{\partial f_m}{\partial h}\nabla h\cdot\nabla\xi_\ell dz\left(f_\ell f_m\nabla\xi_\ell\cdot\nabla h\right)_{z=-h},\end{aligned}\tag{C.1.17}$$

Eqn. (C.1.16) can be written as

$$\begin{aligned}\sum_{\ell=0}^{\infty}\Bigg\{&\xi_\ell\left(-\kappa_m^2g\int_{-h}^{0}f_mf_\ell dz\right)+\nabla\cdot\left[(\nabla\xi_\ell)\left(g\int_{-h}^{0}f_mf_\ell dz\right)\right]\\&+\int_{-h}^{0}g\left(f_m\frac{\partial f_\ell}{\partial h}-f_\ell\frac{\partial f_m}{\partial h}\right)\nabla h\cdot\nabla\xi_\ell dz+\int_{-h}^{0}gf_m\frac{\partial f_\ell}{\partial h}\xi_\ell\nabla^2h\\&+\int_{-h}^{0}gf_m\xi_\ell\frac{\partial^2f_\ell}{\partial h^2}(\nabla h)^2dz+g\left[f_m\xi_\ell\frac{\partial f_\ell}{\partial h}(\nabla h)^2\right]_{z=-h}\Bigg\}=-i2\omega F,\end{aligned}\tag{C.1.18}$$

where

$$f_n(0)=1$$

is applied. Let us denote Eqn. (C.1.18) as

$$\sum_{\ell=0}^{\infty}\left\{\nabla\cdot(A_{m,\ell}\nabla\xi_\ell)+B_{m,\ell}\nabla h\cdot\nabla\xi_\ell+C_{m,\ell}\xi_\ell\right\}=-i2\omega F,\tag{C.1.19}$$

where

$$A_{m,\ell}=g\int_{-h}^{0}\left(f_mf_\ell\right)dz,\tag{C.1.20}$$

$$B_{m,\ell}=g\left(U_{m,\ell}-U_{\ell,m}\right)\tag{C.1.21}$$

with

$$U_{m,\ell}=\int_{-h}^{0}\left(f_m\frac{\partial f_\ell}{\partial h}\right)dz,\tag{C.1.22}$$

and

$$C_{m,\ell}=-\kappa_m^2A_{m,\ell}+gU_{m,\ell}\nabla^2h+gV_{m,\ell}\left(\nabla h\right)^2\tag{C.1.23}$$

with the $A_{m,\ell}$ being Eq. (C.1.20), $U_{m,\ell}$ being Eq. (C.1.22) and

$$V_{m,\ell} = \int_{-h}^{0} \left(f_m \frac{\partial^2 f_\ell}{\partial h^2} \right) dz + \left[f_m \frac{\partial f_\ell}{\partial h} \right]_{z=-h}. \tag{C.1.24}$$

Using Leibniz's rule, we can rewrite $V_{m,\ell}$ as

$$\begin{aligned} V_{m,\ell} &= \frac{\partial}{\partial h} \int_{-h}^{0} \left(f_m \frac{\partial f_\ell}{\partial h} \right) dz - \int_{-h}^{0} \left(\frac{\partial f_m}{\partial h} \frac{\partial f_\ell}{\partial h} \right) dz \\ &= \frac{\partial U_{m,\ell}}{\partial h} - \int_{-h}^{0} \left(\frac{\partial f_m}{\partial h} \frac{\partial f_\ell}{\partial h} \right) dz. \end{aligned} \tag{C.1.25}$$

Now let us obtain $A_{m,\ell}$, $B_{m,\ell}$, $C_{m,\ell}$ as follows. Due to the orthogonality of functions f_m and f_ℓ, $A_{m,\ell}$ is simply

$$A_{m,\ell} = \begin{cases} \frac{gh}{2\cos^2 \kappa_\ell h} \left(1 + \frac{\sin 2\kappa_\ell h}{2\kappa_\ell h} \right) & \text{if, } m = l \\ 0 & \text{if , } m \neq l \end{cases} \tag{C.1.26}$$

By inspecting Eq. (C.1.21), it is obvious that the $B_{m,\ell}$ is zero when $m = \ell$. Therefore, the $B_{m,\ell}$ is

$$B_{m,\ell} = \begin{cases} 0 & \text{when, } m = \ell, \\ g\left(U_{m,\ell} - U_{\ell,m} \right), & \text{when, } m \neq \ell. \end{cases} \tag{C.1.27}$$

with $U_{m,\ell}$, Eq.(C.1.22), being obtained as follows (see Appendix C.4 for details). For $m = \ell$,

$$U_{m,m} = \frac{\sin 2\kappa_m h - 2\kappa_m h \cos 2\kappa_m h}{4\cos^2 (\kappa_m h) \left(2\kappa_m h + \sin 2\kappa_m h \right)}, \tag{C.1.28}$$

for $m \neq \ell$,

$$U_{m,\ell} = -\frac{\kappa_\ell^2}{\cos \kappa_m h \cos \kappa_\ell h \left(\kappa_\ell^2 - \kappa_m^2 \right)}. \tag{C.1.29}$$

Furthermore, $C_{m,\ell}$ is obtained as follows.

$$C_{m,\ell} = \begin{cases} -\kappa_m^2 A_{m,m} + g U_{m,m} \nabla^2 h + g V_{m,m} \left(\nabla h \right)^2, & \text{if, } m = l \\ g U_{m,\ell} \nabla^2 h + g V_{m,\ell} \left(\nabla h \right)^2, & \text{if , } m \neq l \end{cases} \tag{C.1.30}$$

with $U_{m,\ell}$ being Eq. (C.1.28) and (C.4.7) and $V_{m,\ell}$ being the following equations. For $m = \ell$,

$$V_{m,m} = \frac{-\kappa_m \sec^2(\kappa_m h)}{12\left(2\kappa_m h + \sin 2\kappa_m h\right)^3}\left[\left(2\kappa_m h\right)^4 + 4\left(2\kappa_m h\right)^3 \sin 2\kappa_m h + 9\sin\left(2\kappa_m h\right)\sin 4\kappa_m h\right.$$
$$\left. -12\kappa_m h\left(\kappa_m h + \sin 2\kappa_m h\right)\left(\cos^2 2\kappa_m h - 2\cos 2\kappa_m h + 3\right)\right], \tag{C.1.31}$$

For $m \neq \ell$,

$$V_{m,\ell} = \frac{-2\kappa_\ell \sec\kappa_m h \sec\kappa_\ell h}{\left(2\kappa_\ell h + \sin 2\kappa_\ell h\right)} \frac{\left[4\kappa_\ell^2\kappa_m^2 + \left(\kappa_\ell^4 - \kappa_m^4\right)\sin^2\kappa_\ell h\right]}{\left(\kappa_\ell^2 - \kappa_m^2\right)^2}. \tag{C.1.32}$$

C.2 Derivation of $\frac{\partial\kappa_m}{\partial h}$

κ_m satisfies

$$\frac{\omega^2}{g} = -\kappa_m \tan\kappa_m h. \tag{C.2.1}$$

Taking the derivative of the preceding equation in respect with h, we obtain

$$\begin{aligned} 0 &= \frac{\partial\kappa_m}{\partial h}\tan\kappa_m h + \kappa_m\left(h\frac{\partial\kappa_m}{\partial h} + \kappa_m\right)\frac{1}{\cos^2\kappa_m h} \\ &= \frac{\partial\kappa_m}{\partial h}\left[\frac{\kappa_m h}{\cos^2\kappa_m h} + \tan\kappa_m h\right] + \frac{\kappa_m^2}{\cos^2\kappa_m h}. \end{aligned} \tag{C.2.2}$$

Therefore,

$$\frac{\partial\kappa_m}{\partial h} = -\frac{2\kappa_m^2}{2\kappa_m h + \sin 2\kappa_m h}. \tag{C.2.3}$$

C.3 Derivation of $\frac{\partial f_m}{\partial h}$

f_m is defined as

$$f_m = \frac{\cos\kappa_m\left(z + h\right)}{\cos\kappa_m h}. \tag{C.3.1}$$

Taking the derivative of the preceding equation in respect with h, we obtain

$$\begin{aligned}\frac{\partial f_m}{\partial h} &= -\left[\frac{\partial \kappa_m}{\partial h}(z+h)+\kappa_m\right]\frac{\sin\kappa_m(z+h)}{\cos\kappa_m h}+\left(\frac{\partial \kappa_m}{\partial h}h+\kappa_m\right)\frac{\cos\kappa_m(z+h)}{\cos^2\kappa_m h}\sin\kappa_m h \\ &= \frac{1}{\cos\kappa_m h}\frac{\partial\kappa_m}{\partial h}\left[-(z+h)\sin\kappa_m(z+h)+h\sin\kappa_m h\frac{\cos\kappa_m(z+h)}{\cos\kappa_m h}\right] \\ &\quad+\frac{1}{\cos\kappa_m h}\frac{\partial\kappa_m}{\partial h}\frac{\kappa_m}{(\partial\kappa_m/\partial h)}\left[-\sin\kappa_m(z+h)+\sin\kappa_m h\frac{\cos\kappa_m(z+h)}{\cos\kappa_m h}\right].\end{aligned} \tag{C.3.2}$$

Making use of Eqn. (C.2.3), we obtain

$$\frac{\kappa_m}{(\partial\kappa_m/\partial h)} = -\left(\frac{\sin\kappa_m h\cos\kappa_m h}{\kappa_m}+h\right). \tag{C.3.3}$$

Putting the preceding equation into Eqn. (C.3.2), we get

$$\begin{aligned}\frac{\partial f_m}{\partial h} = \frac{1}{\cos\kappa_m h}\frac{\partial\kappa_m}{\partial h}\Big\{&-z\sin\kappa_m(z+h)+\frac{\sin\kappa_m h}{\kappa_m}\left[\cos\kappa_m h\sin\kappa_m(z+h)\right.\\ &\left.-\cos\kappa_m(z+h)\sin\kappa_m h\right]\Big\}.\end{aligned} \tag{C.3.4}$$

Since

$$\sin(z_1-z_2)=\sin z_1\cos z_2-\cos z_1\sin z_2, \tag{C.3.5}$$

we obtain

$$\frac{\partial f_m}{\partial h} = \frac{1}{\cos\kappa_m h}\frac{\partial\kappa_m}{\partial h}\left[-z\sin\kappa_m(z+h)+\frac{\sin\kappa_m h\sin\kappa_m z}{\kappa_m}\right]. \tag{C.3.6}$$

C.4 Derivation of $U_{m,\ell}$

Let us recall that $U_{m,\ell}$, Eq. (C.1.22), is defined as

$$U_{m,\ell}=\int_{-h}^{0} f_m\frac{\partial f_\ell}{\partial h}dz. \tag{C.4.1}$$

For $m = \ell$,

$$\begin{aligned} U_{m,m} &= \int_{-h}^{0} f_m \frac{\partial f_m}{\partial h} dz \\ &= \left(\frac{\partial \kappa_m}{\partial h}\right) \frac{1}{\cos^2 \kappa_m h} \int_{-h}^{0} \left[-z \sin \kappa_m (z+h) \cos \kappa_m (z+h)\right] dz \\ &\quad + \left(\frac{\partial \kappa_m}{\partial h}\right) \frac{\sin \kappa_m h}{\kappa_m \cos^2 \kappa_m h} \int_{-h}^{0} \left[\sin \kappa_m z \cos \kappa_m (z+h)\right] dz \\ &= \frac{\sin 2\kappa_m h - 2\kappa_m h \cos 2\kappa_m h}{4 \cos^2 (\kappa_m h) (2\kappa_m h + \sin 2\kappa_m h)}. \end{aligned} \tag{C.4.2}$$

For $m \neq \ell$,

$$\begin{aligned} U_{m,\ell} &= \int_{-h}^{0} f_m \frac{\partial f_\ell}{\partial h} dz \\ &= \left(\frac{\partial \kappa_\ell}{\partial h}\right) \frac{1}{\cos \kappa_m h \cos \kappa_\ell h} \int_{-h}^{0} \left[-z \sin \kappa_\ell (z+h) \cos \kappa_m (z+h)\right] dz \\ &\quad + \left(\frac{\partial \kappa_\ell}{\partial h}\right) \frac{1}{\cos \kappa_m h \cos \kappa_\ell h} \frac{\sin \kappa_\ell h}{\kappa_\ell} \int_{-h}^{0} \left[\sin \kappa_\ell z \cos \kappa_m (z+h)\right] dz \end{aligned} \tag{C.4.3}$$

with

$$\frac{\partial \kappa_\ell}{\partial h} = -\frac{2\kappa_\ell^2}{\sin 2\kappa_\ell h + 2\kappa_\ell h}. \tag{C.4.4}$$

Let us define $L_{m,\ell}$ to be

$$L_{m,\ell} = \int_{-h}^{0} \left[-z \sin \kappa_\ell (z+h) \cos \kappa_m (z+h)\right] dz, \tag{C.4.5}$$

and $\widehat{L}_{m,\ell}$ to be

$$\widehat{L}_{m,\ell} = \frac{\sin \kappa_\ell h}{\kappa_\ell} \int_{-h}^{0} \left[\sin \kappa_\ell z \cos \kappa_m (z+h)\right] dz, \tag{C.4.6}$$

so that $U_{m,\ell}$ can be written as

$$U_{m,\ell} = -\left(\frac{2\kappa_\ell^2}{\sin 2\kappa_\ell h + 2\kappa_\ell h}\right) \frac{L_{m,\ell} + \widehat{L}_{m,\ell}}{\cos \kappa_\ell h \cos \kappa_m h}. \tag{C.4.7}$$

After evaluating the integrals of $L_{m,\ell}$ and $\widehat{L}_{m,\ell}$, we got

$$L_{m,\ell} = \frac{1}{2}\left[-\frac{\sin\left(\kappa_\ell + \kappa_m\right)h}{\left(\kappa_\ell + \kappa_m\right)^2} - \frac{\sin\left(\kappa_\ell - \kappa_m\right)h}{\left(\kappa_\ell - \kappa_m\right)^2} + \frac{2\kappa_\ell h}{\kappa_\ell^2 - \kappa_m^2}\right], \tag{C.4.8}$$

and

$$\widehat{L}_{m,\ell} = \frac{\sin\kappa_\ell h\left(\cos\kappa_\ell h - \cos\kappa_m h\right)}{\kappa_\ell^2 - \kappa_m^2}. \tag{C.4.9}$$

Thus

$$\begin{aligned} L_{m,\ell} + \widehat{L}_{m,\ell} =& \frac{4\kappa_\ell\left(-\kappa_\ell \sin\kappa_\ell h\cos\kappa_m h + \kappa_m\cos\kappa_\ell h\sin\kappa_m h\right)}{2\left(\kappa_\ell^2 - \kappa_m^2\right)^2} \\ &+ \frac{\left(\kappa_\ell^2 - \kappa_m^2\right)\left(2\kappa_\ell h + \sin 2\kappa_\ell h\right)}{2\left(\kappa_\ell^2 - \kappa_m^2\right)^2}, \end{aligned} \tag{C.4.10}$$

so

$$\frac{L_{m,\ell} + \widehat{L}_{m,\ell}}{\cos\kappa_m h\cos\kappa_\ell h} = \frac{2\kappa_\ell\left(-\kappa_\ell\tan\kappa_\ell h + \kappa_m\tan\kappa_m h\right)}{\left(\kappa_\ell^2 - \kappa_m^2\right)^2} + \frac{\left(2\kappa_\ell h + \sin 2\kappa_\ell h\right)}{2\left(\kappa_\ell^2 - \kappa_m^2\right)}. \tag{C.4.11}$$

Since k_m and k_ℓ satisfy Eq. (C.2.1), Eq. (C.4.11) becomes

$$\frac{L_{m,\ell} + \widehat{L}_{m,\ell}}{\cos\kappa_m h\cos\kappa_\ell h} = \frac{\left(2\kappa_\ell h + \sin 2\kappa_\ell h\right)}{2\cos\kappa_m h\cos\kappa_\ell h\left(\kappa_\ell^2 - \kappa_m^2\right)}. \tag{C.4.12}$$

Putting the preceding equation into Eq. (C.4.7), we then obtain

$$U_{m,\ell} = -\frac{\kappa_\ell^2}{\cos\kappa_m h\cos\kappa_\ell h\left(\kappa_\ell^2 - \kappa_m^2\right)}. \tag{C.4.13}$$

In summary, $U_{m,\ell}$ is

$$U_{m,m} = \frac{\sin 2\kappa_m h - 2\kappa_m h\cos 2\kappa_m h}{4\cos^2\left(\kappa_m h\right)\left(2\kappa_m h + \sin 2\kappa_m h\right)} \quad , m = \ell, \tag{C.4.14}$$

$$U_{m,\ell} = -\frac{\kappa_\ell^2}{\cos\kappa_m h\cos\kappa_\ell h\left(\kappa_\ell^2 - \kappa_m^2\right)}, \quad , m \neq \ell. \tag{C.4.15}$$

C.5 Derivation of $V_{m,\ell}$

From Eq. (C.1.25), $V_{m,\ell}$ is defined as

$$V_{m,\ell} = \frac{\partial U_{m,\ell}}{\partial h} - \int_{-h}^{0} \left(\frac{\partial f_m}{\partial h} \frac{\partial f_\ell}{\partial h} \right) dz. \tag{C.5.1}$$

For $m = \ell$,

$$\begin{aligned} \frac{\partial U_{m,m}}{\partial h} &= \frac{\partial}{\partial h} \left[\frac{\sin 2\kappa_m h - 2\kappa_m h \cos 2\kappa_m h}{4\cos^2(\kappa_m h)\,(2\kappa_m h + \sin 2\kappa_m h)} \right] \\ &= \frac{\kappa_m \sec^2 \kappa_m h}{4\,(2\kappa_m h + \sin 2\kappa_m h)^3} \left\{ 4\kappa_m h \sin^2 2\kappa_m h\,(2\kappa_m h + \sin 2\kappa_m h) \right. \\ &\quad + 2\,(\sin 2\kappa_m h - 2\kappa_m h \cos 2\kappa_m h) \left[2\sin^2 \kappa_m h\,(2\kappa_m h + \sin 2\kappa_m h) \right. \\ &\quad \left. \left. - \sin 2\kappa_m h\,(1 + \cos 2\kappa_m h) \right] \right\}, \end{aligned} \tag{C.5.2}$$

$$\begin{aligned} -\int_{-h}^{0} \left(\frac{\partial f_m}{\partial h} \frac{\partial f_m}{\partial h} \right) dz = \frac{\kappa_m \sec^2 \kappa_m h}{12\,(2\kappa_m h + \sin 2\kappa_m h)^2} \left[-3\,(2\kappa_m h)^2 \sin(2\kappa_m h) \right. \\ \left. + 12\kappa_m h - 3\sin(4\kappa_m h) - (2\kappa_m h)^3 \right]. \end{aligned} \tag{C.5.3}$$

Therefore, combining Eqns. (C.5.2) and (C.5.3), we obtain

$$\begin{aligned} V_{m,m} &= \frac{\partial U_{m,m}}{\partial h} - \int_{-h}^{0} \left(\frac{\partial f_m}{\partial h} \frac{\partial f_m}{\partial h} \right) dz \\ &= \frac{-\kappa_m \sec^2(\kappa_m h)}{12\,(2\kappa_m h + \sin 2\kappa_m h)^3} \left[(2\kappa_m h)^4 + 4\,(2\kappa_m h)^3 \sin 2\kappa_m h \right. \\ &\quad + 9\sin(2\kappa_m h) \sin 4\kappa_m h - 12\kappa_m h\,(\kappa_m h + \sin 2\kappa_m h) \times \\ &\quad \left. \left(\cos^2 2\kappa_m h - 2\cos 2\kappa_m h + 3 \right) \right]. \end{aligned} \tag{C.5.4}$$

For $m \neq \ell$,

$$\begin{aligned} \frac{\partial U_{m,\ell}}{\partial h} &= \frac{\partial}{\partial h} \left[-\frac{\kappa_\ell^2}{\cos \kappa_m h \cos \kappa_\ell h\,(\kappa_\ell^2 - \kappa_m^2)} \right] \\ &= \frac{4\kappa_\ell^2 \kappa_m^2 \sec \kappa_m h \sec \kappa_\ell h}{(\kappa_\ell^2 - \kappa_m^2)^2} \left[-\frac{\kappa_\ell}{2\kappa_\ell h + \sin 2\kappa_\ell h} + \frac{\kappa_m}{2\kappa_m h + \sin 2\kappa_m h} \right] \\ &\quad - \frac{\kappa_\ell^2 \sec \kappa_m h \sec \kappa_\ell h}{(\kappa_\ell^2 - \kappa_m^2)} \left[\frac{2\kappa_m \sin^2 \kappa_m h}{2\kappa_m h + \sin 2\kappa_m h} + \frac{2k_\ell \sin^2 \kappa_\ell h}{2\kappa_\ell h + \sin 2\kappa_\ell h} \right], \end{aligned} \tag{C.5.5}$$

or equivalently,

$$\begin{aligned}\frac{\partial U_{m,\ell}}{\partial h} = &\frac{\sec\kappa_m h \sec\kappa_\ell h}{\left(\kappa_\ell^2-\kappa_m^2\right)^2\left(2\kappa_\ell h+\sin 2\kappa_\ell h\right)\left(2k_m h+\sin 2k_m h\right)}\left\{-4\kappa_\ell^3\kappa_m^2\sin 2\kappa_m h\right.\\ &+4\kappa_\ell^2\kappa_m^3\sin 2\kappa_\ell h-2\kappa_\ell^5\sin^2\kappa_\ell h\sin 2\kappa_m h+2\kappa_\ell^3\kappa_m^2\sin^2\kappa_\ell h\sin 2\kappa_m h\\ &-4\kappa_\ell^5\kappa_m h\sin^2\kappa_\ell h+4\kappa_\ell^3\kappa_m^3 h\sin^2\kappa_\ell h-4\kappa_\ell^5\kappa_m h\sin^2\kappa_m h+4\kappa_\ell^3\kappa_m^3 h\sin^2\kappa_m h\\ &\left.-2\kappa_\ell^4\kappa_m\sin^2\kappa_m h\sin 2\kappa_\ell h+2\kappa_\ell^2\kappa_m^3\sin^2\kappa_m h\sin 2\kappa_\ell h\right\}\end{aligned} \tag{C.5.6}$$

and

$$\begin{aligned}-\int_{-h}^{0}\left(\frac{\partial f_m}{\partial h}\frac{\partial f_\ell}{\partial h}\right)dz = &\frac{\sec\kappa_m h\sec\kappa_\ell h}{\left(\kappa_\ell^2-\kappa_m^2\right)^2\left(2\kappa_\ell h+\sin 2\kappa_\ell h\right)\left(2k_m h+\sin 2k_m h\right)}\times\\ &\left\{-16\kappa_m^3\kappa_\ell^3 h-2\kappa_m^3\kappa_\ell^2\sin^2\kappa_m h\sin 2\kappa_\ell h+2\kappa_\ell^4\kappa_m\sin^2\kappa_m h\sin 2\kappa_\ell h\right.\\ &-2\kappa_\ell^3\kappa_m^2\sin^2\kappa_\ell h\sin 2\kappa_m h+2\kappa_\ell\kappa_m^4\sin^2\kappa_\ell h\sin 2\kappa_m h\\ &-4\kappa_\ell^3\kappa_m^3 h\sin^2\kappa_m h+4\kappa_\ell^5\kappa_m h\sin^2\kappa_m h-4\kappa_\ell^3\kappa_m^2\sin 2\kappa_m h\\ &\left.+4\kappa_\ell\kappa_m^5 h\sin^2\kappa_\ell h-4\kappa_\ell^3\kappa_m^3 h\sin^2\kappa_\ell h-4\kappa_\ell^2\kappa_m^3\sin 2\kappa_\ell h\right\}.\end{aligned} \tag{C.5.7}$$

Combining Eqns. (C.5.6) and (C.5.7), we obtain

$$\begin{aligned}V_{m,\ell} &= \frac{\partial U_{m,\ell}}{\partial h}-\int_{-h}^{0}\left(\frac{\partial f_m}{\partial h}\frac{\partial f_\ell}{\partial h}\right)dz\\ &= \frac{\sec\kappa_m h\sec\kappa_\ell h}{\left(\kappa_\ell^2-\kappa_m^2\right)^2\left(2k_\ell h+\sin 2k_\ell h\right)\left(2k_m h+\sin 2k_m h\right)}\left\{-8\kappa_\ell^3\kappa_m^2\sin 2\kappa_m h\right.\\ &\quad -2\kappa_\ell^5\sin^2\kappa_\ell h\sin 2\kappa_m h-4\kappa_\ell^5\kappa_m h\sin^2\kappa_\ell h-16\kappa_m^3\kappa_\ell^3 h\\ &\quad \left.+2\kappa_\ell\kappa_m^4\sin^2\kappa_\ell h\sin 2\kappa_m h+4\kappa_\ell\kappa_m^5 h\sin^2\kappa_\ell h\right\},\end{aligned} \tag{C.5.8}$$

or equivalently,

$$\begin{aligned}V_{m,\ell} &= \frac{\partial U_{m,\ell}}{\partial h}-\int_{-h}^{0}\left(\frac{\partial f_m}{\partial h}\frac{\partial f_\ell}{\partial h}\right)dz\\ &= \frac{-2\kappa_\ell\sec\kappa_m h\sec\kappa_\ell h}{\left(2\kappa_\ell h+\sin 2\kappa_\ell h\right)}\frac{\left[4\kappa_\ell^2\kappa_m^2+\left(\kappa_\ell^4-\kappa_m^4\right)\sin^2\kappa_\ell h\right]}{\left(\kappa_\ell^2-\kappa_m^2\right)^2}.\end{aligned} \tag{C.5.9}$$

Appendix D

Fourier expression for $\mathcal{Q}$

To calculate the forcing function $\mathcal{Q}$,

$$\mathcal{Q}(r,\theta) = \widehat{\beta}\left[2\eta^{(T)} + \eta^{(S)}\right]\eta^{(S)} + \bar{\beta}\left[2\nabla\eta^{(T)} + \nabla\eta^{(S)}\right]\nabla\eta^{(S)}, \tag{D.1.1}$$

we shall first abbreviate the first-order progressive waves as

$$\eta^{(T)} = \sum_{m=-\infty}^{\infty} T_m(r)e^{im\theta}, \tag{D.1.2}$$

with

$$T_m(r) = Ai^m J_m(kr)\cos m\theta_I, \tag{D.1.3}$$

and the first-order scattered waves as

$$\eta^{(S)} = \sum_{m=-\infty}^{\infty} S_m(r)e^{im\theta}, \tag{D.1.4}$$

where

$$S_m(r) = i^m \alpha_m H_m(kr), \tag{D.1.5}$$

and T_m, S_m, α_m are even in m.

We now calculate $\mathcal{Q}$ according to Eq. (D.1.1). Each quadratic product in Eq.

(4.3.3) are obtained as follows

$$\eta^{(T)}\eta^{(S)} = \sum_{m=-\infty}^{\infty} T_m e^{im\theta} \sum_{n=-\infty}^{\infty} S_n e^{in\theta} = \sum_{m=-\infty}^{\infty} \left[\sum_{n=-\infty}^{\infty} T_{m-n} S_n \right] e^{im\theta}, \tag{D.1.6}$$

$$\eta^{(S)}\eta^{(S)} = \sum_{m=-\infty}^{\infty} S_m e^{im\theta} \sum_{n=-\infty}^{\infty} S_n e^{in\theta} = \sum_{m=-\infty}^{\infty} \left[\sum_{n=-\infty}^{\infty} S_{m-n} S_n \right] e^{im\theta}, \tag{D.1.7}$$

$$\begin{aligned} \nabla\eta^{(T)}\nabla\eta^{(S)} &= \sum_{m=-\infty}^{\infty} \frac{\partial T_m}{\partial r} e^{im\theta} \sum_{n=-\infty}^{\infty} \frac{\partial S_n}{\partial r} e^{in\theta} + \frac{1}{r^2} \sum_{m=-\infty}^{\infty} T_m \frac{\partial e^{im\theta}}{\partial \theta} \sum_{n=-\infty}^{\infty} S_n \frac{\partial e^{in\theta}}{\partial \theta} \\ &= \sum_{m=-\infty}^{\infty} \left[\sum_{n=-\infty}^{\infty} \frac{\partial T_{m-n}}{\partial r} \frac{\partial S_n}{\partial r} \right] e^{im\theta} - \frac{(m-n)n}{r^2} \left[\sum_{n=-\infty}^{\infty} T_{m-n} S_n \right] e^{im\theta}, \end{aligned} \tag{D.1.8}$$

$$\begin{aligned} \nabla\eta^{(S)}\nabla\eta^{(S)} &= \sum_{m=-\infty}^{\infty} \frac{\partial S_m}{\partial r} e^{im\theta} \sum_{n=-\infty}^{\infty} \frac{\partial S_n}{\partial r} e^{in\theta} + \frac{1}{r^2} \sum_{m=-\infty}^{\infty} S_m \frac{\partial e^{im\theta}}{\partial \theta} \sum_{n=-\infty}^{\infty} S_n \frac{\partial e^{in\theta}}{\partial \theta} \\ &= \sum_{m=-\infty}^{\infty} \left[\sum_{n=-\infty}^{\infty} \frac{\partial S_{m-n}}{\partial r} \frac{\partial S_n}{\partial r} \right] e^{im\theta} - \frac{(m-n)n}{r^2} \left[\sum_{n=-\infty}^{\infty} S_{m-n} S_n \right] e^{im\theta}. \end{aligned} \tag{D.1.9}$$

It follows that $\mathcal{Q}$ can be expressed as a Fourier series

$$\mathcal{Q}(r,\theta) = \sum_{m=-\infty}^{\infty} \mathcal{Q}_m(r) e^{im\theta}, \tag{D.1.10}$$

or equivalently

$$\mathcal{Q}(r,\theta) = \sum_{m=0}^{\infty} \epsilon_m \mathcal{Q}_m(r) \cos m\theta, \tag{D.1.11}$$

with

$$\begin{aligned} \mathcal{Q}_m(r) = \sum_{n=-\infty}^{\infty} \Bigg\{ &\left[\widehat{\beta} - \frac{n(m-n)}{r^2} \bar{\beta} \right] S_n \left(2T_{m-n} + S_{m-n} \right) \\ &+ \bar{\beta} \frac{\partial S_n}{\partial r} \left(2\frac{\partial T_{m-n}}{\partial r} + \frac{\partial S_{m-n}}{\partial r} \right) \Bigg\}. \end{aligned} \tag{D.1.12}$$

Appendix E

Equivalence to Stokes waves

We show here that Eqs. (4.4.7) and (4.4.8) are equivalent to Stokes waves of the following standard form:

$$\begin{pmatrix} \Phi_2^I \\ \Phi_2^R \end{pmatrix}_{Stokes} = -\frac{3i\omega}{4}\frac{\cosh 2k\,(z+h)}{\sinh^4 kh}\frac{A^2}{4}e^{i2kr\cos(\theta\mp\theta_I)-2i\omega t} + *, \tag{E.1.1}$$

$$\begin{aligned}\left(\Phi_2^{IR}\right)_{Stokes} = &-\frac{iA^2\omega}{2g}\frac{1+2\cos 2\theta_I - 3\tanh^2 kh}{\tanh kh\left[2\cos\theta_I \tanh\left(2kh\cos\theta_I\right) - 4\tanh kh\right]}\times \\ &\frac{\cosh\left[2k(z+h)\cos\theta_I\right]}{\cosh\left(2kh\cos\theta_I\right)}e^{i2kr\cos\theta_I\cos\theta-2i\omega t} + *.\end{aligned} \tag{E.1.2}$$

To show this we first get from (3.2.3),

$$\widehat{\beta} - \bar{\beta}k^2 = \frac{3\omega k}{\sinh kh\cosh kh}, \tag{E.1.3}$$

$$\widehat{\beta} - \bar{\beta}k^2\cos\left(2\theta_I\right) = \frac{ik\omega}{\tanh kh}\left[1+2\cos(2\theta_I) - 3\tanh^2 kh\right]. \tag{E.1.4}$$

The Stokes wave potential can be rewritten as

$$\begin{pmatrix} \Phi_2^I \\ \Phi_2^R \end{pmatrix}_{Stokes} = -\left[\frac{\cosh kh}{4k\sinh^3 kh}\cosh 2k\,(z+h)\right]\left(\widehat{\beta} - \bar{\beta}k^2\right)\frac{A^2}{4}e^{i2kr\cos(\theta-\theta_I)-2i\omega t} + *, \tag{E.1.5}$$

$$\left(\Phi_2^{IR}\right)_{Stokes} = -\frac{iA^2\omega}{2g}\frac{\widehat{\beta}-\bar{\beta}k^2\cos\left(2\theta_I\right)}{\left[2\cos\theta_I\tanh\left(2kh\cos\theta_I\right)-4\tanh kh\right]}\times \\ \frac{\cosh\left[2k(z+h)\cos\theta_I\right]}{\cosh\left(2kh\cos\theta_I\right)}e^{i2kr\cos\theta_I\cos\theta-2i\omega t}+*. \tag{E.1.6}$$

Let us expand $\cosh 2k(z+h)$ and $\cosh\left[2k(z+h)\cos\theta_I\right]$in terms of the vertical eigenfunctions

$$\cosh 2k\left(z+h\right)=\sum_{\ell=0}^{\infty}a_\ell f_\ell, \qquad \cosh\left[2k(z+h)\cos\theta_I\right]=\sum_{\ell=0}^{\infty}b_\ell f_\ell, \tag{E.1.7}$$

where

$$f_\ell=\frac{\cos k_\ell\left(z+h\right)}{\cos\kappa_\ell h}. \tag{E.1.8}$$

By using the orthogonality of f_ℓ, the dispersion relation as well as the identities

$$2\tanh 2kh-4\tanh kh=-\frac{4\sinh^3 kh}{\cosh kh\cosh 2kh}, \quad \kappa_\ell\tan\kappa_\ell h=-\frac{4\omega^2}{g}=-4k\tanh kh, \tag{E.1.9}$$

we obtain

$$a_\ell=-\frac{g}{A_{\ell,\ell}}\frac{4k\sinh^3 kh}{\cosh kh}\frac{1}{4k^2+\kappa_\ell^2}, \tag{E.1.10}$$

$$b_\ell=-\frac{g}{A_{\ell,\ell}}\frac{\left[2k\cos\theta_I\tanh\left(2kh\cos\theta_I\right)-4k\tanh kh\right]\cosh\left(2kh\cos\theta_I\right)}{\left(4k^2+\kappa_\ell^2\right)}, \tag{E.1.11}$$

where $A_{\ell,\ell}$ is given by (3.2.13). The equivalence of (E.1.5) and (4.4.7) and of (E.1.6) and (4.4.8) is evident.

Appendix F

Weak radiation condition for ξ_0^Q

F.1 Asymptotic behavior of ξ_0^Q

In order to verify the weak radiation condition and to ensure the convergence of certain infinite integrals, we need the asymptotic behavior of ξ_0^Q for $kr \gg 1$. Recall that ξ_0^Q satisfies the inhomogeneous Helmholtz equation, Eq. (4.2.10). The forcing terms $\mathcal{Q}$ involves the products of $\eta^{(T)}$ and $\eta^{(S)}$ and the products of their gradients. For large kr, the first-order scattered wave behaves as

$$\eta^{(S)} \approx \mathcal{F}(\theta)\frac{e^{ikr}}{\sqrt{kr}} \tag{F.1.1}$$

hence

$$\eta^{(S)}\eta^{(T)} = \frac{A}{2}\mathcal{F}\left\{\frac{e^{ikr[\cos(\theta-\theta_I)+1]}}{\sqrt{kr}} + \frac{e^{ikr[\cos(\theta+\theta_I)+1]}}{\sqrt{kr}}\right\}, \tag{F.1.2}$$

and

$$\begin{aligned}\nabla\eta^{(S)}\cdot\nabla\eta^{(T)} &\approx \frac{\partial\eta^{(S)}}{\partial r}\frac{\partial\eta^{(T)}}{\partial r} \\ &= \frac{A}{2}\mathcal{F}\left\{k^2\cos(\theta-\theta_I)\frac{e^{ikr[\cos(\theta-\theta_I)+1]}}{\sqrt{kr}} + k^2\cos(\theta+\theta_I)\frac{e^{ikr[\cos(\theta+\theta_I)+1]}}{\sqrt{kr}}\right\}.\end{aligned} \tag{F.1.3}$$

The remaining term is negligible because

$$\frac{1}{r^2}\frac{\partial \eta^{(S)}}{\partial \theta}\frac{\partial \eta^{(T)}}{\partial \theta} = O\left(r^{-3/2}\right). \tag{F.1.4}$$

It is easy to see that products of $\eta^{(S)}$ and itself is of the order $O\left(e^{ir2k}/kr\right)$. Therefore, $\mathcal{Q}$ is dominated by

$$\begin{aligned}\mathcal{Q} \approx & \left[\widehat{\beta} - \bar{\beta}k^2\cos\left(\theta-\theta_I\right)\right]\frac{A}{2}\mathcal{F}(\theta)\frac{e^{irk[\cos(\theta-\theta_I)+1]}}{\sqrt{kr}} \\ & + \left[\widehat{\beta} - \bar{\beta}k^2\cos\left(\theta+\theta_I\right)\right]\frac{A}{2}\mathcal{F}(\theta)\frac{e^{irk[\cos(\theta+\theta_I)+1]}}{\sqrt{kr}} + O((kr)^{-1}).\end{aligned} \tag{F.1.5}$$

From the governing Helmholtz equation Eq. (4.2.10), it can be seen that

$$\xi_0^Q \approx F(\theta)\frac{e^{ikr[\cos(\theta-\theta_I)+1]}}{\sqrt{kr}} + \widehat{F}(\theta)\frac{e^{ikr[\cos(\theta+\theta_I)+1]}}{\sqrt{kr}} \tag{F.1.6}$$

where $F(\theta)$ and $\widehat{F}(\theta)$ are known functions of θ.

F.2 Weak radiation condition

We show here that the following line integral vanishes

$$I = \int_{\partial F}\left(\xi_0^Q\frac{\partial G_0}{\partial r} - G_0\frac{\partial \xi_0^Q}{\partial r}\right)dS \to 0. \tag{F.2.1}$$

where ∂F is a semi-circle of unboundedly large radius.

Since G_0 satisfies the strong radiation condition,

$$G_0 \approx \frac{H(\theta)}{\left(\widehat{\kappa}_0 r\right)^{1/2}}e^{i\widehat{\kappa}_0 r} \tag{F.2.2}$$

Putting the asymptotic expressions of ξ_0^Q and G_0 into Eq. (F.2.1), we obtain for large

kr,

$$
\begin{aligned}
I &= \int_0^{\pi} r d\theta\, H(\theta) F(\theta) \frac{e^{i\widehat{\kappa}_0 r}}{\left(\widehat{\kappa}_0 r\right)^{1/2}} \frac{e^{irk[\cos(\theta-\theta_I)+1]}}{\sqrt{kr}} \left[-ik\cos\left(\theta-\theta_I\right) - ik + i\widehat{\kappa}_0\right] \\
&\quad + \int_0^{\pi} r d\theta\, H(\theta) \widehat{F}(\theta) \frac{e^{i\widehat{\kappa}_0 r}}{\left(\widehat{\kappa}_0 r\right)^{1/2}} \frac{e^{irk[\cos(\theta+\theta_I)+1]}}{\sqrt{kr}} \left[-ik\cos\left(\theta+\theta_I\right) - ik + i\widehat{\kappa}_0\right] \\
&= i\int_0^{\pi} d\theta \frac{H(\theta)}{\sqrt{\widehat{\kappa}_0}} \frac{F(\theta)}{\sqrt{k}} e^{ir[\widehat{\kappa}_0 + k\cos(\theta-\theta_I)+k]} \left[-k\cos\left(\theta-\theta_I\right) - k + \widehat{\kappa}_0\right] \\
&\quad + i\int_0^{\pi} d\theta \frac{H(\theta)}{\sqrt{\widehat{\kappa}_0}} \frac{\widehat{F}(\theta)}{\sqrt{k}} e^{ir[\widehat{\kappa}_0 + k\cos(\theta+\theta_I)+k]} \left\{-k\cos\left(\theta+\theta_I\right) - k + \widehat{\kappa}_0\right] .
\end{aligned}
\tag{F.2.3}
$$

For large r, we use the method of stationary phase, and let

$$
\varphi(\theta) = k\cos\left(\theta-\theta_I\right) + k + \widehat{\kappa}_0, \qquad \widehat{\varphi}(\theta) = k\cos\left(\theta+\theta_I\right) + k + \widehat{\kappa}_0, \tag{F.2.4}
$$

be the phase function. Since

$$
\varphi' = -k\sin\left(\theta-\theta_I\right), \quad \widehat{\varphi}' = -k\sin\left(\theta+\theta_I\right),
$$

and

$$
\pi < \theta_I < 2\pi,
$$

the stationary phase points are at

$$
\theta = \theta_0 = -\pi + \theta_I, \quad \varphi'' = -k\cos\left(\theta_0-\theta_I\right) = k,
$$

and

$$
\theta = \widehat{\theta}_0 = 2\pi - \theta_I, \quad \widehat{\varphi}'' = -k\cos\left(\widehat{\theta}_0 + \theta_I\right) = -k.
$$

Using the fact that

$$
\int_{\infty}^{\infty} e^{\pm it\theta^2} = \sqrt{\frac{\pi}{t}} e^{\pm i\pi/4},
$$

we obtain

$$I \approx \left\{ i\frac{F(\theta_0)}{\sqrt{\widehat{\kappa}_0}}\frac{H(\theta_0)}{\sqrt{k}}e^{ir(\widehat{\kappa}_0+2k)}\widehat{\kappa}_0 e^{i\pi/4} + i\frac{\widehat{F}(\widehat{\theta}_0)}{\sqrt{\widehat{\kappa}_0}}\frac{H(\widehat{\theta}_0)}{\sqrt{k}}e^{ir\widehat{\kappa}_0}(\widehat{\kappa}_0 - 2k)e^{-i\pi/4} \right\} \sqrt{\frac{2\pi}{kr}}. \tag{F.2.5}$$

Clearly

$$I = O\left(\frac{1}{\sqrt{kr}}\right) \to 0, \quad kr \to \infty, \tag{F.2.6}$$

hence the weak radiation condition is satisfied.

Appendix G

Evaluation of Infinite Integrals

By following Chau and Eatock Taylor (1992) [10], the evaluation of the infinite integrals in Eq. (4.4.65) are shown as follows. As can be seen from Eq. (4.4.65), the typical forms of the infinite integrals are as follows form

$$I^{(1)}_{\iota,\tau,m} = \int_{r_s}^{\infty} r dr H^{(1)}_{\iota}(kr)\, H^{(1)}_{\tau}(kr)\, H^{(1)}_{m}(\widehat{\kappa}_0 r)\,, \tag{G.1.1}$$

and

$$I^{(2)}_{\iota,\tau,m} = \int_{r_s}^{\infty} r dr H^{(2)}_{\iota}(kr)\, H^{(1)}_{\tau}(kr)\, H^{(1)}_{m}(\widehat{\kappa}_0 r)\,. \tag{G.1.2}$$

Making use of Hankel's asymptotic expansions as defined by Abramowitz and Stegun (1972)[1]

$$H^{(1)}_{m}(x) = \left(\frac{2}{\pi x}\right)^{1/2} [X_m(x) + iY_m(x)]\, e^{i(x-\gamma_m)}, \tag{G.1.3}$$

where

$$\gamma_m = \frac{1}{2}m\pi + \frac{1}{4}\pi, \tag{G.1.4}$$

$$X_m(x) = \sum_{\iota=0}^{\infty} \frac{(-1)^{\iota}\,\Gamma\left(\frac{1}{2}+m+2\iota\right)}{(2\iota)!\Gamma\left(\frac{1}{2}+m-2\iota\right)(2x)^{2\iota}}, \tag{G.1.5}$$

$$Y_m(x) = \sum_{\iota=0}^{\infty} \frac{(-1)^{\iota}\,\Gamma\left(\frac{3}{2}+m+2\iota\right)}{(2\iota)!\Gamma\left(-\frac{1}{2}+m-2\iota\right)(2x)^{2\iota+1}}, \tag{G.1.6}$$

When $\iota > \frac{1}{2}m$, the remainder after ι terms in the expansion of $X_m(x)$ will not exceed the $\iota+1$ term in absolute value(Abramowitz and Stegun (1972)[1]). This is also the case for $Y_m(x)$. Therefore, we can truncate $X_m(x)$ and $Y_m(x)$ at $\iota = M_m = \frac{1}{2}m + 2$. The Hankel function can be written as

$$H_m^{(1)}(kr) \approx \left(\frac{2}{\pi kr}\right)^{1/2} e^{i(kr-\gamma_m)} \sum_{\iota=0}^{M_m} C_{m,\iota} (kr)^{-\iota}, \tag{G.1.7}$$

where

$$C_{m,0} = 1 \tag{G.1.8}$$

$$C_{m,\iota} = \frac{i^\iota (4m^2-3)\cdots\left[4m^2-(2\iota-1)^2\right]}{\iota! 8^\iota} \tag{G.1.9}$$

and then a recursive relationship for $C_{m,\iota+1}$ is obtained as

$$C_{m,\iota+1} = \frac{i\left[4m^2-(2\iota+1)^2\right]}{(\iota+1)\,8} C_{m,\iota}. \tag{G.1.10}$$

Therefore, the infinite integral can be written as

$$I^{(1)}_{\iota,\tau,m} = \frac{2}{\pi k}\left(\frac{2}{\pi\widehat{\kappa}_0}\right)^{1/2} e^{-i(\gamma_\iota+\gamma_\tau+\gamma_m)} \sum_{p,q,s} C_{\iota p} C_{\tau q} C_{ms} k^{-(p+q)} \widehat{\kappa}_0^{-s} \int_{r_s}^{\infty} dr \frac{e^{i(2k+\widehat{\kappa}_0)r}}{r^{p+q+s+\frac{1}{2}}}. \tag{G.1.11}$$

Similar for $I^{(2)}_{\iota,\tau,m}$ as

$$I^{(2)}_{\iota,\tau,m} = \frac{2}{\pi k}\left(\frac{2}{\pi\widehat{\kappa}_0}\right)^{1/2} e^{-i(-\gamma_\iota+\gamma_\tau+\gamma_m)} \sum_{p,q,s} (-1)^p C_{\iota p} C_{\tau q} C_{ms} k^{-(p+q)} \widehat{\kappa}_0^{-s} \int_{r_s}^{\infty} dr \frac{e^{i\widehat{\kappa}_0 r}}{r^{p+q+s+\frac{1}{2}}}. \tag{G.1.12}$$

The integrals are of the form

$$A_\nu = \int_{r_s}^{\infty} dr \frac{e^{i\beta r}}{r^{\nu+1/2}} \tag{G.1.13}$$

with $\beta = 2k + \widehat{\kappa}_0$ for Eq. (G.1.11) or $\beta = \widehat{\kappa}_0$ Eq. (G.1.12). The infinite integrals, $I^{(1)}_{\iota,\tau,m}$ and $I^{(2)}_{\iota,\tau,m}$, can now be evaluated by the methods of asymptotic expansion of integrals. Using integration by parts we obtain

$$A_\nu = \frac{i}{\beta}\frac{e^{i\beta r_s}}{r_s^{\nu+\frac{1}{2}}} + \frac{\nu+\frac{1}{2}}{i\beta}A_{\nu+1} \tag{G.1.14}$$

which leads to the power series

$$A_\nu = \frac{i}{\beta}\frac{e^{i\beta r_s}}{r_s^{\nu+\frac{1}{2}}} + \frac{\nu+\frac{1}{2}}{i\beta}\left(\frac{i}{\beta}\frac{e^{i\beta r_s}}{r_s^{\nu+1+\frac{1}{2}}} + \frac{\nu+1+\frac{1}{2}}{i\beta}\left(\frac{i}{\beta}\frac{e^{i\beta r_s}}{r_s^{\nu+2+\frac{1}{2}}} + \frac{\nu+2+\frac{1}{2}}{i\beta}(\cdots)\right)\right) \tag{G.1.15}$$

and can be written as

$$A_\nu = -\sum_{j=1}^{N}\frac{(\nu+j-\frac{3}{2})!}{(\nu-\frac{1}{2})!}\frac{1}{(i\beta)^j}\frac{e^{i\beta r_s}}{r^{\nu+j-\frac{1}{2}}} + E_N. \tag{G.1.16}$$

The truncation error E_N is

$$E_N = \frac{(\nu+N-\frac{1}{2})!}{(\nu-\frac{1}{2})!}\frac{1}{(i\beta)^N}\int_{r_s}^{\infty} dr\frac{e^{i\beta r}}{r^{\nu+N+\frac{1}{2}}}. \tag{G.1.17}$$

Therefore

$$\begin{aligned} |E_N| &\leq \left|\frac{(\nu+N-\frac{1}{2})!}{(\nu-\frac{1}{2})!}\frac{1}{(i\beta)^N}\int_{r_s}^{\infty} dr\frac{e^{i\beta r}}{r^{\nu+N+\frac{1}{2}}}\right| \\ &= \frac{(\nu+N-\frac{3}{2})!}{(\nu-\frac{1}{2})!}\frac{1}{\beta^N}\frac{1}{r_s^{\nu+N-\frac{1}{2}}}. \end{aligned} \tag{G.1.18}$$

It can be seen that E_N always has the same order of magnitude as the last remaining term in the series Eq. (G.1.16). Let us consider The ratio of the $N+1$th term in Eq. (G.1.16) to the Nth term is

$$\left|\frac{N+1\text{th term}}{N\text{th term}}\right| = \frac{\nu+N-\frac{1}{2}}{\beta r_s} \tag{G.1.19}$$

The successive terms decrease as long as $\nu + N - 1/2 < \beta r_s$, but increase unboundedly with increasing N. The best estimate for A_ν can then be obtained by choosing N as

$$N = \text{greatest integer less than } [\beta r_s - \nu]. \tag{G.1.20}$$

Appendix H

Jointly Gaussian distribution

Let the joint probability density function (PDF) of the N random variables $\{ x_1, x_2, \cdots, x_N \}$ be denoted as $f(x_1, x_2, \cdots, x_N)$. The expectation of a function $G(x_1, x_2, \cdots, x_N)$ is obtained from

$$\langle G(x_1, x_2, \cdots, x_N) \rangle = \int \cdots \int f(x_1, x_2, \cdots, x_N) G(x_1, x_2, \cdots, x_N) dx_1 dx_2 \cdots dx_N \tag{H.0.1}$$

where $< \cdot >$ denotes the expectation value. The joint characteristic function, which is derived to be the N-dimensional Fourier transformation of the joint PDF

$$\begin{aligned} \widetilde{f}(x_1, x_2, \cdots, x_N) &= \left\langle \exp\left(-i \sum_{j=1}^{N} \alpha_j x_j \right) \right\rangle \\ &= \int \cdots \int f(x_1, x_2, \cdots, x_N) \exp\left(-i \sum_{j=1}^{N} \alpha_j x_j \right) dx_1 dx_2 \cdots dx_N. \end{aligned} \tag{H.0.2}$$

Since we can expand the exponential function $\exp(-i\alpha x)$ as power series

$$e^{-i\alpha x} = 1 + (-i\alpha) x + \frac{(-i\alpha)^2}{2!} x^2 + \cdots + \frac{(-i\alpha)^n}{n!} x^n + \cdots = \sum_{m=0}^{\infty} \frac{(-i\alpha_1)^m}{m!} x_1^m, \tag{H.0.3}$$

the expansion of $\left\{\exp\left(-i\sum_{j=1}^{N}\alpha_j x_j\right)\right\}$ can be obtained as

$$\exp\left(-i\sum_{j=1}^{N}\alpha_j x_j\right)=\left[\sum_{m=0}^{\infty}\frac{(-i\alpha_1)^m}{m!}x_1^m\right]\left[\sum_{n=0}^{\infty}\frac{(-i\alpha_2)^n}{n!}x_2^n\right]\cdots\left[\sum_{p=0}^{\infty}\frac{(-i\alpha_N)^p}{p!}x_N^p\right]. \tag{H.0.4}$$

Making use of the above equation, the joint characteristic function can be expanded as

$$\begin{aligned}\widetilde{f}\left(\alpha_1,\alpha_2,\cdots,\alpha_N\right)&=\left\langle\exp\left(-i\sum_{j=1}^{N}\alpha_j x_j\right)\right\rangle\\&=1+\left(-i\alpha_1\right)\left\langle x_1\right\rangle+\left(-i\alpha_2\right)\left\langle x_2\right\rangle+\cdots+\left(-i\alpha_N\right)\left\langle x_N\right\rangle\\&\quad+\left(-i\alpha_1\right)\left(-i\alpha_2\right)\left\langle x_1x_2\right\rangle+\left(-i\alpha_1\right)\left(-i\alpha_3\right)\left\langle x_1x_3\right\rangle+\cdots,\\&\quad+\left(-i\alpha_1\right)\left(-i\alpha_2\right)\left(-i\alpha_3\right)\left\langle x_1x_2x_3\right\rangle+\left(-i\alpha_1\right)\left(-i\alpha_2\right)\left(-i\alpha_4\right)\left\langle x_1x_2x_4\right\rangle+\cdots.\end{aligned} \tag{H.0.5}$$

Therefore, the joint moments are generated as

$$\left\langle x_1^{p1}x_2^{p2}\cdots x_N^{p_N}\right\rangle=\left[\frac{\partial^{p_1}}{\partial\left(-i\alpha_1\right)^{p_1}}\frac{\partial^{p_2}}{\partial\left(-i\alpha_2\right)^{p_2}}\cdots\frac{\partial^{p_N}}{\partial\left(-i\alpha_N\right)^{p_N}}\right]\widetilde{f}\left(\alpha_1,\alpha_2,\cdots,\alpha_N\right)\\ @\,\alpha_1=0,\,\alpha_2=0,\,\cdots,\,\alpha_N=0. \tag{H.0.6}$$

The joint Gaussian distribution of N random variables is

$$f\left(x_1,x_2,\cdots,x_N\right)=\frac{1}{\sqrt{\left(2\pi\right)^N\det\left[\mathbf{C}\right]}}\exp\left[-\frac{1}{2}\sum_{m,n}\left(\mathbf{C}\right)_{m,n}^{-1}\left(x_m-\lambda_m\right)\left(x_n-\lambda_n\right)\right], \tag{H.0.7}$$

where $\lambda_m=\left\langle x_m\right\rangle$, the matrix C is the correlation matrix,

$$\mathbf{C}_{m,n}=\left\langle\left(x_m-\lambda_m\right)\left(x_n-\lambda_n\right)\right\rangle, \tag{H.0.8}$$

and C^{-1} is its inverse. In addition, the corresponding joint characteristic function is

$$\widetilde{f}\left(\alpha_1,\alpha_2,\cdots,\alpha_N\right)=\exp\left[\sum_{m}-i\alpha_m\lambda_m-\sum_{m,n}\frac{1}{2}\mathbf{C}_{m,n}\alpha_m\alpha_n\right]. \tag{H.0.9}$$

For $\langle x_m \rangle = \lambda_m = 0$, the joint characteristic function becomes

$$\widetilde{f}\left(\alpha_1, \alpha_2, \cdots, \alpha_N\right) = \exp\left(-\sum_{i,j} \frac{1}{2} \mathbf{C}_{i,j} \alpha_i \alpha_j\right). \tag{H.0.10}$$

Putting Eqn. (H.0.10) into (H.0.6), we can get that and

$$\begin{aligned} \langle x_m x_n \rangle &= \left[\frac{\partial}{\partial\left(-i\alpha_m\right)} \frac{\partial}{\partial\left(-i\alpha_n\right)}\right] \exp\left(-\sum_{i,j} \frac{1}{2} \mathbf{C}_{i,j} \alpha_i \alpha_j\right), \ @\, \alpha_1 = 0, \cdots, \alpha_N = 0 \\ &= \mathbf{C}_{m,n}. \end{aligned} \tag{H.0.11}$$

and

$$\begin{aligned} \langle x_m x_n x_p \rangle = \left[\frac{\partial}{\partial\left(-i\alpha_m\right)} \frac{\partial}{\partial\left(-i\alpha_n\right)} \frac{\partial}{\partial\left(-i\alpha_p\right)}\right] \exp\left(-\sum_{i,j} \frac{1}{2} \mathbf{C}_{i,j} \alpha_i \alpha_j\right), \\ @\, \alpha_1 = 0, \cdots, \ \alpha_N = 0, \\ = 0. \end{aligned} \tag{H.0.12}$$

and all the remaining odd moments are zero. Besides, all the even moment can be obtained by grouping the random variables into pairs, e.g.

$$\begin{aligned} \langle x_m x_n x_p x_q \rangle &= \mathbf{C}_{mn}\mathbf{C}_{pq} + \mathbf{C}_{mp}\mathbf{C}_{nq} + \mathbf{C}_{mq}\mathbf{C}_{np} \\ &= \langle x_m x_n \rangle \langle x_p x_q \rangle + \langle x_m x_p \rangle \langle x_n x_q \rangle + \langle x_m x_q \rangle \langle x_n x_p \rangle. \end{aligned} \tag{H.0.13}$$

(Cf. Root and Pitcher 1955, Theorem 2. [40]).

Appendix I

Weak radiation condition for $\xi_0^Q(\omega_1, \omega_2)$

I.1 Asymptotic behavior of $\xi_0^Q(\omega_1, \omega_2)$

In order to verify the weak radiation condition and to ensure the convergence of certain infinite integrals, we need the asymptotic behavior of $\xi_0^Q(\omega_1, \omega_2)$ for $kr \gg 1$. Recall that ξ_0^Q satisfies the inhomogeneous Helmholtz equation, Eq. (9.2.5). The forcing terms $\mathcal{Q}(\omega_1, \omega_2)$ involves the products of $\Gamma_1^{(T)}$ and $\Gamma_1^{(S)}$ and the products of their gradients. For large kr, the first-order scattered wave behaves as

$$\Gamma_1^{(S)}(\omega_1) \approx \mathcal{F}(\theta, \omega_1) \frac{e^{ik(\omega_1)r}}{\sqrt{|k(\omega_1)|r}}, \tag{I.1.1}$$

hence

$$\Gamma_1^{(S)}(\omega_2)\Gamma_1^{(T)}(\omega_1) = \mathcal{F}(\theta, \omega_2) \left\{ \frac{e^{ir[k(\omega_1)\cos(\theta-\theta_I)+k(\omega_2)]}}{\sqrt{|k(\omega_2)|r}} + \frac{e^{ir[k(\omega_1)\cos(\theta+\theta_I)+k(\omega_2)]}}{\sqrt{|k(\omega_2)|r}} \right\}, \tag{I.1.2}$$

$$\Gamma_1^{(S)}(\omega_1)\Gamma_1^{(T)}(\omega_2) = \mathcal{F}(\theta, \omega_1) \left\{ \frac{e^{ir[k(\omega_2)\cos(\theta-\theta_I)+k(\omega_1)]}}{\sqrt{|k(\omega_1)|r}} + \frac{e^{ir[k(\omega_2)\cos(\theta+\theta_I)+k(\omega_1)]}}{\sqrt{|k(\omega_1)|r}} \right\}, \tag{I.1.3}$$

and

$$\begin{aligned}\nabla\Gamma_1^{(S)}(\omega_2)\cdot\nabla\Gamma_1^{(T)}(\omega_1) &\approx \frac{\partial\Gamma_1^{(S)}(\omega_2)}{\partial r}\frac{\partial\Gamma_1^{(T)}(\omega_1)}{\partial r}\\ &= -k(\omega_1)k(\omega_2)\mathcal{F}(\theta,\omega_2)\left\{\cos(\theta-\theta_I)\frac{e^{ir[k(\omega_1)\cos(\theta-\theta_I)+k(\omega_2)]}}{\sqrt{|k(\omega_2)|r}}\right.\\ &\quad\left.+\cos(\theta+\theta_I)\frac{e^{ir[k(\omega_1)\cos(\theta+\theta_I)+k(\omega_2)]}}{\sqrt{|k(\omega_2)|r}}\right\},\end{aligned}\tag{I.1.4}$$

$$\begin{aligned}\nabla\Gamma_1^{(S)}(\omega_1)\cdot\nabla\Gamma_1^{(T)}(\omega_2) &\approx \frac{\partial\Gamma_1^{(S)}(\omega_1)}{\partial r}\frac{\partial\Gamma_1^{(T)}(\omega_2)}{\partial r}\\ &= -k(\omega_1)k(\omega_2)\mathcal{F}(\theta,\omega_1)\left\{\cos(\theta-\theta_I)\frac{e^{ir[k(\omega_2)\cos(\theta-\theta_I)+k(\omega_1)]}}{\sqrt{|k(\omega_1)|r}}\right.\\ &\quad\left.+\cos(\theta+\theta_I)\frac{e^{ir[k(\omega_2)\cos(\theta+\theta_I)+k(\omega_1)]}}{\sqrt{|k(\omega_1)|r}}\right\}.\end{aligned}\tag{I.1.5}$$

The remaining terms are negligible because

$$\frac{1}{r^2}\frac{\partial\Gamma_1^{(S)}(\omega_2)}{\partial\theta}\frac{\partial\Gamma_1^{(T)}(\omega_1)}{\partial\theta} = O\left(r^{-3/2}\right),\tag{I.1.6}$$

$$\frac{1}{r^2}\frac{\partial\Gamma_1^{(S)}(\omega_1)}{\partial\theta}\frac{\partial\Gamma_1^{(T)}(\omega_2)}{\partial\theta} = O\left(r^{-3/2}\right).\tag{I.1.7}$$

It is easy to see that products of $\Gamma_1^{(S)}(\omega_1)$ and $\Gamma_1^{(S)}(\omega_2)$is of the order $O(1/r)$. Therefore, $\mathcal{Q}(\omega_1,\omega_2)$ is dominated by

$$\begin{aligned}\mathcal{Q}(\omega_1,\omega_2) \approx{}& [\beta_1(\omega_1,\omega_2)-\beta_2(\omega_1,\omega_2)k(\omega_1)k(\omega_2)\cos(\theta-\theta_I)]\times\\ &\left\{\mathcal{F}(\theta,\omega_2)\frac{e^{ir[k(\omega_1)\cos(\theta-\theta_I)+k(\omega_2)]}}{\sqrt{|k(\omega_2)|r}}+\mathcal{F}(\theta,\omega_1)\frac{e^{ir[k(\omega_2)\cos(\theta-\theta_I)+k(\omega_1)]}}{\sqrt{|k(\omega_1)|r}}\right\}\\ &+[\beta_1(\omega_1,\omega_2)-\beta_2(\omega_1,\omega_2)k(\omega_1)k(\omega_2)\cos(\theta+\theta_I)]\times\\ &\left\{\mathcal{F}(\theta,\omega_2)\frac{e^{ir[k(\omega_1)\cos(\theta+\theta_I)+k(\omega_2)]}}{\sqrt{|k(\omega_2)|r}}+\mathcal{F}(\theta,\omega_1)\frac{e^{ir[k(\omega_2)\cos(\theta+\theta_I)+k(\omega_1)]}}{\sqrt{|k(\omega_1)|r}}\right\}.\end{aligned}\tag{I.1.8}$$

From the governing Helmholtz equation Eq. (9.2.5), it can be seen that

$$\begin{aligned}\xi_0^Q(\omega_1,\omega_2) \approx & \mathcal{F}_1(\theta)\frac{e^{ir[k(\omega_1)\cos(\theta-\theta_I)+k(\omega_2)]}}{\sqrt{|k(\omega_2)|r}} + \mathcal{F}_2(\theta)\frac{e^{ir[k(\omega_2)\cos(\theta-\theta_I)+k(\omega_1)]}}{\sqrt{|k(\omega_1)|r}} \\ & + \mathcal{F}_3(\theta)\frac{e^{ir[k(\omega_1)\cos(\theta+\theta_I)+k(\omega_2)]}}{\sqrt{|k(\omega_2)|r}} + \mathcal{F}_4(\theta)\frac{e^{ir[k(\omega_2)\cos(\theta+\theta_I)+k(\omega_1)]}}{\sqrt{|k(\omega_1)|r}}\end{aligned} \tag{I.1.9}$$

where $\mathcal{F}_1$, $\mathcal{F}_2$, $\mathcal{F}_3$ and $\mathcal{F}_4$ are known functions of θ.

I.2 Weak radiation condition

We show here that the following line integral vanishes

$$I = \int_{\partial F}\left(\xi_0^Q(\omega_1,\omega_2)\frac{\partial G_0(\omega_1,\omega_2)}{\partial r} - G_0(\omega_1,\omega_2)\frac{\partial \xi_0^Q(\omega_1,\omega_2)}{\partial r}\right)dS \to 0. \tag{I.2.1}$$

where ∂F is a semi-circle of unboundedly large radius.

Since $G_0(\omega_1,\omega_2)$ satisfies the strong radiation condition,

$$G_0 \approx \frac{H(\theta)}{(\widehat{\kappa}_0 r)^{1/2}}e^{i\widehat{\kappa}_0 r} \tag{I.2.2}$$

Putting the asymptotic expressions of ξ_0^Q and G_0 into Eq. (I.2.1), we obtain for large kr,

$$\begin{aligned}I = & \int_0^\pi d\theta\,\frac{H(\theta)\mathcal{F}_1(\theta)}{\sqrt{\widehat{\kappa}_0|k(\omega_2)|}}e^{ir[k(\omega_1)\cos(\theta-\theta_I)+k(\omega_2)+\widehat{\kappa}_0]}\left[-ik(\omega_1)\cos(\theta-\theta_I)-ik(\omega_2)+i\widehat{\kappa}_0\right] \\ & \int_0^\pi d\theta\,\frac{H(\theta)\mathcal{F}_2(\theta)}{\sqrt{\widehat{\kappa}_0|k(\omega_1)|}}e^{ir[k(\omega_2)\cos(\theta-\theta_I)+k(\omega_1)+\widehat{\kappa}_0]}\left[-ik(\omega_2)\cos(\theta-\theta_I)-ik(\omega_1)+i\widehat{\kappa}_0\right] \\ & \int_0^\pi d\theta\,\frac{H(\theta)\mathcal{F}_3(\theta)}{\sqrt{\widehat{\kappa}_0|k(\omega_2|)}}e^{ir[k(\omega_1)\cos(\theta+\theta_I)+k(\omega_2)+\widehat{\kappa}_0]}\left[-ik(\omega_1)\cos(\theta+\theta_I)-ik(\omega_2)+i\widehat{\kappa}_0\right] \\ & \int_0^\pi d\theta\,\frac{H(\theta)\mathcal{F}_4(\theta)}{\sqrt{\widehat{\kappa}_0|k(\omega_1)|}}e^{ir[k(\omega_2)\cos(\theta+\theta_I)+k(\omega_1)+\widehat{\kappa}_0]}\left[-ik(\omega_2)\cos(\theta+\theta_I)-ik(\omega_1)+i\widehat{\kappa}_0\right].\end{aligned} \tag{I.2.3}$$

For large r, we use the method of stationary phase, and let

$$\varphi_1(\theta) = k(\omega_1)\cos(\theta - \theta_I) + k(\omega_2) + \widehat{\kappa}_0, \qquad \varphi_2(\theta) = k(\omega_2)\cos(\theta - \theta_I) + k(\omega_1) + \widehat{\kappa}_0,$$

$$\varphi_3(\theta) = k(\omega_1)\cos(\theta + \theta_I) + k(\omega_2) + \widehat{\kappa}_0, \qquad \varphi_4(\theta) = k(\omega_2)\cos(\theta + \theta_I) + k(\omega_1) + \widehat{\kappa}_0,$$

be the phase function. Since

$$\varphi_1' = -k(\omega_1)\sin(\theta - \theta_I), \quad \varphi_2' = -k(\omega_2)\sin(\theta - \theta_I),$$

$$\varphi_3' = -k(\omega_1)\sin(\theta + \theta_I), \quad \varphi_4' = -k(\omega_1)\sin(\theta + \theta_I),$$

and

$$\pi < \theta_I < 2\pi,$$

the stationary phase points are at

$$\theta = \theta_1 = -\pi + \theta_I,$$

$$\varphi_1'' = -k(\omega_1)\cos(\theta_1 - \theta_I) = k(\omega_1), \quad \varphi_2'' = -k(\omega_2)\cos(\theta_1 - \theta_I) = k(\omega_2),$$

and

$$\theta = \theta_2 = 2\pi - \theta_I,$$

$$\varphi_3'' = -k(\omega_1)\cos(\theta_2 + \theta_I) = -k(\omega_1), \quad \varphi_4'' = -k(\omega_2)\cos(\theta_2 + \theta_I) = -k(\omega_2).$$

Using the fact that

$$\int_{\infty}^{\infty} e^{\pm it\theta^2} d\theta = \sqrt{\frac{\pi}{t}} e^{\pm i\pi/4},$$

we obtain

$$
\begin{aligned}
I \approx & i\frac{H(\theta_1)}{\sqrt{\widehat{\kappa}_0}}\frac{\mathcal{F}_1(\theta_1)}{\sqrt{|k(\omega_2)|}}e^{ir[\widehat{\kappa}_0+k(\omega_1)+k(\omega_2)]}\left[k(\omega_1)-k(\omega_2)+\widehat{\kappa}_0\right]e^{i\pi/4}\sqrt{\frac{2\pi}{|k(\omega_1)|r}} \\
& + i\frac{H(\theta_1)}{\sqrt{\widehat{\kappa}_0}}\frac{\mathcal{F}_2(\theta_1)}{\sqrt{|k(\omega_1)|}}e^{ir(\widehat{\kappa}_0+k(\omega_1)+k(\omega_2))}\left[k(\omega_2)-k(\omega_1)+\widehat{\kappa}_0\right]e^{i\pi/4}\sqrt{\frac{2\pi}{|k(\omega_2)|r}} \\
& + i\frac{H(\theta_2)}{\sqrt{\widehat{\kappa}_0}}\frac{\mathcal{F}_3(\theta_2)}{\sqrt{|k(\omega_2)|}}e^{ir[\widehat{\kappa}_0+k(\omega_2)-k(\omega_1)]}\left[\widehat{\kappa}_0+k(\omega_1)-k(\omega_2)\right]e^{-i\pi/4}\sqrt{\frac{2\pi}{|k(\omega_1)|r}} \\
& + i\frac{H(\theta_2)}{\sqrt{\widehat{\kappa}_0}}\frac{\mathcal{F}_4(\theta_2)}{\sqrt{|k(\omega_1)|}}e^{ir[\widehat{\kappa}_0+k(\omega_1)-k(\omega_2)]}[\widehat{\kappa}_0+k(\omega_2)-k(\omega_1)]e^{-i\pi/4}\sqrt{\frac{2\pi}{|k(\omega_2)|r}}.
\end{aligned}
\tag{I.2.4}
$$

Clearly

$$
I = O\left(\frac{1}{\sqrt{r}}\right) \to 0, \quad r \to \infty, \tag{I.2.5}
$$

hence the weak radiation condition is satisfied.

Appendix J

Derivation of H_{31}

Since the random variable $A(\omega_i)$,with $i = 1, 2, 3, 4$, is Gaussian, so $A(\omega_i)$ are jointly normally distributed and independent.

$$\overline{A^*(\omega_1) A^*(\omega_2) A(\omega_3) A(\omega_4)} = \overline{A^*(\omega_1) A(\omega_2)} \quad \overline{A(\omega_3) A(\omega_4)} + \overline{A^*(\omega_1) A(\omega_3)} \quad \overline{A(\omega_2) A(\omega_4)} + \overline{A^*(\omega_1) A(\omega_4)} \quad \overline{A(\omega_2) A(\omega_3)}. \tag{J.1.1}$$

Hence, we obtain

$$H_{31}(t,\tau) = \iiiint_{-\infty}^{\infty} d\omega_1 d\omega_2 d\omega_3 d\omega_4 \left[\overline{A^*(\omega_1) A(\omega_2)} \quad \overline{A(\omega_3) A(\omega_4)} + \overline{A^*(\omega_1) A(\omega_3)} \quad \overline{A(\omega_2) A(\omega_4)} + \overline{A^*(\omega_1) A(\omega_4)} \quad \overline{A(\omega_2) A(\omega_3)}\right] \times \Gamma_1(x, y, \omega_1) \Gamma_3^*(x, y, \omega_2, \omega_3, \omega_4) e^{-i(-\omega_1+\omega_2+\omega_3+\omega_4)t} e^{i\omega_1\tau}. \tag{J.1.2}$$

Each ensemble average in Eqn. (J.1.2) is given as follows.

$$\overline{A^*(\omega_1) A(\omega_2)} \quad \overline{A(\omega_3) A(\omega_4)} = S_A(\omega_1) \delta(\omega_1 - \omega_2) S_A(\omega_3) \delta(\omega_3 + \omega_4), \tag{J.1.3}$$

$$\overline{A^*(\omega_1) A(\omega_3)} \quad \overline{A(\omega_2) A(\omega_4)} = S_A(\omega_1) \delta(\omega_1 - \omega_3) S_A(\omega_2) \delta(\omega_2 + \omega_4), \tag{J.1.4}$$

$$\overline{A^*(\omega_1) A(\omega_4)} \quad \overline{A(\omega_2) A(\omega_3)} = S_A(\omega_1) \delta(\omega_1 - \omega_4) S_A(\omega_2) \delta(\omega_2 + \omega_3). \tag{J.1.5}$$

Therefore, Eq. (8.5.47) becomes

$$\begin{aligned}
&\overline{A(\omega_1)\,A^*(\omega_2)\,A^*(\omega_3)\,A^*(\omega_4)} \\
&\quad = S_A(\omega_1)\,\delta(\omega_1-\omega_2)\,S_A(\omega_3)\,\delta(\omega_3+\omega_4) + S_A(\omega_1)\,\delta(\omega_1-\omega_3)\,S_A(\omega_2)\,\delta(\omega_2+\omega_4) \\
&\qquad + S_A(\omega_1)\,\delta(\omega_1-\omega_4)\,S_A(\omega_2)\,\delta(\omega_2+\omega_3)\,.
\end{aligned} \tag{J.1.6}$$

Thus the first integral in Eqn. (J.1.2) becomes

$$\begin{aligned}
\text{term } 1 &= \iiiint_{-\infty}^{\infty} d\omega_1 d\omega_2 d\omega_3 d\omega_4 \left\{ \overline{A^*(\omega_1)\,A(\omega_2)} \quad \overline{A(\omega_3)\,A(\omega_4)} \times \right. \\
&\qquad \left. \Gamma_1^*(x,y,\omega_1)\,\Gamma_3(x,y,\omega_2,\omega_3,\omega_4)\,e^{-i(-\omega_1+\omega_2+\omega_3+\omega_4)t} e^{i\omega_1\tau} \right\} \\
&= \iiiint_{-\infty}^{\infty} d\omega_1 d\omega_2 d\omega_3 d\omega_4 \left\{ S_A(\omega_1)\,\delta(\omega_1-\omega_2)\,S_A(\omega_3)\,\delta(\omega_3+\omega_4) \times \right. \\
&\qquad \left. \Gamma_1(x,y,\omega_1)\,\Gamma_3^*(x,y,\omega_2,\omega_3,\omega_4)\,e^{-i(-\omega_1+\omega_2+\omega_3+\omega_4)t} e^{i\omega_1\tau} \right\}
\end{aligned} \tag{J.1.7}$$

Because of $\delta(\omega_1-\omega_2)$ and $\delta(\omega_3+\omega_4)$, Term 1 becomes

$$\text{term } 1 = \int_{-\infty}^{\infty}\int_{-\infty}^{\infty} S_A(\omega_1)\,S_A(\omega_3)\,\Gamma_1^*(x,y,\omega_1)\,\Gamma_3(x,y,\omega_1,\omega_3,-\omega_3)\,e^{i\omega_1\tau} d\omega_1 d\omega_3 \tag{J.1.8}$$

Let us change the notation and replace variable ω_3 by ω_2 and get

$$\text{term } 1 = \int_{-\infty}^{\infty}\int_{-\infty}^{\infty} S_A(\omega_1)\,S_A(\omega_2)\,\Gamma_1^*(x,y,\omega_1)\,\Gamma_3(x,y,\omega_1,\omega_2,-\omega_2)\,e^{i\omega_1\tau} d\omega_1 d\omega_2 \tag{J.1.9}$$

The second integral in Eqn. (J.1.2) is

$$\begin{aligned}
\text{term } 2 &= \iiiint_{-\infty}^{\infty} d\omega_1 d\omega_2 d\omega_3 d\omega_4 \left\{ \overline{A^*(\omega_1)\,A(\omega_3)} \quad \overline{A(\omega_2)\,A(\omega_4)} \times \right. \\
&\qquad \left. \Gamma_1^*(x,y,\omega_1)\,\Gamma_3(x,y,\omega_2,\omega_3,\omega_4)\,e^{-i(-\omega_1+\omega_2+\omega_3+\omega_4)t} e^{i\omega_1\tau} \right\} \\
&= \iiiint_{-\infty}^{\infty} d\omega_1 d\omega_2 d\omega_3 d\omega_4 \left\{ S_A(\omega_1)\,\delta(\omega_1-\omega_3)\,S_A(\omega_2)\,\delta(\omega_2+\omega_4) \times \right. \\
&\qquad \left. \Gamma_1^*(x,y,\omega_1)\,\Gamma_3(x,y,\omega_2,\omega_3,\omega_4)\,e^{-i(-\omega_1+\omega_2+\omega_3+\omega_4)t} e^{i\omega_1\tau} \right\}
\end{aligned} \tag{J.1.10}$$

Because of $\delta(\omega_1 - \omega_3)$ and $\delta(\omega_2 + \omega_4)$, Term 2 becomes

$$\text{term } 2 = \int_{-\infty}^{\infty}\int_{-\infty}^{\infty} S_A(\omega_1) S_A(\omega_2) \Gamma_1^*(x,y,\omega_1) \Gamma_3(x,y,\omega_2,\omega_1,-\omega_2) e^{i\omega_1\tau} d\omega_1 d\omega_2 \tag{J.1.11}$$

The third integral in Eqn. (J.1.2) is

$$\begin{aligned}\text{term } 3 = &\iiiint_{-\infty}^{\infty} d\omega_1 d\omega_2 d\omega_3 d\omega_4 \left\{ \overline{A^*(\omega_1) A(\omega_4)} \quad \overline{A(\omega_2) A(\omega_3)} \times \right. \\ &\left. \Gamma_1^*(x,y,\omega_1) \Gamma_3(x,y,\omega_2,\omega_3,\omega_4) e^{-i(\omega_1-\omega_2-\omega_3-\omega_4)t} e^{i(\omega_2+\omega_3+\omega_4)\tau} \right\} \\ = &\iiiint_{-\infty}^{\infty} d\omega_1 d\omega_2 d\omega_3 d\omega_4 \left\{ S_A(\omega_1) \delta(\omega_1 - \omega_4) S_A(\omega_2) \delta(\omega_2 + \omega_3) \times \right. \\ &\left. \Gamma_1(x,y,\omega_1) \Gamma_3^*(x,y,\omega_2,\omega_3,\omega_4) e^{-i(-\omega_1+\omega_2+\omega_3+\omega_4)t} e^{i\omega_1\tau} \right\}\end{aligned} \tag{J.1.12}$$

Because of $\delta(\omega_1 - \omega_4)$ and $\delta(\omega_2 + \omega_3)$, Term 3 becomes

$$\text{term } 3 = \int_{-\infty}^{\infty}\int_{-\infty}^{\infty} S_A(\omega_1) S_A(\omega_2) \Gamma_1^*(x,y,\omega_1) \Gamma_3(x,y,\omega_2,-\omega_2,\omega_1) e^{i\omega_1\tau} d\omega_1 d\omega_2 \tag{J.1.13}$$

In summary, $H_{31}(t,\tau)$ is

$$\begin{aligned}H_{31}(x,y,\tau) = &\int_{-\infty}^{\infty} d\omega_1 e^{i\omega_1\tau} \left\{ S_A(\omega_1) \Gamma_1^*(\omega_1) \int_{-\infty}^{\infty} S_A(\omega_2) \left[\Gamma_3(\omega_1,\omega_2,-\omega_2) \right.\right. \\ &\left.\left. + \Gamma_3(\omega_2,\omega_1,-\omega_2) + \Gamma_3(\omega_2,-\omega_2,\omega_1) \right] d\omega_2 \right\} \\ = &\int_{-\infty}^{\infty} \mathbf{S}_{31}(\omega_1) e^{i\omega_1\tau} d\omega_1.\end{aligned} \tag{J.1.14}$$

The corresponding frequency spectrum is

$$\begin{aligned}\mathbf{S}_{31}(\omega_1) = &S_A(\omega_1) \Gamma_1^*(\omega_1) \int_{-\infty}^{\infty} S_A(\omega_2) \left[\Gamma_3(\omega_1,\omega_2,-\omega_2) \right. \\ &\left. + \Gamma_3(\omega_2,\omega_1,-\omega_2) + \Gamma_3(\omega_2,-\omega_2,\omega_1) \right] d\omega_2.\end{aligned} \tag{J.1.15}$$

Let us change the notation and replace variable ω_1 by ω and ω_2 by ω_1 get

$$\begin{aligned}\mathbf{S}_{31}(\omega) = S_A(\omega)\,\Gamma_1^*(\omega)\int_{-\infty}^{\infty} S_A(\omega_1)\,[\Gamma_3(\omega,\omega_1,-\omega_1) \\ +\Gamma_3(\omega_1,\omega,-\omega_1)+\Gamma_3(\omega_1,-\omega_1,\omega)]\,d\omega_1.\end{aligned} \tag{J.1.16}$$

Bibliography

[1] M. Abramowitz and I. A. Stegun. *Handbook of mathematical functions with formulas, graphs and mathematical tables.* Dover, 1972.

[2] Y. Agnon and C. C. Mei. Long-period oscillations in a harbour induced by incident short waves. *J. Fluid Mech.*, 208:595–608, 1989.

[3] G. A. Athanssoulis and K. A. Belibassakis. A consistent couple-mode theory for the propagation of small-amplitude water aves over variable bathymetry regions. *J. Fluid Mech.*, 389:275–301, 1999.

[4] K. J. Bai and R. Yeung. Numerical solutions of free-surface and flow problems. *Proc. 10th Symp. Naval Hydrodyn. Office of Naval Research*, pages 609–641, 1974.

[5] K. A. Belibassakis, G. A. Athanssoulis, and Th. P. Gerostathis. A couple-mode theory for refraction-diffraction of linear waves over steep three-dimensional bathymatry. *Applied Ocean Research*, 23:319–336, 2001.

[6] J. C. W. Berkhoff. Computation of combined refraction-diffraction. *Proc. 13th Conf. Coastal Eng. ASCE*, 1:471–490, 1972.

[7] E. Bouws, H. Günther, W. Rosenthal, and C. L. Vincent. Similarity of the wind wave spectrum in finite depth water: 1. spectral form. *J. Geophys. Res.*, 90:975–986, 1985.

[8] E. C. Bowers. Harbour resonance due to set-down beneath wave groups. *J. Fluid Mech.*, 79:71–92, 1977.

[9] P. G. Chamberlain and D. Porter. The modified mild-slope equation. *J. Fluid Mech.*, 291:393–407, 1995.

[10] F. P. Chau and R. Eatock Taylor. Second-order wave diffraction by a vertical cylinder. *J. Fluid Mech.*, 240:571–599, 1992.

[11] H. S. Chen and C. C. Mei. Oscillations and wave forces in an offshore harbor. Technical Report 190, Parsons Lab. MIT, Dept. Civil and Environm. Eng., MIT, Cambridge, 1974.

[12] R. Eatock Taylor and S. M. Hung. Second-order diffraction forces on a vertical cylinder in regular waves. *Applied Ocean Research*, 9:19–30, 1987.

[13] J. R. Houston. Long beach harbor numerical analysis of harbor - alternate plans for pier j completion and tanker terminal project oscillations. Technical Report 2, Hydraulics lab. U.S. army engineer waterways experiment station, P.O. box 631, vicksburg, Miss. 39180, 1976.

[14] J. R. Houston. Combined refraction and diffraction of short waves using the finite element method. *Applied Ocean Research*, 3(4):163–170, 1981.

[15] Hualien Harbour Baureau. *Hualien harbour oscillation study and improvement conference*, Taiwan, Oct. 1996.

[16] L. S. Hwang and E. O. Tuck. On the oscillation of harbours of arbitrary shape. *J. Fluid Mech.*, 42:447–464, 1970.

[17] M.-H. Kim and D. K. P. Yue. The complete second-order diffraction solution for an axisymmetric body. part 1 monochromatic incident waves. *J. Fluid Mech.*, 200:235–264, 1989.

[18] M.-H. Kim and D. K. P. Yue. The complete second-order diffraction solution for an axisymmetric body. part 2 bichromatic incident waves and body motions. *J. Fluid Mech.*, 211:557–593, 1990.

[19] S. A. Kitaigorodskii, V. P. Krasitskii, and M. M. Zaslavskii. On phillips' theory of equilibrium range in the spectra of wind-generated gravity waves. *J. Phys. Oceanogr.*, 5(3):410–420, 1975.

[20] C. C. Lautenbacher. Gravity wave refraction by islands. *J. Fluid Mech.*, 41:655–672, 1970.

[21] J. J. Lee. Wind-induced oscillation in harbors of arbitrary geometry. *J. Fluid Mech.*, 45:375–394, 1971.

[22] S. R. Massel. Extended refraction-diffraction equation for surface waves. *Coastal Eng.*, 19:97–126, 1993.

[23] F. Mattioli. Wave-induced oscillations in harbors of variable depth. *Computers and Fluids*, 6:161–172, 1978.

[24] C. C. Mei. *The applied dynamics of ocean surface waves*. Word scientific, 1989.

[25] C. C. Mei. Mild-slope approximation for long waves generated by short waves. *J. Eng. Math*, 35:43–57, 1999.

[26] C. C. Mei and P. L.-F. Liu. Surface waves and coastal dynamics. *Annu. Rev. Fluid Mech.*, 25:215–40, 1993.

[27] J. W. Miles and W. Munk. Harbor paradox. *J. Waterways and Harbor Div. ASCE*, 87:111–30, 1961.

[28] B. Molin. Second-order diffraction loads upon three-dimensional bodies. *Applied Ocean Research*, 1(4):197–202, 1979.

[29] M. K. Ochi. *Ocean waves, the stochastic approach.* Cambridge Universuty press, 1998.

[30] J. N. O.M. Faltinsen, Newman and T. Vinje. Nonlinear wave loads on a slender vertical cylinder. *J. Fliud Mech*, 289:179ff, 1995.

[31] D. Porter and D. J. Staziker. Extensions of the mild-slope equation. *J. Fluid Mech.*, 300:367–382, 1995.

[32] Prot & Harbour Res. Inst. *Proc. Informal Symp. on Port & Harbour Tech. - countermeasures for long-period waves and secondary oscillations in harbours*, Japan, Feb. 1998.

[33] P. D. Sclavounos. Radiation and diffraction of second-order surface waves by floating bodies. *J. Fluid Mech.*, 196:65–91, 1988.

[34] P. D. Sclavounos. On the quadratic effect of random gravity waves on a vertical boundary. *J. Fluid Mech.*, 242:475–489, 1992.

[35] R. Smith and T. Sprinks. Scattering of surface waves by a conical island. *J. Fluid Mech.*, 72:373–384, 1975.

[36] J. J. Stoker. *Water waves; the mathematical theory with applications.* New York, Interscience Publishers, 1957.

[37] W. Zhu T.-K. Tsay and P. L.-F. Liu. A finite element model for wave refraction diffraction, reflection and dissipation. *Applied Ocean Research*, 11(1):33–38, 1989.

[38] Ü. Ünlüata and C. C. Mei. Long wave excitation in harbors- an analytic study. Technical Report 171, M.I.T., Dept. of Civil Engineering, M.I.T., Cambridge, 1973.

[39] Ü. Ünlüata and C. C. Mei. Resonant scattering by a harbor with two coupled basins. *J. Eng. Math.*, 10:333–353, 1978.

[40] W. L. William and T. S. Pitcher. On the fourier-series expansion of random functions. *Annals of Math. Statistics*, 26:313–318, 1955.

[41] J.-K. Wu and P. L.-F. Liu. Harbour excitations by incident wave groups. *J. Fluid Mech.*, 217:595–613, 1990.

[42] D. K. P. Yue, H. S. Chen, and C. C. Mei. Water wave forces on three-dimensional bodies by a hybrid element method. *Parsons Laboratory, Dept. of Civil Engineering, Massachusetts Institute Of Technology Technical Report*, 215, 1976.

[43] D. K. P. Yue, H. S. Chen, and C. C. Mei. A hybrid element method for diffraction of water waves by three-dimensional bodies. *Int. J. Num. Methods Engineering*, 12:245–266, 1978.

[44] C. Zhou and P. L.-F. Liu. Second-order low-frequency wave forces on a vertical circular cylinder. *J. Fluid Mech.*, 175:143–155, 1987.